International Journal of Polymer Science

Silsesquioxanes: Recent Advancement and Novel Applications

Guest Editors: Yoshiro Kaneko, E. Bryan Coughlin, Takahiro Gunji, Maki Itoh, Kimihiro Matsukawa, and Kensuke Naka

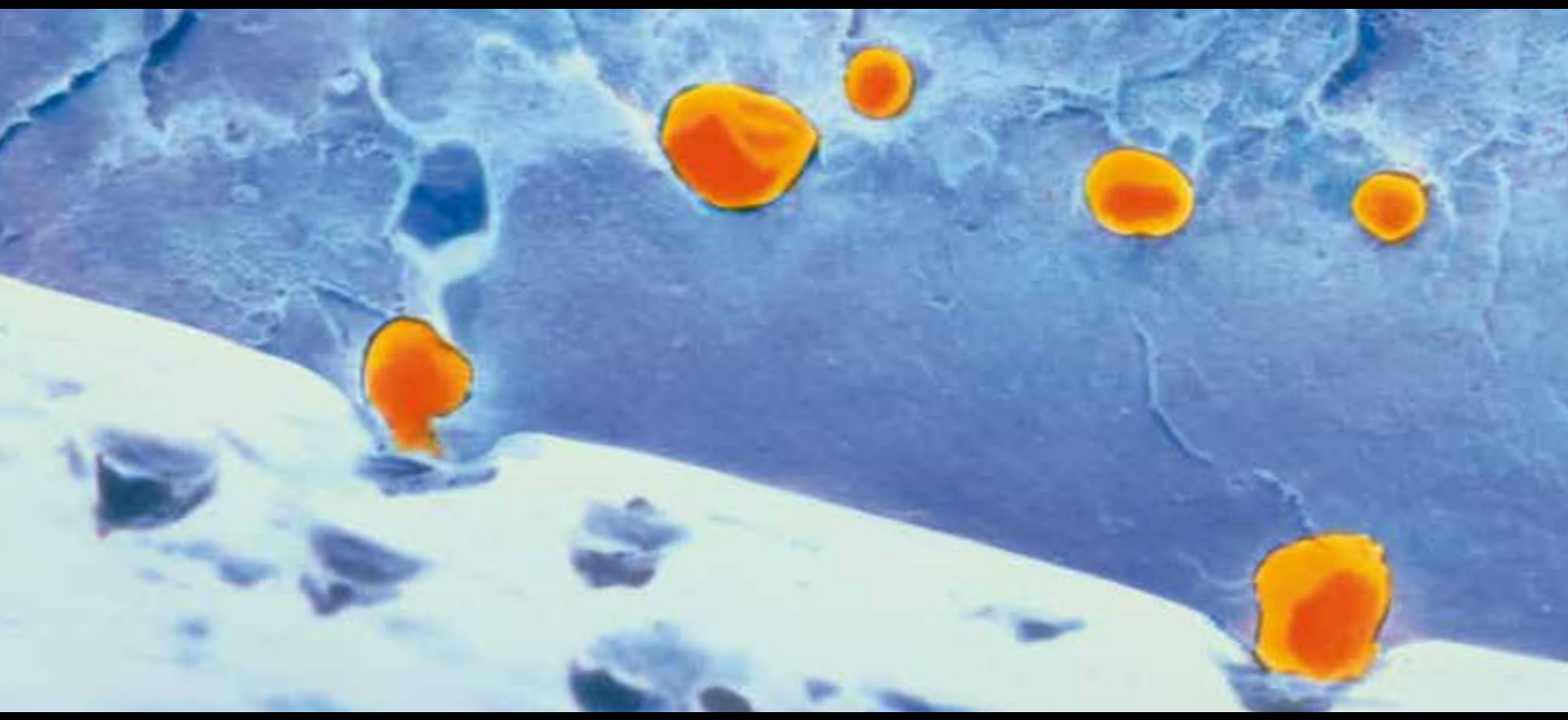

Silsesquioxanes: Recent Advancement and Novel Applications

International Journal of Polymer Science

Silsesquioxanes: Recent Advancement and Novel Applications

Guest Editors: Yoshiro Kaneko, E. Bryan Coughlin, Takahiro Gunji, Maki Itoh, Kimihiro Matsukawa, and Kensuke Naka

Editorial Board

Contents

Silsesquioxanes: Recent Advancement and Novel Applications, Yoshiro Kaneko, E. Bryan Coughlin, Takahiro Gunji, Maki Itoh, Kimihiro Matsukawa, and Kensuke Naka
Volume 2012, Article ID 453821, 2 pages

Iron Oxide Arrays Prepared from Ferrocene- and Silsesquioxane-Containing Block Copolymers, Raita Goseki, Tomoyasu Hirai, Masa-aki Kakimoto, and Teruaki Hayakawa
Volume 2012, Article ID 692604, 10 pages

Synthesis of a Novel Family of Polysilsesquioxanes Having Oligothiophenes with Well-Defined Structures, Ichiro Imae, Shotaro Takayama, Daisuke Tokita, Yousuke Ooyama, Kenji Komaguchi, Joji Ohshita, and Yutaka Harima
Volume 2012, Article ID 484523, 10 pages

Preparation of Ionic Silsesquioxanes with Regular Structures and Their Hybridization, Yoshiro Kaneko, Hisaya Toyodome, Miki Shoiriki, and Nobuo Iyi
Volume 2012, Article ID 684278, 14 pages

Polysilsesquioxanes for Gate-Insulating Materials of Organic Thin-Film Transistors, Kimihiro Matsukawa, Mitsuru Watanabe, Takashi Hamada, Takashi Nagase, and Hiroyoshi Naito
Volume 2012, Article ID 852063, 10 pages

A Theoretical Study of the Insertion of Atoms and Ions into Titanosilsequioxane (Ti-POSS) in Comparison with POSS, Yosuke Komagata, Takaaki Iimura, Nobuhiro Shima, and Takako Kudo
Volume 2012, Article ID 391325, 14 pages

Sol-Gel Preparation of Highly Water-Dispersible Silsesquioxane/Zirconium Oxide Hybrid Nanoparticles, Yoshiro Kaneko and Tomoyuki Arake
Volume 2012, Article ID 984501, 6 pages

Design and Synthesis of Functional Silsesquioxane-Based Hybrids by Hydrolytic Condensation of Bulky Triethoxysilanes, Hideharu Mori
Volume 2012, Article ID 173624, 17 pages

Characterization and Some Insights into the Reaction Chemistry of Polymethylsilsesquioxane or Methyl Silicone Resins, Maki Itoh, Fukuyo Oka, Michitaka Suto, Simon D. Cook, and Norbert Auner
Volume 2012, Article ID 526795, 17 pages

Nonacyclic Ladder Silsesquioxanes and Spectral Features of Ladder Polysilsesquioxanes, Masafumi Unno, Tomoe Matsumoto, and Hideyuki Matsumoto
Volume 2012, Article ID 723892, 4 pages

Evolution of Mesopores in Monolithic Macroporous Ethylene-Bridged Polysilsesquioxane Gels Incorporated with Nonionic Surfactant, Atsushi Mushiake, Kazuyoshi Kanamori, and Kazuki Nakanishi
Volume 2012, Article ID 460835, 6 pages

Synthesis and Properties of Polysilsesquioxanes Having Ethoxysulfonyl Group as a Side Chain, Takahiro Gunji, Kazuki Yamamoto, Akira Tomobe, Noritaka Abe, and Yoshimoto Abe
Volume 2012, Article ID 568301, 5 pages

A Synthetic Route to Quaternary Pyridinium Salt-Functionalized Silsesquioxanes, Nataliya Kostenko, Jochen Gottfriedsen, Liane Hilfert, and Frank T. Edelmann
Volume 2012, Article ID 586594, 9 pages

Hindawi Publishing Corporation
International Journal of Polymer Science
Volume 2012, Article ID 453821, 2 pages
doi:10.1155/2012/453821

Editorial

Silsesquioxanes: Recent Advancement and Novel Applications

Yoshiro Kaneko,[1] E. Bryan Coughlin,[2] Takahiro Gunji,[3] Maki Itoh,[4] Kimihiro Matsukawa,[5] and Kensuke Naka[6]

[1] *Department of Chemistry, Biotechnology, and Chemical Engineering, Graduate School of Science and Engineering, Kagoshima University, Kagoshima, Kagoshima 890-0065, Japan*
[2] *Department of Polymer Science and Engineering, University of Massachusetts Amherst, Amherst, MA 01003, USA*
[3] *Department of Pure and Applied Chemistry, Faculty of Science and Technology, Tokyo University of Science, Noda, Chiba 278-8510, Japan*
[4] *Electronics Solutions S&T, Dow Corning, Ichihara, Chiba 299-0108, Japan*
[5] *Electronic Material Research Division, Osaka Municipal Technical Research Institute, Osaka, Osaka 536-8553, Japan*
[6] *Department of Chemistry and Materials Technology, Graduate School of Science and Technology, Kyoto Institute of Technology, Kyoto, Kyoto 606-8585, Japan*

Correspondence should be addressed to Yoshiro Kaneko, ykaneko@eng.kagoshima-u.ac.jp
and Maki Itoh, maki.itoh@dowcorning.com

Received 6 November 2012; Accepted 6 November 2012

Among the products in silicone industry, silicone oils or elastomers are based on linear polysiloxanes mainly consisting of D ($R_2SiO_{2/2}$) unit, which is the predominant material in this industry mostly as polydimethylsiloxane. In contrast, silicone resins are network polymers consisting mainly of T ($RSiO_{3/2}$) and Q ($SiO_{4/2}$) units. Silsesquioxanes are one class of silicone resins that consist only of the T unit. The first commercialization of silicones started with silicone resins consisting primarily of silsesquioxanes for electrical insulation at high temperatures, in an effort to develop materials much more thermally stable and tougher than plastics but more flexible than glass [1]. Development research was started in the 1930s in Corning Glass Works and General Electric Company on the basis of academic work by Kipping. The research work at Corning Glass Works, led by Hyde, and scale-up production of the raw materials at Dow Chemical resulted in formation of Dow Corning in 1943. General Electric, where Patnode and Rochow were acting as pioneers, started commercial production of silicones in 1946 [2].

Most of the industrial silicone resin materials can be classified either into a DT type, which consists of D and T units, and an MQ type, which comprise M ($R_3SiO_{1/2}$) and Q units [3]. Silsesquioxanes could be considered as one of the DT silicone reins in which the content of the D unit is zero. In other words, T units without other components can form a material that we can call a silicone resin. Another characteristic of silsesquioxane is the defined structures like cages, known as polyhedral oligomeric silsesquioxanes (POSSs), which is drawing attentions both from academia and industry. Linear polymers could be characterized mostly by molecular weight and molecular weight distribution. However, the trifunctional nature of silsesquioxanes allows to form a variety of structures from oligomeric cages to ladder-like structures to three-dimensional network structures based on the ring structures. This could open up the possibility of creating unmet properties by structural control.

Silicones, including silsesquioxanes, are characterized with their high thermal/photo stability, electric insulation and so on. Compared with silica, silsesquioxanes or silicone resins can provide additional features including lower k, flowability, flexibility, functionality, and interaction with organic molecules from the combination of siloxane backbone and organic substitution. Combination of these characteristics and the numerous possibility of structural permutations provide the unique attributes of silsesquioxane

materials. This special issue highlights the recent significant progress in silsesquioxanes and their novel applications.

This special issue contains four review papers and eight research articles. One research article, "*A synthetic route to quaternary pyridinium salt-functionalized silsesquioxanes,*" describes synthesis of POSS derivatives having a pendant quaternized 4-(2-ethyl)pyridyl group aiming for potential antimicrobial property. The possible benefit of using POSS is its thermal stability and the spacing of the functionality by the cubic octamers. A 4-(2-ethyl)pyridine POSS derivative was prepared by reacting the corresponding trichlorosilane either directly with cyclohexyl-substituted $[RSiO_{3/2}]_4[RSi(OH)O_{2/2}]_3$ or after converting the SiOH to SiOLi. Another characteristic of such defined cage structures is entrapment of gas molecules, cations, or anions. Computer simulation for the insertion reaction of various guest species for Ti-POSS, $[HTiO_{3/2}]_n$, $n = 8$ and 10, is discussed in "*A theoretical study of the insertion of atoms and ions into titanosilsequioxane (Ti-POSS) in comparison with POSS*" in comparison with that for Si-POSS, exploring the similarity and difference between Ti-POSS and Si-POSS. Presence of cage compounds in products by the hydrolytic polycondensation of methyltrichlorosilane in excess water is clarified in "*Characterization and some insights into the reaction chemistry of polymethylsilsesquioxane or methyl silicone resins*". An experimental evidence that such cage molecules are formed by siloxane bond rearrangement from molecules of similar molecular weight rather than simple condensation of precursor molecules is presented. The presence of such cage molecules in industrial DT type silicone resins is also described. Preparation of block copolymers of methacrylates having POSS and ferrocene in the side chain by anionic polymerization is described in "*Iron oxide arrays prepared from ferrocene- and silsesquioxane-containing block copolymers.*" The materials showed microphase-separated nanostructures, and the array is expected to be a promising catalytic material for the creation of carbon nanotube thin films.

Another form of defined structure for silsesquioxane is a ladder structure. Proven ladder structure of silsesquioxanes can be found in those synthesized by stepwise reactions. The first nonacyclic ladder silsesquioxanes with isopropyl substituent are reported in "*Nonacyclic ladder silsesquioxanes and spectral features of ladder polysilsesquioxanes*", as formed by the reaction of bicyclic silanol with tricyclic tetrachloride. A review paper, "*Preparation of ionic silsesquioxanes with regular structures and their hybridization,*" describes the preparation of ladder-like polysilsesquioxanes by self-organization of ammonium salt, for which anion exchange behavior is investigated. In this review, control of conformational structures of the polysilsesquioxanes by the introduction of chiral moieties is also reported.

Various polysilsesquioxanes including hybrids aiming for specific functions are presented. Polysilsesquioxanes bearing ethoxysulfonyl groups in side chains were prepared for a proton-conductive film, by the hydrolytic polycondensation of 4-(2-methyl-3-triethoxysilylpropoxy)benzenesulfonate as discussed in "*Synthesis and properties of polysilsesquioxanes having ethoxysulfonyl group as a side chain.*" Polymethylsilsesquioxane-based organic-inorganic hybrid materials for gate insulating layer in organic thin film transistors (TFTs) are reviewed in "*Polysilsesquioxanes for gate insulating materials of organic thin-film transistors,*" referring to the possibility for flexible TFTs. Water-soluble polysilsesquioxanes, including hydroxyl-functional and cationic silsesquioxanes, are reviewed including the hybrids of $SiO_{1.5}/SiO_2$ and $RSiO_{1.5}/TiO_2$ and stimuli-responsive materials in "*Design and synthesis of functional silsesquioxane-based hybrids by hydrolytic condensation of bulky triethoxysilanes.*" Hybrid nanoparticles with other metal oxides are also reported for poly-3-aminopropyl-silsiesquioxane and zirconia having the estimated refractive index of 1.66, which can form highly transparent water dispersion as discussed in "*Sol-gel preparation of highly water-dispersible silsesquioxane/zirconium oxide hybrid nanoparticles*."

The last set of materials is so-called bridged silsesquioxanes. Ethylene-bridged polysilsesquioxane gels with hierarchical macropores and mesopores are prepared by combining the micellar templating in nanometer-scale with the polymerization-induced phase separation in micrometer-scale for well defined mesoporous structures as described in "*Evolution of mesopores in monolithic macroporous ethylene-bridged polysilsesquioxane gels incorporated with nonionic surfactant.*" Synthesis and properties of oligo-thiophene bridged polysilsesquioxanes are reviewed in "*Synthesis of a novel family of polysilsesquioxanes having oligothiophenes with well-defined structures.*" The polymers anchored on SiO_2 or ITO substrates showed excellent mechanical hardness based on the three-dimensional siloxane network structure with chemical linkage between the polymer and the surface of the metal-oxide substrates.

Acknowledgment

The editors are grateful to the contributing authors and reviewers for their efforts in compiling this special issue.

Yoshiro Kaneko
E. Bryan Coughlin
Takahiro Gunji
Maki Itoh
Kimihiro Matsukawa
Kensuke Naka

References

[1] E. L. Warrick, "Years of firsts," in *The Recollections of a Dow Corning Pioneer*, chapter 1, pp. 1–45, McGraw-Hill, New York, NY, USA, 1990.

[2] E. G. Rochow, *Silicon and Silicones*, Springer, Berlin, Germany, 1987.

[3] R. H. Baney, M. Itoh, A. Sakakibara, and T. Suzuki, "Silsesquioxanes," *Chemical Reviews*, vol. 95, no. 5, pp. 1409–1430, 1995.

Hindawi Publishing Corporation
International Journal of Polymer Science
Volume 2012, Article ID 692604, 10 pages
doi:10.1155/2012/692604

Research Article

Iron Oxide Arrays Prepared from Ferrocene- and Silsesquioxane-Containing Block Copolymers

Raita Goseki, Tomoyasu Hirai, Masa-aki Kakimoto, and Teruaki Hayakawa

Department of Organic and Polymeric Materials, Tokyo Institute of Technology, 2-12-1-S8-36 Ookayama, Meguro-ku, Tokyo 152-8552, Japan

Correspondence should be addressed to Teruaki Hayakawa, hayakawa.t.ac@m.titech.ac.jp

Received 13 August 2012; Accepted 11 October 2012

Academic Editor: Maki Itoh

Arrays of iron oxides as precursors of iron clusters were prepared by oxygen plasma treatment of block copolymer microphase-separated nanostructures in thin films. Block copolymers composed of ferrocene-containing and silsesquioxane-containing polymethacrylate (PMAPOSS-*b*-PMAHFC) were successfully prepared, with different molecular weights and compositions and narrow molecular weight distributions, by living anionic polymerization. The formed microphase-separated nanostructures in the bulk were characterized by wide- and small-angle X-ray scattering (WAXS and SAXS), scanning electron microscopy (SEM), and transmission electron microscopy (TEM). Thin films were prepared from a solution of PMAPOSS-*b*-PMAHFC in tetrahydrofuran by spin coating onto silicon wafers. Fingerprint-type line nanostructures were formed in the PMAPOSS-*b*-PMAHFCs thin films after solvent annealing with carbon disulfide. Oxygen plasma treatment provided the final line arrays of iron oxides based on the formed nanostructural patterns.

1. Introduction

Microphase-separated nanostructures of block copolymer thin films have been studied widely because they offer simple and low-cost pattern formation on the nanometer scale. In particular, they can be used as membranes, lithography masks, and as a variety of templates for the fabrication of a variety of devices [1–7]. For the creation of unique self-assembled nanostructures and the advancement of novel functions in these applications, various block segments consisting not only of conventional organic polymers, but also of organometallic and organic-inorganic polymers have been synthesized by recently developed controlled and living polymerization methods [8–14]. The size and spacing of the microdomains can be tailored on the scale of several tens of nanometers by varying the relative molar masses of the polymer segments within the blocks and the total molar masses of the copolymers.

Carbon nanotubes (CNTs) have attracted a great deal of attention in many areas of electronics because of their exceptional electrical properties, chemical stability, and mechanical strength [15, 16]. Among the numerous potential applications, CNTs in the form of thin films are particularly interesting for use in flexible integrated circuits [17]. CNTs properties strongly depend on the geometric arrangement of carbon atoms and the diameters of the individual tubes [18–21]. Therefore, gaining adequate control of tube diameter and geometry is essential in the protocols used for synthesizing CNTs [22–26]. One promising route to controlling the size and geometry of CNTs is a growth method using a catalytic template with iron oxides based on block copolymer thin films. Lu and coworkers have shown that iron clusters generated by reduction of iron oxides prepared from polystyrene-*block*-poly(ferrocenylsilane) (PS-*b*-PFS) [22] and poly(dimethyl siloxane)-*block*-poly(ferrocenylsilane) (PDMS-*b*-PFS) [27] diblock copolymers act as an effective catalyst for the growth of CNTs. They first attempted to prepare arrays of iron oxides as precursors of iron clusters from PS-*b*-PFS thin films, but a mixture of single- and multiwalled CNTs was obtained. This was attributed to the different sizes of iron oxides generated during the high-temperature CNT growth procedure (700°C). The arrays of iron oxide generated by PS-*b*-PFS thin films have low thermal stability

because of occurring aggregation of iron oxides at the high temperature. They subsequently, improved the block copolymers in order to provide thermally and structurally stable arrays of iron oxides by using PDMS-*b*-PFS. The PDMS was able to convert to thermally stable silica that surrounded the iron structures and prevented their aggregation during CNT growth. The resulting catalytic arrays of irons provided uniform single-walled CNTs. In general, silicone-containing block copolymers can form well-ordered microphase-separated nanostructures; however, dewetting often occurs during film preparation in the PDMS-based diblock copolymer system because of its low glass transition temperatures (T_g), below −100°C. This induces difficulty in forming the desired uniform thin films for producing ordered arrays of iron oxides. Therefore, a challenge remains in the preparation of silicone-containing block copolymer thin films with well-defined and stable microphase-separated nanostructures containing iron and silicon species.

We recently developed a novel series of block copolymers containing a polyhedral oligomeric silsesquioxane (POSS)-containing block copolymers such as PS-*block*-POSS containing poly(methyl methacrylate) (PMAPOSS), PMMA-*block*-PMAPOSS, and poly(ethylene oxide)-*block*-PMAPOSS [28–32]. The PMAPOSS polymers have much higher T_g values than that of PDMS and depend on the organic substituents of the POSS silicon atoms. They are able to stay stable and can be converted to silica using an oxidation process without dewetting. The POSS-containing block copolymers have also demonstrated good segregation during microphase separation and form much smaller periodic nanofeatures compared with many conventional block copolymers [33]. Furthermore, the etch resistance of PMAPOSS to oxygen plasma is much higher than that of polymers consisting purely of hydrocarbons, such as PEO, PMMA, and PS. Therefore, they can act not only as block copolymer lithographic materials, but also as silica thin film templates.

Herein, we report the creation of arrays of iron oxides within a silica matrix in thin films based on microphase-separated nanostructures of a series of PMAPOSS-containing block copolymers. In this study, we designed and synthesized a new PMAPOSS-containing block copolymer where one block contained a ferrocene moiety in the side chain, namely, PMAPOSS-*b*-PMAHFC. Typical examples of ferrocene-containing side chain polymers include poly(ferrocenyl methacrylate) (PFMMA) and poly(vinyl ferrocene) (PVFc), which have relatively high T_g values (PFMMA T_g: 185°C) [34–39]. In order to obtain well-ordered nanostructures in block copolymer thin films, thermal and/or solvent annealing is often necessary. However, this is not easy for polymers with high T_g values because of the crucial annealing conditions required for reassembly of the polymer chains. Therefore, in this study, we also attempted to improve the design of the ferrocene-containing polymer to reduce its T_g to a level suitable for forming well-ordered microphase-separated nanostructures under mild annealing conditions. A new ferrocene-containing methacrylate monomer with an alkyl spacer (MAHFC) was synthesized and used for living anionic polymerization to create a new series of diblock copolymers, PMAPOSS-*b*-PMAHFCs. We also describe the characterization of the resulting microphase-separated nanostructures in the bulk and thin films by small- and wide-angle X-ray scattering (SAXS and WAXS), transmission electron microscopy (TEM), and scanning electron microscopy (SEM). The oxygen plasma-treated PMAPOSS-*b*-PMAHFC thin films were then characterized by SEM and X-ray photoelectron spectroscopy (XPS).

2. Experimental

2.1. Materials. *sec*-Butyllithium (*sec*-BuLi) was purchased from Kanto Chemical Co. (Tokyo, Japan). 3-(3,5,7,9,11,13,15-heptaisobutylpentacyclo-[9.5.1.^{3,9}1.^{5,15}1^{7,13}]octasiloxane-1-yl)propyl methacrylate (MAPOSS) was purchased from Hybrid Plastics Inc. (USA). The other reagents were purchased from TCI Co. (Tokyo, Japan). Prior to use, tetrahydrofuran (THF) was distilled over sodium/benzophenone in a nitrogen atmosphere until a deep purple color was achieved. MAPOSS was purified by recrystallization from methanol. 1,1-diphenylethylene (DPE) was distilled over *n*-butyllithium under reduced pressure, and lithium chloride (LiCl) was baked under vacuum at 180°C for 24 h. The other reagents were used as received.

2.2. Instrumentation and Characterization. For TEM analysis, bulk samples were embedded in epoxy resin and cured at 70°C for 24 h. The embedded samples were then microtomed using a DIATOME diamond knife at room temperature to a preset thickness of 70 nm using Microtome. The sections were placed on TEM grids and viewed directly using a JEOL JEM-200CX at 100 kV. WAXS and SAXS measurements on the bulk samples were performed on the BL17B3 beamline at the National Synchrotron Radiation Research Center (NSRRC). Monochromatic X-ray beams of 10.5 keV (λ = 1.1809 Å) were used. IR spectra were recorded on a JASCO FT/IR-460 Plus spectrometer. ^{1}H, ^{13}C, and ^{29}Si NMR spectra were recorded on a JEOL JNM-AL 300 spectrometer at 300 MHz, 75 MHz, and 59.4 MHz, respectively. Thermal analyses of the compounds, thermogravimetric analysis (TGA), and differential scanning calorimetry (DSC) were carried out using a Seiko SSC/6000 (TG/DTA 6200 and DSC6200) thermal analyzer with ca. 5 mg of samples at a heating rate of 10°C min^{-1}. Nitrogen was used as the purge gas at a flow rate of 50 mL min^{-1} for both the TGA and DSC measurements. Size-exclusion chromatography (SEC) measurements were carried out using a Shodex GPC-101, two columns (Shodex KF-802 and Shodex KF-806 M), and a Shodex RI-71 detector. THF was used as the eluent with a 1 mL min^{-1} flow rate at 40°C. SEM imaging was carried out using a Hitachi S-4800 SEM with a field-emission source at 1.0 kV. XPS was carried out using AlKα radiation ($h\nu$ = 1486.6 eV) as the photo source and was used to investigate the surface properties of the sample.

2.3. Synthesis. Hydroxymethylferrocene was synthesized according to the literature [40]. Iodomethane (21.9 g, 0.155 mol) in methanol (25 mL) was treated dropwise with dimethylamino (dimethylferoccene) (25 g, 0.103 mol) in

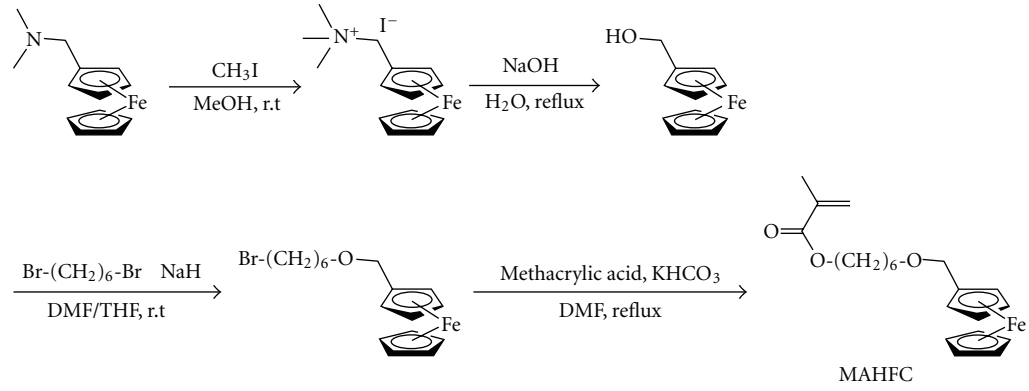

Figure 1: Synthesis of MAHFC monomer.

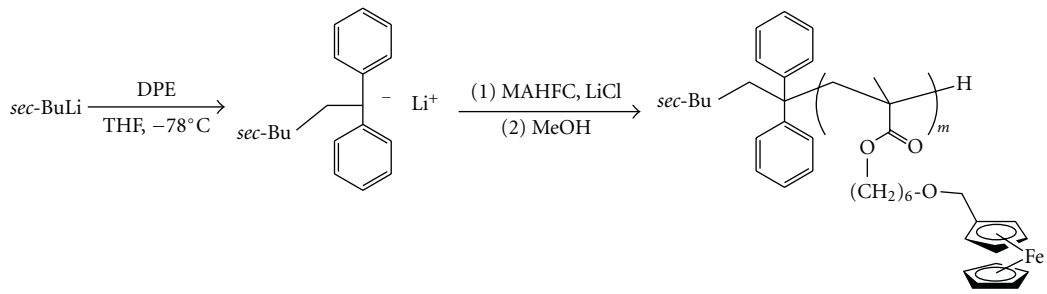

Figure 2: Synthesis of PMAHFC homopolymer by living anion polymerization.

methanol (20 mL) and stirred for 4 h at room temperature. Diethyl ether was then added to the mixture and the resulting precipitate was filtered and dried *in vacuo* at 30°C for 3 h (37.2 g, 94%).

N,N,N-trimethylaminomethyl-ferrocene iodine (20.0 g, 0.052 mol) was added to a 2N sodium hydroxide solution (200 mL) and the mixture was refluxed overnight. The reaction mixture was then diluted with diethyl ether and washed with brine. The organic layer was dried over magnesium sulfate ($MgSO_4$), filtered, and evaporated. The yellow residue was purified by recrystallization from *n*-hexane. The yellow needles were dried *in vacuo* at 30°C for 4 hours (8.1 g, 72%); m.p.; 77-78°C; ^{1}H NMR ($CDCl_3$, r.t): δ 1.53 (1H, –OH), 4.24 (7H, H), 4.26 (2H, H), 4.32 (2H, $–CH_2$).

2.4. 1-Bromo-6-ferrocenylmethoxy-hexane. A round-bottomed flask was charged with sodium hydride (0.79 g, 0.033 mol) and THF (10 mL) in a nitrogen atmosphere. A solution of 1,6-dibromohexane (8.08 g, 0.033 mmol) and hydroxymethylferrocene (7.25 g, 0.033 mmol) in *N,N*-dimethylformamide (DMF)/THF (20 mL each) was added to the mixture and the mixture was kept at 0°C using an ice bath. After 24 h, the reaction mixture was diluted with *n*-hexane and washed with brine several times to remove the DMF and excess sodium hydride. The organic layer was dried over $MgSO_4$, filtered, and evaporated. The dark red residue was purified by column chromatography on silica using *n*-hexane. The solvent was removed and the dark red liquid was dried *in vacuo* at room temperature for 3 h (7.20 g, 18.9 mmol, 57%). IR (KBr): 3094, 2954, 2867, 1100, 1000, 654 cm^{-1}.; ^{1}H NMR ($CDCl_3$, rt): δ 4.89 and 4.26–4.09 (9H, cyclopentadienyl), 3.40 (m, 4H, $–CH_2–O–CH_2–$ferrocene), 1.84 (m, 2H, $Br–CH_2–CH_2–$), 1.58 (m, 4H, alkyl chain), 1.38 (m, 4H, alkyl chain); ^{13}C NMR ($CDCl_3$, rt): δ 83.6, 77.2, 69.7, 69.4, 69.0, 68.3, 33.9, 32.7, 29.5, 27.9, 25.3 ppm.

2.5. Synthesis of MAHFC. A round-bottomed flask was charged with 1-bromo-6-ferrocenylmethoxy-hexane (1.50 g, 3.95 mmol) in DMF (24 mL). The methacrylic acid salt was prepared by mixing methacrylic acid (0.68 g, 7.90 mmol) and sodium hydrogen carbonate (0.79 g, 7.90 mmol) and was added to the flask along with a small amount of hydroquinone as an inhibitor. The resulting solution was heated to 100°C over the course of 6 h in a nitrogen atmosphere. The reaction mixture was then diluted with *n*-hexane and washed with brine. The organic layer was dried over $MgSO_4$, filtered, and evaporated. The dark red residue was purified by column chromatography on silica using *n*-hexane. The solvent was removed and a dark red liquid was obtained (1.31 g, 3.42 mmol, 86%). IR (KBr): 3093, 2951, 2869, 1730, 1640, 1100, 1000 cm^{-1}. ^{1}H NMR ($CDCl_3$, rt): δ 6.10 (s, 1H, $C=CH_2$), 5.56 (s, 1H, $C=CH_2$), 4.26–4.13 (br, 11H, cyclopentadienyl and $–COO–CH_2–$), 3.39 (br, 2H, $–O–CH_2–$ferrocene), 1.95 (s, 3H, $–CH_3$), 1.54 (m, 4H, alkyl chain), 1.34 (s, 4H, alkyl chain); ^{13}C NMR ($CDCl_3$, rt): δ 1637.3, 136.3, 127.2, 125.0, 83.5, 79.7, 77.4, 69.6, 69.2, 68.9, 68.2, 64.5, 29.4, 28.4, 25.7, 18.2 ppm.

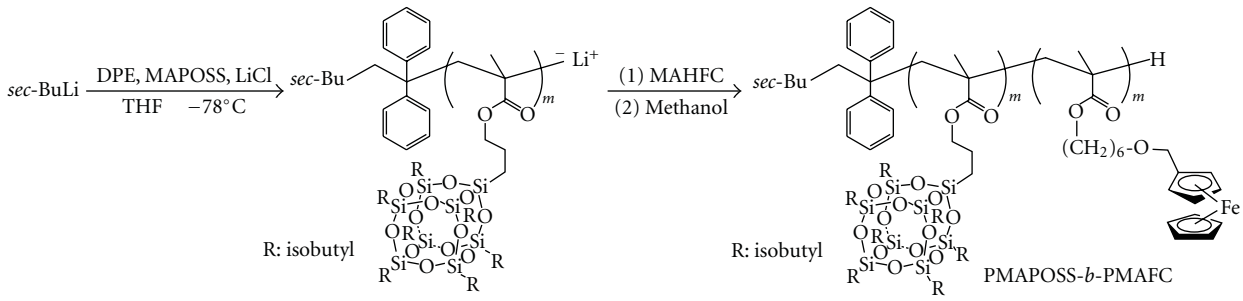

Figure 3: Synthesis of PMAPOSS-*b*-PMAHFC by living anion polymerization.

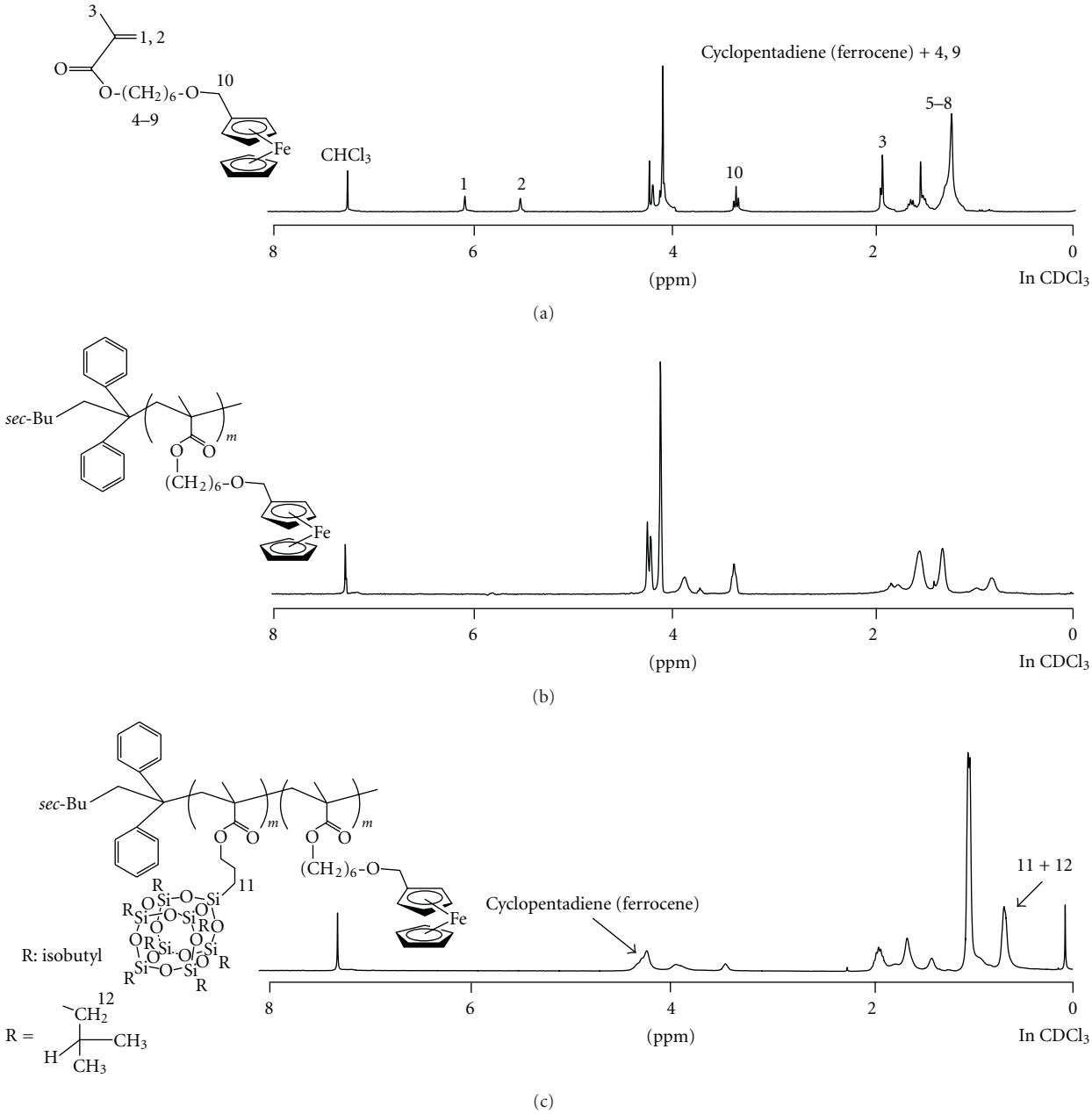

Figure 4: ^{1}H NMR spectra of (a) MAHFC, (b) PMAHFC, and (c) PMAPOSS-*b*-PMAHFC.

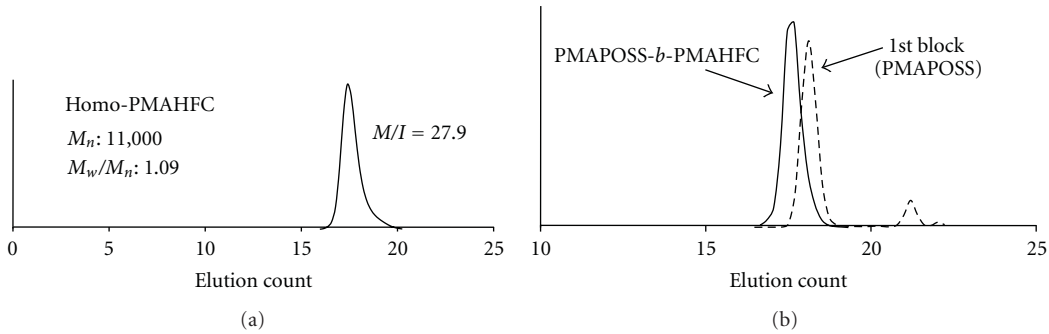

Figure 5: SEC curves of (a) PMAHFC homopolymer and (b) PMAPOSS-*b*-PMAHFC (solid line) and PMAPOSS (dashed line).

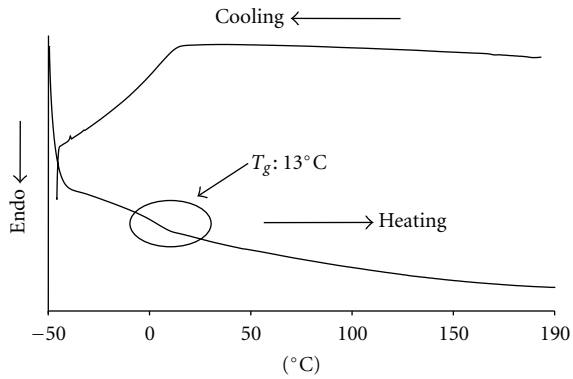

Figure 6: DSC trace of PMAPOSS-*b*-PMAHFC **2** (from −50°C to 190°C).

2.6. Synthesis of PMAHFC Homopolymer by Living Anionic Polymerization. THF (40 mL) was transferred to a glass reactor equipped with stir bar containing dry LiCl (15 mg, 0.36 mmol) and cooled to −78°C. After 5 min, *sec*-BuLi was added until the color changed to slightly yellow. The reactor was removed from the cooling bath and allowed to reach room temperature, upon which the solution became colorless. The reactor was cooled back to −78°C, and 1.07 M *sec*-BuLi solution in hexane/cyclohexane (0.025 mL, 0.027 mmol) was added. After 5 min, DPE (0.025 mL, 0.14 mmol) was added to the reactor, resulting in the formation of a deep red color. After 30 min, MAHFC that had been dried under reduced pressure for several hours (0.30 g, 0.78 mmol) was dissolved in THF (4.0 mL) and transferred from the monomer reservoir to the polymerization flask via cannula with vigorous stirring. The solution changed from deep red to orange. After 8 h at −78°C, excess of methanol was added to the reactor to obtain the proton-terminated polymer. This was then precipitated into a large excess amount of methanol, filtered, and dried *in vacuo* at 80°C for 6 h, yielding 0.28 g of polymer. IR (KBr): 3093, 2951, 2869, 1730, 1640, 1100, 1000 cm^{-1}. ^{1}H NMR ($CDCl_3$, rt): δ 4.26-4.13 (br, cyclopentadienyl), 3.89 (br, –O–CH_2−ferrocene), 3.40 (br, –O–CH_2–CH_2,), 1.85−1.78 (m, main chain), 1.56–1.34 (br, alkyl side chain), 0.85 (m, αCH_3); ^{13}C NMR ($CDCl_3$, rt): δ 177.7, 83.7, 69.8, 69.4, 69.0, 68.44, 68.40, 54.1, 51.8, 44.8, 44.5, 29.6, 28.1, 25.8 ppm.

2.7. Synthesis of PMAPOSS-b-PMAHFC by Living Anionic Polymerization. THF (40 mL) was transferred to a glass reactor equipped with a stirrer bar containing dry LiCl (15 mg, 0.36 mmol), and then cooled to −78°C. After 5 min, *sec*-BuLi was added until the color changed to slightly yellow. The reactor was removed from the cooling bath and allowed to reach room temperature upon which the solution became colorless. The reactor was cooled back to −78°C and 1.07 M *sec*-BuLi solution in hexane/cyclohexane (0.025 mL, 0.027 mmol) was added. After 5 additional minutes, DPE (0.025 mL, 0.14 mmol) was added to the reactor resulting in the formation of a deep red color. After 30 min, MAPOSS (0.5 g, 0.5 mmol) was dissolved in THF (4.0 mL) and transferred from the monomer reservoir to the polymerization flask via cannula with vigorous stirring. The deep red color changed to colorless. In a second sample, MAHFC (0.4 g, 0.78 mmol) was dissolved in THF (4.0 mL). After 8 h, the MAHFC solution was transferred to the polymerization flask via cannula. After additional 8 h at −78°C, excess methanol was added to the reactor yielding the proton terminated diblock copolymer. This was then precipitated into methanol, filtered, and dried *in vacuo* at 60°C for 8 h. IR (KBr): 3094, 2953, 2868, 1730, 1643, 1260, 1100, 1000 cm^{-1}. ^{1}H NMR ($CDCl_3$, rt): δ 4.25–4.10 (br, ferrocene, PMAHFC), 3.86 (br, –O–CH_2–ferrocene), 3.37 (br, –O–CH_2–CH_2, PMAHFC), 1.84–1.78 (br, main chain –CH_2, –CH, PMAPOSS, PMAHFC), 1.53–1.31 (br, alkyl side chain, PMAHFC), 0.98 (br, isobutyl –$C(CH_3)_2$, PMAPOSS), 0.81 (m, αCH_3, PMAPOSS and PMAHFC), 0.55 (br, -$SiCH_2$, PMAPOSS); ^{13}C NMR ($CDCl_3$, rt): δ 177.7, 176.9, 83.7, 69.8, 69.4, 69.0, 68.44, 68.40, 67.2, 54.1, 51.8, 45.2, 44.8, 44.5, 29.6, 28.1, 26.0, 25.8, 25.7, 25.5, 24.0, 23.8, 22.5, 22.4, 21.8, 8.4 ppm.; ^{29}Si NMR ($CDCl_3$, rt): δ −67.6, −67.9 ppm.

3. Results and Discussion

3.1. Synthesis and Polymerization of Ferrocene-Containing Monomer. The procedure for synthesizing MAHFC, with a hexyl chain between the ferrocene moiety and methacrylate group, is illustrated in Figure 1. The role of the hexyl chain is to prevent strong interactions between ferrocene groups. The hydroxymethylferrocene was first prepared according

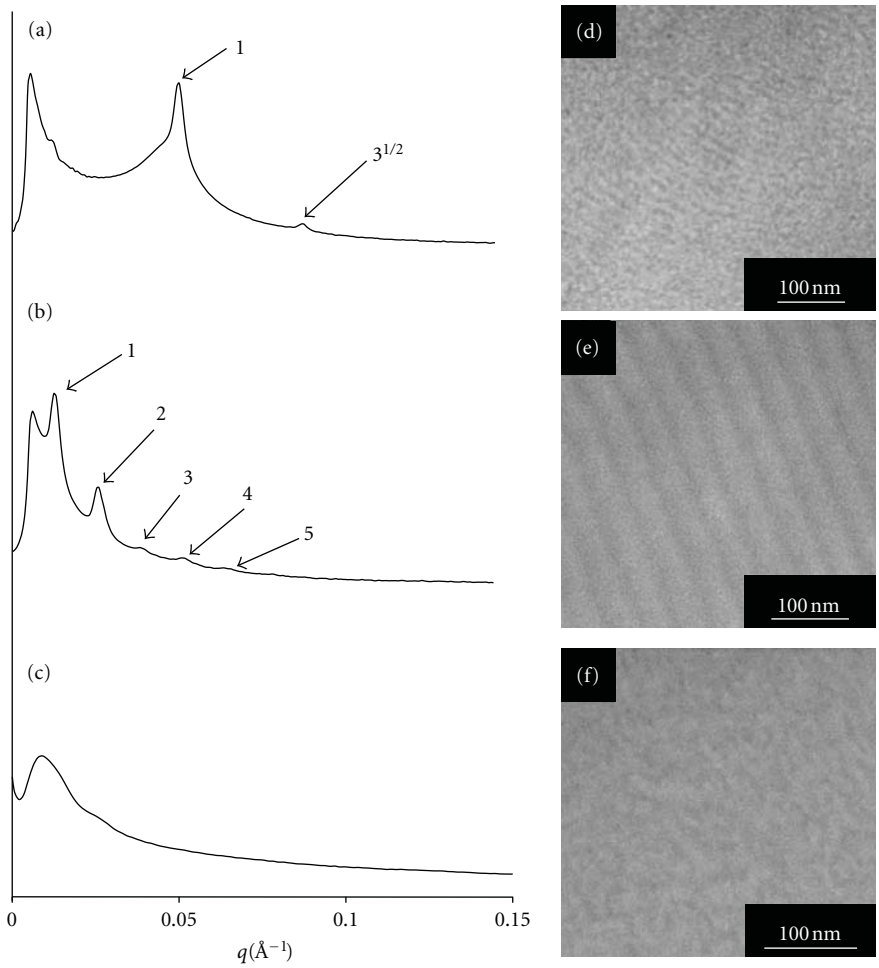

Figure 7: SAXS profiles (a, b, c) and TEM images (d, e, f) of PMAPOSS-*b*-PMAHFC **1**−**3**; (a) and (d) PMAPOSS-*b*-PMAHFC **1**; (b) and (e) PMAPOSS-*b*-PMAHFC **2**; (c) and (f) PMAPOSS-*b*-PMAHFC **3**. Brighter region corresponds to PMAPOSS domain and darker region corresponds to PMAHFC domain.

to the literature. It then underwent etherification with 1,6-dibromohexane to obtain 1-bromo-6-ferrocenylmethoxy-hexane. Finally, the MAHFC monomer was yielded as a dark red liquid after esterification of methacrylic acid. The monomer was characterized by ^{1}H and ^{13}C NMR and IR spectroscopy. Figure 4(a) shows ^{1}H NMR spectrum of MAHFC, which exhibits the resonance signals of the double bond (peaks a and b) and the ferrocene moiety. The characteristic peaks of the two carbons of the double bond appear at 136.3 and 125.0 ppm in the ^{13}C NMR spectrum. There is also a series of peaks between 68.4 and 69.8 ppm from the ten carbons of the ferrocene group. These observations indicate that the desired MAHFC was successfully obtained.

Living anionic polymerization of MAHFC was employed in order to control both the molecular weights and molecular weight distributions of the resulting block copolymers. The polymerization was carried out using 1,1-diphenyl-3-methyl-pentyllithium as the initiator, prepared by the reaction of *sec*-BuLi and DPE in the presence of a 5-fold excess of LiCl in THF at −78°C for 8 h to ensure complete conversion was achieved (Figure 2). Finally, the active chains were terminated at −78°C using degassed methanol, and the products were precipitated in a large volume of methanol at room temperature. After precipitation, the methanol solution remained colorless, thereby verifying the absence of unreacted monomers and oligomers. The purification was carried out by reprecipitation into a large volume of methanol, twice, and PMAHFC was obtained as a yellowish-orange powder. All the signals and peaks of PMAHFC were accurately assigned in the ^{1}H and ^{13}C NMR and IR spectra. SEC was performed on PMAHFC to determine its number average molecular weight (M_n) and polydispersity index (PDI). The chromatogram demonstrates a sharp unimodal peak (Figure 5(a)). The M_n and PDI were found to be 11 000 g mol^{-1} and 1.09, respectively, indicating that the living anionic polymerization of MAHFC successfully afforded the polymer with a controlled M_n and narrow PDI.

Based on the success of the homopolymerization of MAHFC, the synthesis of the block copolymer PMAPOSS-*b*-PMAHFC was carried out (Figure 3). The MAHFC was added as a second monomer to the living PMAPOSS reaction

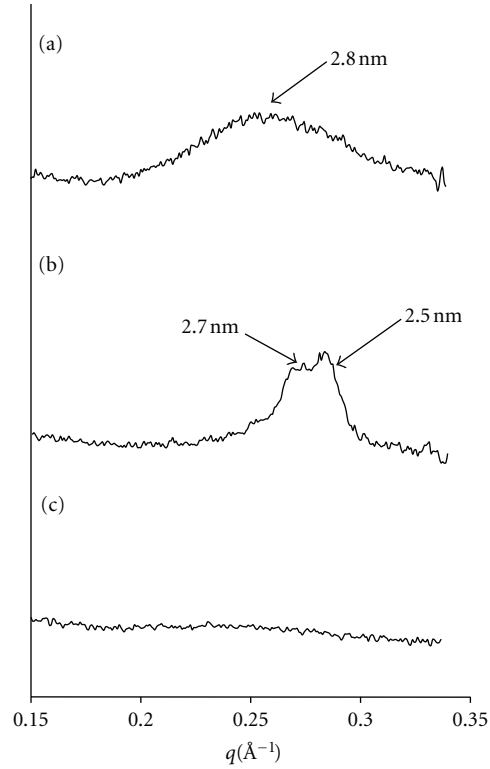

Figure 8: WAXS profiles of (a) PMAPOSS-*b*-PMAHFC **1**, (b) PMAPOSS-*b*-PMAHFC **2**, and (c) PMAPOSS-*b*-PMAHFC **3**.

mixture and the polymerization proceeded homogeneously, with no precipitation observed until the reaction was terminated. In this study, three PMAPOSS-*b*-PMAHFCs, **1**, **2**, and **3**, with different molecular weights and compositions were prepared (Table 1). The chemical compositions of the block copolymers were characterized by ^{1}H, ^{13}C, and ^{29}Si NMR and IR spectroscopies, and the M_n values were measured using SEC. Figure 4 shows the ^{1}H NMR spectra of the MAHFC monomer, PMAHFC homopolymer, and PMAPOSS-*b*-PMAHFC. The ^{1}H NMR spectrum of PMAPOSS-*b*-PMAHFCs clearly shows that the incorporation of each block was successful, which is indicated by the appearance of methylene ($-OSiCH_2$) protons corresponding to PMAPOSS at 0.59 ppm and cyclopentadienyl protons corresponding to ferrocene groups in PMAHFC at 4.1–4.3 ppm. The SEC chromatograms of the polymers show that the M_n increased in a controlled manner, which is reflected by the shift to the higher molecular weight region (Figure 5(b)). The SEC analysis showed that the PDI for all polymers was below 1.08. The compositions of PMAPOSS-*b*-PMAHFCs were ascertained by using the ^{1}H NMR spectra integration ratios of methylene protons for PMAPOSS and ferrocene protons from PMAHFC, along with the M_n values. The thermal properties of PMAHFC and the PMAPOSS-*b*-PMAHFCs were investigated using TGA and DSC. To eliminate the effect of thermal histories of the samples, the samples were heated to 200°C and held for 10 min at this temperature before cooling to −50°C at a rate of 10°C min^{-1}. The DSC trace of PMAPOSS-*b*-PMAHFC **2** on the second heating showed baseline shifts at 13°C corresponding to the T_g of the PMAHFC block segment (Figure 6). The T_g of PMAHFC is significantly lower than that of poly(ferrocenyl methacrylate) (185°C). The alkyl chain in the ferrocene-tethered side chains might decrease the interactions between the ferrocene moieties increasing the conformational flexibility of the side chains.

3.2. Bulk Morphological Characterization. The morphologies of the PMAPOSS-*b*-PMAHFCs in their bulk state were studied using WAXS, SAXS, and TEM. The samples were prepared by slow evaporation from chloroform at room temperature. For TEM measurement, all samples were imaged without staining as the contrast between the ferrocene-containing block (dark regions) and the POSS-containing block (bright regions) was sufficient for achieving high-quality images.

Figure 7 shows SAXS and TEM results for PMAPOSS-*b*-PMAHFCs **1**–**3**. The SAXS profile of the PMAPOSS-*b*-PMAHFC **1** exhibits first-order and second-order diffraction peaks, with ratios of 1 and $3^{1/2}$, respectively. The TEM image of PMAPOSS-*b*-PMAHFC **1** shows PMAHFC cylindrical nanostructures, which is strongly supported by the SAXS results. On increasing the PMAHFC wt% to 0.33, clear microphase-separated nanostructures were observed. The scattering profiles show up to five peaks with a characteristic ratio of 1 : 2 : 3 : 4 : 5, indicating a lamellar morphology. The lamellar *d*-spacing was found to be 49 nm, which is in good agreement with values obtained from the TEM image. Although the molecular weight and the composition of PMAPOSS-*b*-PMAHFC **3** are theoretically sufficient to enable microphase separation, the TEM image shows no well-defined microphase-separated nanostructures. In order to investigate this sample further, WAXS measurements were performed. The WAXS patterns of PMAPOSS-*b*-PMAHFC **1** and **2** (Figure 8) show some peaks in the high *q* region corresponding to a *d* spacing of 2.5−2.7 nm, but no diffraction peaks are evident for PMAPOSS-*b*-PMAHFC **3**. As previously reported, these diffraction peaks correspond to the distance between the PMAPOSS chains in the self-assembled structures [30]. These results indicate that the microphase separation and the aggregation of PMAPOSS chains can only occur when the content of PMAHFC in the PMAPOSS-*b*-PMAHFC copolymer is low.

3.3. Thin Film Nanostructures and Oxygen Plasma Treatment. In order to investigate the nanostructures of the thin films, solutions of the PMAPOSS-*b*-PMAHFCs in THF (1.0%−2.0%, w/w) were spin coated onto silicon wafers. Prior to coating, the substrates were cleaned with piranha solution (30% H_2O_2/70% H_2SO_4, v/v) at 110°C for 2 h, rinsed thoroughly with distilled water, and dried under a stream of nitrogen. The morphology of the thin films of the PMAPOSS-*b*-PMAHFCs was characterized by SEM, and the thickness of the films was estimated using ellipsometry. The as-cast thin film prepared from a THF solution of PMAPOSS-*b*-PMAHFC **2** had a thickness of 47 nm and did not show any ordered nanostructures caused by microphase

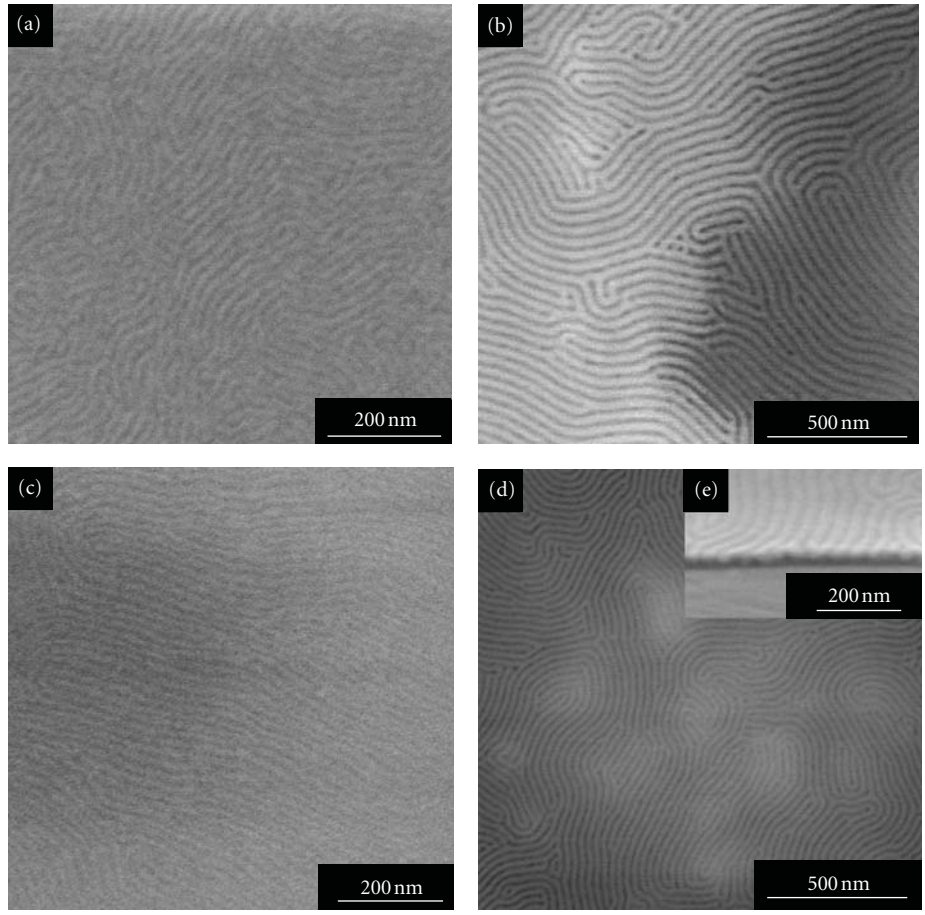

Figure 9: SEM images of thin films (a) PMAPOSS-*b*-PMAHFC **1**, (b) PMAPOSS-*b*-PMAHFC **2**, (c) oxygen plasma treated PMAPOSS-*b*-PMAHFC **1**, and (d) oxygen plasma treated PMAPOSS-*b*-PMAHFC **2**, the inset (e) is the cross-sectional SEM image of (d).

Table 1: Characteristics of block copolymers based on SEC and ^{1}H NMR analyses.

PMAPOSS-*b*-PMAHFC	M_n[a]	M_w[a]	PDI[a]	wt% PMAPOSS[b]	wt% PMAHFC[b]
1	16,300	17,300	1.06	75	25
2	49,000	52,600	1.07	67	33
3	56,100	60,400	1.08	42	58

[a]Measured by SEC, relative to PS linear standard. [b]The numbers refer to the final composition determined by SEC calibrated against PS linear standard and integrations from ^{1}H NMR spectrum.

separation. Solvent and thermal annealing were carried out in order to initiate reassembly of the polymer chains to induce microphase separation. However, the thermal annealing did not affect the results with a wide range of temperatures and annealing times tested. Solvent annealing was therefore subsequently investigated. Solvent annealing of PMAPOSS-*b*-PMAHFC was performed using carbon disulfide (CS_2) because it was found that it could swell both PMAHFC and PMAPOSS. Thin films of PMAPOSS-*b*-PMAHFC **1** and **2** were annealed in saturated CS_2 vapor at room temperature for 5 min and 10 min, respectively. SEM images of the resulting films showed line nanostructures on the surface with *d* spacings of 19 nm (Figure 9(a)) and 46 nm (Figure 9(b)), respectively. Under these specific solvent annealing conditions, no dewetting was seen to occur. In Figure 9, the brighter region corresponds to the PMAPOSS blocks. Because the PMAPOSS blocks tend to discharge more secondary electrons than the PMAHFC blocks.

Finally, in order to create the arrays of iron oxides, oxygen plasma treatment was carried out for 30 s on the series of PMAPOSS-*b*-PMAHFC thin films. The SEM images of the exposed films clearly show the remaining microphase-separated nanostructures. As shown in Figure 9(e), the cross-sectional SEM image of the PMAPOSS-*b*-PMAHFC **2** thin film treated with oxygen plasma indicates that perpendicular lamella formed through the entire 47 nm thick film. The XPS spectrum of PMAPOSS-*b*-PMAHFC **1** shown in Figure 10 exhibits a peak corresponding to $Fe_{2p3/2}$ at 711 eV (Figure 10). This indicates that iron oxides

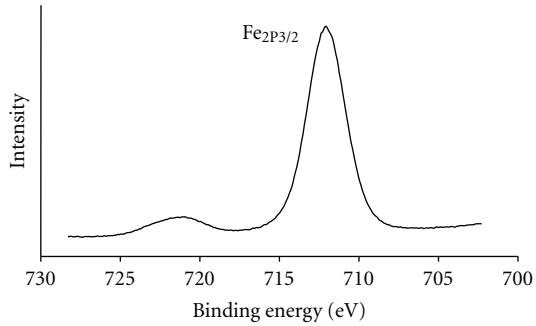

Figure 10: XPS spectrum in the range 730–700 eV for oxygen plasma-treated PMAPOSS-*b*-PMAHFC **1** thin film.

were generated by oxidation of the ferrocene moiety on the PMAPOSS-*b*-PMAHFCs at the thin film surface. These characterizations show that a well-defined line array of iron oxides was obtained, without any collapse, by simple oxygen plasma treatment of PMAPOSS-*b*-PMAHFC thin films. The catalytic ability for CNT growth is still under investigation, and will be described in a subsequent report.

4. Conclusion

In conclusion, a new series of POSS-containing block copolymers with a ferrocene-containing side-chain polymer of PMAHFC was prepared using living anionic polymerization. The use of this method enabled control of the molecular weights and the achievement of a narrow PDI below 1.08. PMAHFC demonstrated a T_g at 13°C, which is much lower than that of conventional ferrocene-containing side-chain polymers such as PFMMA. Microphase separation occurred only when the content of PMAHFC in the PMAPOSS-*b*-PMAHFC copolymer was below 33 wt%. The line nanostructures in the thin films were formed using solvent annealing, and subsequent oxygen plasma treatment provided line arrays of iron oxides based on the microphase-separated nanostructures. This array is expected to be a promising catalytic material for the creation of CNT thin films.

Acknowledgments

The authors thank Ryohei Kikuchi, National University Corporation Tokyo Institute of Technology Center for Ascended Materials Analysis, for the TEM. The authors acknowledge NSRRC, Taiwan, for facilitating the SAXS and WAXS experiments performed as part of this work and Dr. U-Ser Jeng of NSRRC for assistance with these experiments. R. Goseki and T. Hayakawa gratefully thank Professor Sang-Ouk Kim (Korea Advanced Institute of Science and Technology) for his useful discussions.

References

[1] M. Lazzari and M. A. López-Quintela, "Block copolymers as a tool for nanomaterial fabrication," *Advanced Materials*, vol. 15, no. 19, pp. 1583–1594, 2003.

[2] C. Park, J. Yoon, and E. L. Thomas, "Enabling nanotechnology with self assembled block copolymer patterns," *Polymer*, vol. 44, no. 22, pp. 6725–6760, 2003.

[3] J. Y. Cheng, C. A. Ross, H. I. Smith, and E. L. Thomas, "Templated self-assembly of block copolymers: top-down helps bottom-up," *Advanced Materials*, vol. 18, no. 19, pp. 2505–2521, 2006.

[4] M. Park, C. Harison, P. M. Chaikin, R. A. Register, and D. H. Adamson, "Block copolymer lithography: periodic arrays of ~ 1011 holes in 1 square centimeter," *Science*, vol. 276, no. 5317, pp. 1401–1404, 1997.

[5] C. J. Hawker and T. P. Russell, "Block copolymer lithography: merging "bottom-up" with "top-down" processes," *MRS Bulletin*, vol. 30, no. 12, pp. 952–966, 2005.

[6] J. Bang, U. Jeong, D. Y. Ryu, T. P. Russell, and C. J. Hawker, "Block copolymer lithography: translation of molecular level control to nanoscale patterns," *Advanced Materials*, vol. 21, no. 47, pp. 4769–4792, 2009.

[7] A. V. Ruzette and L. Leibler, "Block copolymers in tomorrow's plastics," *Nature Materials*, vol. 4, no. 1, pp. 19–31, 2005.

[8] A. S. Abd-El-Aziz and I. Manners, *Frontiers in Transition Metal-Containing Polymers*, Wiley-Interscience, Hoboken, NJ, USA, 2007.

[9] I. Manners, *Synthetic Metal-Containing Polymers*, VCH, Weinheim, Germany, 2004.

[10] D. Wohrle and A. D. Pomogailo, *Metal Complexes and Metals in Macromolecules: Synthesis, Structure and Properties*, Wiley-VCH, Weinheim, Germany, 2003.

[11] C. E. Carraher, A. S. Abd-El-Aziz, C. Pittman, J. Sheats, and M. Zeldin, *A Half Century of Metal and Metalloid Containing Polymers*, Wiley, New York, NY, USA, 2003.

[12] M. Rehahn, "Organic-inorganic hybrid polymers," in *Synthesis of Polymers: A Volume of the Materials Science and Technology Series*, A. D. Schluter, Ed., Wiley-VCH, Weinheim, Germany, 1999.

[13] P. Nguyen, P. Gómez-Elipe, and L. Manners, "Organometallic polymers with transition metals in the main chain," *Chemical Reviews*, vol. 99, no. 6, pp. 1515–1548, 1999.

[14] I. Manners, "Polymer science with transition metals and main group elements: towards functional, supramolecular inorganic polymeric materials," *Journal of Polymer Science A*, vol. 40, no. 2, pp. 179–191, 2002.

[15] W. A. De Heer, A. Châtelain, and D. Ugarte, "A carbon nanotube field-emission electron source," *Science*, vol. 270, no. 5239, pp. 1179–1180, 1995.

[16] S. J. Tans, A. R. M. Verschueren, and C. Dekker, "Room-temperature transistor based on a single carbon nanotube," *Nature*, vol. 393, no. 6680, pp. 49–52, 1998.

[17] D. H. Lee, D. O. Shin, W. J. Lee, and S. O. Kim, "Hierarchically organized carbon nanotube arrays from self-assembled block copolymer nanotemplates," *Advanced Materials*, vol. 20, no. 13, pp. 2480–2485, 2008.

[18] A. Javey and H. Dai, "Regular arrays of 2 nm metal nanoparticles for deterministic synthesis of nanomaterials," *Journal of the American Chemical Society*, vol. 127, no. 34, pp. 11942–11943, 2005.

[19] Y. Li, W. Kim, Y. Zhang, M. Rolandi, D. Wang, and H. Dai, "Growth of single-walled carbon nanotubes from discrete catalytic nanoparticles of various sizes," *Journal of Physical Chemistry B*, vol. 105, no. 46, pp. 11424–11431, 2001.

[20] C. L. Cheung, A. Kurtz, H. Park, and C. M. Lieber, "Diameter-controlled synthesis of carbon nanotubes," *Journal of Physical Chemistry B*, vol. 106, no. 10, pp. 2429–2433, 2002.

[21] L. An, J. M. Owens, L. E. McNeil, and J. Liu, "Synthesis of nearly uniform single-walled carbon nanotubes using identical metal-containing molecular nanoclusters as catalysts," *Journal of the American Chemical Society*, vol. 124, no. 46, pp. 13688–13689, 2002.

[22] J. Q. Lu, T. E. Kopley, N. Moll et al., "High-quality single-walled carbon nanotubes with small diameter, controlled density, and ordered locations using a polyferrocenylsilane block copolymer catalyst precursor," *Chemistry of Materials*, vol. 17, no. 9, pp. 2227–2231, 2005.

[23] J. Lu, S. S. Yi, T. Kopley, C. Qian, J. Liu, and E. Gulari, "Fabrication of ordered catalytically active nanoparticles derived from block copolymer micelle templates for controllable synthesis of single-walled carbon nanotubes," *Journal of Physical Chemistry B*, vol. 110, no. 13, pp. 6655–6660, 2006.

[24] S. Lastella, Y. J. Jung, H. Yang et al., "Density control of single-walled carbon nanotubes using patterned iron nanoparticle catalysts derived from phase-separated thin films of a polyferrocene block copolymer," *Journal of Materials Chemistry*, vol. 14, no. 12, pp. 1791–1794, 2004.

[25] K. Temple, K. Kulbaba, K. N. Power-Billard et al., "Spontaneous vertical ordering and pyrolytic formation of nanoscopic ceramic patterns from poly(styrene-b-ferrocenylsilane)," *Advanced Materials*, vol. 15, no. 4, pp. 297–300, 2003.

[26] C. Hinderling, Y. Keles, T. Stöckli et al., "Organometallic block copolymers as catalyst precursors for templated carbon nanotube growth," *Advanced Materials*, vol. 16, no. 11, pp. 876–879, 2004.

[27] J. Q. Lu, D. A. Rider, E. Onyegam et al., "Carbon nanotubes with small and tunable diameters from poly(ferrocenylsilane)-*block*-Polysiloxane diblock copolymers," *Langmuir*, vol. 22, no. 11, pp. 5174–5179, 2006.

[28] T. Hirai, M. Leolukman, C. C. Liu et al., "One-step direct-patterning template utilizing self-assembly of POSS-containing block copolymers," *Advanced Materials*, vol. 21, no. 43, pp. 4334–4338, 2009.

[29] T. Hirai, M. Leolukman, S. Jin et al., "Hierarchical self-assembled structures from POSS-containing block copolymers synthesized by living anionic polymerization," *Macromolecules*, vol. 42, no. 22, pp. 8835–8843, 2009.

[30] Y. Ishida, Y. Tada, T. Hirai et al., "Directed self-assembly of cage silsesquioxane containing block copolymers via graphoepitaxy techniques," *Journal of Photopolymer Science and Technology*, vol. 23, no. 2, pp. 155–159, 2010.

[31] Y. Ishida, T. Hirai, R. Goseki, M. Tokita, M. Kakimoto, and T. Hayakawa, "Synthesis and self-assembly of thermotropic block copolymer with long alkyl tethered cage silsesquioxane in the side chain," *Journal of Polymer Science A*, vol. 49, no. 12, pp. 2653–2664, 2011.

[32] R. Goseki, T. Hirai, Y. Ishida, M. Kakimoto, and T. Hayakawa, "Rapid and reversible morphology control in thin films of poly(ethylene oxide)-*block*-POSS containing poly(methacrylate)," *Polymer Journal*, vol. 44, pp. 658–664, 2012.

[33] Y. Tada, H. Yoshida, Y. Ishida et al., "Directed self-assembly of POSS containing block copolymer on lithographically defined chemical template with morphology control by solvent vapor," *Macromolecules*, vol. 45, no. 1, pp. 292–304, 2012.

[34] C. U. Pittman, "Anionic homopolymerization of ferrocenylmethyl methacrylate," *Journal of Polymer Science Part A*, vol. 15, no. 7, pp. 1677–1686, 1977.

[35] T. Higashihara and R. Faust, "Synthesis of novel block copolymers comprised of polyisobutylene and poly(vinylferrocene) segments," *Macromolecules*, vol. 40, no. 21, pp. 7453–7463, 2007.

[36] F. Yan, T. Higashihara, R. Mosurkal et al., "Self organization and redox behavior of poly(vinylferrocene)-*block*-poly (isobutylene)-*block*-poly(vinylferrocene) triblock copolymer," *Journal of Macromolecular Science A*, vol. 45, no. 11, pp. 911–914, 2008.

[37] Y. Yang, Z. Xie, and C. Wu, "Novel synthesis and characterization of side-chain ferrocene-containing polymers," *Macromolecules*, vol. 35, no. 9, pp. 3426–3432, 2002.

[38] M. Gallei, B. V. K. J. Schmidt, R. Klein, and M. Rehahn, "Defined poly[styrene-*block*-(ferrocenylmethyl methacrylate)] diblock copolymers via living anionic polymerization," *Macromolecular Rapid Communications*, vol. 30, no. 17, pp. 1463–1469, 2009.

[39] M. Gallei, S. Tockner, R. Klein, and M. Rehahn, "Silacydobutane-based diblock copolymers with vinylferrocene, ferrocenylmethyl methacrylate, and [1]dimethylsilaferrocenophane," *Macromolecular Rapid Communications*, vol. 31, no. 9-10, pp. 889–896, 2010.

[40] J. K. Lindsay and C. R. Hauser, "Aminomethylation of ferrocene to form N,N-dimethylaminomethylferrocene and its conversion to the corresponding alcohol and aldehyde," *Journal of Organic Chemistry*, vol. 22, no. 4, pp. 355–358, 1957.

Hindawi Publishing Corporation
International Journal of Polymer Science
Volume 2012, Article ID 484523, 10 pages
doi:10.1155/2012/484523

Review Article

Synthesis of a Novel Family of Polysilsesquioxanes Having Oligothiophenes with Well-Defined Structures

Ichiro Imae, Shotaro Takayama, Daisuke Tokita, Yousuke Ooyama, Kenji Komaguchi, Joji Ohshita, and Yutaka Harima

Department of Applied Chemistry, Graduate School of Engineering, Hiroshima University, 1-4-1 Kagamiyama, Hiroshima, Higashi-Hiroshima 739-8527, Japan

Correspondence should be addressed to Ichiro Imae, imae@hiroshima-u.ac.jp

Received 12 June 2012; Accepted 21 October 2012

Academic Editor: Kimihiro Matsukawa

Our recent results on the synthesis and properties of a novel family of polysilsesquioxanes having oligothiophenes were reviewed. The polymers anchored on SiO_2 or ITO substrates showed excellent mechanical hardness due to the formation of a three-dimensional siloxane network structure and chemical linkage between polymer and the surface of metal-oxide substrates. Optical, electrochemical, and electrical properties of polymers were also investigated.

1. Introduction

Organic-inorganic hybrid materials have been opening a new field of materials science because of a wide range of possible applications. Among a variety of organic-inorganic hybrid materials, hybrid materials based on a siloxane network are very attractive due to the robust nature of the siloxane bond [1, 2] and thus are studied intensively. From the viewpoints of synthetic approach and the resulting materials structure, the siloxane-based hybrid materials can be divided into two classes [3]. Class I corresponds to nanocomposite materials, which are synthesized by an inorganic hydrolytic polycondensation (sol-gel reaction) of tetraalkoxysilane monomer in the presence of low molecular weight organic compounds as dopants. In this class of hybrid materials, the organic dopants are just embedded in the inorganic matrix and are likely to be isolated due to phase separation. Class II corresponds to nanostructured hybrid materials prepared from a sol-gel reaction of trialkoxysilane-based precursor monomers having organic substituents in the molecular chains. The resulting network polymers are called polysilsesquioxanes (PSQs), where the organic substituents bound covalently to the siloxane network are fixed strongly and homogeneously in the polymer bulk. When the sol-gel reaction occurs on the surface of glass or ITO, terminal silanol groups of PSQs react with hydroxy groups of the metal-oxide surface (Scheme 1), so that the organic functional groups can be fixed on the metal-oxide substrates through the siloxane network in PSQs. PSQs have been used as novel high-performance materials such as water-repellent agents for automobiles, catalyst supports, adsorbents, optics, and biosensors [4–8].

Recently, we introduced oligothiophenes in PSQ for applying PSQs to transparent and conductive films with tunable electrical properties. Oligothiophenes are well studied as photo- and electroactive materials and their electrical conductivities can be changed by chemical or electrochemical oxidation (p-doping) [9–11]. In addition, conductive and energetic properties of oligothiophenes can be controlled by changing a π-conjugation length or by introducing electron donating or withdrawing groups on the π-conjugated chains.

In this paper, synthesis of a novel family of polysilsesquioxanes having oligothiophenes (Figure 1) and their electrochemical, optical, electrical, and mechanical properties are described [12–15].

2. Synthesis of Triethoxysilane Monomers

2.1. Direct Silylation. We firstly succeeded in the introduction of silyl groups to sexithiophene [13] and octithiophene

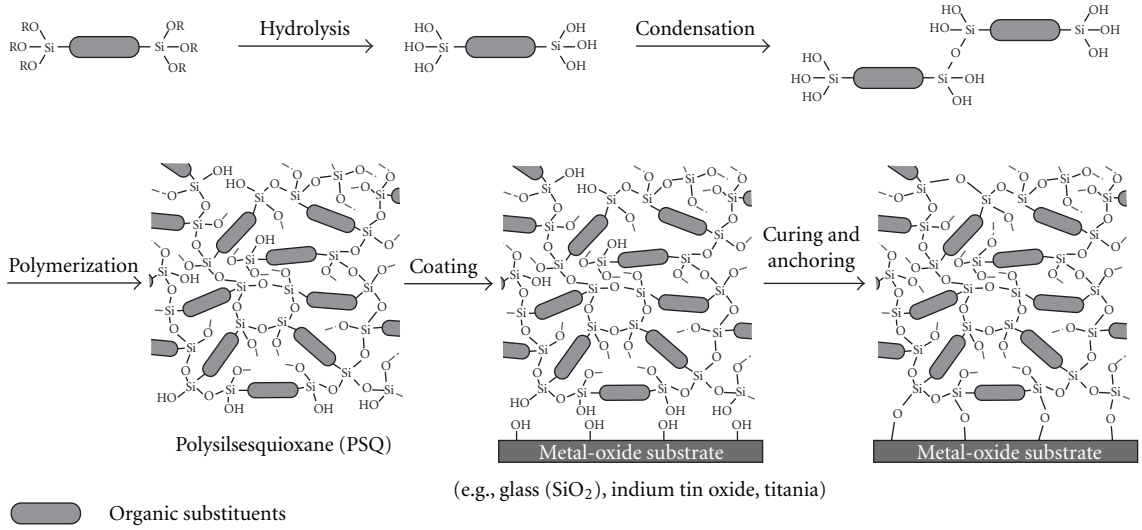

Scheme 1: Sol-gel reactions of trialkoxysilane monomer and coating of PSQs on metal-oxide substrates.

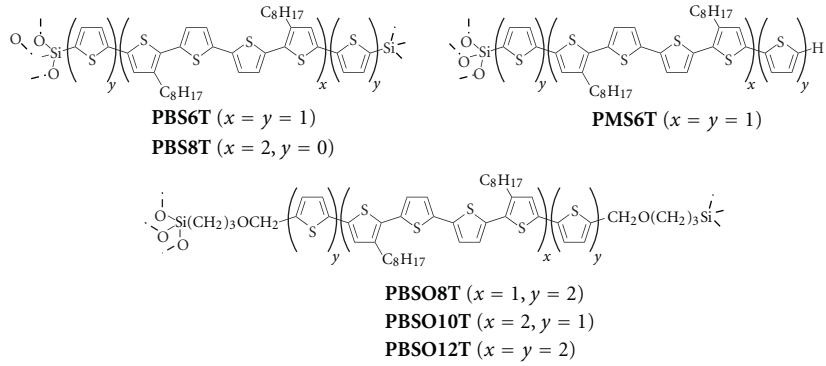

Figure 1: Chemical structures of PSQs having oligothiophenes.

[12–14] using a coupling reaction between triethoxychlorosilane and lithiated oligothiophenes obtained by the reaction of oligothiophenes and *n*-butyllithium (Scheme 2). The crude products mainly contained **BS*n*T** ($n = 6$ and 8) and they could be purified by preparative GPC. Small amount of mono(triethoxysilyl)-substituted oligothiophenes (**MS*n*T**) was isolated as a major byproduct.

2.2. Indirect Silylation. We tried also to synthesize bis(triethoxysilyl)-substituted deca- and dodecathiophene in the same manner as shown in Scheme 2. However, the reactivity of these oligothiophenes with *n*-butyllithium was low, and the lithiation reaction did not proceed at −78°C. Although the reaction was made at room temperature to increase the reactivity, the selectivity of lithiation became low, and bulky triethoxysilyl groups were introduced not only at α-positions but also at β-position of thienylene units. The formation of multisilylated oligothiophenes is unfavorable for developing electrically highly conductive materials because the steric hindrances may reduce effective π-conjugation lengths of oligothiophenes.

We have designed a new synthetic pathway, as shown in Scheme 3, in order to introduce triethoxysilyl groups only at α-positions of both terminal thienyl groups of oligothiophenes [15]. Although Scheme 3 consists of much more reaction steps than Scheme 2, we have found that silyl groups could be surely introduced only at the α-position of terminal thienyl groups, and reaction steps included in this route proceed with reasonable yields.

3. Polymerization of Monomers and Anchoring of Polymers

Polycondensation process of monomers monitored by GPC is shown in Figure 2. When a dilute hydrochloric acid (0.1 M) as a polymerization catalyst was added into the THF solution of monomers, the molecular weight of the formed polymers started to increase soon after the addition of the acid catalyst and leveled off at 6 hr, although the reaction solution remained homogenous. However, once the solvent was removed from the polymer solution, orange or reddish-orange solids which were insoluble in common organic

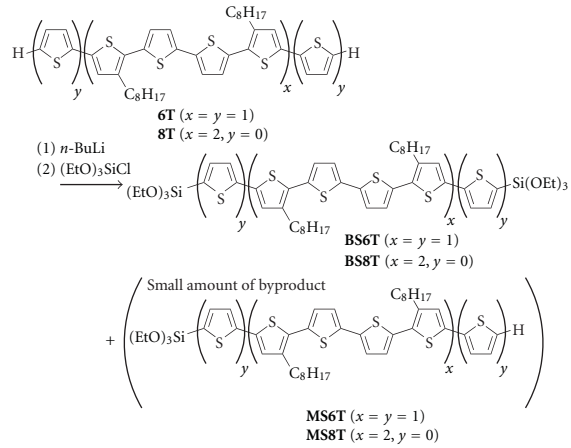

Scheme 2: Synthesis of **BS*n*T** and **MS*n*T** ($n = 6$ and 8).

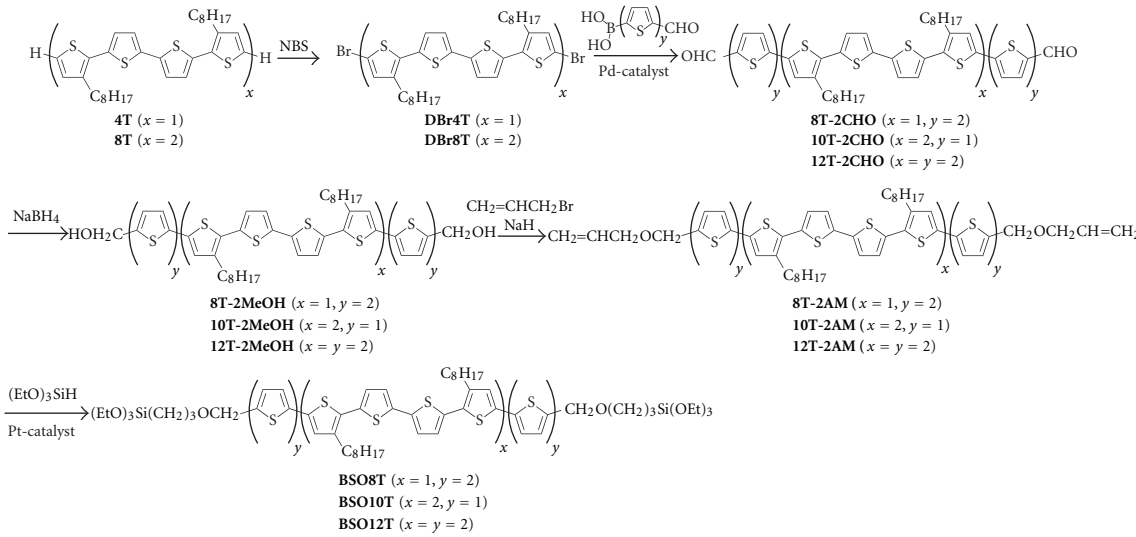

Scheme 3: Synthesis of **BSO*n*T** ($n = 8$, 10, and 12).

solvents were obtained. The FT-IR spectra of polymers showed a broad and strong peak at 1000–1200 cm^{-1} due to an Si–O–Si stretching vibration, which was not observed in the FT-IR spectra of monomers. These findings suggest, first, that the polymerization proceeds by the sol-gel reaction of the triethoxysilyl group to form a siloxane-bond network and, second, that the polymers in THF still have active sites which can react partly with hydroxyl groups on the surface of glass or ITO substrate, leading to the formation of insoluble polymer films fixed covalently on the substrate. The insoluble nature of polymer films is of a great use for the fabrication of multilayered molecular devices by a wet process. PSQs obtained from the polymerization reaction are named hereafter as **PBS*n*T** ($n = 6$ and 8), **PMS6T**, and **PBSO*n*T** ($n = 8$, 10 and 12) (Figure 1).

To confirm the role of the PSQ network, the polymer film in class I was prepared by the sol-gel method using a mixture of tetraethoxysilane (TEOS) and octithiophene (**8T**), and the morphology of the class I film was compared with that of **PBS8T** (class II film). In the class I film, the sea-and-island morphology was observed due to the phase separation between **8T** (island) and SiO_2 from TEOS (sea) (Figure 3(b)). The phase separation is not favorable for electrical conduction because a conducting pathway will be segmented due to the isolation of conductive oligothiophene phases in the insulating SiO_2 matrix. It was also found that **8T** was removed readily by dipping the sol-gel film into acetone, showing that the **8T** molecules were just embedded in SiO_2 matrix without forming covalent bonds. In contrast, the **PBS8T** film was very smooth and homogeneous (Figure 3(a)) and was insoluble in common organic solvents.

4. Electrochemical Properties

Stability of the polymer films was examined by cyclic voltammetry (CV) in tetraethylammonium perchlorate (TEAP)

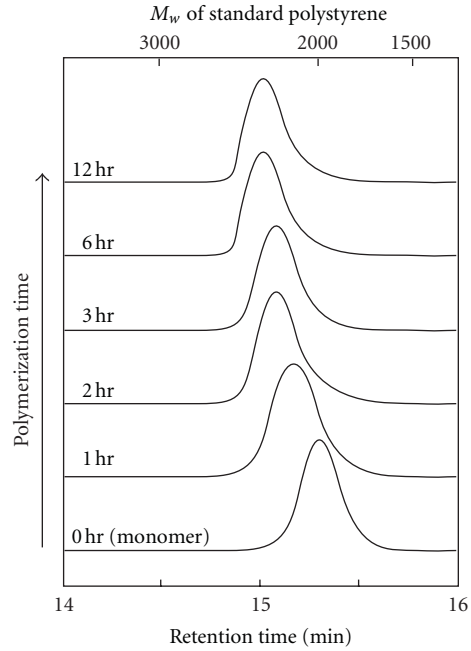

Figure 2: GPC curves of reaction solutions during polymerization of **BS8T**.

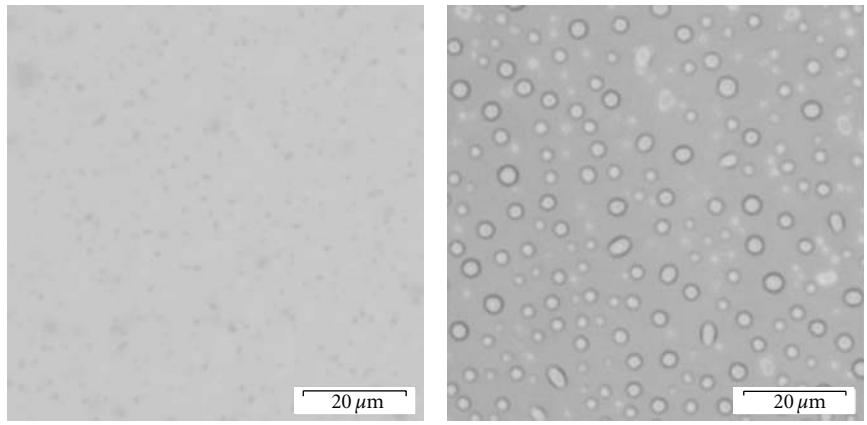

Figure 3: Optical microscope images of (a) **PBS8T** film and (b) film obtained from TEOS and **8T**.

(0.1 M)/acetonitrile (Figure 4). The **PBS8T** film exhibited broad oxidation peaks at 0.6 and 0.8 V versus Ag/Ag^+, while two oxidation peaks were observed at 0.5 and 0.7 V for the **PBSO8T** film. Four alkyl groups are introduced in octithiophene moiety in **PBS8T**, compared with two alkyl groups for **PBSO8T**. By this difference, π-conjugation length of octithienylene units in **PBSO8T** will be well expanded because of less stertic hindrance, which may cause the negative shift of the oxidation potential relative to those of **PBS8T**. **PBSO10T** also showed two oxidation peaks centered at 0.3 and 0.6 V, but **PBSO12T** showed a broad oxidation peak in the potential range from 0.2 to 0.7 V.

Although **PBS6T** showed an irreversible CV curve and its current density gradually decreased by the repeated potential cycling, other PSQ films (**PBS8T** and **PBSO*n*T**) showed broad but reversible redox waves, suggesting the electrochemical stability of oligothiophenes longer than hexamer. Corriu et al. reported the synthesis and electrochemical properties of PSQs having oligothiophenes with short π-conjugation units (monomer to trimer) [16]. In their report, when the polymers were chemically or electrochemically oxidized, oligothiophene moieties were eliminated and polymerized due to the poor stability of the oxidized species. In contrast to their results, **PBS8T** and **PBSO*n*T** showed a good electrochemical stability due to delocalization of charges formed on the well expanded π-conjugation unit and a good adhesion of the polymer to the ITO substrate.

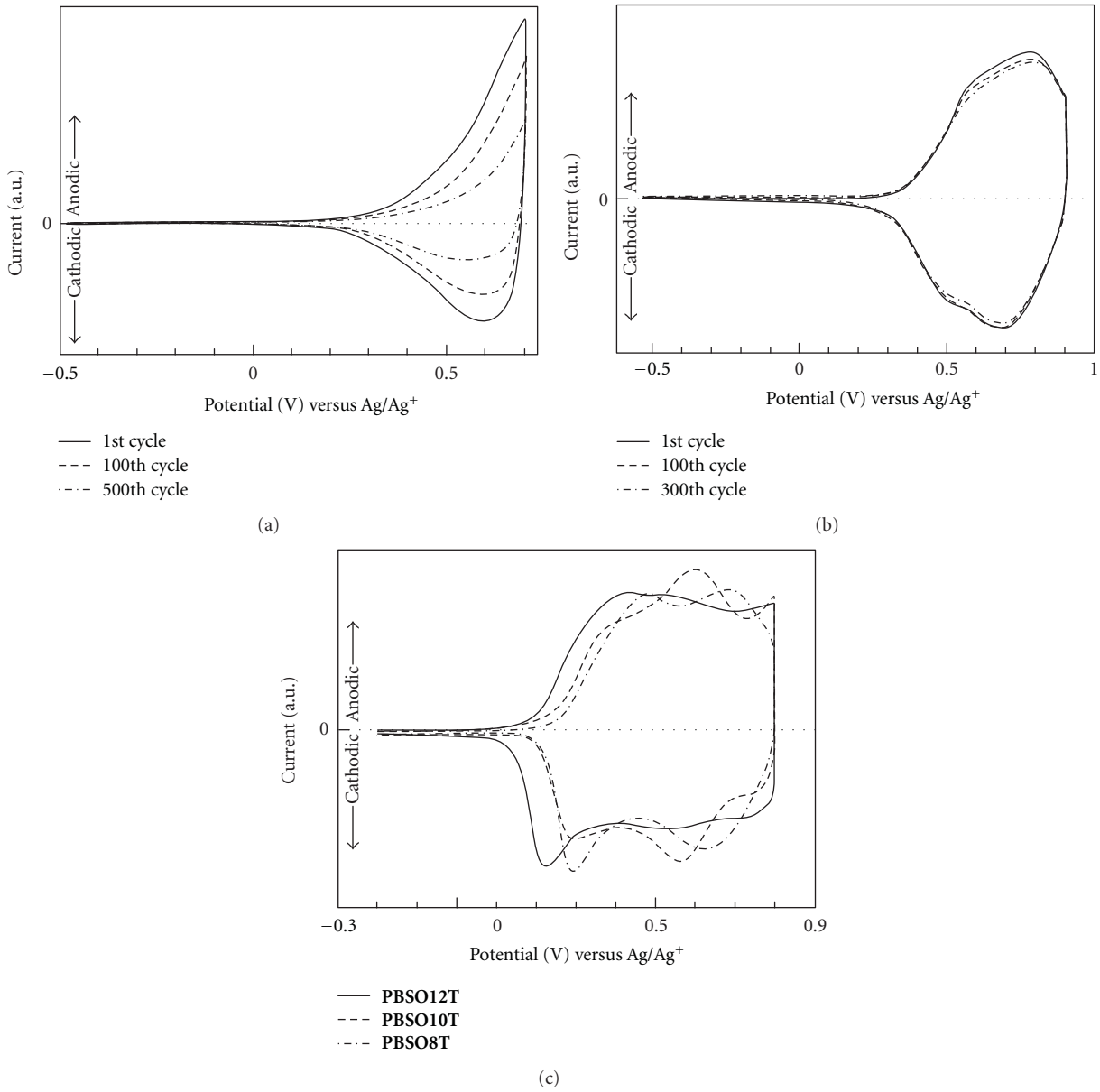

Figure 4: Cyclic voltammograms of (a) **PBS6T**, (b) **PBS8T**, and (c) **PBSO*n*T** (n = 8, 10, and 12) films in TEAP (0.1 M)/acetonitrile at a scan rate of 50 mV s^{-1}.

5. Spectroelectrochemistry

Absorption spectra of PSQ films biased at different potentials were measured in TEAP (0.1 M)/acetonitrile to identify chemical species to be formed at different oxidation states of PSQs (Figure 5, Table 1). As shown in the inset of Figure 5, the neutral **PBS8T** film showed a single absorption band at 445 nm due to π-π^* transition of a neutral octithiophene moiety. When the **PBS8T** film was oxidized at 0.6 V, the intensity of the 445-nm band decreased, and instead two absorption bands appeared at 749 and 1204 nm, which were ascribed to the one-electron oxidized species (monocation radical or π-dimer) of octithienylene unit. The **PBS8T** film oxidized at 0.9 V was almost colorless and showed a single broad band at 970 nm, being ascribed to the two-electron oxidized species (dication) of octithienylene unit. Similar results were obtained with **PBSO8T**. The π-π^* absorption bands in the neutral **PBSO10T** and **PBSO12T** were red-shifted relative to those of **PBS8T** and **PBSO8T**, reflecting that the effective π-conjugation length of deca- and dodecathiophene is longer than that of octithiophene. Furthermore, the absorption bands of their oxidized species in the polymers were also red-shifted with increasing the number of thiophene rings. In all cases except **PBS6T**, polymer films could be one- and two-electron oxidized in the potential range from 0 to 0.9 V versus Ag/Ag^+.

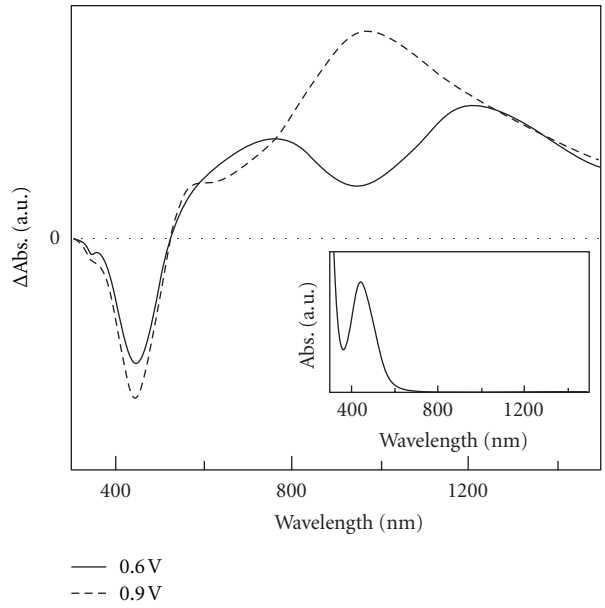

Figure 5: Difference absorption spectra of **PBS8T** film at 0.6 and 0.9 V referred to spectrum of neutral **PBS8T** film. The inset shows absorption spectrum of neutral **PBS8T** film.

Table 1: Absorption maxima of neutral and oxidized polymers.

Polymers	Wavelength/nm		
	Neutral state	One-electron oxidized state[a]	Two-electron oxidized state[b]
PBS6T	435	—[c]	—[c]
PBS8T	445	749, 1204	970
PBSO8T	447	697, 1211	1099
PBSO10T	482	708, 1335	1252
PBSO12T	486	752, 1405	1247

[a]Oxidized at 0.6 V for **PBS8T**, at 0.5 V for **PBSO8T**, and at 0.4 V for **PBSO10T** and **PBSO12T**.
[b]Oxidized at 0.9 V for **PBS8T** and at 0.8 V for **PBSO*n*T**.
[c]Not observed.

6. Electrical Properties

Doping levels and electrical conductivities were measured by using an *in situ* electrochemical technique (Figure 6). In concert with the electrochemical oxidation process of the **PBS8T** film (Figure 4), the doping level gradually increased and finally reached around 25% at 0.9 V, which corresponds to 200% doping per octithienylene unit and suggests that all octithienylene units are completely two-electron oxidized at 0.9 V. The plot of log(doping level) versus potential fits a straight line in a low doping region, and the inverse of its slope value is around 100 mV/decade, which is larger than 60 mV/decade for a common one-electron transfer process at room temperature. We have already revealed that the slope value is a measure of distribution of effective π-conjugation lengths in conjugated oligomers and polymers [17–19]. In the **PBS8T** film, since both terminal thiophene rings of octithienylene unit are tightly fixed with silsesquioxane network, their conformation is partially restricted not to spread the π-conjugation all over the oligothienylene unit (*vide infra*). The electrical conductivity also increased with increasing the electrode potential from 0.3 to 0.7 V, showed a maximum value of 5.6×10^{-3} S cm^{-1}, and then decreased to 3.0×10^{-3} S cm^{-1} at 0.9 V (Figure 6(b)).

The doping levels and electrical conductivities of **PBSO*n*T** (n = 8, 10, and 12) changed with the electrode potential similarly to those of **PBS8T**. The electrical conductivities of **PBSO*n*T** increased with the increase in the chain length of oligothienylene units in PSQs.

To get an insight into charge transport properties of the polymer films, apparent mobilities of charge carriers were estimated by combining doping level and conductivity data. The mobilities are plotted in Figure 7 as a function of doping level. In all cases, the mobilities at the low doping level below 1% are 1-2 $\times$ 10^{-6} cm^2 V^{-1} s^{-1}, which can be explained by the interchain hopping transport of monocation radicals (polarons). The mobility plots showed maxima at doping levels of 10%–15%, in which one- and two-electron oxidized states coexist. When the doping level was increased beyond 20%, the mobilities of **PBS8T** and **PBSO8T** greatly decreased, while the mobilities of

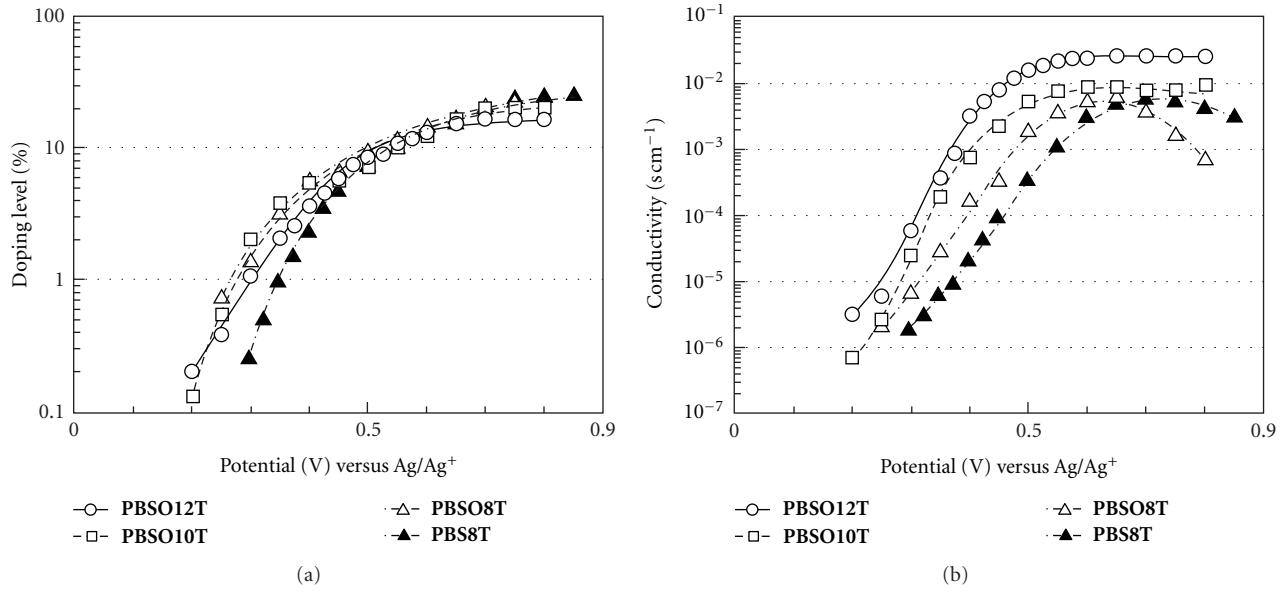

Figure 6: (a) Doping levels and (b) electrical conductivities plotted against electrode potential for ▲: **PBS8T**, Δ: **PBSO8T**, □: **PBSO10T**, and ◯: **PBSO12T** films.

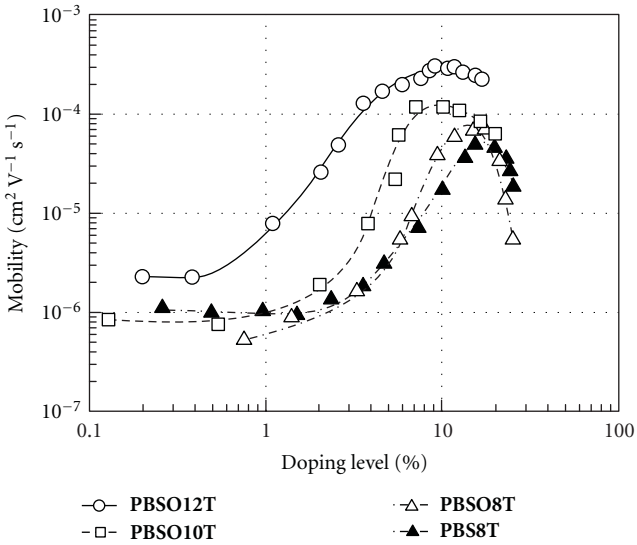

Figure 7: Apparent mobilities of charge carriers plotted against doping level for ▲: **PBS8T**, Δ: **PBSO8T**, □: **PBSO10T**, and ◯: **PBSO12T** films.

PBSO10T and **PBSO12T** did not decrease considerably. A plausible reason for this difference may be explained by the length of oligothienylene unit in the polymer; almost all oligothienylene units are two electrons oxidized at a doping level of 20%, so that it becomes difficult for the positive charges to move among the oligothienylene units because of a Coulombic repulsion. However, the degree of the Coulombic repulsion will become smaller when the chain length of oligothienylene unit is longer. Thus, the degree of decrease of the mobilities becomes smaller with the increase of the number of thiophene rings.

7. Effect of Silsesquioxane Network

The mechanical hardness of the PSQ films was measured by a pencil hardness test according to the ASTM Standard D 3363-92 [20] and the results are summarized in Table 2. For the comparison, monomer films were prepared on glass or ITO substrate by spin-coating of a BSOnT solution of THF containing no polymerization catalyst [15]. The **PBSO12T** film did not show any damages by being scratched with 4H pencil, while the **BSO12T** film showed some damages even by B pencil. Similar results were obtained with other PSQ films. In the cases of PEDOT-PSS and common polymer films such as poly(styrene) (PSt) and poly(methyl methacrylate) (PMMA), appreciable damages were caused even by soft pencils (2B for PEDOT-PSS and PSt, 2H for PMMA). These results demonstrate clearly that the mechanical hardness of the PSQ films is much higher than those of trialkoxysilane monomers and other type of polymers having no chemical linkage with substrates, indicative of a hard network structure of silsesquioxane polymers and adhesion to metal oxides.

Figure 8 shows the absorption spectra of **BSO12T** and **PBSO12T** films in the neutral states. While the **PBSO12T** film exhibits a broad structureless spectrum with λ_{max} = 486 nm, the spectrum of the **BSO12T** film displays a vibronic fine structure. Also, the absorption tail of **BSO12T** is redshifted by about 15 nm relative to that of **PBSO12T**. This redshift suggests the expansion of the effective π-conjugation length of the oligothienylene unit in **BSO12T**, where the oligothiophene units are not restricted by the siloxane network.

Table 2: Results of pencil hardness test for **PBSO12T**, **BSO12T**, PMMA, PSt, and PEDOT-PSS.

Hardness of pencils		**PBSO12T**	**BSO12T**	PMMA	PSt	PEDOT-PSS
(Hard)	6H	Damaged	Damaged	Damaged	Damaged	Damaged
	5H					
	4H	Not damaged				
	3H					
	2H					
	H					
	F					
	HB					
	B					
	2B		Not damaged	Not damaged	Not damaged	Not damaged
	3B					
	4B					
	5B					
(Soft)	6B					

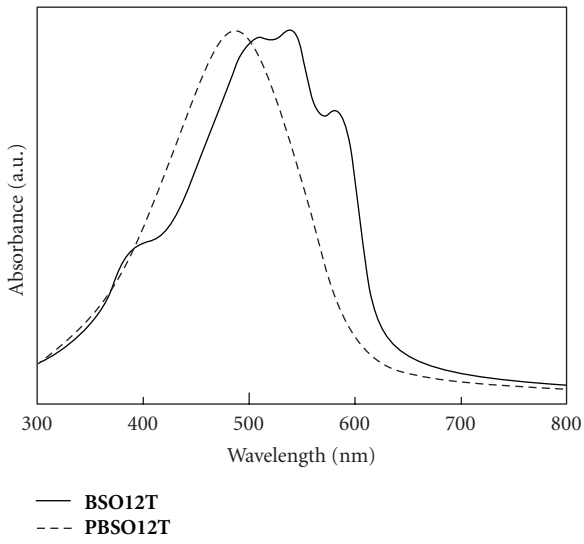

Figure 8: Absorption spectra of neutral **BSO12T** and **PBSO12T** films.

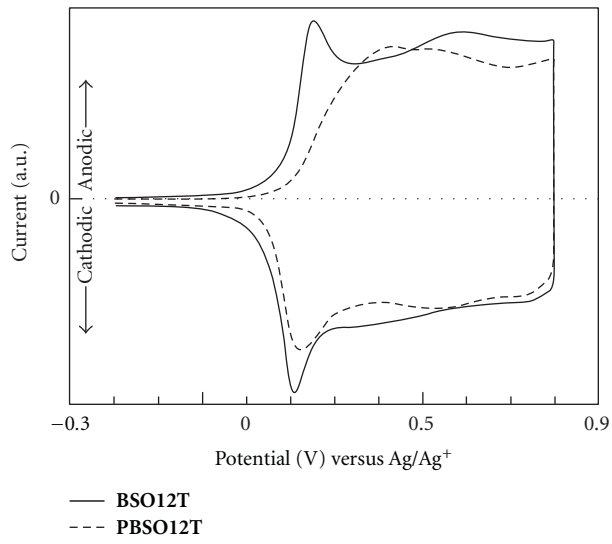

Figure 9: Cyclic voltammograms of **BSO12T** and **PBSO12T** films in TEAP (0.1 M)/acetonitrile at a scan rate of 50 mV s^{-1}.

A clear difference was seen also in cyclic voltammograms of **BSO12T** and **PBSO12T** films in TEAP (0.1 M)/acetonitrile (Figure 9). The cyclic voltammogram of the **BSO12T** film shows a sharp oxidation peak at 0.25 V versus Ag/Ag^+, compared with a broad oxidation peak for the **PBSO12T** film. The difference in shape of the cyclic voltammograms is reflected in the plots of log(doping level) versus potential shown in Figure 10. The inverse of the slope value of the plot in the low potential region is around 130 mV/decade for the **PBSO12T**, much greater than 80 mV/decade for the **BSO12T**. The value of 80 mV/decade for the **BSO12T** monomer film is slightly greater than the theoretical value of 60 mV/decade for a common one-electron transfer process at room temperature, suggesting that the effective π-conjugation length of oligothienylene unit is somewhat distributed [18]. From the difference in the slope value, one can conclude that the effective π-conjugation length in the **PBSO12T** polymer film is distributed much wider than that in the **BSO12T** monomer film. It is likely that this may be caused by the rigid nature of the siloxane network.

Since we obtained a mono(triethoxysilyl)-substituted monomer, **MS6T**, as a byproduct by chance during the synthesis of **BS6T**, we attempted the polymerization of **MS6T** to obtain **PMS6T** (the chemical structure is shown in Figure 1), where one terminal of sexithiophene moiety is linked to silsesquioxane polymer. Compared with **PBS6T**, the cyclic voltammogram of **PMS6T** showed a clear redox wave (Figure 11), suggesting the higher flexibility of sexithienylene unit in the polymer film. This finding also supports the rigid siloxane network of PSQs.

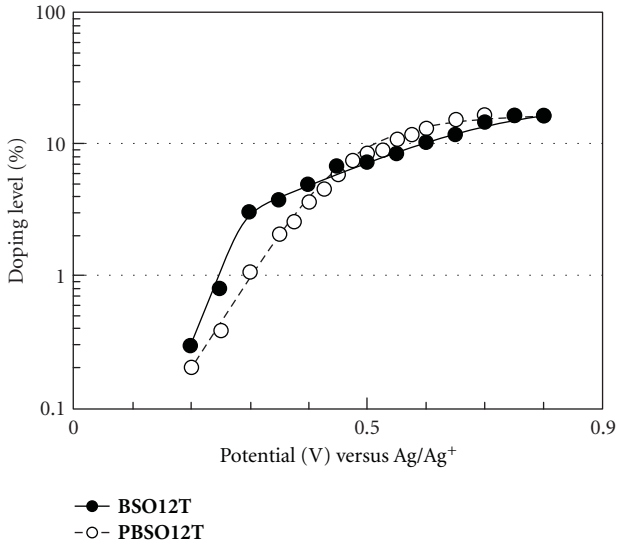

Figure 10: Doping levels plotted against electrode potential for ●: **BSO12T** and ◯: **PBSO12T** films.

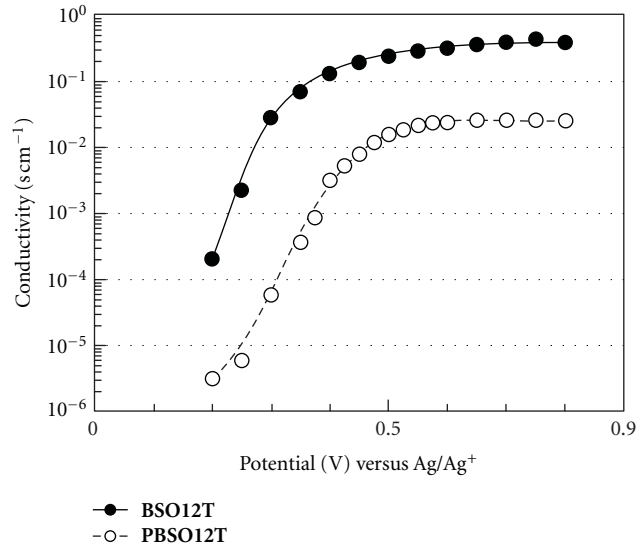

Figure 12: *In situ* electrical conductivities plotted against electrode potential for ●: **BSO12T** and ◯: **PBSO12T** films.

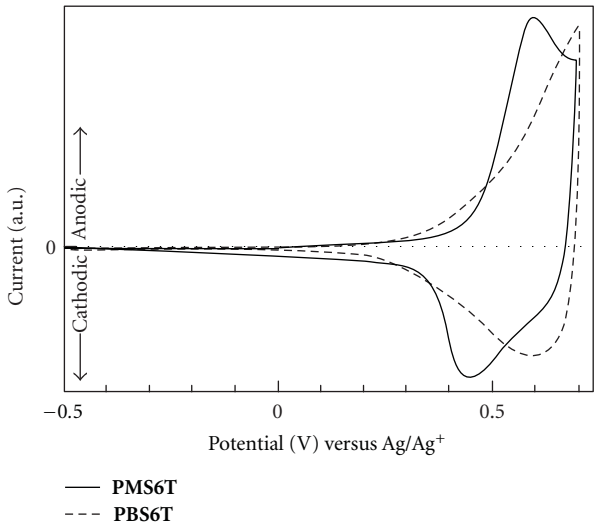

Figure 11: Cyclic voltammograms of **PMS6T** and **PBS6T** films in TEAP (0.1 M)/acetonitrile at a scan rate of 50 mV s^{-1}.

It was found that the maximum conductivity of **BSO12T** was 4.0×10^{-1} S cm^{-1}, which was by one order of magnitude greater than that of **PBSO12T** (Figure 12). There may be two plausible reasons for the difference in conductivity between **BSO12T** and **PBSO12T**. The first reason originates from the positional disorder. Silsesquioxane polymer may be amorphous, so that the position of oligothiophenes in the polymer is disordered. Thus, the pathway of the charge transport will become much longer than the case for the monomer film. The second reason arises from the energetic disorder. As mentioned above, the conformation is partially restricted not to spread the π-conjugation all over the oligothienylene unit. Thus, oligothienylene units with different effective π-conjugation length coexist in the polymer, which means that some of oligothienylene site will act as trapping sites for the charge transport.

A study on the modification on polymerization conditions and polymer structures is currently under way to enhance the effective π-conjugation length, leading to higher conductivities, by controlling the flexibility of the silsesquioxane network. For example, we have found that 3,4-ethylenedioxythiophene (EDOT) unit can enhance the π-conjugation length, and an EDOT-containing polymer showed an excellent electrical conductivity [21]. So, EDOT-containing oligothiophenes will become good candidates as oligothienylene units in PSQs.

8. Summary

Synthesis and physicochemical properties of polysilsesquioxanes incorporating oligothiophenes were reviewed. We found that with increasing the chain length of oligothienylene units in the polymers, Coulombic repulsion between oxidized polymer chains became smaller, the absorption bands of neutral and oxidized films showed red-shift, and the electrical conductivity and charge carrier mobility increased. The comparison with the monomer film revealed that the siloxane network enhanced the mechanical hardness of the polymer film, but its rigidity restricted a conformational change of oligothienylene units, leading to low conductivities of the PSQ films.

Acknowledgments

This work was supported in part by a Grant-in-Aid for scientific research from the Japan Society for the Promotion of Science (JSPS) (no. 22550198) and Adaptable and Seamless Technology Transfer Program through Target-Driven R&D (A-STEP) from the Japan Science and Technology Agency

(JST), the Furukawa Technology Promotion Foundation, and the Hitachi Metals-Materials Science Foundation.

References

[1] N. Auner and J. Weis, *Organosilicon Chemistry VI, from Molecules to Materials*, Wiley-VCH, Weinheim, Germany, 2005.

[2] S. J. Clarson, J. J. Fitzgerald, M. J. Owen, S. D. Smith, and M. E. Van Dyke, *Science and Technology of Silicones and Silicone-Modified Materials*, ACS Symposium Series 964, Oxford University Press, Washington, DC, USA, 2007.

[3] C. Sanchez and F. Ribot, "Design of hybrid organic-inorganic materials synthesized via sol-gel chemistry," *New Journal of Chemistry*, vol. 18, no. 10, pp. 1007–1047, 1994.

[4] K. J. Shea and D. A. Loy, "Bridged polysilsesquioxanes. Molecular-engineered hybrid organic−inorganic materials," *Chemistry of Materials*, vol. 13, no. 10, pp. 3306–3319, 2001.

[5] A. Walcarius, "Electrochemical applications of silica-based organic−inorganic hybrid materials," *Chemistry of Materials*, vol. 13, no. 10, pp. 3351–3372, 2001.

[6] R. Corriu, "Organosilicon chemistry and nanoscience," *Journal of Organometallic Chemistry*, vol. 686, no. 1-2, pp. 32–41, 2003.

[7] A. Walcarius, D. Mandler, J. A. Cox, M. Collinson, and O. Lev, "Exciting new directions in the intersection of functionalized sol-gel materials with electrochemistry," *Journal of Materials Chemistry*, vol. 15, no. 35-36, pp. 3663–3689, 2005.

[8] F. Lerouge, G. Cerveau, and R. J. P. Corriu, "Supramolecular self-organization in non-crystalline hybrid organic-inorganic nanomaterials induced by van der Waals interactions," *New Journal of Chemistry*, vol. 30, no. 10, pp. 1364–1376, 2006.

[9] D. Fichou, Ed., *Handbook of Oligo- and Polythiophenes*, Wiley-VCH, Weinheim, Germany, 1999.

[10] P. Bäuerle, "Oligothiophenes," in *Electronic Materials: the Oligomer Approach*, K. Müllen and G. Wegner, Eds., chapter 2, pp. 105–1197, Wiley-VCH, Weinheim, Germany, 1998.

[11] A. Mishra, C. Q. Ma, and P. Bäuerle, "Functional oligothiophenes: molecular design for multidimensional nanoarchitectures and their applications," *Chemical Reviews*, vol. 109, no. 3, pp. 1141–1276, 2009.

[12] I. Imae, S. Takayama, D. Tokita et al., "Development of anchored oligothiophenes on substrates for the application to the tunable transparent conductive films," *Polymer*, vol. 50, no. 26, pp. 6198–6201, 2009.

[13] Y. Harima, J. Ohshita, I. Imae, T. Sugioka, and K. Kanehira, "Electrically conductive laminates having organic compounds on surfaces and their manufacture, doped electrically conductive materials, and electrochromic materials," JP 2010266727 A 20101125, Japan Kokai Tokkyo Koho, 2010.

[14] I. Imae, D. Tokita, Y. Ooyama, K. Komaguchi, J. Ohshita, and Y. Harima, "Charge transport properties of polymer films comprising oligothiophene in silsesquioxane network," *Polymer Chemistry*, vol. 2, no. 4, pp. 868–872, 2011.

[15] I. Imae, D. Tokita, Y. Ooyama, K. Komaguchi, J. Ohshita, and Y. Harima, "Oligothiophenes incorporated in a polysilsesquioxane network: application to tunable transparent conductive films," *Journal of Materials Chemistry*, vol. 22, pp. 16407–16415, 2012.

[16] R. J. P. Corriu, J. J. E. Moreau, P. Thepot, and M. W. C. Man, "Trialkoxysilyl Mono-, Bi-, and terthiophenes as molecular precursors of hybrid organic-inorganic materials," *Chemistry of Materials*, vol. 6, no. 5, pp. 640–649, 1994.

[17] Y. Harima, Y. Kunugi, K. Yamashita, and M. Shiotani, "Determination of mobilities of charge carriers in electrochemically anion-doped polythiophene film," *Chemical Physics Letters*, vol. 317, no. 3–5, pp. 310–314, 2000.

[18] J. Yano, M. Kobayashi, S. Yamasaki, Y. Harima, and K. Yamashita, "Mean redox potentials of polyaniline determined by chronocoulometry," *Synthetic Metals*, vol. 119, no. 1–3, pp. 315–316, 2001.

[19] Y. Harima, T. Eguchi, and K. Yamashita, "Enhancement of carrier mobilities in poly(3-methylthiophene) by an electrochemical doping," *Synthetic Metals*, vol. 95, no. 1, pp. 69–74, 1998.

[20] The American Society for Testing and Materials (ASTM) D, 3363- 92, *Test Method for Film Hardness by Pencil Test*.

[21] I. Imae, S. Imabayashi, K. Korai et al., "Electrosynthesis and charge-transport properties of poly(3′,4′-ethylenedioxy-2,2′:5′,2′′-terthiophene)," *Materials Chemistry and Physics*, vol. 131, no. 5, pp. 752–756, 2012.

Hindawi Publishing Corporation
International Journal of Polymer Science
Volume 2012, Article ID 684278, 14 pages
doi:10.1155/2012/684278

Review Article

Preparation of Ionic Silsesquioxanes with Regular Structures and Their Hybridization

Yoshiro Kaneko,[1] Hisaya Toyodome,[1] Miki Shoiriki,[1] and Nobuo Iyi[2]

[1] *Graduate School of Science and Engineering, Kagoshima University, 1-21-40 Korimoto, Kagoshima 890-0065, Japan*
[2] *Functional Geomaterials Group, National Institute for Materials Science (NIMS), 1-1 Namiki, Tsukuba 305-0044, Japan*

Correspondence should be addressed to Yoshiro Kaneko, ykaneko@eng.kagoshima-u.ac.jp

Received 19 June 2012; Accepted 22 August 2012

Academic Editor: Maki Itoh

This paper deals with our recent studies on the preparation of ionic silsesquioxanes (SQs) with regular structures. Cationic ladder-like polySQs (PSQs) with hexagonally stacked structures were successfully prepared by the sol-gel reactions of amino group-containing organotrialkoxysilanes in strong acid aqueous solutions. Self-organization of an ion pair (a salt) prepared from the amino group in the organotrialkoxysilane and an acid is the key factor for the formation of such regular structures of the PSQs. It is also reported that the control of the conformational structure of the PSQs was performed by the introduction of the chiral moieties. In addition, we investigated the correlation between the pK_as of acid-catalysts and the structures of SQs prepared by the hydrolytic condensation of amino group-containing organotrialkoxysilane, that is, the use of the superacid aqueous solution resulted in the formation of cage-like octaSQ, while the ladder-like PSQs with hexagonally stacked structures were formed from the strong acid aqueous solutions under the same reaction conditions. Furthermore, anion-exchange behaviors of the cationic ladder-like PSQ were investigated with various organic and inorganic compounds, such as anionic surfactants, a polymer, and layered clay minerals, to obtain the functional hybrid materials.

1. Introduction

Silsesquioxanes (SQs), the materials containing the structure of $RSiO_{1.5}$, have attracted much attention in the research fields of organic-inorganic hybrid materials for academic and application reasons [1, 2] because they can contain the various functional groups as side-chains (R) and are inorganic materials indicating the remarkable compatibility with organic materials such as polymers [3–6], in addition to exhibiting superior thermal, mechanical, and chemical stabilities derived from siloxane (Si–O–Si) bond frameworks with high bond energy compared with C–C bonds.

However, even though various kinds of polyhedral oligomeric SQs (POSS) are known as SQs with controlled molecular structures (Scheme 1(a)) [7–12], the regularly structured polySQs (PSQs) have only been obtained in the limited cases. This is because PSQs are prepared by polycondensation of the trifunctional silane monomers such as organotrialkoxysilanes and organotrichlorosilanes. These multifunctional monomers generally result in the formation of insoluble polymers with irregular three-dimensional network structures of Si–O–Si bonds (Scheme 1(b)) [2]. If the structures of PSQs can be controlled, they are expected to be applicable for a wide range of materials research fields.

Ladder-structured PSQs are one of a few PSQs with controlled molecular structures (Scheme 1(c)) [13–17]. These structures are classified into two types: "perfect ladder structure" (Scheme 1(c-i)) and "ladder-like structure" (Scheme 1(c-ii)) [18]. The latter has slight defects in Si–O–Si bond main-chain. Even though oligomeric SQ with "perfect ladder structure" could be synthesized by a step-by-step method and its characterization methods were established [19], it is difficult to prepare PSQs with such structures and to characterize them. In most cases, the ladder-structured PSQs probably do not have "perfect ladder structure" but have "ladder-like structure" as shown in Scheme 1(c-ii).

The ladder-like PSQs exhibit rigidity and anisotropy in addition to the aforementioned superior physical properties

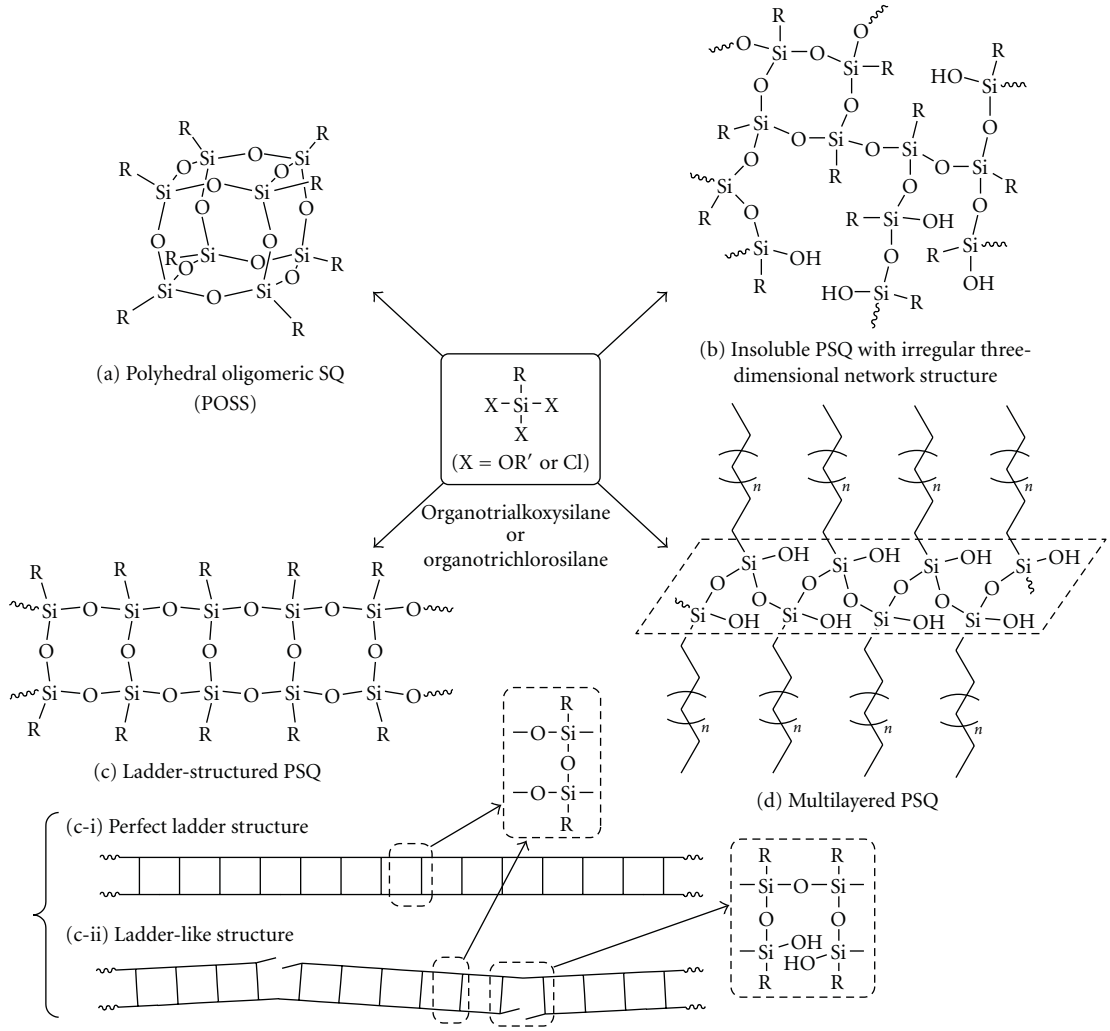

Scheme 1: Preparation of silsesquioxanes (SQs) with various structures.

of SQs because they have one-dimensional network structures of Si–O–Si bonds. Furthermore, ladder-like PSQs are colorless materials due to no absorptions of Si–O–Si bonds in the visible light region and can be used as transparent solutions owing to good solubility in any solvents. These properties of ladder-like PSQs would be useful for versatile applications, in particular, as inorganic compounds due to hybridization with organic functional materials.

Furthermore, the control of the higher-ordered structures (nanostructures) of PSQs would also be significant to apply to various supramolecular organic-inorganic hybrid materials. For example, it has been reported that trifunctional silane monomers containing long alkyl chains were hydrolyzed to form amphiphilic molecules having silanol groups, resulting in the formation of multilayered PSQs by polycondensation (Scheme 1(d)) [20, 21]. Another method for controlling higher-ordered structures of PSQs is sol-gel reaction (hydrolytic polycondensation) of 1,4-bis(trialkoxysilyl)benzene as a monomer in the presence of surfactants [22]. The resulting material has a hexagonal array of mesopores and crystal-like frameworks. Self-organization of long alkyl chains by hydrophobic interactions is a driving force to form such regular higher-ordered structures.

From the aforementioned background, it is evident that the development of PSQs with regularly controlled molecular and higher-ordered structures is one of the important issues for research fields of SQs. Therefore, the present paper reviews our recent researches on the preparation of ionic PSQs with regular structures. In the second part, we describe the preparation of cationic ladder-like PSQs with hexagonally stacked structures by sol-gel reaction of amino group-containing organotrialkoxysilane monomers and their detailed characterizations. In the third part, the introduction of the chiral moieties into the ladder-like PSQ is described to investigate the conformational structures of the resulting PSQs. In the fourth part, we report the correlation between the pK_a of acid-catalysts and the structures of cationic SQs prepared by hydrolytic condensation of an amino group-containing organotrialkoxysilane monomer. The fifth part deals with anion-exchange reactions of the

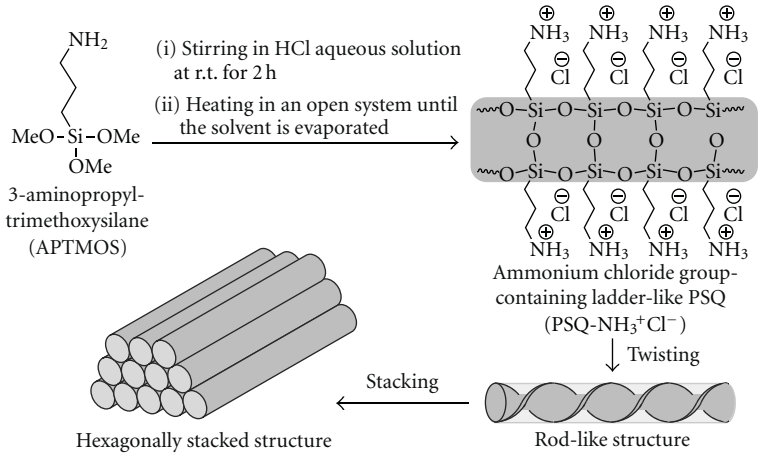

Scheme 2: Preparation of an ammonium chloride group-containing ladder-like PSQ (PSQ-$NH_3^+Cl^-$) with a hexagonally stacked structure by sol-gel method.

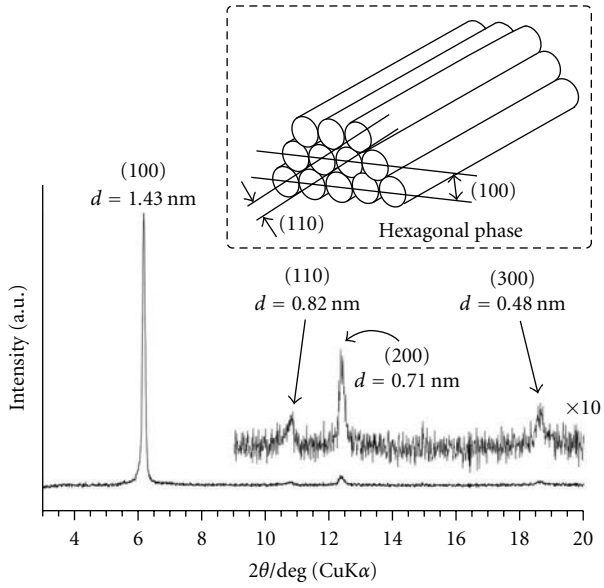

Figure 1: XRD pattern of PSQ-$NH_3^+Cl^-$. Relative humidity (RH) during XRD measurements was 50%.

cationic ladder-like PSQ with various organic and inorganic compounds, such as anionic surfactants, a polymer, and layered clay minerals, to obtain the functional hybrid materials.

2. Preparation of Ammonium Group-Containing Ladder-Like PSQs with Hexagonally Stacked Structures

We have developed the preparation method for ammonium group-containing PSQs with controlled molecular and higher-ordered structures by sol-gel reaction of organotrialkoxysilane monomers containing amino groups in aqueous inorganic acids [23–26].

2.1. Sol-Gel Reaction of 3-Aminopropyltrimethoxysilane. The first example of monomer to prepare the aforementioned PSQs was 3-aminopropyltrimethoxysilane (APTMOS) [23]. The sol-gel reaction of APTMOS was performed by stirring in an acid, for example, a hydrochloric acid (HCl), aqueous solution at room temperature for 2 h, followed by heating (*ca.* 50–60°C) in an open system until the solvent was completely evaporated (Scheme 2). The resulting product was dissolved in water, and this aqueous solution was lyophilized to obtain a water-soluble ammonium chloride group-containing PSQ (PSQ-$NH_3^+Cl^-$). Here, a feed molar ratio of HCl to APTMOS is a very important factor for the formation of the regular structures of the PSQ, that is, HCl/APTMOS ratio needs more than one. The higher-ordered structure of the product was mainly characterized by the X-ray diffraction (XRD) measurements, while the molecular structure was discussed using the results of ^{29}Si NMR, XRD, and static light-scattering (SLS) measurements.

The XRD pattern of the cast film prepared by drying PSQ-$NH_3^+Cl^-$ aqueous solution showed diffraction peaks with the *d*-value ratio of $1 : 1/\sqrt{3} : 1/2 : 1/3$, strongly indicating that PSQ-$NH_3^+Cl^-$ had a hexagonal phase (Figure 1). These peaks were assigned to the (100), (110), (200), and (300) peaks, respectively. However, based on only these data, it could not be determined whether this hexagonal phase originated from a porous-type structure or a stacking of rod-like polymers. Therefore, the influence of relative humidity (RH) was investigated on the *d*-value in the XRD measurements of PSQ-$NH_3^+Cl^-$. As shown in Figure 2, the diffraction peaks shifted by varying RH that is, the *d*-value increased for a high RH and decreased for a low RH although the *d*-value ratios of (110)/(100) and (200)/(100) did not change. Such a behavior cannot be expected for hexagonal-structured porous materials. Therefore, we assumed that this hexagonal phase originated from the stacking of rod-like polymers.

We next discuss the molecular structure of PSQ-$NH_3^+Cl^-$. The analysis method to prove ladder structure of oligoSQs has already been established [19]. Because

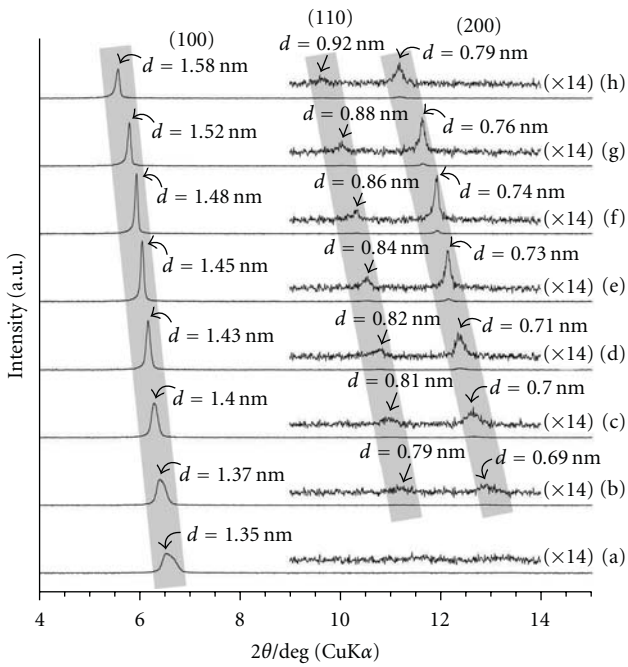

FIGURE 2: XRD patterns of PSQ-$NH_3^+Cl^-$ under various RH conditions: (a) 20, (b) 30, (c) 40, (d) 50, (e) 60, (f) 70, (g) 80, and (h) 90% RH. Amount of each product on glass was *ca.* 2.0 mg/cm^2.

this material forms a single crystal, its ladder structure can be confirmed by single crystal XRD measurements. In addition, the formation of ladder structure of oligoSQs can be discussed by IR spectra because the theoretical absorption peaks have been calculated [27]. On the other hand, decisive analysis methods for the ladder-like structure of PSQ have not yet been established. This is because it is difficult to obtain the single crystal of PSQ and to calculate the theoretical absorption peaks in IR spectra due to high molecular weight. Therefore, the evidence necessary to confirm the molecular structure was collected by performing multiple analyses. The ladder-like PSQ simultaneously satisfies the following conditions: (i) to be soluble in solvents, (ii) relatively high molecular weight, (iii) relatively small width of the molecule, and (iv) observation of large T^3 peak and small T^2 peak in ^{29}Si NMR spectrum.

PSQ-$NH_3^+Cl^-$ had a rod-like structure with relatively small diameter, that is, short molecular width (*ca.* 1.6–1.7 nm, estimated from *d*-value of (100) peak in XRD pattern of Figure 1), in spite of forming highly dense Si–O–Si bond network structure, which was confirmed by the observation of large T^3 peak in the ^{29}Si NMR spectrum of Figure 3. In addition, PSQ-$NH_3^+Cl^-$ was soluble in water, despite its M_w was relatively high (*ca.* 12000, estimated by *Zimm* plot method using the SLS in water), which indicated no formation of three-dimensional network structure. These results satisfy the aforementioned conditions. All these things considered, it is reasonable to assume that the present PSQ has one-dimensional ladder-like molecular structure as shown in Scheme 1(c-ii).

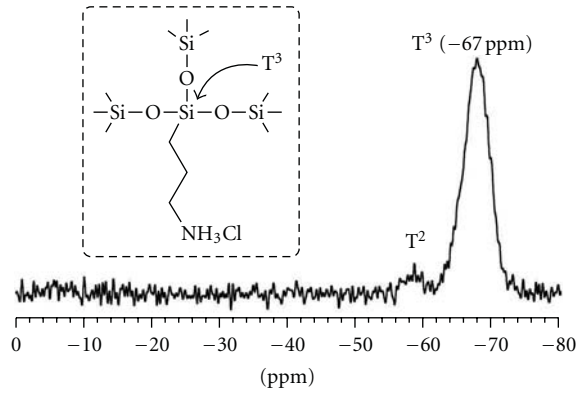

FIGURE 3: Solid-state ^{29}Si NMR spectrum of PSQ-$NH_3^+Cl^-$.

We supposed that ladder-like PSQ-$NH_3^+Cl^-$ was twisted to form rigid rod-like structure in the solid state, resulting in the formation of the hexagonally stacked structure. The driving force for the formation of the twisted conformation is probably intramolecular charge repulsion between the ammonium cations in side-chain groups of PSQ-$NH_3^+Cl^-$. Therefore, to investigate correlation between intramolecular charge repulsion and regular structure of PSQ-$NH_3^+Cl^-$, the XRD measurements were performed with changing RH. Stability of the ammonium cations is affected with RH because of hydration with water molecules. The XRD patterns of PSQ-$NH_3^+Cl^-$ with RH higher than 30% indicated three diffraction peaks derived from hexagonal phase (Figures 2(b)–2(h)), meanwhile those with RH lower than 20% did not show such the diffraction peaks (Figure 2(a)). Because these results indicate the presence of correlation between the formation of the hexagonally stacked structure and higher RH, it is assumed that the twisted structure caused by intramolecular charge repulsion between the ammonium cations is plausible conformation of PSQ-$NH_3^+Cl^-$.

When the sol-gel reaction of APTMOS was performed under alkaline conditions using ammonia (NH_3) aqueous solution, insoluble PSQ with three-dimensional network structure was prepared. On the basis of all results as described above, we considered that self-organization of the ion pair prepared from the amino group of APTMOS and the acid was the driving force for the formation of regular molecular and higher-ordered structures of the PSQ.

2.2. Sol-Gel Reaction of (3-(2-Aminoethylamino)propyl)-trimethoxysilane. As another monomer, organotrialkoxysilane containing two amino groups, that is, (3-(2-aminoethylamino)propyl)trimethoxysilane (AEAPTMOS), was employed for the preparation of regular-structured PSQ [24]. The procedure for sol-gel reaction of AEAPTMOS was similar to that of APTMOS.

The XRD pattern of the resulting product film showed three diffraction peaks with the *d*-value ratio of $1 : 1/\sqrt{3} : 1/2$, indicating that the product had a hexagonal phase. The *d*-values of the diffraction peaks changed by varying the RH, although the *d*-value ratios of (110)/(100) and (200)/(100) did not change (Table 1). The same behavior was observed

Table 1: *d*-Values of diffraction peaks in the XRD patterns of the PSQ obtained from AEAPTMOS under various RH conditions.

RH (%)	*d*-value (nm)		
	(100)	(110)	(200)
20	1.68	0.97	0.84
30	1.74	1.01	0.87
40	1.80	1.04	0.89
50	1.85	1.07	0.93
60	1.93	1.12	0.97
70	2.00	1.16	0.99
80	2.06	1.20	1.03
90	2.15	—	—

with the aforementioned PSQ-$NH_3^+Cl^-$ (Figure 2). Therefore, the PSQ containing double-ammonium groups in one repeating unit also had a hexagonal phase, which originated from the stacking of rod-like polymers. The *d*-value of (100) peak of this PSQ (1.85 nm for RH of *ca*. 50%) was larger than that of PSQ-$NH_3^+Cl^-$ (1.43 nm for RH of *ca*. 50%). This is because of difference in side-chain lengths between these PSQs.

3. Preparation of Ladder-Like PSQs Containing Chiral and Ammonium Chloride Side-Chain Groups

In the previous part, we described the assumption that the ladder-like PSQ was twisted to form the rod-like structure, resulting in the formation of the hexagonally stacked structure. However, the twisting direction would not be controlled, that is, the twisted ladder-like PSQ was probably obtained in racemic form. We suppose that controlling the conformational structure of the PSQ, for example, formation of the chiral conformation that is motif for biological macromolecules such as DNA, protein, and amylose, is one of the important subjects. Such a conformational structure of the biological macromolecules is generally caused by chiral moieties of monomer units. In this part, therefore, the introduction of the chiral moieties into the ladder-like PSQs is described to control not only the molecular and higher-ordered structures of PSQs but also their conformational structures.

3.1. Preparation by Copolymerization Method. To prepare chiral ladder-like PSQs, the introduction of the chiral moieties into the PSQs was first investigated by acid-catalyzed copolycondensation of two organotrialkoxysilanes containing chiral and amino groups, respectively [28]. The chiral trialkoxysilanes (R and S monomers) were synthesized by reaction of 3-(triethoxysilyl)propyl isocyanate with (R)-(+)- or (S)-(−)-1-phenylethylamine in dichloromethane at room temperature for 15 min, respectively, followed by evaporation of the dichloromethane. The sol-gel copolycondensation of the resulting chiral trialkoxysilanes with 3-aminopropyltriethoxysilane (APTEOS) (feed molar ratio = 1 : 9) was performed in a mixed solvent of aqueous hydrochloric acid and methanol by heating in an open system until the solvent was completely evaporated (Scheme 3(a)).

The compositional ratio of the chiral groups to the ammonium chloride groups in the products was calculated to be 6 : 94 from the ^{1}H NMR spectra. Therefore, the resulting PSQs are denoted as R_6- and S_6-PSQs, according to the stereostructure and functionality of the chiral groups. In the IR spectra of R_6- and S_6-PSQs, large absorption bands at 1135 and 1040 cm^{-1} assigned to the Si–O–Si bonds were observed. In addition, the ^{29}Si NMR spectra in DMSO-d_6 at 40°C of these PSQs exhibited the large peaks in the regions of T^3. These results indicate the complete progress of sol-gel copolycondensation of the chiral trialkoxysilanes and APTEOS, and the formation of Si–O–Si bonds. The M_ws of R_6- and S_6-PSQs estimated by the *Zimm* plot method using SLS in water were assessed to be 10700 and 9800, respectively, indicating that the products were not oligomeric compounds but polymers.

The XRD patterns of the films of R_6- and S_6-PSQs showed three diffraction peaks with the *d*-value ratio of $1 : 1/\sqrt{3} : 1/2$, indicating the formation of the hexagonal phases. Because these PSQs were soluble in water and DMSO, it was supposed that these hexagonal phases originated from the stacking of rod-like polymers. The diameters of the rod-like PSQs calculated from *d*-values of (100) peaks (1.47–1.48 nm) were assessed to be *ca*. 1.7 nm.

As aforementioned, R_6- and S_6-PSQs had rod-like structures with relatively small diameter (*ca*. 1.7 nm) in spite of the presence of large T^3 peak in the ^{29}Si NMR spectrum. In addition, these PSQs were soluble in water and DMSO, despite the M_ws of the PSQs were relatively high (*ca*. 9800–10700). These results satisfy the aforementioned conditions for ladder-like structure of PSQ. Therefore, the present chiral PSQs would also have one-dimensional ladder-like structure as shown in Scheme 1(c-ii).

The vibrational circular dichroism (VCD) spectra of R_6- and S_6-PSQs showed the reversed absorptions at *ca*. 1145–1165 cm^{-1}, respectively (Figure 4), corresponding to the absorptions assigned to Si–O–Si bond of polymer main-chains. These results indicate that R_6- and S_6-PSQs had chiral conformations of main-chains.

3.2. Preparation by Polymer Reaction Method. To prepare ladder-like PSQs containing higher compositional ratios of chiral side-chain groups, the aforementioned acid-catalyzed copolycondensation was investigated with a higher feed molar ratio of chiral trialkoxysilanes (>20%). However, the resulting PSQs were insoluble in all solvents owing to the formation of three-dimensional cross-linked network structures. This is because the number of ion pairs formed by the amino groups of APTEOS and the acid-catalysts decreased. Therefore, to prepare soluble ladder-like PSQs containing higher ratio of chiral groups, that is, a lower ratio of ammonium chloride groups, the polymer reaction of chiral isocyanate compounds with the aforementioned PSQ-$NH_3^+Cl^-$ was investigated [29].

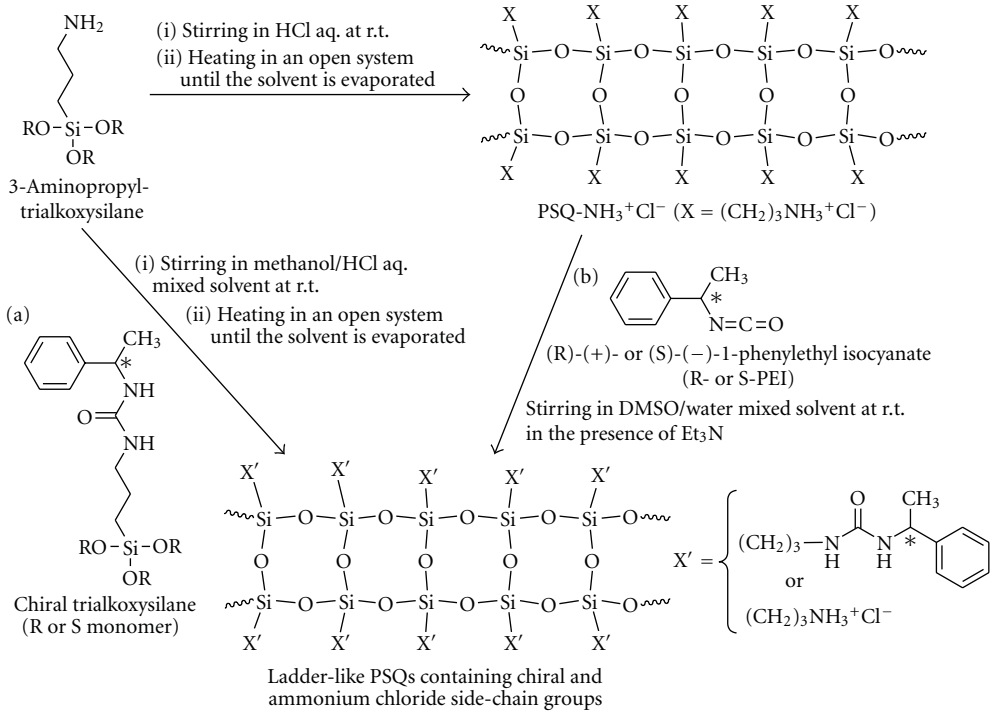

Scheme 3: Preparation of ladder-like PSQs containing chiral and ammonium chloride side-chain groups by (a) copolycondensation method and (b) polymer reaction method.

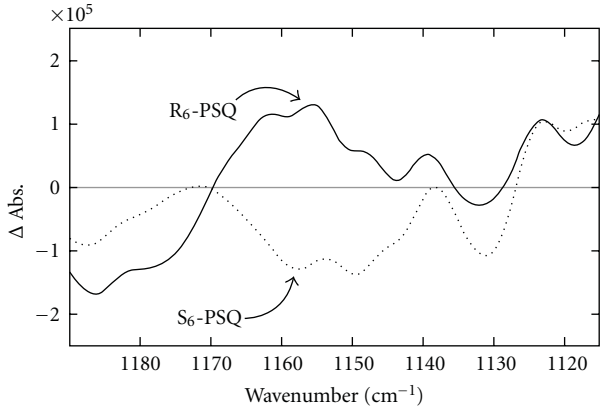

Figure 4: VCD spectra in DMSO of R_6- and S_6-PSQs.

The preparation was performed by reaction of (R)-(+)- or (S)-(−)-1-phenylethyl isocyanate (R- or S-PEI) with PSQ-$NH_3^+Cl^-$ in the presence of triethylamine in DMSO/water mixed solvent at room temperature for 10 min (Scheme 3(b)). The compositional ratios of chiral groups to ammonium chloride groups in the resulting products were estimated from their ^{1}H NMR spectra and were found to depend on the feed molar ratio of PEI to ammonium chloride group of PSQ-$NH_3^+Cl^-$. Here, soluble PSQs with the compositional ratio of chiral groups to ammonium chloride groups = *ca*. 80 : 20 were prepared. These PSQs are denoted as R_{80}- and S_{80}-PSQs, respectively. The M_ws of R_{80}- and S_{80}-PSQs were estimated by the *Zimm* plot method using SLS in methanol and were assessed to be *ca*. 54000 and 46000, respectively.

The diffraction peaks in the XRD patterns of the PSQs were broadened compared with those of PSQ-$NH_3^+Cl^-$. This is due to the decrease in the number of ion pairs, that is, ammonium chloride groups. As described above, the ion pair has an important role in the construction of a regular higher-ordered structure. However, because the XRD pattern of the product film showed diffraction peaks with *d*-value of 1.80 nm, indicating a relatively regular stacking structure, the rigid structures of PSQs would be maintained.

The chiral conformations of many kinds of helical polymers are stabilized by intramolecular interaction, for example, hydrogen bonding [30]. Therefore, specific rotations of these polymers are generally changed by varying the solvents because their intramolecular interactions are affected by the nature of the solvent. The specific rotations $[\alpha]_D^{22}$ of R_{80}- and S_{80}-PSQs in methanol were +17.4° and −18.9°, respectively, while those in DMF were +8.6° and −8.5°, respectively. Because these PSQs have urea groups as side-chains, which are involved in intramolecular hydrogen bonding, their $[\alpha]_D^{22}$ values were probably affected by solvent effects. Such a solvent effect on specific rotations indicates the presence of chiral conformations of these PSQs.

3.3. Chiral Induction Behavior from Chiral PSQ to Anionic Porphyrin Compound. Self-assembled hybrids formed by noncovalent interactions between photofunctional compounds and chiral molecules have attracted much attention because of their potential applications in circularly polarized

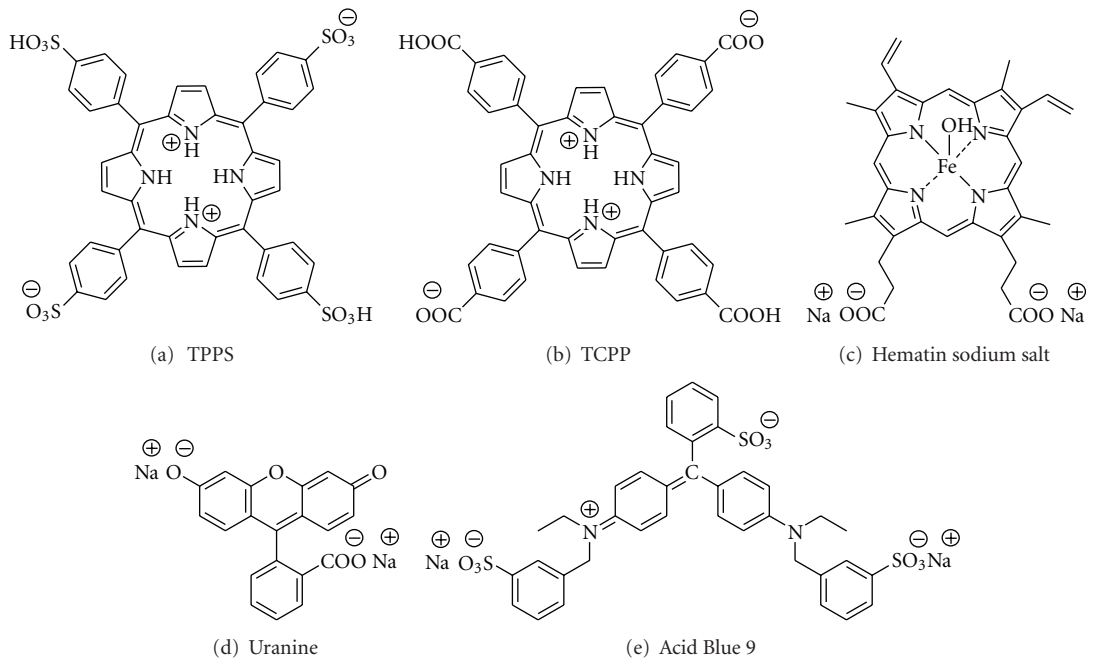

(a) TPPS (b) TCPP (c) Hematin sodium salt

(d) Uranine (e) Acid Blue 9

Figure 5: Structures of various dye compounds.

luminescent (CPL) materials. To achieve the preparation of these supramolecular hybrids by chiral induction from chiral molecules to photofunctional compounds, several combinations have been investigated, for example, anionic dye/cationic chiral surfactants [31], laser dye/cholesteric liquid crystal [32], pyrene derivatives/cyclodextrins [33], porphyrins/helical polyacetylene [34], and π-conjugated polymers/polysaccharides such as amylose [35], and schizophyllan [36]. On the other hand, there have been no reports regarding hybridization using inorganic compounds such as siloxane (SiO)-based materials as chiral inductors. The chiral inductors derived from SiO-based materials may enable the development of durable and thermostable hybrids with photofunctional compounds because the SiO-based materials exhibit superior thermal, mechanical, and chemical stabilities. Therefore, the aforementioned ladder-like PSQs containing chiral and ammonium groups were applied to chiral inductors for hybridization with a dye compound such as an anionic achiral porphyrin, tetraphenylporphine tetrasulfonic acid (TPPS) (Figure 5(a)), by ionic interaction [28, 29].

In the UV-Vis spectra of TPPS/R_6- and S_6-PSQs aqueous mixtures (4 μmol/L and 100 μmol unit/L, resp.), absorptions due to the Soret band of TPPS in these mixtures were blue shifted (to 400 nm) compared with that of TPPS alone and indicated monomeric state with protonated (at 434 nm) and deprotonated (at 414 nm) species (Figure 6(a)). These results indicate that the negatively charged TPPS formed H aggregates along the positively charged ammonium groups as side-chains of the PSQs.

The electronic circular dichroism (ECD) spectra of these TPPS/PSQs aqueous mixtures showed the reversed absorptions due to the Soret bands of TPPS aggregates, corresponding to R_6- and S_6-PSQs as templates, respectively (Figure 6(b)), indicating that TPPS aggregates have chiralities induced from the chiral PSQs. However, these mixtures did not show fluorescence emissions due to self-quenching of the excited state of the TPPS aggregate. Therefore, to inhibit the formation of H-aggregates of TPPS by extension of the distance between the ammonium side-chains of PSQs, the same analyses were performed using R_{80}- and S_{80}-PSQs as chiral inductors.

The ECD spectra of TPPS/R_{80}- and S_{80}-PSQs mixtures in methanol (4 μmol/L and 100 μmol unit/L, resp.) exhibited the reverse absorptions (Figure 6(d)), corresponding to the absorptions assigned to the Soret bands of TPPS at 418 nm in the UV-Vis spectrum (Figure 6(c)). The absorption wavelength of this mixture was almost the same as that of dilute methanol solution of sole TPPS (concentration = 4 μmol/L), indicating that TPPS maintained the monomeric state in the mixture. These results indicate that the chiral induction from PSQs to TPPS was achieved without the formation of H-aggregate of TPPS. In the present mixture, because of no formation of H-aggregate, the fluorescence spectrum excited at 420 nm showed an emission peak at 654 nm.

3.4. Influence of the Structures of Dye Compounds on Chiral Induction Behavior. To investigate the influence of the structures of dye compounds on the aforementioned chiral induction behavior, we performed the ECD and UV-Vis measurements of the mixtures in methanol of R_{80}- and S_{80}-PSQs with various dye compounds as shown in Figure 5. When tetrakis(4-carboxyphenyl)porphyrin (TCPP) (Figure 5(b)) was used as a dye compound, the reverse absorptions assigned to TCPP in these mixtures were observed in the ECD spectra (Figure 7(b)). These behaviors

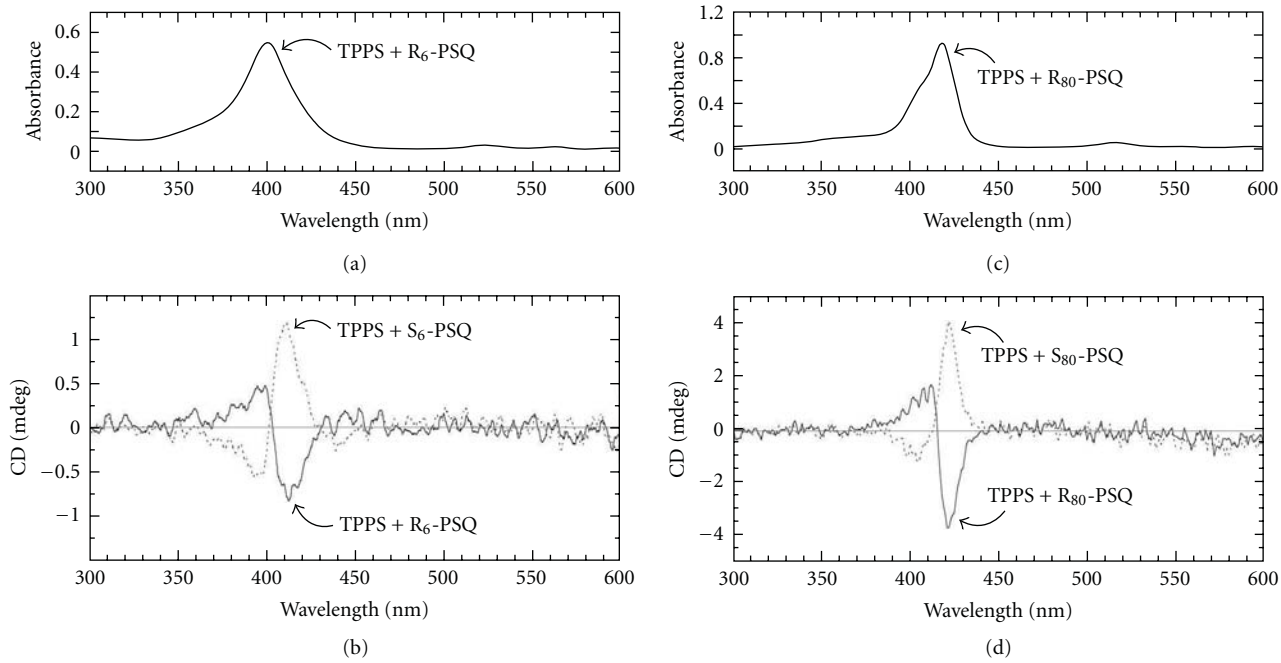

Figure 6: (a) UV-Vis spectrum of TPPS/R_6-PSQ aqueous mixture, (b) ECD spectra of TPPS/R_6- and S_6-PSQs aqueous mixtures, (c) UV-Vis spectrum of TPPS/R_{80}-PSQ mixture in methanol, and (d) ECD spectra of TPPS/R_{80}- and S_{80}-PSQs mixtures in methanol.

were similar to those using TPPS and indicated that the chiral induction from PSQs to TCPP was occurred. On the other hand, such the absorptions in the ECD spectra did not appear using Hematin sodium salt (Figure 5(c)), Uranine (Figure 5(d)), and Acid Blue 9 (Figure 5(e)) as dye compounds (Figures 7(d), 7(f), and 7(h)). Difference in the structures between the dye compounds indicated chiral induction (TPPS and TCPP) and the others (Hematin sodium salt, Uranine, and Acid Blue 9) are point symmetry, that is, the former had point-symmetric structure and the later did not have it. Therefore, we assumed that point symmetry of dye compounds was an important factor for the chiral induction behavior from R_{80}- and S_{80}-PSQs to these dye compounds.

4. Correlation between the pK_a of Acid-Catalysts and the Structures of SQs Prepared by Hydrolytic Condensation of APTMOS

As described above, the sol-gel reaction of APTMOS using HCl aqueous solution resulted in the formation of ladder-like PSQ with hexagonally stacked structure [23–26]. Furthermore, when another acid, for example, nitric acid (HNO_3) aqueous solution was used, we confirmed the formation of similarly structured PSQ [23]. On the other hand, when the hydrolytic condensation of APTMOS was performed using a superacid trifluoromethanesulfonic acid (CF_3SO_3H) aqueous solution under the same reaction conditions as those used for the preparation of the ladder-like PSQ as described above, we found that cage-like octa(3-aminopropyl)SQ trifluoromethanesulfonate (OAP-POSS-CF_3SO_3) was prepared in *ca.* 93% yield with a total reaction time of *ca.* 5-6 h (Scheme 4) [37]. In the preparation of OAP-POSS, these values are considerably high yield and a short reaction time compared with those of the previous studies [7–9].

For the confirmation of the OAP-POSS-CF_3SO_3 structure as shown in Scheme 4, the ^{29}Si NMR, matrix-assisted laser desorption ionization time of flight mass (MALDI-TOF MS), electrospray ionization mass (ESI MS), and IR measurements were carried out. The ^{29}Si NMR spectrum in DMSO-d_6 at 40°C of the product showed only a T^3 signal at *ca.* −66 ppm. This indicates that the product has only one type of Si atoms, which are substituted with three siloxane bonds (i.e., the absence of a silanol group). Furthermore, in the MALDI-TOF MS spectrum of the product, only one significant peak was observed, which corresponded to the mass of OAP-POSS without $CF_3SO_3^-$ as counterions (*m*/*z* 881.9 $[M+H]^+$). To support the mass result from the MALDI-TOF MS spectrum, we performed an ESI MS measurement of the product. Consequently, peaks corresponding to the mass of OAP-POSS were also observed. Additionally, the counterions of the product were exchanged (from $CF_3SO_3^-$ to Cl^-) by treatment with the mixed solvent of 0.5 mol/L methanolic HCl and acetone to more easily evaluate the Si−O−Si stretching absorption band in the IR spectrum. The IR spectrum of the product with Cl^- as the counterion showed only one absorption peak at 1125 cm^{-1} derived from Si−O−Si bonds. It has been reported that the IR spectra of cage-like octaSQs showed a single peak due to the Si−O−Si stretching absorption band because of their highly symmetrical structures [27]. From these results, it was

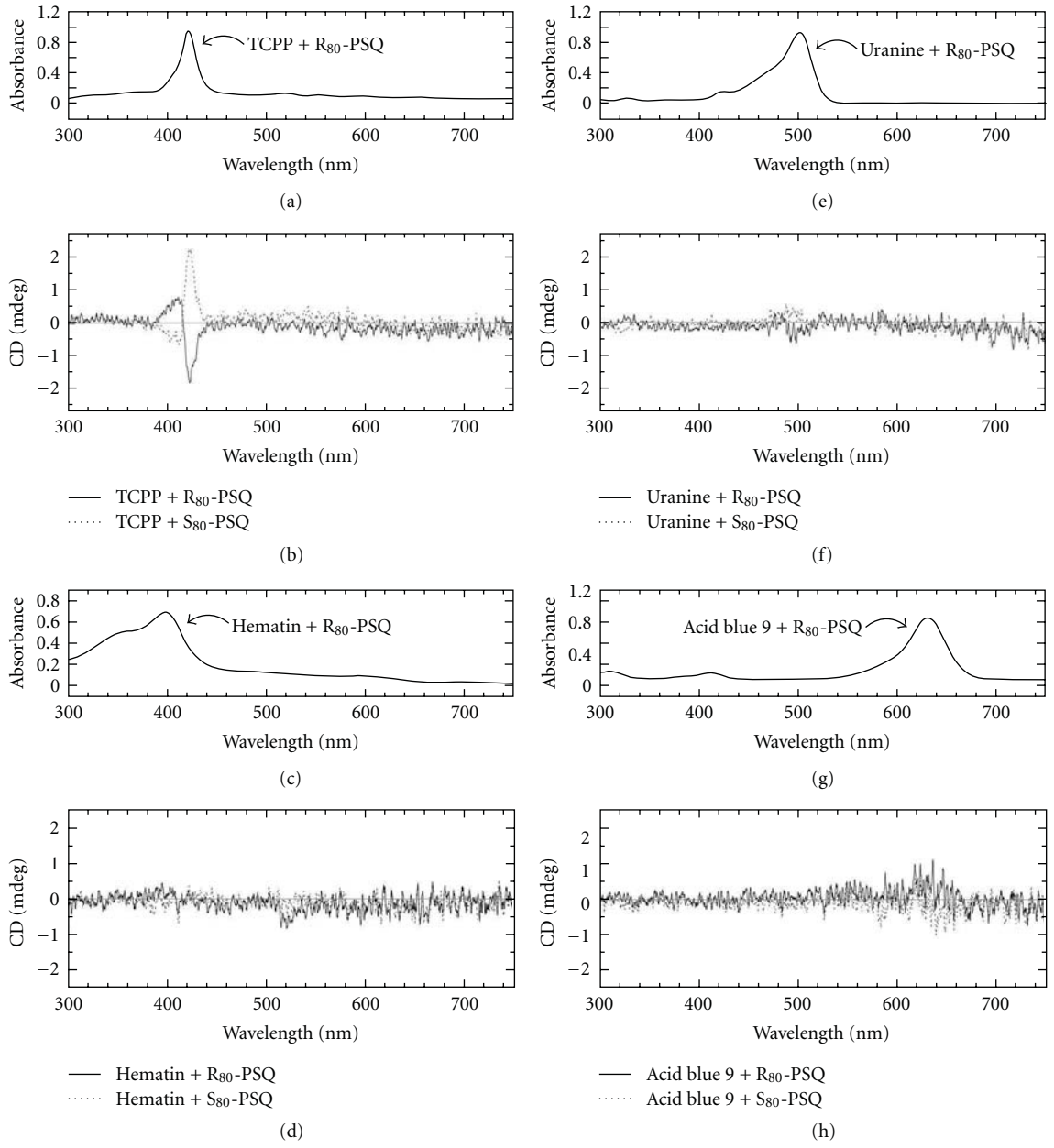

Figure 7: (a) UV-Vis spectrum of TCPP/R_{80}-PSQ mixture, (b) ECD spectra of TCPP/R_{80}- and S_{80}-PSQs mixtures, (c) UV-Vis spectrum of Hematin/R_{80}-PSQ mixture, (d) ECD spectra of Hematin/R_{80}- and S_{80}-PSQs mixtures, (e) UV-Vis spectrum of Uranine/R_{80}-PSQ mixture, (f) ECD spectra of Uranine/R_{80}- and S_{80}-PSQs mixtures, (g) UV-Vis spectrum of Acid Blue 9/R_{80}-PSQ mixture, and (h) ECD spectra of Acid Blue 9/R_{80}- and S_{80}-PSQs mixtures. In all cases, methanol was employed as a solvent, and the molar ratios of dye compound to one unit of PSQ were 1 : 25.

concluded that the product had cage-like structure as shown in Scheme 4.

As aforementioned, the ladder-like PSQs with hexagonally stacked structures can be prepared from APTMOS using the strong acids such as HCl and HNO_3 aqueous solutions under the same reaction conditions as those used for the preparation of OAP-POSS-CF_3SO_3. The differences between the CF_3SO_3H ($pK_a = -13$) and the acids used for the formation of the ladder-like PSQs (HCl and HNO_3, pK_as $= -3.7$ and -1.8, resp.) are associated with their acidity and bulkiness. The pK_a of trifluoroacetic acid (CF_3COOH, $pK_a = 0.3$) is higher than that of CF_3SO_3H (i.e., the acidity of CF_3COOH is lower than that of CF_3SO_3H) although the bulkiness of both acids is similar. Therefore, to investigate the effect of these properties of the acids on the structures of the synthesized SQs, the hydrolytic condensation of APTMOS was performed using CF_3COOH aqueous solution. Consequently, we found that a hexagonally structured PSQ was obtained, as confirmed by XRD measurements. In addition, the ^{29}Si NMR spectrum showed a slight T^2 peak, indicating

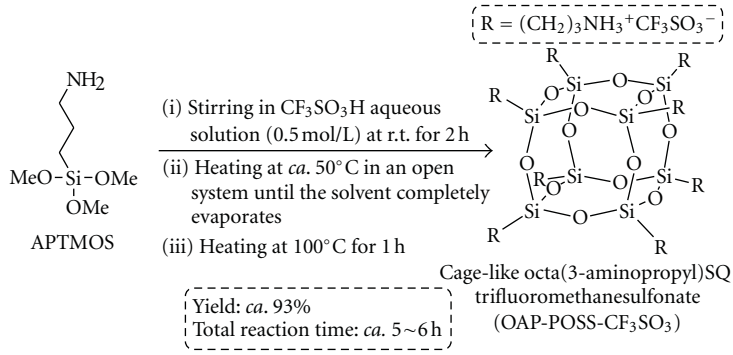

Scheme 4: Preparation of OAP-POSS-CF_3SO_3 using CF_3SO_3H aqueous solution in higher yield with a shorter reaction time.

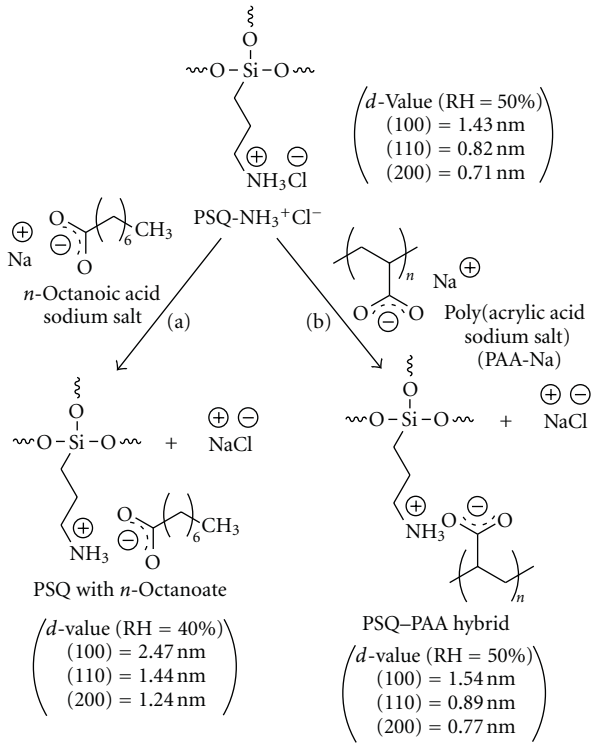

Scheme 5: Ion-exchange reactions of PSQ-$NH_3^+Cl^-$ with (a) *n*-octanoic acid sodium salt and (b) poly(acrylic acid sodium salt).

that there was no formation of the OAP-POSS-CF_3SO_3 structure, which was confirmed by the presence of silanol groups. These results indicate that the lower pK_a of the acid is an important factor for the preparation of OAP-POSS-CF_3SO_3.

On the basis of these results, we concluded that the pK_a of the acids was important to control the structures of SQs prepared by hydrolytic condensation of APTMOS, that is, the use of the superacid aqueous solution resulted in the formation of cage-like octaSQ, while the ladder-like PSQs with hexagonally stacked structures were formed from the strong acid aqueous solutions under the same reaction conditions (Figure 8). Detailed studies on the hydrolytic condensations of APTMOS using other acid-catalysts with various pK_a levels are now in progress.

5. Ion-Exchange Behaviors of Cationic Ladder-Like PSQs with Various Anionic Compounds

Because the aforementioned PSQ-$NH_3^+Cl^-$ has ammonium groups as side-chains and chloride anions (Cl^-) as counterions, the anion-exchange property can be expected. Therefore, ion-exchange reactions of the PSQs were performed with various anionic compounds.

5.1. Ion-Exchange with Fatty Acids. First, a fatty acid salt such as *n*-octanoic acid sodium salt was employed as an anionic compound (Scheme 5(a)) [23]. By pouring PSQ-$NH_3^+Cl^-$ aqueous solution into aqueous solution of *n*-octanoic acid sodium salt, precipitation immediately occurred. The XRD pattern of the resulting water-insoluble product showed peaks for a typical hexagonal phase and the *d*-value of (100) peak increase more than those of the original PSQs (PSQ-$NH_3^+Cl^-$), indicating that the diameter of the rod-like PSQ increased when the Cl^- as the counterion was exchanged with the bulky *n*-octanoate. Thus, the hexagonal phase of the rod-like PSQ was maintained, in spite of the increase in the *d*-value by the ion-exchange reaction with *n*-octanoic acid sodium salt.

On the other hand, when the ion-exchange reactions were performed using the fatty acid salts containing longer alkyl chains (*n*-decanoic acid sodium salt, *n*-dodecanoic acid sodium salt, and *n*-tetradecanoic acid sodium salt), the peaks due to the typical hexagonal phase were not obtained. This is because the hydrophobic interaction between the guest fatty acid salts containing longer alkyl chains was too strong to maintain the hexagonally stacked structure of rod-like PSQ.

5.2. Ion-Exchange with Anionic Organic Polymer. Hybrids composed of organic and inorganic materials usually exhibit improved performance properties compared with conventional composites, mixtures on a micrometer scale (μm), due to their unique phase morphology, and improved interfacial properties. For these reasons, nanostructured

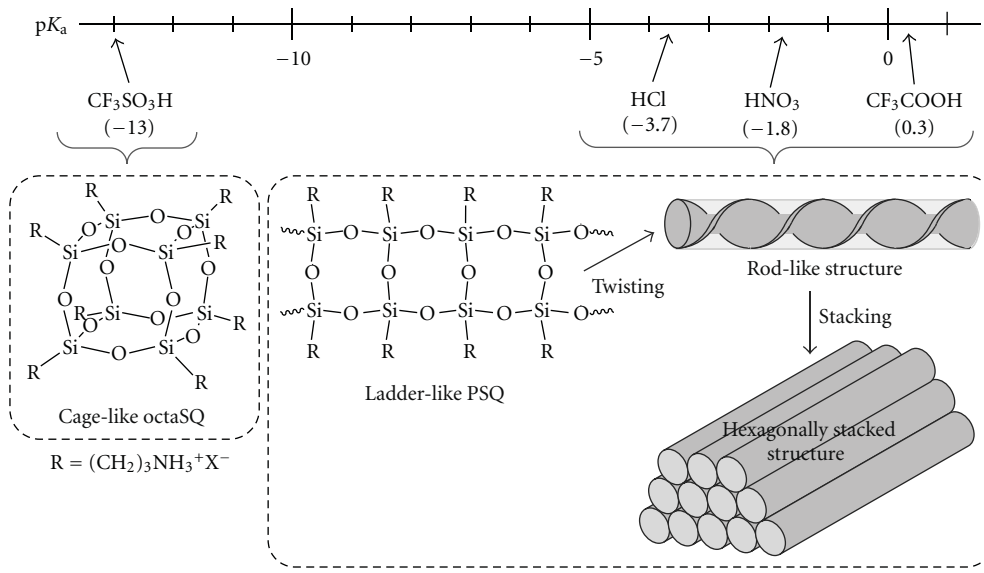

Figure 8: Correlation between the pK_a of acid-catalysts and the structures of SQs prepared by hydrolytic condensation of APTMOS.

organic-inorganic hybrids have attracted considerable attention from both fundamental research and applications points of view [38, 39]. In particular, the organic-inorganic hybrids obtained from the synthetic polymers as organic species are important industrial materials.

Here, we describe the preparation of an organic-inorganic polymer hybrid (PSQ-PAA) with regular higher-ordered structure composed of the aforementioned PSQ-$NH_3^+Cl^-$ as the inorganic species and poly(acrylic acid sodium salt) (PAA-Na) as the organic species by an ion-exchange reaction [40]. To obtain PSQ-PAA, the ion-exchange reaction was performed by pouring PSQ-$NH_3^+Cl^-$ aqueous solution into PAA-Na aqueous solution (Scheme 5(b)).

The IR spectrum of PSQ-PAA indicated that the product consisted of both organic and inorganic polymers. The CHN elemental analysis data showed that the C/N molar ratio for the product was 5.92. From this value, the ratio of the functional groups of the two polymers, that is, NH_3^+ and COO^-, was calculated to be *ca.* 1 : 1. The XRD pattern of PSQ-PAA showed the formation of a hexagonal phase, and the *d*-values of the diffraction peaks were different from those of PSQ-$NH_3^+Cl^-$ (Scheme 5(b)), indicating the formation of not a macroscopic mixture but the molecular-scale hybrid of two polymers.

5.3. Ion-Exchange with Layered Clay Minerals. There have been intense research activities on layered silicates pillared with inorganic or organic clusters, which are called pillared interlayer clays (PILCs) [41–43]. PILCs have much higher surface areas and pore volumes than those of the original clays. Such properties make them useful catalysts, ion-exchangers, and adsorbents. These materials are usually prepared by the intercalative ion-exchange of layered clay minerals with a variety of nanosized pillars, such as organic ions [44], inorganic ions [45], and sol particles [46].

Even though the preparation of various polymer/clay hybrids has already been reported [47], there have been a few studies on the preparation of PILCs using polymers. Because the polymers generally have a flexible structure, expansion of the interlayer space of clays by polymer incorporation is not enough for providing more free space.

The aforementioned PSQ-$NH_3^+Cl^-$ has motivated us to develop new PILCs, because PSQ-$NH_3^+Cl^-$ has rigidity and bulkiness to expand the interlayer of clays and ability to intercalate molecules into the interlayer of anionic clays by the ion-exchange reaction due to the presence of ammonium cations in side-chains of PSQ-$NH_3^+Cl^-$. Therefore, we describe the preparation of a clay pillared with rod-like cationic PSQ-$NH_3^+Cl^-$ [48].

The preparation was performed by pouring PSQ-$NH_3^+Cl^-$ aqueous solution into an aqueous suspension of Na-saturated saponite (Na-SAP) as a clay mineral to obtain the clay pillared with PSQ-$NH_3^+Cl^-$ (PSQ-SAP) (Scheme 6). The resulting product was mainly characterized by IR, XRD, and nitrogen adsorption-desorption isotherm measurements.

The IR spectrum of PSQ-SAP showed the absorption assigned to the ammonium ion of the PSQ component, indicating that the PSQ was inserted into the interlayer of SAP. The XRD pattern of PSQ-SAP was completely different from that of Na-SAP and PSQ-$NH_3^+Cl^-$. Accordingly, PSQ-SAP was not a mixture, but an intercalated nanoorder material, that is, a hybrid.

From the nitrogen adsorption-desorption isotherms at 77 K, the surface area and pore volume of PSQ-SAP derived from the *t*-plot were estimated to be 370 m^2/g and 0.15 cm^3/g, respectively. This indicates that a porous material was prepared from the starting materials with dense structures (BET surface areas of Na-SAP and PSQ-$NH_3^+Cl^-$ were *ca.* 26 and 5 m^2/g, resp.).

When a clay mineral with high cation-exchange capacity (CEC) such as Li-saturated taeniolite was employed, such a

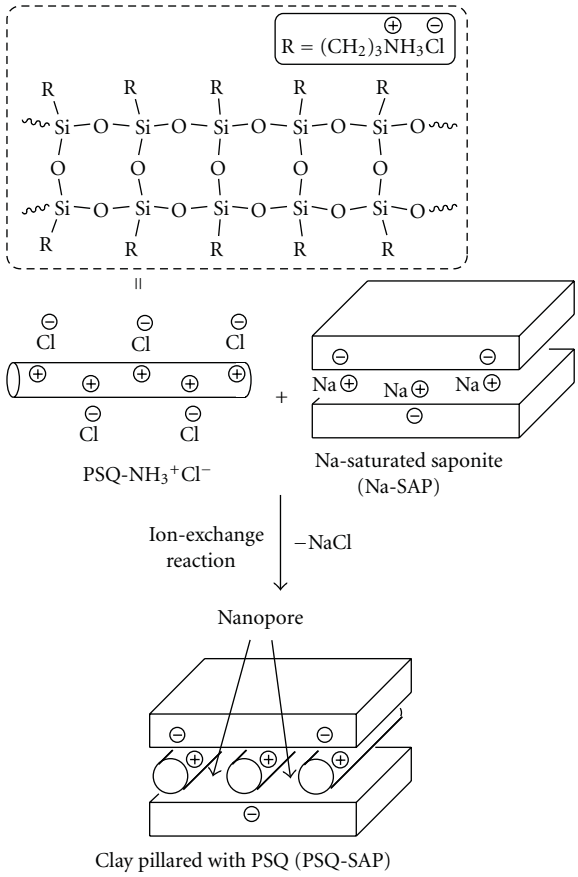

Scheme 6: Preparation of a clay pillared with PSQ by ion-exchange reaction of PSQ-$NH_3^+Cl^-$ with Na-saturated saponite.

porous material was not obtained by combination with PSQ-$NH_3^+Cl^-$ (BET surface area of the resulting product was *ca.* 53 m^2/g), although a sufficient interlayer spacing existed as confirmed by the XRD measurement. Because the distance between the PSQs in the interlayer of taeniolite is short due to the higher CEC of the Li-saturated taeniolite, sufficient space was not provided. Furthermore, when polyallylamine hydrochloride (PAA-Cl), a common cationic polymer, was used for pillaring in the SAP interlayer, a porous structure was not obtained (BET surface area of the product was *ca.* 52 m^2/g). It was difficult for PAA-Cl to pillar the interlayer of SAP due to the lack of rigidity and bulkiness. From these results, it was considered that the rigidity and bulkiness of the guest polymers and a sufficient distance between charges in the host layered clay minerals are necessary for preparing clays pillared with polymers.

6. Conclusion

In this review, we described the preparation of cationic ladder-like PSQs with hexagonally stacked structures by the sol-gel reaction of amino group-containing organotrialkoxysilane monomers in the acid solutions. It was considered that self-organization of the ion pairs prepared from the monomers and the acids was the driving force for the formation of regular molecular and higher-ordered structures of the PSQs. In addition, to control the conformational structure of PSQ, the introduction of the chiral moieties into PSQ was performed. Furthermore, we found that the pK_a of the acid-catalysts was important to control the structures of the ammonium group-containing SQs prepared by hydrolytic condensation of APTMOS, that is, the use of the superacid aqueous solution resulted in the formation of cage-like octaSQ, while the ladder-like PSQs with hexagonally stacked structures were formed from the strong acid aqueous solutions under the same reaction conditions. Finally, because the present ladder-like PSQs indicated the anion-exchange properties due to existence of cationic functional groups as side-chains, we described the anion-exchange behaviors with various organic and inorganic compounds, such as anionic surfactants, a polymer, and layered clay minerals, to obtain the functional hybrid materials.

Acknowledgments

This work was supported in part by a research grant from the Mazda Foundation and a Grant-in-Aid for Scientific Research (C) from Ministry of Education, Culture, Sports, Science, and Technology, Japan (no. 24550138). The authors acknowledge Prof. H. Sato of Graduate School of Science and Engineering, Ehime University (Japan) and Dr. T. Mizumo of Graduate School of Engineering, Hiroshima University (Japan) for their valuable technical advices. of a clay pillared with PSQ by ion-exchange reaction of PSQ-$NH_3^+Cl^-$

References

[1] R. H. Baney, M. Itoh, A. Sakakibara, and T. Suzuki, "Silsesquioxanes," *Chemical Reviews*, vol. 95, no. 5, pp. 1409–1430, 1995.

[2] D. A. Loy, B. M. Baugher, C. R. Baugher, D. A. Schneider, and K. Rahimian, "Substituent effects on the sol-gel chemistry of organotrialkoxysilanes," *Chemistry of Materials*, vol. 12, no. 12, pp. 3624–3632, 2000.

[3] J. Choi, J. Harcup, A. F. Yee, Q. Zhu, and R. M. Laine, "Organic/inorganic hybrid composites from cubic silsesquioxanes," *Journal of the American Chemical Society*, vol. 123, no. 46, pp. 11420–11430, 2001.

[4] K. M. Kim and Y. Chujo, "Organic-inorganic hybrid gels having functionalized silsesquioxanes," *Journal of Materials Chemistry*, vol. 13, pp. 1384–1391, 2003.

[5] X. Yu, S. Zhong, X. Li et al., "A giant surfactant of polystyrene-(carboxylic acid-functionalized polyhedral oligomeric silsesquioxane) amphiphile with highly stretched polystyrene tails in micellar assemblies," *Journal of the American Chemical Society*, vol. 132, no. 47, pp. 16741–16744, 2010.

[6] F. Wang, X. Lu, and C. He, "Some recent developments of polyhedral oligomeric silsesquioxane (POSS)-based polymeric materials," *Journal of Materials Chemistry*, vol. 21, no. 9, pp. 2775–2782, 2011.

[7] F. J. Feher and K. D. Wyndham, "Amine and ester-substituted silsesquioxanes: synthesis, characterization and use as a core for starburst dendrimers," *Chemical Communications*, no. 3, pp. 323–324, 1998.

[8] R. M. Laine, C. Zhang, A. Sellinger, and L. Viculis, "Polyfunctional cubic silsesquioxanes as building blocks for organic/inorganic hybrids," *Applied Organometallic Chemistry*, vol. 12, no. 10-11, pp. 715–723, 1998.

[9] Z. Zhang, G. Liang, and T. Lu, "Synthesis and characterization of cage octa(aminopropylsilsesquioxane)," *Journal of Applied Polymer Science*, vol. 103, no. 4, pp. 2608–2614, 2007.

[10] D. B. Cordes, P. D. Lickiss, and F. Rataboul, "Recent developments in the chemistry of cubic polyhedral oligosilsesquioxanes," *Chemical Reviews*, vol. 110, no. 4, pp. 2081–2173, 2010.

[11] K. Tanaka, F. Ishiguro, and Y. Chujo, "POSS ionic liquid," *Journal of the American Chemical Society*, vol. 132, no. 50, pp. 17649–17651, 2010.

[12] K. Tanaka and Y. Chujo, "Advanced functional materials based on polyhedral oligomeric silsesquioxane (POSS)," *Journal of Materials Chemistry*, vol. 22, no. 5, pp. 1733–1746, 2012.

[13] J. F. Brown Jr., L. H. Vogt Jr., and P. I. Prescott, "Double chain polymers of phenylsilsesquioxane," *Journal of the American Chemical Society*, vol. 82, no. 23, pp. 6194–6195, 1960.

[14] J. F. Brown Jr., L. H. Vogt Jr., and P. I. Prescott, "Preparation and characterization of the lower equilibrated phenylsilsesquioxanes," *Journal of the American Chemical Society*, vol. 86, no. 6, pp. 1120–1125, 1964.

[15] M. Unno, S. Chang, and H. Matsumoto, "cis-trans-cis-tetrabromotetramethylcyclotetrasiloxane: a versatile precursor of ladder silsesquioxanes," *Bulletin of the Chemical Society of Japan*, vol. 78, no. 6, pp. 1105–1109, 2005.

[16] X. Zhang, P. Xie, Z. Shen et al., "Confined synthesis of a cis-isotactic ladder polysilsesquioxane by using a π-stacking and h-bonding superstructure," *Angewandte Chemie—International Edition*, vol. 45, no. 19, pp. 3112–3116, 2006.

[17] H. Seki, T. Kajiwara, Y. Abe, and T. Gunji, "Synthesis and structure of ladder polymethylsilsesquioxanes from sila-functionalized cyclotetrasiloxanes," *Journal of Organometallic Chemistry*, vol. 695, no. 9, pp. 1363–1369, 2010.

[18] Y. Abe and T. Gunji, "Oligo- and polysiloxanes," *Progress in Polymer Science*, vol. 29, no. 3, pp. 149–182, 2004.

[19] M. Unno, A. Suto, and H. Matsumoto, "Pentacyclic ladder-siloxane," *Journal of the American Chemical Society*, vol. 124, no. 8, pp. 1574–1575, 2002.

[20] A. N. Parikh, M. A. Schivley, E. Koo et al., "*n*-Alkylsiloxanes: from single monolayers to layered crystals. The formation of crystalline polymers from the hydrolysis of *n*-octadecyltrichlorosilane," *Journal of the American Chemical Society*, vol. 119, no. 13, pp. 3135–3143, 1997.

[21] A. Shimojima, Y. Sugahara, and K. Kuroda, "Inorganic-organic layered materials derived via the hydrolysis and polycondensation of trialkoxy(alkyl)silanes," *Bulletin of the Chemical Society of Japan*, vol. 70, no. 11, pp. 2847–2853, 1997.

[22] S. Inagaki, S. Guan, T. Ohsuna, and O. Terasaki, "An ordered mesoporous organosilica hybrid material with a crystal-like wall structure," *Nature*, vol. 416, no. 6878, pp. 304–307, 2002.

[23] Y. Kaneko, N. Iyi, K. Kurashima, T. Matsumoto, T. Fujita, and K. Kitamura, "Hexagonal-structured polysiloxane material prepared by sol-gel reaction of aminoalkyltrialkoxysilane without using surfactants," *Chemistry of Materials*, vol. 16, no. 18, pp. 3417–3423, 2004.

[24] Y. Kaneko, N. Iyi, T. Matsumoto, and K. Kitamura, "Synthesis of rodlike polysiloxane with hexagonal phase by sol-gel reaction of organotrialkoxysilane monomer containing two amino groups," *Polymer*, vol. 46, no. 6, pp. 1828–1833, 2005.

[25] Y. Kaneko and N. Iyi, "Sol-gel synthesis of rodlike polysilsesquioxanes forming regular higher-ordered nanostructure," *Zeitschrift für Kristallographie*, vol. 222, no. 11, pp. 656–662, 2007.

[26] Y. Kaneko and N. Iyi, "Sol-gel synthesis of water-soluble polysilsesquloxanes with regular structures," *Kobunshi Ronbunshu*, vol. 67, no. 5, pp. 280–287, 2010.

[27] E. S. Park, H. W. Ro, C. V. Nguyen, R. L. Jaffe, and D. Y. Yoon, "Infrared spectroscopy study of microstructures of poly(silsesquioxane)s," *Chemistry of Materials*, vol. 20, no. 4, pp. 1548–1554, 2008.

[28] Y. Kaneko and N. Iyi, "Sol-gel synthesis of ladder polysilsesquioxanes forming chiral conformations and hexagonal stacking structures," *Journal of Materials Chemistry*, vol. 19, no. 38, pp. 7106–7111, 2009.

[29] Y. Kaneko, H. Toyodome, and H. Sato, "Preparation of chiral ladder-like polysilsesquioxanes and their chiral induction to anionic dye compound," *Journal of Materials Chemistry*, vol. 21, no. 41, pp. 16638–16641, 2011.

[30] H. Zhao, F. Sanda, and T. Masuda, "Transformation of helical sense of poly(*N*-propargylamides) controlled by competition between structurally different enantiomeric amino acids," *Macromolecules*, vol. 37, no. 24, pp. 8888–8892, 2004.

[31] D. Franke, M. Vos, M. Antonietti, N. A. J. M. Sommerdijk, and C. F. J. Faul, "Induced supramolecular chirality in nanostructured materials: ionic self-assembly of perylene-chiral surfactant complexes," *Chemistry of Materials*, vol. 18, no. 7, pp. 1839–1847, 2006.

[32] M. Uchimura, Y. Watanabe, F. Araoka, J. Watanabe, H. Takezoe, and G. I. Konishi, "Development of laser dyes to realize low threshold in dye-doped cholesteric liquid crystal lasers," *Advanced Materials*, vol. 22, no. 40, pp. 4473–4478, 2010.

[33] K. Kano, H. Matsumoto, Y. Yoshimura, and S. Hashimoto, "Binding sites of pyrene and related compounds and chiral excimer formation in the cavities of cyclodextrins and branched cyclodextrins," *Journal of the American Chemical Society*, vol. 110, no. 1, pp. 204–209, 1988.

[34] H. Onouchi, T. Miyagawa, K. Morino, and E. Yashima, "Assisted formation of chiral porphyrin homoaggregates by an induced helical poly(phenylacetylene) template and their chiral memory," *Angewandte Chemie—International Edition*, vol. 45, no. 15, pp. 2381–2384, 2006.

[35] M. Ikeda, Y. Furusho, K. Okoshi et al., "A luminescent poly(phenylenevinylene)-amylose composite with supramolecular liquid crystallinity," *Angewandte Chemie—International Edition*, vol. 45, no. 39, pp. 6491–6495, 2006.

[36] C. Li, M. Numata, A. H. Bae, K. Sakurai, and S. Shinkai, "Self-assembly of supramolecular chiral insulated molecular wire," *Journal of the American Chemical Society*, vol. 127, no. 13, pp. 4548–4549, 2005.

[37] Y. Kaneko, M. Shoiriki, and T. Mizumo, "Preparation of cage-like octa(3-aminopropyl)silsesquioxane trifluoromethanesulfonate in higher yield with a shorter reaction time," *Journal of Materials Chemistry*, vol. 22, no. 29, pp. 14475–14478, 2012.

[38] A. Usuki, Y. Kojima, M. Kawasumi et al., "Synthesis of nylon 6-clay hybrid," *Journal of Materials Research*, vol. 8, no. 5, pp. 1179–1184, 1993.

[39] Y. Chujo, "Organic-inorganic hybrid materials," *Current Opinion in Solid State and Materials Science*, vol. 1, no. 6, pp. 806–811, 1996.

[40] Y. Kaneko, N. Iyi, T. Matsumoto, and K. Kitamura, "Preparation of higher-ordered inorganic-organic nanocomposite composed of rodlike cationic polysiloxane and polyacrylate," *Journal of Materials Chemistry*, vol. 15, no. 15, pp. 1572–1575, 2005.

[41] K. Ohtsuka, "Preparation and properties of two-dimensional microporous pillared interlayered solids," *Chemistry of Materials*, vol. 9, no. 10, pp. 2039–2050, 1997.

[42] J. T. Kloprogge, "Synthesis of smectites and porous pillared clay catalysts: a review," *Journal of Porous Materials*, vol. 5, no. 1, pp. 5–41, 1998.

[43] Z. Ding, J. T. Kloprogge, R. L. Frost, G. Q. Lu, and H. Y. Zhu, "Porous clays and pillared clays-based catalysts. part 2: a review of the catalytic and molecular sieve applications," *Journal of Porous Materials*, vol. 8, no. 4, pp. 273–293, 2001.

[44] M. Ogawa, M. Takahashi, C. Kato, and K. Kuroda, "Oriented microporous film of tetramethylammonium pillared saponite," *Journal of Materials Chemistry*, vol. 4, no. 4, pp. 519–523, 1994.

[45] M. Pichowicz and R. Mokaya, "Stability of Pillared Clays: effect of compaction on the physicochemical properties of al-pillared clays," *Chemistry of Materials*, vol. 16, no. 2, pp. 263–269, 2004.

[46] S. Yamanaka, Y. Inoue, M. Hattori, F. Okumura, and M. Yoshikawa, " Preparation and properties of clays pillared with SiO_2–TiO_2 sol particles," *Bulletin of the Chemical Society of Japan*, vol. 65, no. 9, pp. 2494–2500, 1992.

[47] T. J. Pinnavaia and G. W. Beall, *Polymer-Clay Nanocomposites*, John Wiley and Sons, Chichester, UK, 2000.

[48] Y. Kaneko, N. Iyi, T. Matsumoto, and K. Kitamura, "Preparation of a clay pillared with rodlike cationic polysiloxane," *Chemistry Letters*, vol. 33, no. 11, pp. 1486–1487, 2004.

Hindawi Publishing Corporation
International Journal of Polymer Science
Volume 2012, Article ID 852063, 10 pages
doi:10.1155/2012/852063

Review Article

Polysilsesquioxanes for Gate-Insulating Materials of Organic Thin-Film Transistors

Kimihiro Matsukawa,[1] Mitsuru Watanabe,[1] Takashi Hamada,[2] Takashi Nagase,[3] and Hiroyoshi Naito[3]

[1] *Electronic Material Research Division, Osaka Municipal Technical Research Institute, Osaka 536-8553, Japan*
[2] *JST Innovation Plaza Osaka, Osaka 594-1131, Japan*
[3] *Department of Physics and Electronics, Osaka Prefecture University, Osaka 599-8531, Japan*

Correspondence should be addressed to Kimihiro Matsukawa, kmatsu@omtri.or.jp

Received 11 August 2012; Accepted 11 September 2012

Academic Editor: Yoshiro Kaneko

Printable organic thin-film transistor (O-TFT) is one of the most recognized technical issues nowadays. Our recent progress on the formation of organic-inorganic hybrid thin films consists of polymethylsilsesquioxane (PMSQ), and its applications for the gate-insulating layer of O-TFTs are introduced in this paper. PMSQ synthesized in toluene solution with formic acid catalyst exhibited the electric resistivity of higher than 10^{14} Ω cm after thermal treatment at 150°C, and the very low concentration of residual silanol groups in PMSQ was confirmed. The PMSQ film contains no mobile ionic impurities, and this is also important property for the practical use for the gate-insulating materials. In the case of top-contact type TFT using poly(3-hexylthiophene) (P3HT) with PMSQ gate-insulating layer, the device properties were comparable with the TFTs having thermally grown SiO_2 gate-insulating layer. The feasibility of PMSQ as a gate-insulating material for O-TFTs, which was fabricated on a flexible plastic substrate, has been demonstrated. Moreover, by the modification of PMSQ, further functionalities, such as surface hydrophobicity, high permittivity that allows low driving voltage, and photocurability that allows photolithography, could be appended to the PMSQ gate-insulating layers.

1. Introduction

Organic thin-film transistor (O-TFT) is an indispensable component in the development of large-area, flexible, and low-cost electronic devices, such as paper-like displays, radio frequency identification tags, and high-performance sensors. However, as the conventional method of O-TFT fabrication, which includes multiple steps of vacuum processing, is complicated and costly, the convenient fabrication process for O-TFT is required in the industrial demand. Thus, the solution based method has attracted increasing attention to achieve low-cost fabrication of O-TFTs. Printable organic semiconductors have been widely investigated [1, 2] and the wide technology for printed electronics is progressing rapidly. As a solution processible gate-insulating layer for O-TFT devices, various organic polymers have been examined, including polyvinylphenol (PVP) [3, 4], polymethylmethacrylate [5], polyimide [6], and polyvinylalcohol [7], so far. Since organic polymer based gate-insulating materials exhibited lower electric and chemical resistivity than that of inorganic dielectrics, those organic polymers are not the optimum material for the insulating layer of multilayered electronic devices. On the other hand, organic-inorganic hybrid materials will be the most promising materials that can solve these problems, because organic-inorganic hybrids are expected to have specific properties derived from both organic and inorganic component, that is, solution processibility, flexibility, and high resistivity. In the point of view from organic-inorganic hybrids, we have developed novel organic-inorganic hybrid materials that can make a gate-insulating layer of O-TFT by a simple solution process. In this paper, our recent progresses on the construction of organic-inorganic hybrid thin films consist of polysilsesquioxane, and its applications for the gate-insulating layer of O-TFTs are introduced.

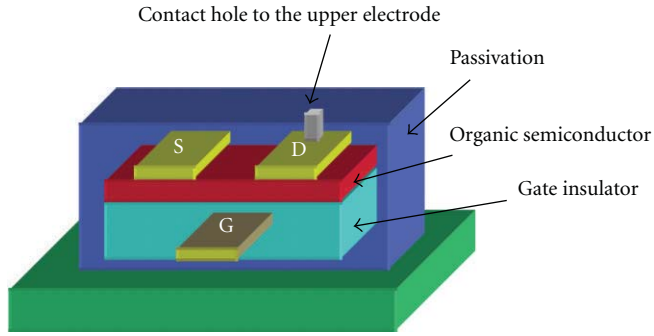

Figure 1: Device structure of O-TFT (bottom-gate/top-contact type).

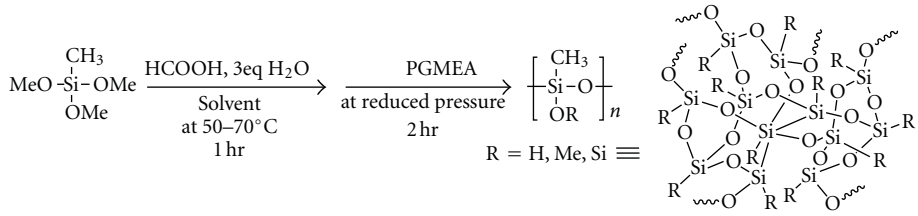

Figure 2: Synthesis of polymethylsilsesquioxane (PMSQ).

2. Required Properties of Gate-Insulating Layer for O-TFT

As shown in Figure 1, a bottom-gate/top-contact type O-TFT consists of a gate electrode, gate-insulating layer, organic semiconductor layer, and source and drain electrodes, respectively. Furthermore, in order to keep the high durability of O-TFT component, the O-TFT must be covered by a passivation layer, and an upper electrode is formed on the passivation layer. The upper electrode is connected with the drain electrode through a contact hole in the passivation layer, which transfers electric signals from O-TFT to a driving electrode of devices such as liquid crystal or electric paper ink. In those components of O-TFT, electric resistivity and permittivity of the gate-insulating layer are known to largely affect the electric performance of the O-TFT, because charge transfer through the channel, that is, the gap between the source and drain electrodes, is strictly controlled by applied gate-voltage (V_G), which induces electric field through the gate-insulating layer and results in charge accumulation at the interface between the gate-insulating layer and the organic semiconductor layer. In general, the well-known inorganic gate-insulating films, such as silicon nitrate by plasma CVD [8], aluminum oxide [9], and tantalum oxide [10] by sputter process, are prepared by a costly high-temperature vacuum process. There is a requirement of optimized material for gate-insulating layer to manufacture high-performance O-TFTs. In case of fabricating O-TFT onto flexible plastic substrates, the most important requirement is a low-temperature curability, since there is a limitation of process temperature. As a material must form a cross-linked thin film at relatively low temperature, polysilsesquioxane has been recognized as a promising candidate [11–15]. However, previous attempts resulted in low electric resistivity and stability [14, 15], because residual silanol groups in polysilsesquioxane have not condensed completely. It is indispensable for polysilsesquioxane to solve this problem, in order to apply as gate-insulating material of O-TFTs. In addition, gate-insulating materials are also required to be low ionic impurity concentration, high permittivity, high-surface smoothness, low-surface free energy, and so forth. We have developed novel polysilsesquioxanes that accomplished these requirements.

3. Synthesis of Polymethylsilsesquioxane (PMSQ)

Materials for gate-insulating layer of O-TFTs should exhibit high electric resistivity (more than $10^{13}\,\Omega\,\text{cm}$) and high permittivity. As a possible material for such requirements, we investigated polymethylsilsesquioxane (PMSQ) that can be synthesized by sol-gel condensation of methyltrimethoxysilane (Figure 2). In order to develop highly cross-linked PMSQ films with low concentration of residual silanol groups, which have reduced electric resistivity, PMSQ was synthesized under various reaction conditions [16]. ^{1}H-NMR spectra of PMSQ prepared in methanol and toluene are shown in Figure 3. The amounts of silanol Si-O$\underline{\text{H}}$ were estimated based on the amount of silylmethyl group Si-C$\underline{\text{H}}_3$, revealing that silanol content was extremely small when PMSQ was prepared in toluene compared to that in

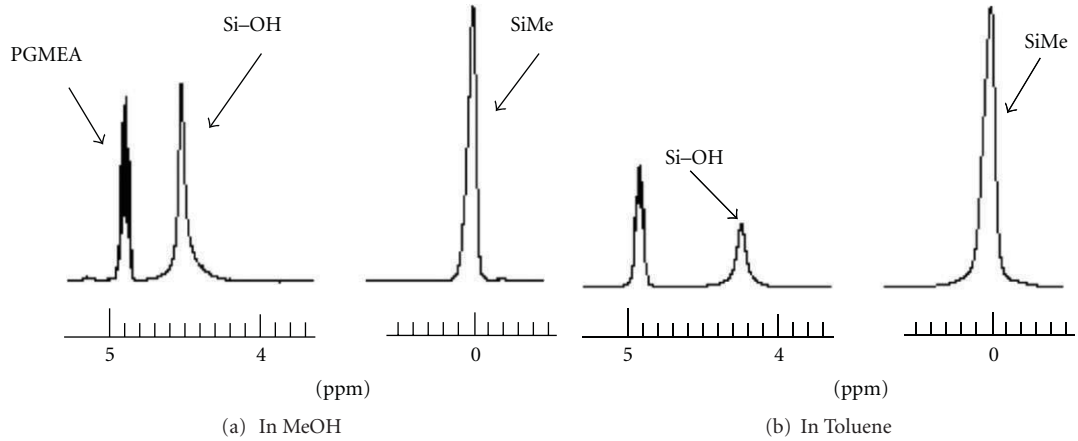

(a) In MeOH (b) In Toluene

Figure 3: ^{1}H-NMR spectra of PMSQ; (a) prepared in methanol, (b) prepared in toluene.

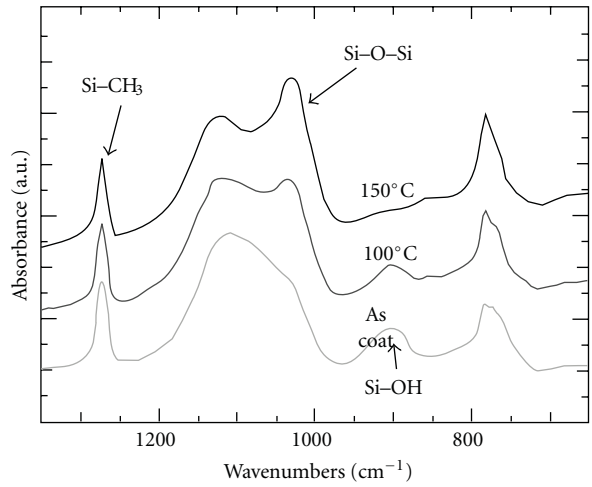

Figure 4: FT-IR spectra of PMSQ films before and after thermal treatment at 100°C and 150°C for 1 h in air.

Table 1: Properties of PMSQ prepared in different solvents.

Solvent	Temperature (°C)	Mw[a]	Mw/Mn	ε (10 kHz)[b]	Ω cm[b]
MeOH	50	6150	8.31	5.4	7.2×10^{12}
Toluene	50	4700	5.79	4.2	1.6×10^{14}
PGMEA	70	3960	3.46	4.3	3.8×10^{13}

[a] Estimated by GPC in THF using polystyrene standards.
[b] Baking temperature: 150°C.

methanol. Also by a measurement of ^{29}Si-NMR, the amount of highly cross-linked T^3 structure, which is corresponding to the silicon atom attached to one alkyl group and three siloxane groups, was twice larger in toluene than that in methanol. This observation indicates also low concentration of silanol groups. It is found that these results were caused by the difference of the polarity of solvents. In the case of the sol-gel reaction under hydrophobic condition in toluene, the collision frequency of silanol groups will increase by hydrophilic interaction, so that enhances the condensation reaction rate, leading to a decrease in the silanol concentration. On the other hand, the excessive water or methanol molecules in the reaction mixture will stabilize silanol groups, which interfere with the condensation reaction to PMSQ with less residual silanols. Therefore, the condensation was carried out under reduced pressure, as shown in Figure 2, to remove methanol and water from propylene glycol monomethyl ether acetate (PGMEA) solution. For the practical use of PMSQ as a gate-insulating material, PMSQ solution should be coated onto the gate electrode, and the thin film was baked to complete consumption of residual silanols. Figure 4 shows the FT-IR spectra of spin-coated PMSQ films before and after thermal treatment at 100 and 150°C for 1 h in air. The absorption bands at 902 cm^{-1}, 1030 cm^{-1}, and 1270 cm^{-1} are attributed to the bonds of Si–OH, Si–O–Si, and Si–CH_3, respectively. The absorption peak of the silanol groups (Si–OH) disappeared completely, and the intensity of the siloxane bonds (Si–O–Si) markedly increased on thermal treatment at 150°C [17]. This result clearly indicated that the cross-linking reaction of the silanol groups proceeded effectively even at low-temperature treatment less than 150°C, forming the higher cross-linked siloxane network.

Electric resistivity and permittivity of PMSQ thin films prepared in different solvents were measured using Al/PMSQ/Al cell structures fabricated on glass substrates and summarized in Table 1. It was found that the electrical resistivity of PMSQ thin films significantly changed in the range from 10^{12} to 10^{14} Ω cm depending on the organic solvent used in the synthesis. The PMSQ synthesized in toluene exhibited a high resistivity of 1.6×10^{14} Ω cm, which were two orders of magnitude higher than that synthesized in methanol. Current density-electric field characteristics shown in Figure 5(a) also revealed the formation of dense siloxane networks in the PMSQ film which were cured at 150°C. The PMSQ film had a very high breakdown field of over 3.0 MV cm^{-1} and exhibited an extremely low leakage current, which was much lower than that of

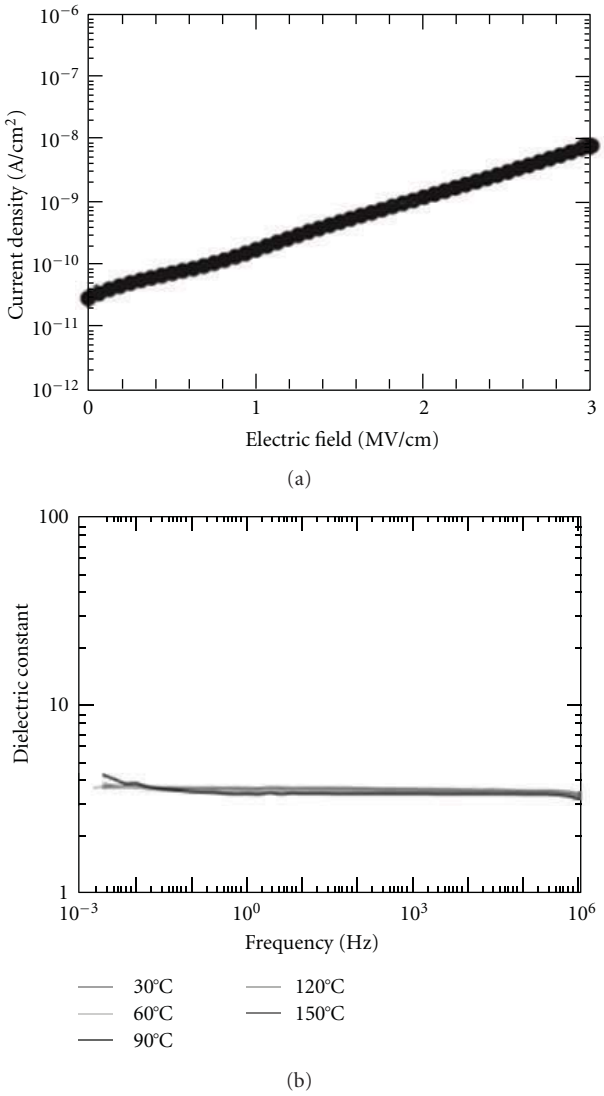

Figure 5: (a) Current density-electric field characteristics and (b) frequency dependence of dielectric constant of PMSQ film cured at 150°C for 1 h in air.

PVP and polyimide [18] and more than two orders of magnitude lower than that of previously reported PMSQ films [14]. Furthermore, since mobile ionic impurities in gate-insulating layer seriously suffer the property of O-TFTs, it is important to confirm their existence by means of impedance spectroscopy, that is, measurement of permittivity as a function of frequency in wide range of temperature [19]. As shown in Figure 5(b), the dielectronic constant ($k \sim 3.6$) did not significantly change for wide frequency sweeps (10 mHz~100 kHz) and wide temperature sweeps (30~150°C), which indicated extremely low concentration of mobile ionic impurities. The reason of the absence of mobile ionic impurities is probably due to the preparation condition of PMSQ. The novel synthetic process introduced here utilizes formic acid as a volatile acid catalyst for the sol-gel reaction, and after the condensation, it was completely removed under reduced pressure with exchanging the solvent by adding PGMEA of higher boiling point.

The PMSQ thin films, which were made by spin-coating and subsequent thermal treatment at 150°C, were not dissolved in common organic solvents such as chloroform, toluene, and xylene, which allows the next coating of soluble organic semiconductors, such as poly(3-hexylthiophene) (P3HT), onto the PMSQ gate-insulating layer. The PMSQ thin films have the pinhole-less smooth surface with average roughness of 0.24 nm, which came out by AFM measurements. Relatively less volatile nature of PGMEA and fluidity of PMSQ before the thermal treatment will be attributable to this surface smoothness of the thin films. Moreover, PMSQ film had a hydrophobic surface exhibiting the water contact angle of 90.7°, and this also satisfies one of the requirements for the gate-insulating layer of O-TFTs.

4. Characteristics of PMSQ as a Gate-Insulating Material

Top-contact P3HT TFTs with gate-insulating layer of PMSQ were fabricated on a glass substrate with an indium-tin-oxide (ITO) gate electrode. The spin-coated PMSQ thin films were cured at 150°C for 1 h in ambient air, which were 450 nm in thickness. A solution of regioregular P3HT in chloroform was spin-coated onto the gate-insulating layer, and the source and drain electrodes were evaporated onto the P3HT layer through a shadow mask, as shown in Figure 6 for TFT structure. Figure 7 shows the I_D-V_D output curves and I_D-V_G transfer curves of the P3HT TFT with PMSQ gate-insulating layer (where I_D, V_D, and V_G stand for drain current, drain voltage, and gate voltage, resp.). In Figure 7(a), all curves display good linear and saturation behaviors with no leakage current at $V_D = 0$ V. Figure 7(b) shows that the device exhibited no hysteresis with respect to a V_G sweep from +20 to −80 V and then from −80 to +20 V, indicating that P3HT TFT with PMSQ gate-insulating layer has stable TFT characteristics significantly. For comparison, P3HT TFT using a highly doped Si substrate with a thermally grown SiO_2 gate-insulating layer (365 nm thickness) were also fabricated. The surfaces of the SiO_2 gate-insulating layers were modified with the hydrophobic self-assembled monolayers (SAMs) of alkyltrichlorosilanes with different alkyl lengths (C_nH_{2n+1}-$SiCl_3$, $n = 2$, 6, 12, and 18). The field-effect mobility (μ) and induced threshold voltage (V_{th}) shift for the V_G sweep of the devices with different gate-insulating layer surfaces are summarized in Table 2. P3HT TFT with PMSQ gate-insulating layer exhibited fair TFT characteristics with $\mu = 7.1 \times 10^{-3}$ cm^2 V^{-1} s^{-1} and $V_{th} = -0.3$ V, whereas the device with untreated SiO_2 gate-insulating layer exhibited one order magnitude of small mobility and larger negative V_{th} shift because of hydrophilic surface. The suppression of hysteresis behavior and smaller negative V_{th} shift of the device with PMSQ gate-insulating layer also indicates that cured PMSQ films may contain a small number of uncross-linked residual silanol groups. The mobility of SAM-modified SiO_2 gate-insulating layer showed a close correlation to the water contact angle; that is, a more

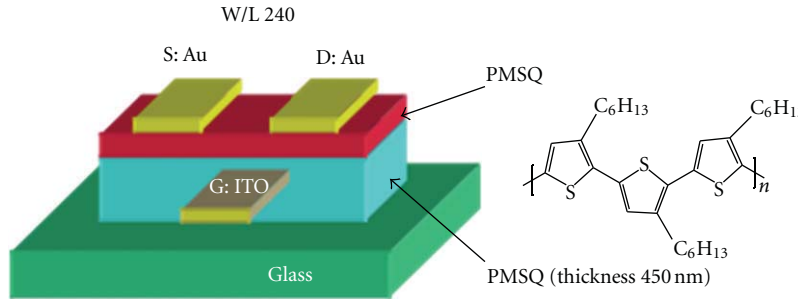

Figure 6: O-TFT (bottom-gate/top-contact type) with PMSQ and P3HT.

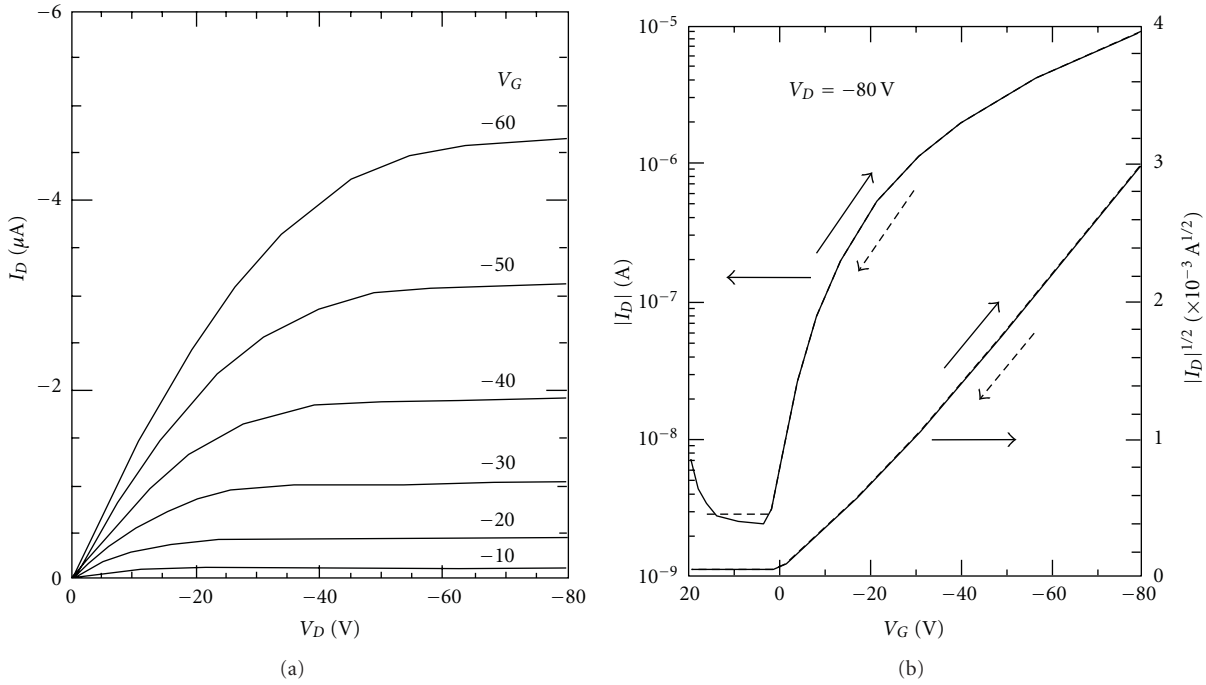

Figure 7: (a) Output and (b) transfer characteristics of P3HT TFT with PMSQ gate insulator.

hydrophobic surface gives a higher mobility. Such behavior has been observed by a number of authors, indicating that mobility enhancement is caused by the improvement in the structural ordering of the P3HT molecules at low-energy surfaces [20–22]. A large contact angle of the PMSQ surfaces would originate from the high density of the methyl groups and the small amount of the residual Si–OH groups, which are responsible for enhanced mobility.

As described above, the spin-coated thin films of PMSQ can be cured at a low temperature of 150°C, which is suitable for a plastic substrate. Thus, fabrications of O-TFTs on flexible plastic substrates were also investigated. Polycarbonate (PC) substrate coated with an indium zinc oxide (IZO) layer was prepatterned by wet etching and used as a gate electrode, a gate-insulating layer of PMSQ was formed by spin-coating and subsequent thermal treatment, followed by spin-coating of P3HT, and source and drain electrodes were thermally deposited [23]. The P3HT TFT fabricated on PC substrate exhibited field-effect mobility of $\mu = 5.8 \times 10^{-3}\,\mathrm{cm^2\,V^{-1}\,s^{-1}}$, which was comparable to those of the devices fabricated on glass substrates. Also, on a polyethylenenaphtalate (PEN) substrate, P3HT TFT with

Table 2: Mobility (μ) and V_{th} with respect to V_G sweep of P3HT TFTs and water contact angle on different insulator surfaces. The alkyltrichlorosilane SAMs are represented as number of alkyl units (n).

Gate insulator	μ ($\mathrm{cm^2\,V^{-1}\,s^{-1}}$)	Water contact angle (degree)	V_{th} (V)
PMSQ	7.1×10^{-3}	93	−0.3
SiO_2	7.8×10^{-4}	25	−2.0
$n = 2$	4.2×10^{-3}	89	−2.5
$n = 6$	1.2×10^{-2}	103	−2.5
$n = 12$	3.0×10^{-2}	106	−2.4
$n = 18$	3.3×10^{-2}	107	−2.4

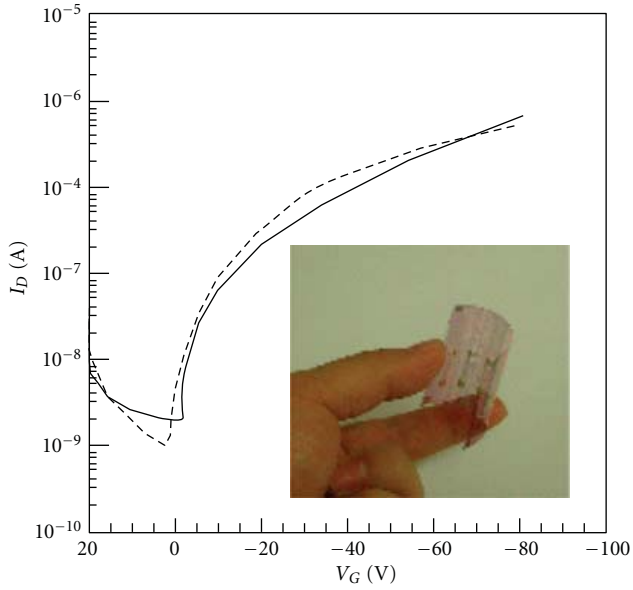

Figure 8: Transfer characteristics of P3HT TFT fabricated on glass substrate (solid line) and PEN substrate (dashed line) at $V_D = -80$ V. Inset: An image of TFT device on PEN substrate (5×5 cm^2).

PMSQ gate-insulating layer has been similarly fabricated [24]. As shown in Figure 8, the transfer characteristic curves of P3HT TFT on a glass substrate and that on a PEN substrate were almost equal each other. The field effect mobility and on/off ratio were also comparable with different substrates as summarized in Table 3. These results demonstrate that low-temperature processible PMSQ is extremely useful gate-insulating material for enhancing electrical stability as well as for a fabrication of printable O-TFTs.

5. Functionalization of PMSQ Gate-Insulating Layer

5.1. Control of Surface Hydrophobicity of PMSQ. As mentioned above, SAM modification on utilizing a thermally grown SiO_2 layer as a gate-insulating layer is essential step for the higher performance of O-TFT. Similarly, we studied to improve the TFT properties by the SAM modification of PMSQ surface [25]. PMSQ was spin-coated on the glass substrates and heated at 80°C for 2 min. At this stage, PMSQ thin films were not completely cured and the silanol could clearly be observed by IR measurement, but as the cross-linked films were not dissolved in organic solvents, the SAM modification could be performed with the remaining silanol group on the surface of PMSQ thin film. After PMSQ thin film on the substrate were immersed in the 5 wt.% various alkyltrichlorosilanes of hexane/chloroform (3 : 1) solution and then washed with hexane as shown in Figure 9, which is a stepwise modification. In order to complete the modification and curing of PMSQ, the substrate was heated at 150°C for 1 h.

Table 3: Device performance (mobility, on/off ratio, and V_{th}) of P3HT TFT on glass and PEN substrate with PMSQ as the gate insulating layers.

Substrate	m ($cm^2\ V^{-1}\ s^{-1}$)	V_{th} (V)	On/off ratio
Glass	4.0×10^{-3}	−18	4.0×10^3
PEN	1.3×10^{-3}	5	4.0×10^3

Table 4: Surface properties of co-PMSQ thin films.

Additive [R-Si(OMe)$_3$] R	mol%	Contact angle (degree)	Surface free energy (mJ m^{-2})
None	—	86.1	28.2
$-(CH_2)_{17}CH_3$	0.5	87.1	28.5
$-(CH_2)_2Ph$	0.5	89.6	27.1
$-(CH_2)_2(CF_2)_5CF_3$	0.5	92.9	24.3
$-(CH_2)_2(CF_2)_5CF_3$	1.0	97.1	22.3

In the case of SAM modification using octadecyltrichlorosilane (OTS), signals of silanol on IR spectra completely disappeared lower than 150°C of thermal treatment, and the film exhibited higher water contact angle of 100°, whereas the nonmodified PMSQ films show lower water contact angle of 89°. To examine the effect of surface modification of PMSQ for O-TFT performance, O-TFTs were fabricated using the nontreated PMSQ and the OTS-treated PMSQ thin films as gate-insulating layers. Figures 10(a) and 10(b) show the output characteristics of P3HT TFTs with the non-treated PMSQ and OTS-treated PMSQ films, respectively. The O-TFT with the OTS-treated PMSQ thin films showed higher mobility and larger on/off ratio compared to that with the nontreated PMSQ films. It will be noteworthy that the mobility of the O-TFT with OTS-treated PMSQ was 4 times larger than that with nontreated PMSQ.

Instead of the SAM modification of PMSQ surface, copolymethylsilsesquoxanes (co-PMSQs), which were prepared from cocondensation of methyltrimethoxysilane and a small amount of alkyltrimethoxysilanes, were used for the direct formation of hydrophobic surface [26]. And co-PMSQ gate-insulating layers were fabricated by a simple spin-coating and subsequent thermal treatment as shown in Figure 11. The relation between the surface free energy of co-PMSQ layer and field effect mobility was investigated. The surface properties of co-PMSQ with several alkyl groups were summarized in Table 4, and it seems that the surface of co-PMSQ thin films were more hydrophobic than that of normal PMSQ, indicating that hydrophobic functional groups migrated and accumulated on the surface. Especially, co-PMSQ derived from tridecafuluoro-1,1,2,2-tetrahydrooctyltrimethoxysilane exhibited very low surface free energy.

Figure 12 shows the relation between the surface free energy and mobility of the O-TFTs fabricated with the co-PMSQ gate-insulating layer. It could be clearly observed that the mobility increased with lower surface free energy. This

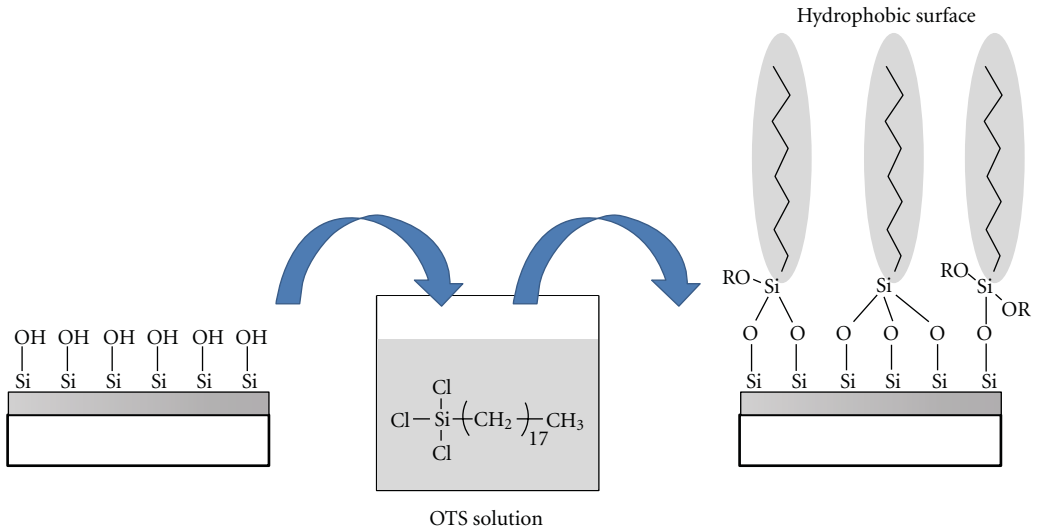

Figure 9: Surface modification of PMSQ film with alkyltrichlorosilane.

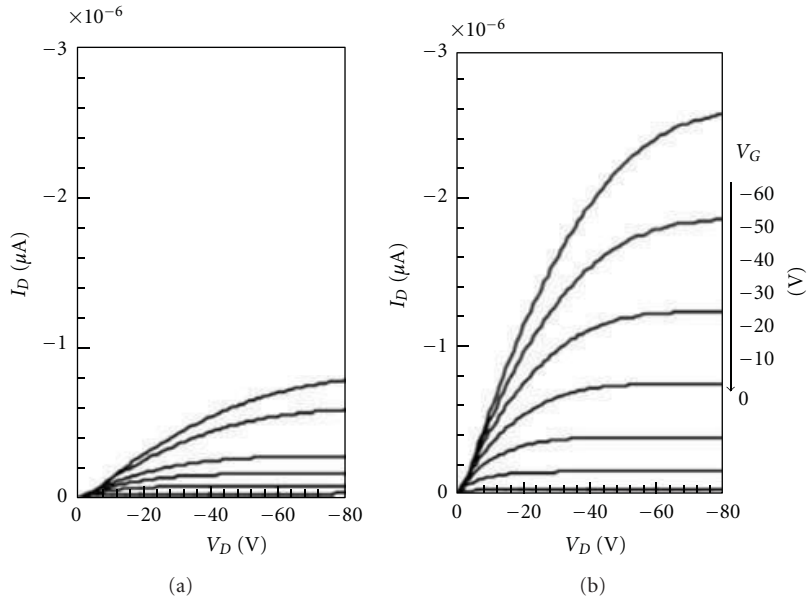

Figure 10: Output characteristics of P3HT TFTs fabricated on (a) non-treated PMSQ film and (b) OTS-treated PMSQ film, at gate voltages $V_G = 0, -10, -20, -30, -40, -50$, and -60 V.

result follows the same tendency of SAM-modified thermal grown SiO_2, and it was concluded that co-PMSQ prepared from cocondensation is an effective gate-insulating materials with a highly hydrophobic surface.

5.2. Improvement of Permittivity of PMSQ. As driving O-TFTs with low operating voltage is an important function for a high performance device, the gate-insulating layer of high permittivity is required. We have also tried to develop polysilsesquioxane having high permittivity. Some modified PMSQs were synthesized by cocondensation of several alkyltrialkoxysilanes and methyltrimethoxysilane. It revealed that the introduction of polar functional groups, such as epoxy and cyano, leads to the co-PMSQs with high permittivity. Co-PMSQ containing epoxy group (PMSQ-epoxy) showed very high permittivity, although TFT properties with PMSQ-epoxy gate-insulating layer was not superior, because hydroxyl groups generated by ring-opening of epoxy groups affected the charge trapping. On the other hand, co-PMSQ containing cyano group (PMSQ-CN), which is a product from cocondensation with cyanoethyltrimethoxysilane, improved permittivity with the increase of cyano group

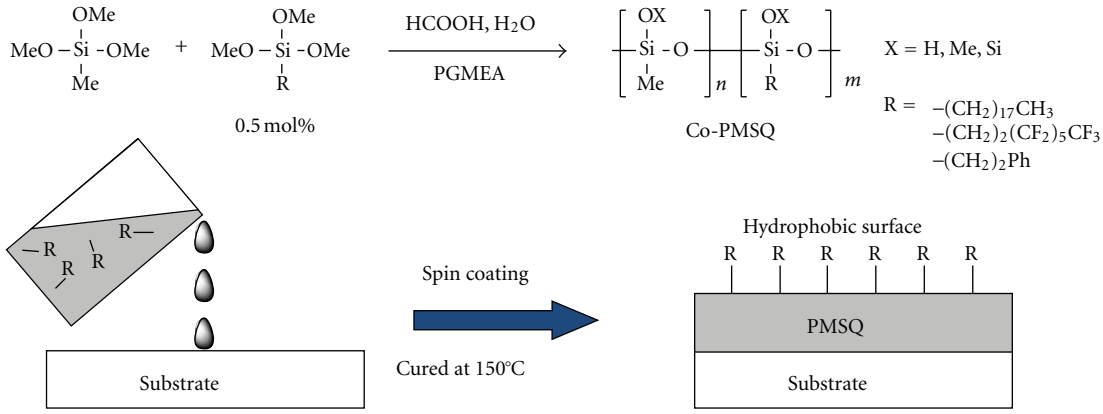

Figure 11: Synthesis of co-PMSQ and fabrication of the hydrophobic gate-insulating layers.

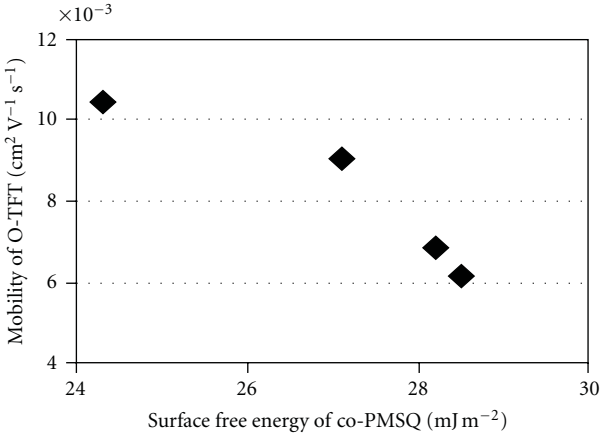

Figure 12: Relationships between mobility of O-TFTs and surface free energy of co-PMSQ gate-insulating layer.

as shown in Figure 13 [24]. When the feed ratio of cyano group was 1 : 1, the permittivity was 3 times larger than that of PMSQ without cyano group. Although PMSQ-CN had slightly less hydrophobic surface than that of normal PMSQ, field-effect mobility using two gate-insulating layer did not differ much. The field-effect mobility (μ) of O-TFTs with PMSQ and PMSQ-CN are 3.7×10^{-3} cm^2 V^{-1} s^{-1} and 2.8×10^{-3} cm^2 V^{-1} s^{-1}, respectively. As clearly shown in Figure 13, I_D of the P3HT TFT with gate-insulating layer of PMSQ-CN was ca. 4 times larger than that of PMSQ without cyano groups at $V_G = -30$ V. This result suggested that required V_G to obtain a certain I_D could be lowered by using PMSQ-CN gate-insulating layer, and thus, PMSQ-CN revealed to be a promising gate-insulating material for the high-performance O-TFT of low-operating voltage.

5.3. Photocurable PMSQ. A photolithography is indispensable process for the fabrication of electric devices using photoresists and UV irradiation. Introduction of photocurability to PMSQ is seemed to become applicable not only for O-TFT, but also various electronic devices. Therefore, the photocurable PMSQ was investigated by introducing photofunctional acrylic groups [27]. As shown in Figure 14, a sol-gel cocondensation of methyltrimethoxysilane and acryloxypropyltrimethoxysilane was carried out under the same condition that have already described above. The spin-coated film of thus obtained copolysilsesquioxane (PMSQ-acryl) with Darocure 1173 as a photoradical initiator was exposed to UV light through a photo mask, then the 250 μm line and space negative-patterns were obtained by the development with 2-propanol. As shown in the inset table in Figure 14, the increasing acrylic groups in PMSQ lead to slightly decrease of electric resistivity. However, these values of resistivity are sufficient for gate-insulating materials of O-TFT. Also, it was found that the thin film from PMSQ-acryl exhibited no permittivity change even in higher temperature by the impedance spectroscopy, which was indicating no existence of ionic impurities. The properties of O-TFT with PMSQ-acryl as a gate-insulating layer were comparable to that with normal PMSQ. These results have suggested that the photo-curable PMSQ is not only useful material as a gate-insulating layer of O-TFT but also promising insulating material for other electronic devices.

6. Conclusion

The term of "printed electronics" refers to electronic devices fabricated by solution processes, which are less energy consumption and cost comparing to vacuum processes. For the sake of achieving printed electronics, there should be close connection between three research steps of material development, process design, and device characterization. We have developed PMSQ derivatives for gate-insulating layer of O-TFT based on three research steps. Possessing the property of both organic and inorganic materials, one of the typical organic-inorganic hybrid materials, polysilsesquioxane, has been revealed to be an important field of materials for printed electronics. The careful investigation of

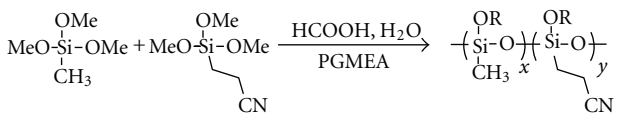

$x:y$	Mw	Mw/Mn	Dielectric constant (10 kHz)	Contact angle
1:0	10600	4.96	4.6	88
3:1	11300	3.9	8.4	85
2:1	7500	3.87	9.9	84
1:1	4200	2.43	13.7	79

(a)

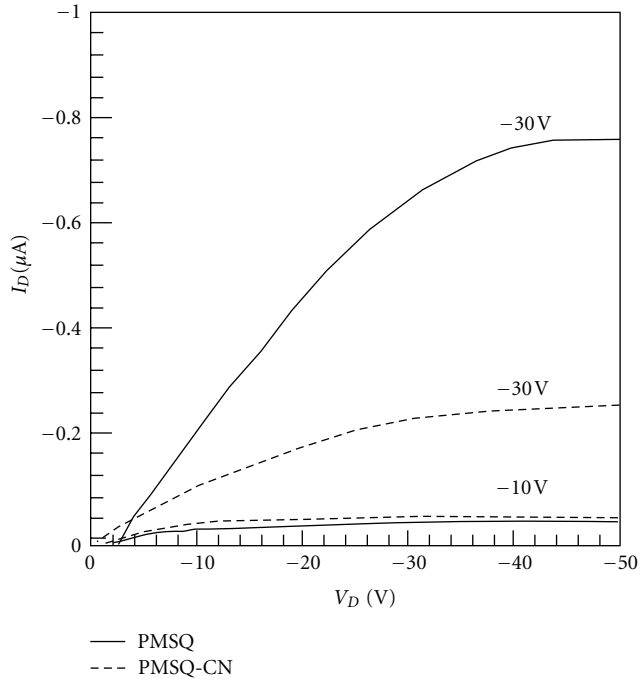

(b)

Figure 13: Synthesis of copolysilsesquioxane (PMSQ-CN) and their properties (a), and output characteristics of P3HT TFT with PMSQ gate-insulating layer (dashed lines) and PMSQ-CN gate-insulating layer (solid lines) at $V_G = -10$ and -30 V (b).

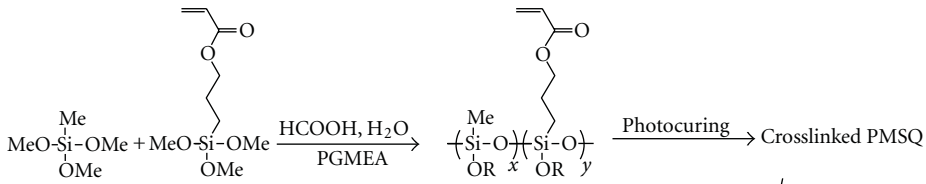

$x:y$	Mw	Mw/Mn	ε	Resistivity (Ωcm)
0.8 : 0.2	4300	2.31	5.3	1×10^{14}
0.5 : 0.5	3000	1.83	5.4	2×10^{13}

(a) Estimated by GPC in THF using polystyrene standards.
(b) Baking temperature: 100°C for 1 h and 150°C for 1 h.
(c) Measured at 1 kHz.

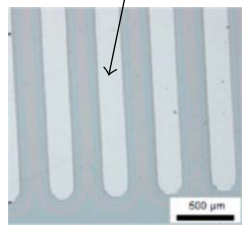

Figure 14: Synthesis of copolysilsesquioxane (PMSQ-acryl) and their properties.

the preparation condition of PMSQs has enabled the development of material suitable for gate-insulating layer of O-TFTs. Recently, we have fabricated flexible O-TFT utilizing PMSQ described above, and succeeded to drive an electric-paper device. The property adjustability of PMSQ, that is, resistivity, surface hydrophobicity, permittivity, and photocurability, suggests further possibility of applications. We are certainly expecting the polysilsesquioxane derivatives to be one of key materials for new electronic devices.

References

[1] H. Sirringhaus, P. J. Brown, R. H. Friend et al., "Two-dimensional charge transport in self-organized, high-mobility

conjugated polymers," *Nature*, vol. 401, no. 6754, pp. 685–688, 1999.

[2] A. Afzali, C. D. Dimitrakopoulos, and T. L. Breen, "High-performance, solution-processed organic thin film transistors from a novel pentacene precursor," *Journal of the American Chemical Society*, vol. 124, no. 30, pp. 8812–8813, 2002.

[3] T. Kawase, H. Sirringhaus, R. H. Friend, and T. Shimoda, "Inkjet printed via-hole interconnections and resistors for all-polymer transistor circuits," *Advanced Materials*, vol. 13, no. 21, pp. 1601–1605, 2001.

[4] H. Klauk, M. Halik, U. Zschieschang, G. Schmid, W. Radlik, and W. Weber, "High-mobility polymer gate dielectric pentacene thin film transistors," *Journal of Applied Physics*, vol. 92, no. 9, p. 5259, 2002.

[5] J. A. Rogers, Z. Bao, A. Makhija, and P. Braun, "Printing process suitable for reel-to-reel production of high-performance organic transistors and circuits," *Advanced Materials*, vol. 11, no. 9, pp. 741–745, 1999.

[6] C. D. Sheraw, D. J. Gundlach, and T. N. Jockson, "Spin-on polymer gate dielectric for high performance organic thin film transistors," *Materials Research Society Symposium Proceedings*, vol. 558, article 403, 2000.

[7] T. B. Singh, F. Meghdadi, S. Günes et al., "High-performance ambipolar pentacene organic field-effect transistors on poly(vinyl alcohol) organic gate dielectric," *Advanced Materials*, vol. 17, no. 19, pp. 2315–2320, 2005.

[8] D. Knipp, R. A. Street, A. Vokel, and J. Ho, "Pentacene thin film transistors on inorganic dielectrics: morphology, structural properties, and electronic transport," *Journal of Applied Physics*, vol. 93, no. 1, article 347, 9 pages, 2003.

[9] J. Wang, X. Yan, Y. Xu, J. Zhang, and D. Yan, "Organic thin-film transistors having inorganic/organic double gate insulators," *Applied Physics Letters*, vol. 85, no. 22, article 5424, 3 pages, 2004.

[10] A. Facchetti, M. H. Yoon, and T. J. Marks, "Gate dielectrics for organic field-effect transistors: new opportunities for organic electronics," *Advanced Materials*, vol. 17, no. 14, pp. 1705–1725, 2005.

[11] Z. Bao, V. Kuck, J. A. Rogers, and M. A. Paczkowski, "Silsesquioxane resins as high-performance solution processible dielectric materials for organic transistor applications," *Advanced Functional Materials*, vol. 12, no. 8, pp. 526–531, 2002.

[12] P. Liu, Y. Wu, Y. Li, B. S. Ong, and S. Zhu, "Enabling gate dielectric design for all solution-processed, high-performance, flexible organic thin-film transistors," *Journal of the American Chemical Society*, vol. 128, no. 14, pp. 4554–4555, 2006.

[13] Y. Wu, P. Lin, and B. S. Ong, "Organic thin-film transistors with poly(methyl silsesquioxane) modified dielectric interfaces," *Applied Physics Letters*, vol. 89, no. 1, Article ID 013505, 2006.

[14] S. Jeong, D. Kim, S. Lee, B. K. Park, and J. Moon, *Applied PhysicsLetters*, vol. 89, Article ID 092101, 2006.

[15] S. Jeong, D. Kim, S. Lee, B. K. Park, and J. Moon, "Influence of silanol groups on the electrical performance of organic thin-film transistors utilizing organosiloxane-based organic-inorganic hybrid dielectrics," *Nanotechnology*, vol. 18, no. 2, Article ID 025204, 2007.

[16] K. Tomatsu, T. Hamada, T. Nagase et al., "Fabrication and characterization of poly(3-hexylthiophene)-based field-effect transistors with silsesquioxane gate insulators," *Japanese Journal of Applied Physics*, vol. 47, no. 4, pp. 3196–3199, 2008.

[17] T. Nagase, T. Hamada, K. Tomatsu et al., "Low-temperature processable organic-inorganic hybrid gate dielectrics for solution-based organic field-effect transistors," *Advanced Materials*, vol. 22, no. 42, pp. 4706–4710, 2010.

[18] S. Y. Yang, S. H. Kim, K. Shin, H. Jeon, and C. E. Park, "Low-voltage pentacene field-effect transistors with ultrathin polymer gate dielectrics," *Applied Physics Letters*, vol. 88, no. 17, Article ID 173507, 3 pages, 2006.

[19] S. Uemura, "Low-frequency dielectric behavior of poly(vinylidene fluoride)," *Journal of Polymer Science*, vol. 12, no. 6, pp. 1177–1188, 1974.

[20] J. Veres, S. Ogier, G. Lloyd, and D. de Leeuw, "Gate insulators in organic field-effect transistors," *Chemistry of Materials*, vol. 16, no. 23, pp. 4543–4555, 2004.

[21] A. Salleo, M. L. Chabinyc, M. S. Yang, and R. A. Street, "Polymer thin-film transistors with chemically modified dielectric interfaces," *Applied Physics Letters*, vol. 81, no. 23, pp. 4383–4385, 2002.

[22] K. P. Pernstich, S. Haas, D. Oberhoff et al., "Threshold voltage shift in organic field effect transistors by dipole monolayers on the gate insulator," *Journal of Applied Physics*, vol. 96, no. 11, pp. 6431–6438, 2004.

[23] S. Yamazaki, T. Hamada, K. Tomatsu et al., "Electrical characteristics of polymer field-effect transistors with poly(methylsilsesquioxane) gate dielectrics on plastic substrates," *Thin Solid Films*, vol. 517, no. 4, pp. 1343–1345, 2008.

[24] T. Hamada, S. Yamazaki, T. Nagase et al., "Chemical design of polysilsesquioxane as a gate insulator for organic thin-film transistors," in *Proceedings of the 15th International Display Workshops (IDW '08)*, pp. 1665–1668, December 2008.

[25] T. Hamada, T. Nagase, T. Kobayashi, K. Matsukawa, and H. Naito, "Effective control of surface property on poly(silsesquioxane) films by chemical modification," *Thin Solid Films*, vol. 517, no. 4, pp. 1335–1339, 2008.

[26] M. Watanabe, K. Muro, T. Hamada et al., "Surface modification of organic-inorganic hybrid insulator for printable organic field-effect transistors," *Chemistry Letters*, vol. 38, no. 1, pp. 34–35, 2009.

[27] T. Hamada, T. Nagase, M. Watanabe, S. Watase, H. Naito, and K. Matsukawa, "Preparation and dielectric property of photocurable polysilsesquioxane hybrids," *Journal of Photopolymer Science and Technology*, vol. 21, no. 2, pp. 319–320, 2008.

Hindawi Publishing Corporation
International Journal of Polymer Science
Volume 2012, Article ID 391325, 14 pages
doi:10.1155/2012/391325

Research Article

A Theoretical Study of the Insertion of Atoms and Ions into Titanosilsequioxane (Ti-POSS) in Comparison with POSS

Yosuke Komagata, Takaaki Iimura, Nobuhiro Shima, and Takako Kudo

Department of Chemistry and Chemical Biology, Graduate School of Engineering, Gunma University, 1-5-1 Tenjin-cho, Kiryu 376-8515, Japan

Correspondence should be addressed to Takako Kudo, tkudo@gunma-u.ac.jp

Received 9 June 2012; Revised 26 August 2012; Accepted 26 August 2012

Academic Editor: Kensuke Naka

The insertion reaction of various guest species, such as rare gases (He, Ne, and Ar), cations of group 1 (Li^+, Na^+, and K^+), and anions of group 17 (F^- and Cl^-) elements, into the Ti analogues of POSS (polyhedral oligomeric silsesquioxanes), Ti-POSS, $[HTiO_{1.5}]_n$ (n = 8 and 10), has been investigated by ab initio molecular orbital and density functional methods. For each case, the properties of the exohedral and endohedral complexes and transition-state structure connecting them on the potential energy surface and energetics are discussed in comparison with the case of POSS. Furthermore, in order to understand the origin of the stability of these structures, the binding energy (ΔE_{comp}) and the energy barrier of the encapsulation are analyzed by an energy decomposition method. As a result, some similarities and differences between Ti-POSS and POSS were explored.

1. Introduction

Polyhedral oligomeric silsesquioxanes (POSS), $[RSiO_{1.5}]_n$ (n = 4, 6, 8, 10, 12, ...), referred to as T_n, have been the focus of considerable experimental and theoretical interest because of their wide variety of practical uses for many years [1–4]. Among a huge number of investigations for these diverse polyhedral compounds, the approach to make use of their cavity for various purposes, such as a container of atomic or molecular species [5–19], medical supplies [20, 21], molecular sieves, or a reaction filed for H_2 formation [22], is one of the extremely attractive research areas of the POSS chemistry. In addition to many interesting experimental observations, theoretical studies have been making considerable contributions in this area. For example, there are systematic and comprehensive studies for the encapsulation of various atomic or ionic species into T_8 and T_{10} by Hossain et al. [9, 13, 15, 16]. Furthermore, incorporation of molecular species such as H_2, N_2, and O_2 inside T_n (n = 6–12) that also been investigated by our group [5, 18, 19]. These studies must give useful information for the future design of the molecular sieve or better drug delivery.

On the other hand, metal-substituted POSS (metallasilsesquioxanes) where the skeletal silicon atoms of POSS are all or partially replaced with various metals such as group 4 (Ti, Zr, and Hf) [23–29] or other heavier group 14 (Ge Sn) [29] elements are also fascinating research targets. The titanosilsequioxanes especially (Ti-T_n) have extensively been studied both by experimental and theoretical chemists because of their potential as useful materials such as promising catalysts. For the experimental works, the titanium-substituted T_8 with the $TiSi_7O_{12}$ core [24, 26] and even the Si/Ti-alternated T_8 with the $Ti_4Si_4O_{12}$ core [23, 25] have already been synthesized and their stability or catalytic activity investigated years ago. On the other hand, not for Ti-POSS but some theoretical studies on the structures and catalytic reactions of the model compounds of titanosilicate or titanium-containing zeolites are available [30, 31]. In the past several years, therefore, we have studied the structures and catalytic ability of the titanium analogues of POSS, $[HTiO_{1.5}]_n$ and $H_8Ti_pSi_{8-p}O_{12}$ [27]. Incidentally, the experimental result [23] for the structure of the Si/Ti-alternated T_8 is in good agreement with our calculational result [27]. Our next target is their various intramolecular

Table 1: Some geometrical parameters (Å and degrees), the averaged net atomic charge, [a]energy level of HOMO and LUMO, and the HOMO-LUMO energy gap (hartree)[c] of Ti-T_8 and Si-T_8 at the B3LYP/6-311+G(d) level.

A	A-O	A-H	<AOA	<OAO	C^b-A	C^a-O
Si	1.644	1.460	148.4	109.2	2.744	2.690
Ti	1.811	1.697	149.1	109.1	3.023	2.951
A	q_A[a]	q_o[a]	HOMO[c]	LUMO[c]	$\Delta E^c_{(H\text{-}L)}$	
Si	2.131 (0.767)	−1.268 (−0.474)	−0.319 [−0.483]	−0.007 [0.052]	0.312 [0.535]	
Ti	1.313 (0.202)	−0.787 (−0.110)	−0.328 [−0.464]	−0.139 [0.019]	0.189 [0.483]	

[a]NBO and Mulliken (in parentheses) net atomic charges on A (Si and Ti) and O atoms.
[b]C is the center of the cage.
[c]The HF/6-311+G(d) values are in square brackets.

reactions. Therefore, in the present study, as a continuation of our theoretical approach for Ti-POSS and to deepen our understanding for POSS, the result of the investigation for the encapsulation of various atoms and ions into Ti-T_8($[HTiO_{1.5}]_8$) is shown and discussed in comparison with the case of the Si analogue, T_8($[HSiO_{1.5}]_8$).

2. Computational Methods

Geometry optimizations were performed for all of the molecules investigated here at the Hartree-Fock (HF) and a hybrid type of the HF and DFT theories, B3LYP [32] levels of theory. For the basis set, 6-311+G(d) [33–35] was finally chosen after the investigation of several kinds of basis sets. We have investigated the effect of six kinds of basis sets (6-31G(d), 6-311G(d), 6-31+G(d), 6-31G(d,p), 6-31+G(d,p), and 6-311+G(d)) for the geometries of exohedral and endohedral complexes between X (He and F^-) and Ti-T_8 at the HF and B3LYP levels of theory. As a result, a set of p functions on hydrogen atoms is found to have small effect so it was not considered in this study. All optimized geometries were characterized as minima or transition states by normal frequency mode analyses. In addition, single point energy calculations on the optimized geometries were carried out at the second-order perturbation (MP2) [36] level of theory for a part of the system involving F^- to obtain more reliable energetics. Finally, the relative energies of the stationary points were corrected by considering the zero point energy (described as "+ZPC").

Furthermore, in order to explore the origin of the stability of the stationary points on the potential energy surface of the encapsulation reactions in detail, we carried out a kind of energy decomposition for the binding energy (ΔE_{comp}) between the guest species and the host Ti-T_n cage. The ΔE_{comp} is the energy accompanying the formation of complexes (exohedral and endohedral complexes, and the transition-state structures connecting them), and it is decomposed into two kinds of energy—(a) the deformation energy (ΔE_{def}) of the host cage caused by the complexation, and (b) the interaction energy (ΔE_{int}) between the guest species and the deformedhost cage:

$$\Delta E_{comp} = \Delta E_{def} + \Delta E_{int}. \quad (1)$$

The former always brings about the destabilization of the system, but even the latter is possible to contribute the destabilization (repulsion) as well as the stabilization. The "minus" value means stabilization, while "plus" does destabilization of the system relative to the referred one for the binding energy (ΔE_{comp}) and both energy components, ΔE_{def} and ΔE_{int}.

The ΔE_{def} is obtained as the energy difference between the deformed cage ($E_{deformed\ cage}$) and the optimized (empty) one ($E_{pure\ cage}$):

$$\Delta E_{def} = E_{deformed\ cage} - E_{pure\ cage}. \quad (2)$$

On the other hand, the ΔE_{int} is defined as the energy difference between the complexes (E_{comp}) and the sum of two energy components as shown as follows:

$$\Delta E_{int} = E_{comp} - \left(E_{deformed\ cage} + E_{guest\ species}\right). \quad (3)$$

As a result, the ΔE_{comp} can be described as another formula as expected:

$$\Delta E_{comp} = E_{comp} - \left(E_{pure\ cage} + E_{guest\ species}\right). \quad (4)$$

All calculations were performed with the Gaussian 03 [37] and GAMESS [38, 39] electronic structure codes.

3. Results and Discussion

3.1. Ti-T_8 versus Si-T_8. Before discussing the encapsulation reaction, it may be worth to compare some properties of the host molecule, Ti-T_8, $(HTiO_{1.5})_8$, with those of the Si analogue, T_8, $(HSiO_{1.5})_8$. Both molecules have highly symmetric O_h structure [27]. The geometric parameters, the averaged NBO [40] and the Mulliken net atomic charge of the skeletal atoms, and the energy levels of the frontier orbitals (the Kohn-Sham orbitals in the DFT results) of both molecules are shown in Table 1. As the table shows, all distances in Ti analogue are longer than those in T_8, suggesting Ti–T_8 has the larger cavity compared to that of the Si analogue. It is convenient for the encapsulation of guest species as well as the extremely floppy titanoxane (Ti–O–Ti) bonds in the framework suggested by our previous study [27]. The two kinds of the bond angles, however, are very similar in both molecules.

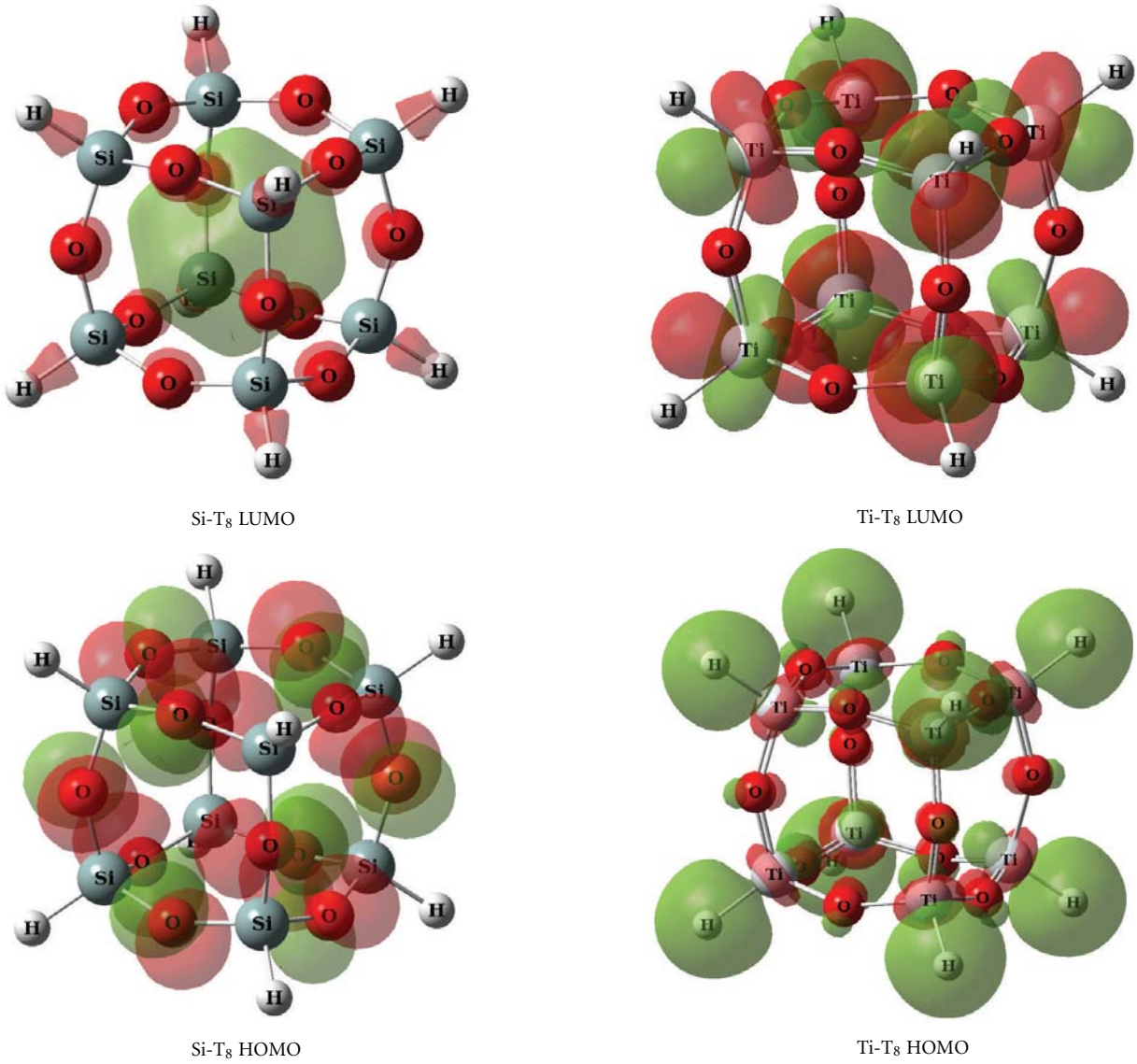

Figure 1: The HOMO and LUMO of T_8 and Ti-T_8 at the B3LYP/6-311+G(d) level.

In addition, the averaged net atomic charges in the table suggest that the Ti–O bond is less polarized compared to the Si–O, which is in agreement with our previous results for the siloxane and titanoxane compounds ($H(OH)_2XOX(OH)_2H$; X = Si and Ti) [29]. In the Si/Ti-mixed POSS, however, Ti atom is found to have larger positive charge than that of Si atoms [27]. As the present basis set involves the diffuse functions, absolute values of the Mulliken charge seem to be remarkably underestimated compared to those of the NBO charge.

On the other hand, the B3LYP level significantly underestimates the HOMO-LUMO gap compared to the corresponding value obtained at the HF level, as expected. According to the HF results, the HOMO is higher and LUMO is lower in Ti-T_8 than in T_8, which makes the HOMO-LUMO energy gap of the T-T_8 slightly smaller compared to that of T_8. Nevertheless, the figures of the orbitals, especially for HOMO, are very similar in the HF and B3LYP levels. As seen from Figure 1, the d orbitals on Ti atoms seem to play an important role for both frontier orbitals in Ti-T_8 while the contribution of the p orbitals on oxygen atoms seems to be large in T_8.

3.2. Insertion of Rare Gas Elements (He, Ne, and Ar). In Scheme 1 displayed is the schematic process of the insertion of some rare gas elements and cations into Ti-T_8. As seen in the scheme, the guest species and Ti-T_8 form exohedral complex (X(Ti-T_8)) where the rare gas elements are above the center of a D_4 ($(HTiO)_4$) face of the cage first. Then the species inserts into the host cage via the transition-state structure with keeping the same C_{4v} symmetry as the first complex. The resultant endohedral complex (X@(Ti-T_8)) has the guest species in the center of the cage so the symmetry is as high as D_{4h} (O_h).

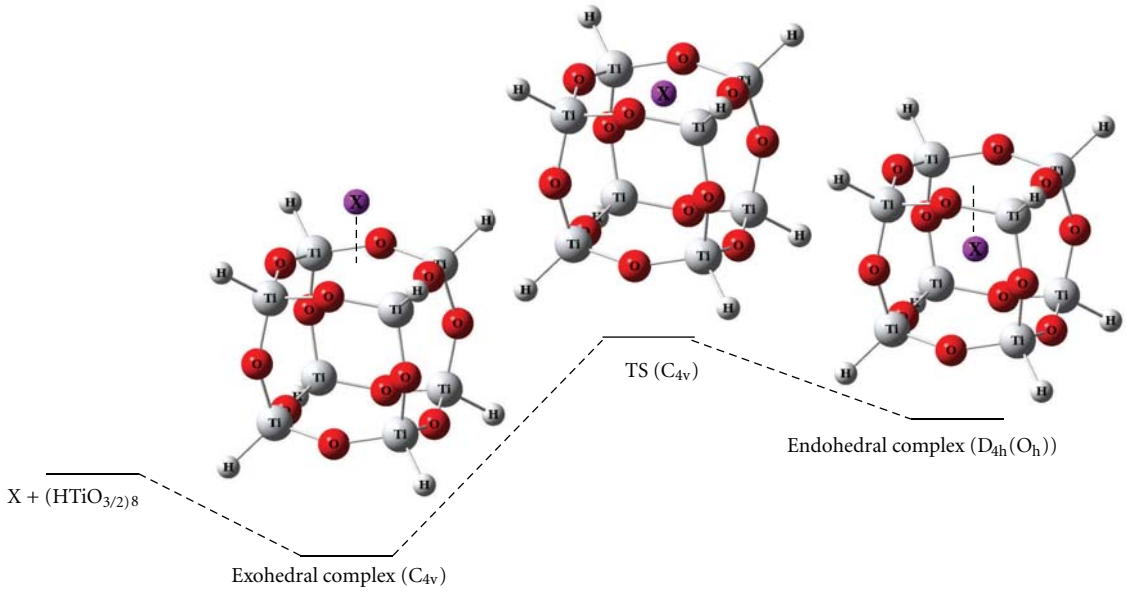

Scheme 1

The B3LYP/6-311+G(d) geometries of these structures are depicted in Tables 2 and 3. For the exohedral complexes, as Table 2 shows, the attached species X is far from the cage (>3 Å). Also, for the endohedral complexes, the geometry of the host cage does not largely change by the inclusion of guest species except for the heaviest rare gas element in this study, Ar atom. On the other hand, for the transition-state structures (see Table 3), the geometry of the D_4 face where the insertion takes place is remarkably expanded and the extent becomes large as the atomic radius of the guest element becomes large in the order He < Ne < Ar as expected. The other faces are not much affected as seen in the H_2 insertion into POSS [18].

The energetics of the insertion reaction in Table 4 show that the energy barrier increases as the atomic radius of the guest element increases as expected from the geometrical change mentioned above. Apparently, the inclusion complex is less stable than the exohedral complex but that may be possible to exist because of the large release energy in all cases.

On the other hand, the binding energies (ΔE_{comp}) together with the result of energy decomposition are summarized in Table 5. For the rare gas elements, ΔE_{comp} and the two energy components (ΔE_{def} and ΔE_{int}) of the exohedral complex are very small. Furthermore, the absolute values of the deformation energy (ΔE_{def}) of the endohedral complex and the transition structure are much smaller than those of the interaction energy (ΔE_{int}). These results suggest that the encapsulation of the rare gas elements has just a small effect for the cage of Ti-T_8 and the origin of the binding energy is mainly the repulsion with the cage and not the deformation of the cage.

The reaction mechanism and the structures of the stationary points are similar to those of the Si analogue by Park et al. [9].

3.3. Insertion of Cations of Alkali Metal Elements (Li^+, Na^+, and K^+). The insertion reaction discussed next is that of the cations of three alkali metal (group 1) elements. Among these, the reaction of the Na^+ and K^+ resembles that of the rare gas elements and the structures of the stationary points are also similar. For the exohedral complexes, the distance between the cations and the cage is smaller than that of the rare gases as shown in Table 2. The same is true in the r(X-O), while the opposite (longer) is seen in the r(X-Ti), for the endohedral complexes. This may be explained from the electrostatic interaction between the plus charge of the guest cations and skeletal $Ti^{\delta+}$ and $O^{\delta-}$ atoms of the host. Such interaction especially in the endohedral complex of Na cation is considered to be significant as the symmetry of the structure of Na^+@Ti-T_8 is reduced from D_{4h} to C_{2v}. This is in sharp contrast to the fact that the Si analogue keeps the highest symmetry in the endohedral complex, Na^+@T_8 [9].

In contrast, the both complexes of Li^+ are quite different with other cases as shown in Figure 2. There is another exohedral complex (exo-2) in addition to the normal C_{4v} structure (exo-1). As the figure shows, Li^+ is attached on one of the skeletal oxygen atoms in "exo-2" while the cation interacts with all oxygen atoms of the D_4 face in "exo-1" and the former is 0.6 kcal/mol less stable than the latter. Furthermore, two types of the endohedral complex ("endo-1" and "endo-2") were located as in the case of the Si analogue [9]. The "endo-1" has the stretched cubic structure with the D_{4h} symmetry, while in "endo-2" the cage is remarkably deformed

Table 2: Some geometrical parameters (Å and degrees) of X(Ti-T_8) and X@(Ti-T_8); X = He, Ne, Ar, Na^+, K^+, Cl^- at the B3LYP/6-311+G(d) level.

X	X(Ti-T_8) (exohedral complex)				X@(Ti-T_8) (endohedral complex)					
	sym	r(X-S[a])	r(X-Ti)	r(X-O)	sym	r(X-S[a])	r(X-Ti)	r(X-O)	<TiOTi	<OTiO
Pure					D_{4h}	1.746	3.023	2.950	149.1	109.1
He	C_{4v}	4.217	4.885	4.396	D_{4h}	1.748	3.028	2.950	149.4	108.9
Ne	C_{4v}	3.504	4.284	3.782	D_{4h}	1.750	3.031	2.954	149.3	109.0
Ar	C_{4v}	5.292	5.838	5.365	D_{4h}	1.757	3.043	2.975	148.8	109.3
Na^+	C_{4v}	2.119	3.247	2.545	C_{2v}	1.716	3.069	2.595	154.9	103.1
K^+	C_{4v}	2.769	3.698	3.028	D_{4h}	1.790	3.101	2.892	157.2	104.7
Cl^-					D_{4h}	1.707	2.959	3.053	139.1	113.7

[a]The center of a D_4 face.

Table 3: Some geometrical parameters (Å and degrees) of the D_4 face where the insertion takes place in the transition structure connecting X(Ti-T8) and X@(Ti-T8); X = He, Ne, Ar, Na^+, K^+, Cl^- at the B3LYP/6-311+G(d) level.

X	sym	r(X-Ti)	r(X-O)	r(Ti-O)	<TiOTi	<OTiO
Pure	D_{4h}	2.468	2.114	1.811	149.1	109.1
He	C_{4v}	2.503	2.160	1.833	148.4	112.7
Ne	C_{4v}	2.510	2.267	1.860	143.5	119.0
Ar	C_{4v}	2.553	2.431	1.924	138.7	126.5
Na^+	C_{4v}	2.629	2.107	1.889	159.6	103.5
K^+	C_{4v}	2.676	2.299	1.951	150.7	112.7
Cl^-	C_{4v}	2.440	2.507	1.906	129.5	136.7

Table 4: The B3LYP/6-311+G(d)+ZPC relative energy (kcal/mol) of the exohedral (X(Ti-T8)) and endohedral (X@(Ti-T8)) complexes (X = He, Ne, Ar, Li^+, Na^+, K^+, and Cl^-) and the transition state (TS) connecting them and the release energy (ΔE) of X from the endohedral complex.

X	X(Ti-T_8)	TS	X@(Ti-T_8)	Release ΔE
He	0.0	31.2	7.6	23.6
Ne	0.0	58.3	11.6	46.7
Ar	0.0	145.2	46.0	99.2
Li^+	0.0	27.8	25.8	2.0
Na^+	0.0	60.7	31.7	29.0
K^+	0.0	150.9	53.6	97.3
Cl^-	0.0	83.5	7.7	75.8

compared to "endo-1." The large deformation of the cage in both structures is brought about by the strong interaction between Li^+ and skeletal oxygens as indicated by the short Li–O distances of 2.181 and 2.081 Å in the planar or tetrahedral Li^+O_4 moiety of "endo-1" and "endo-2," respectively. As a result, the symmetry of "endo-2" is reduced to D_{2d}, and this is found to be more stable than "endo-1" by 2.2 kcal/mol at the B3LYP/6-311+G(d) +ZPC level. These are the same trend in the $Li^+@T_8$ [9].

Figure 3 shows the potential energy surface of the insertion of Li^+ into Ti-T_8. The exo-2 and endo-1 are not involved in the figure. It is noteworthy that Li^+ seems to keep some interaction with several specific oxygens during the insertion process as the transition-state structure is not symmetric with respect to the center.

The energetics of the insertion reaction of these cations can be compared with those of rare gas elements in Table 4. The energy changes with regard to atomic number in both groups resemble each other. As the atom becomes heavy in each group, the energy barrier becomes high and the endohedral complex becomes less stable. However, the stability of the endohedral complex relative to the exohedral complex is smaller in the cations compared to the rare gas elements. For the case of Li^+, especially the release energy is too small (2.0 kcal/mol) for $Li^+@$Ti-T_8 to exist stably. As a result, for the encapsulation of Li^+ in Ti-T_8, only the exohedral complex is predicted to be existable. On the other hand, the endohedral complex of the other cations is kinetically existable but the energy barrier is too high for the exohedral complex to isomerize to the endohedral complex at least in the room temperature.

As Table 5 shows, the deformation energy (ΔE_{def}) of the exohedral complex of the cations is much larger than that of the rare gas elements as expected from the significant

Table 5: Energy decomposition of the binding energy (ΔE_{comp}) (kcal/mol) of the complexes of various guest species and Ti-T8 and the transition state connecting the complexes at the B3LYP/6-311+G(d) level.

	X	sym	ΔE_{def}	ΔE_{int}	ΔE_{comp}	ΔE_{comp} + ZPC
Exo	He	C_{4v}	0.0	−0.2	−0.2	−0.1
	Ne	C_{4v}	0.0	−0.3	−0.3	−0.2
	Ar	C_{4v}	0.0	0.0	0.0	0.0
	Li^+	C_{4v}/C_1	17.4/11.8	−56.9/−50.6	−39.5/−38.8	−38.1/−37.5
	Na^+	C_{4v}	11.7	−33.9	−22.2	−21.6
	K^+	C_{4v}	7.9	−19.9	−12.0	−11.8
	Cl^-	Cs	35.9	−93.6	−57.7	−57.4
Endo	He	D_{4h}	0.1	6.6	6.7	7.5
	Ne	D_{4h}	0.1	10.6	10.7	11.4
	Ar	D_{4h}	1.4	43.7	45.1	46.0
	Li^+	D_{2d}/D_{4h}	31.9/27.7	−45.9/−39.0	−14.0/−11.3	−12.3/−10.1
	Na^+	C_{2v}	16.3	−6.6	9.7	10.1
	K^+	D_{4h}	15.4	25.7	41.1	41.8
	Cl^-	D_{4h}	17.3	−67.5	−50.2	−49.7
TS	He	C_{4v}	2.0	27.3	29.3	31.1
	Ne	C_{4v}	10.2	47.0	57.2	58.1
	Ar	C_{4v}	39.4	106.0	145.4	145.2
	Li^+	C_s	28.3	−40.0	−11.7	−10.3
	Na^+	C_{4v}	22.2	15.6	37.8	39.1
	K^+	C_{4v}	45.6	93.7	139.3	139.1
	F^-	C_1/C_1	50.6/52.8	−136.9/−131.6	−86.3/−78.8	−85.7/−77.9
	Cl^-	C_{4v}	59.0	−32.2	26.8	26.1

geometrical changes mentioned above. The host cage is considerably destabilized as suggested by the large value of ΔE_{def}, but the stabilization by ΔE_{int} overwhelms the disadvantage so the complex becomes more stable than the isolated cation and cage eventually in all cases. The large plus values of ΔE_{def} (destabilization) and large minus values of ΔE_{int} (stabilization) in the cation complexes compared to those of the rare gases may be explained from the electrostatic interaction between the plus charge of the cations and the skeletal elements. For all stationary points of the cations, as ionic radius becomes small, ΔE_{def} becomes large (destabilized) and ΔE_{int} becomes small (largely minus, stabilized) except for ΔE_{def} of the transition-state structure of K^+. Here, it may be interesting to compare the ΔE_{int} of isoelectronic pairs, He/Li^+, Ne/Na^+, and Ar/K^+. The NBO analyses [40] show the plus charge of the free cations (formally 1) is significantly reduced by the complexation, such as Li^+ (exo-1/exo-2 : 0.777/0.912, end-1/endo-2 : 0.509/0.495), Na^+ (exo: 0.883, endo: 0.484), and K^+ (exo: 0.943, endo: 0.558), suggesting the considerable electrostatic interaction with the host cage and this brings about the large stability of the complexes indicated by the largely minus ΔE_{comp}.

For the endohedral complex of the cations, however, the destabilization caused by the significant geometrical changes mentioned above is more serious compared to the exohedral complexes, as indicated by the larger value of ΔE_{def}. The strong interaction between the cations and skeletal atoms may be the main reason for the large ΔE_{def} as suggested from the geometrical parameters in Table 2. As a result, ΔE_{comp} is still minus for the Li^+@Ti-T_8 while K^+@Ti-T_8 gives remarkably plus value so severe steric repulsion between the guest with large ionic radius and host may be expected in the case of K^+. The value of Na^+@Ti-T_8 is the intermediate between the cases of Li^+ and K^+. Incidentally, ΔE_{comp} of the transition-state structure for the Li^+ case is minus, −11.7 (−10.3 with ZPC) kcal/mol, too. This minus value is caused by the largely minus ΔE_{int} as shown in Table 5. This stabilization may be explained from the unique structure (Figures 2 and 3) mentioned above and makes the TS of the insertion of Li^+ lower compared to that of the other cations and the endohedral complex kinetically unstable.

3.4. Insertion of Anions of Halogen Elements (F^- and Cl^-). Next guests are the minus ions of halogen (group 7). The structures of the complexes and reaction paths of the halogen anions investigated here (especially F^-) are significantly different with those of the rare gas or cationic elements in the preceding sections. Incidentally, there are many comprehensive studies for the encapsulation of F^- into POSS, and it is well known that the endohedral complex F^-@T_8 has been observed experimentally [7, 8, 12].

First, the properties of the complexes between the halogen anions and Ti cage are explained in detail. For F^-, as Figure 4 shows, various kinds of exohedral ((a)–(d)) and endohedral (e) complexes were located but we could not find the exohedral structure with the higher C_{4v} symmetry like the rare gas or cationic species. F^- tends to interact strongly with small number (1 or 2) of skeletal Ti atoms. Among

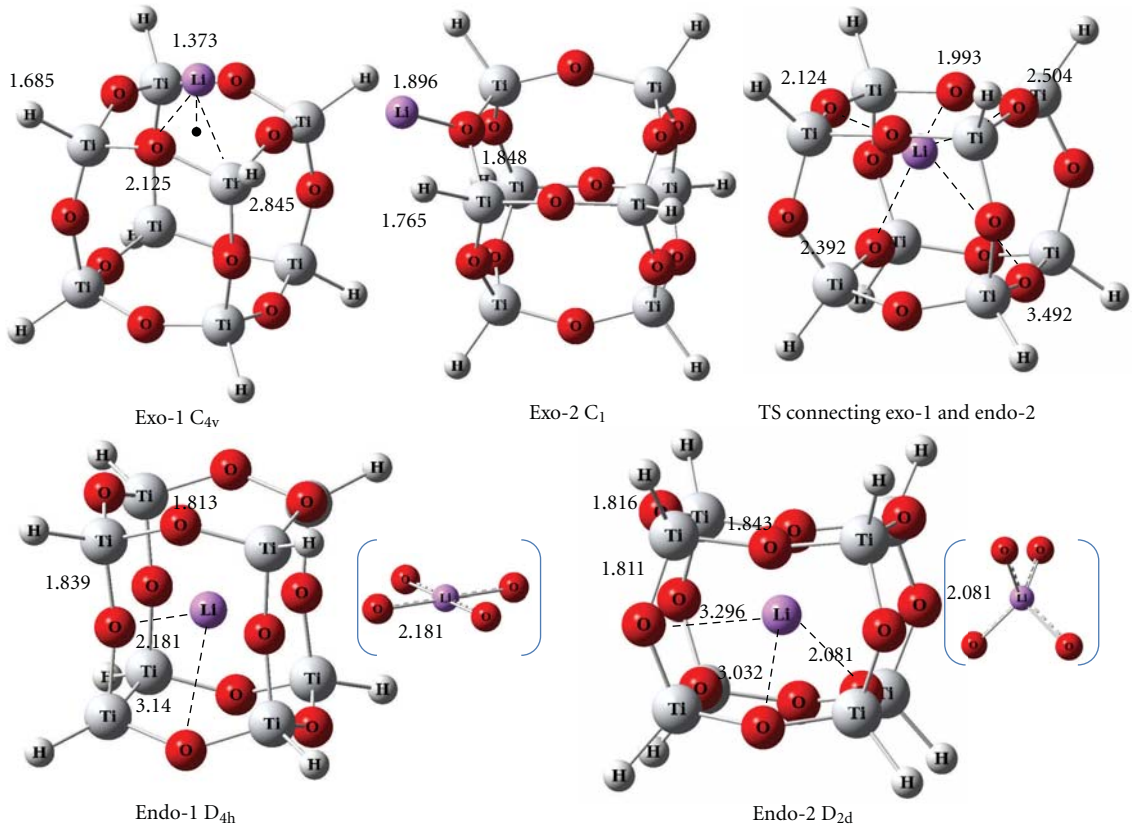

FIGURE 2: The B3LYP/6-311+G(d) optimized geometries of the exohedral and endohedral complexes and the transition state connecting "Exo-1" and "Endo-2" of Li^+ and Ti-T_8 in angstroms.

these, (a) and (b) have the partial triangular bipyramidal structure so we call each of them as "axial" and "equatorial" complex, respectively (see Scheme 2). The similar exohedral complexes are observed in the Si analogue too, though the "equatorial" conformation is not an equilibrium structure [9]. F^- interacts with one Ti atom in (a) and (b) while it does with more than two Ti atoms in the others in Figure 4. Apparently in the diagonally bridged structures, "diagonal-bridge" (d), the Ti-T_8 cage is considerably deformed as suggesting with the largest ΔE_{def}, so it is remarkably less stable than other isomers as seen in Table 6.

On the other hand, the structure of the endohedral complex "endo" (e) is quite interesting since F^- is notthe center of the cage but close to a specific skeletal Ti atom, which is completely different with the initial expectation. As a result, this complex also seems to have the partial triangular bipyramidal structure with F^- at the axial position in a corner of the cage. This is also different with the fact that the F^- is encapsulated in the center of the silicon analogue, T_8 [9]. Nevertheless, Tossell has found that in the larger POSS such as T_{10} and T_{12} with the double-decker structure F^- is bound at the Si atom in a corner of the cage so the present result resembles that [12].

The distance between F^- and the Ti in (e) is 2.321 Å so it is rather longer than 1.814 Å in (a). As apparent from Table 6, the smallest deformation energy among the isomers suggests that this structure does not bring about such a severe energetic damage of the cage seen in the other structures. That is the reason why the endohedral complex (e) is most stable in spite of the smallest interaction energy among the five isomers. The relative stability was found to increase (−3.2 to −7.6 kcal/mol) at the more reliable MP2 level. In order to confirm whether the small space of T_8 triggers such a unique structure, we have investigated the case of larger Ti-T_{10}. However, as Figure S1 (in Supporting Information available online at doi:10.1155/2012/391325) shows, the similar endohedral (endo) complex was also located, and the F-Ti distance is ca. 0.1 Å shorter than that in "endo" (e) of Ti-T_8. Interestingly, in contrast, it is found that Ti-T_6 with a smaller titanoxane cage (a prismatic shape) has a F^- in the center of the cage like in the case of F^-@T_8 at the same B3LYP/6-311+G(d) level (see Figure S2). This means the cavity of Ti-T_8 is large enough for a F^- moves rather freely compared with that of Ti-T_6. Therefore, the limited space of Ti-T_8 is found not to be the reason for the strange behavior of F^- in the endohedral complex but the strong electrostatic interaction between F^- and Ti atom of Ti-T_n (n = 8 and 10) may be the plausible explanation. Furthermore, in consideration of the Tossell results for F^-@T_n (n = 10 and 12) [12], F^- seems to prefer to interact with a specific Ti or Si rather than with plural skeletal atoms at the same time if there is enough space to allow that in the cage.

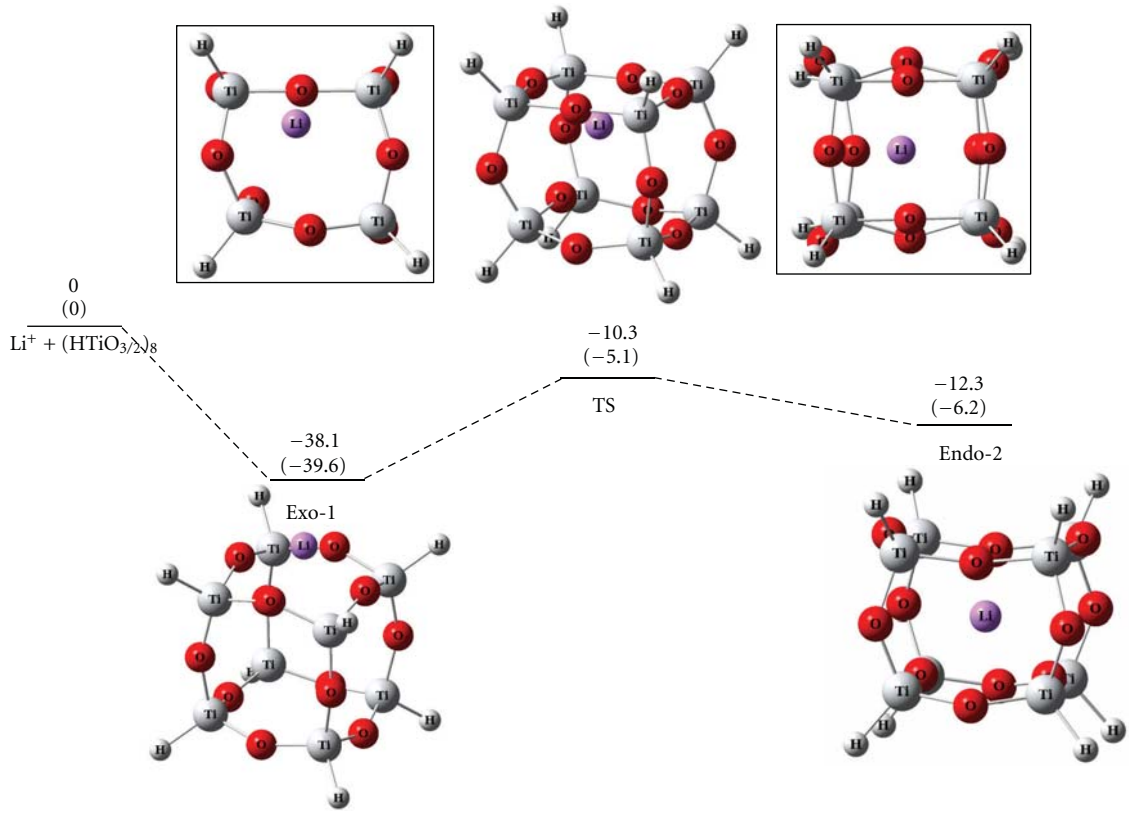

Figure 3: The potential energy surface (kcal/mol) of the insertion reaction of Li^+ into Ti-T_8 with the structures of the exohedral complex (Exo-1), the transition state (TS), and endohedral complex (Endo-2) at the B3LYP/6-311+G(d)+ZPC and HF/6-311+G(d)+ZPC (in parentheses) levels. For the transition state, the side view is in the left quadrangle while the top view is in the right one.

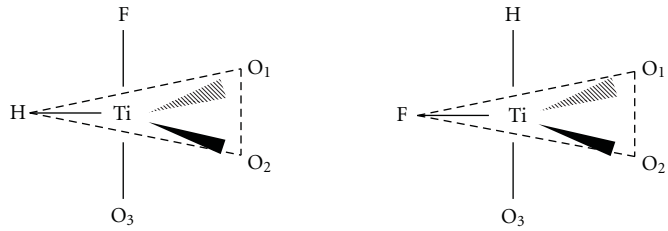

Scheme 2

On the other hand, the isomerization between "axial" and "equatorial" exohedral complexes of F^-(Ti-T_8) takes place via the transition structure also shown in Figure 4. The "equatorial" structure is less stable than "axial" by 3.6 (2.7 at the HF/6-311+G(d)+ZPC level) kcal/mol at the B3LYP/6-311+G(d)+ZPC level, while the extremely low energy barrier (0.3 kcal/mol at the HF level) needed for the isomerization to "axial" is further reduced to less than 0.1 kcal/mol at the B3LYP level. Therefore, for the exohedral complex of F^-(Ti-T_8), "axial" is the main structure but the interconversion of the two conformations is possible to take place very easily.

In contrast with the F^- case, the situation of the encapsulation of Cl^- into Ti-T_8 cage is quite simple. The "axial" is a unique exohedral complex and the endohedral complex has a Cl^- at the center of the cage with the D_{4h} symmetry like those of the rare gases and K^+ as shown in Figure 5. As seen from Table 4, the endohedral complex is less stable only by 7.7 kcal/mol than the exohedral complex. This is in sharp contrast with the fact that the endohedral complex is largely less stable than the exohedral complex in the isoelectronic Ar and K^+ as shown in Table 4. This is explained from the small ΔE_{def} (17.3 kcal/mol) and large absolute value of the ΔE_{int} (−67.5 kcal/mol) of the endohedral complex of Cl^-@Ti-T_8 (see Table 5). As a result, the endohedral complex is not so unstable compared to the other cases.

Incidentally, the deformation energy (ΔE_{def}) of the complexes of F^- and Ti-T_8 is larger than that of the complexes of Cl^- and Ti-T_8 probably because of the larger geometrical

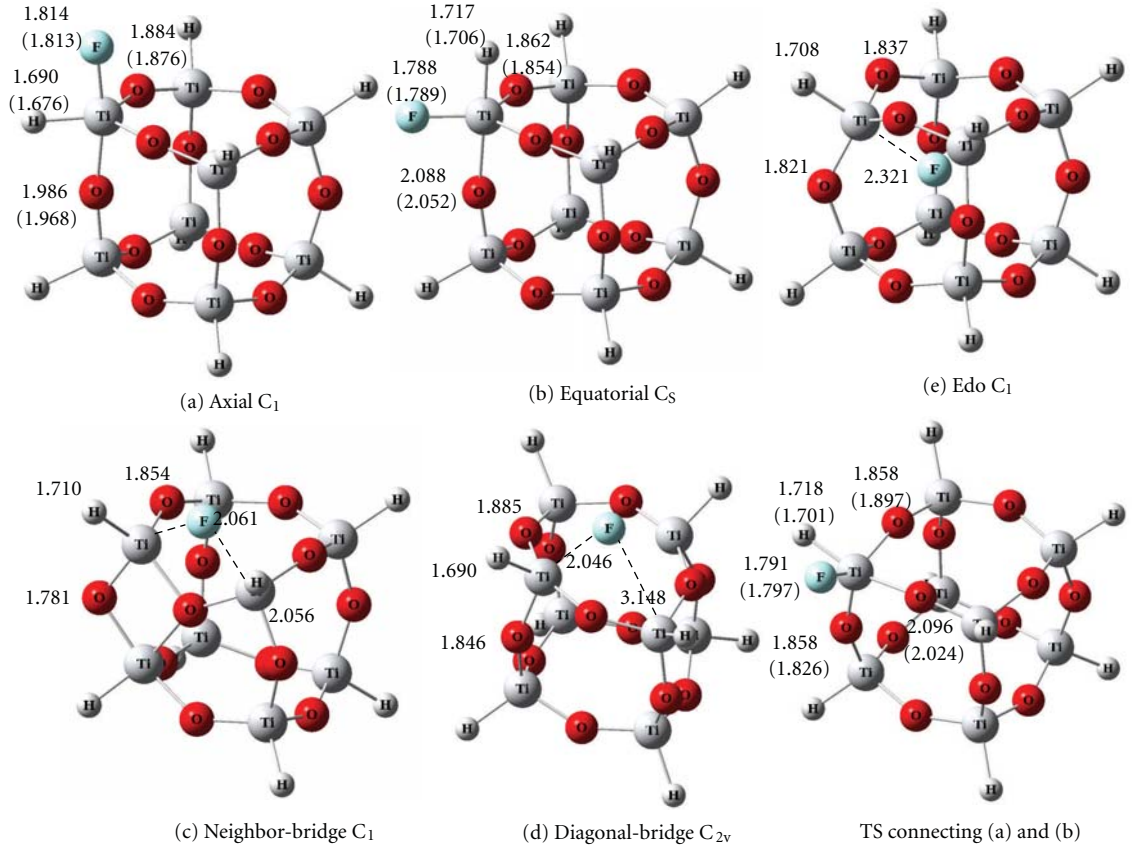

Figure 4: The B3LYP/6-311+G(d) and HF/6-311+G(d) (in parentheses) optimized geometries of exohedral and endohedral complexes of F^- and Ti-T_8 and the transition state for the "Axial" (a) "Equatorial" (b) isomerization in angstroms.

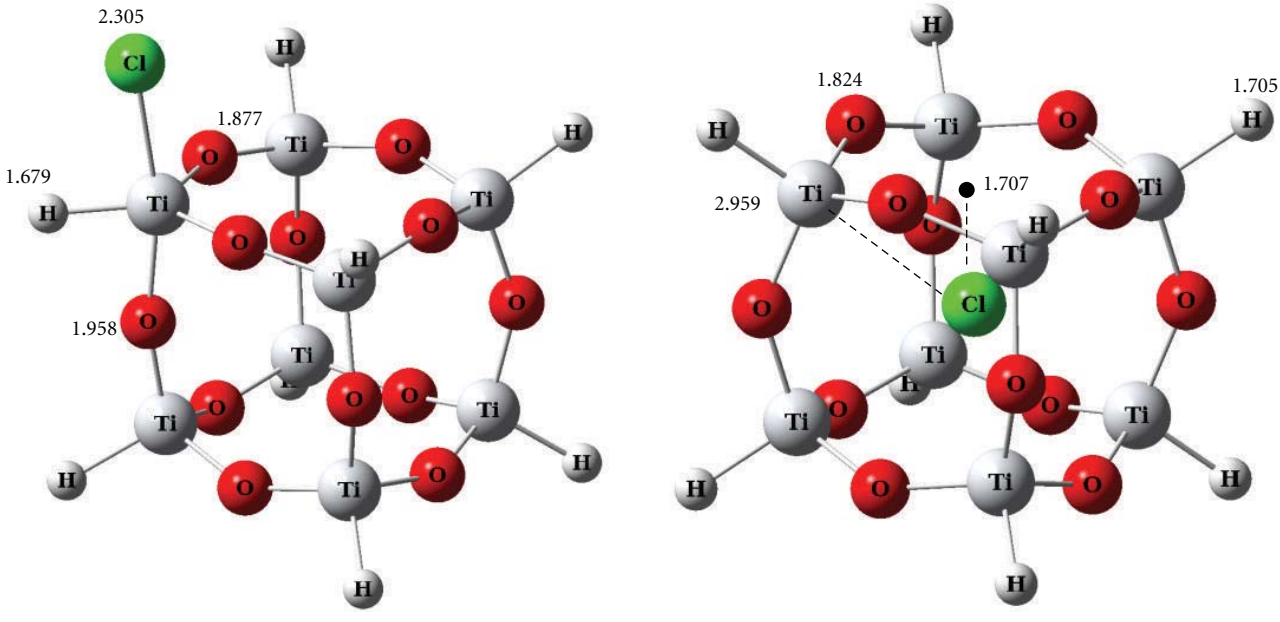

Figure 5: The B3LYP/6-311+G(d) optimized geometries of the exohedral (Axial) and endohedral (Endo) complexes of Cl^- and Ti-T_8 in angstroms.

Table 6: Energy decomposition of the binding energy (ΔE_{comp}) (kcal/mol) of the complexes of F^- and Ti-T_8 and the energies relative to "axial" (ΔE) in each system based on the B3LYP/6-311+G(d)+ZPC and MP2/6-311+G(d)//B3LYP/6-311+G(d)[a] energies.

	Isomer	Sym	ΔE_{def}	ΔE_{int}	ΔE_{comp}	ΔE_{comp} + ZPC	ΔE
F^-+Ti-T_8	(a) Axial	C_1	35.9	−135.1	−99.1	−98.4	0.0 [*0.0*]
	(b) Equatorial	Cs	55.6	−150.6	−95.0	−94.8	3.6
	(c) Neighbor bridge	C_1	56.3	−151.4	−95.1	−93.7	4.7
	(d) Diagonal bridge	C_{2v}	63.9	−149.5	−85.6	−84.7	13.7
	(e) Endo	C_1	23.2	−125.3	−102.1	−101.6	−3.2 [*−7.6*]

[a]The values in italics are in square brackets.

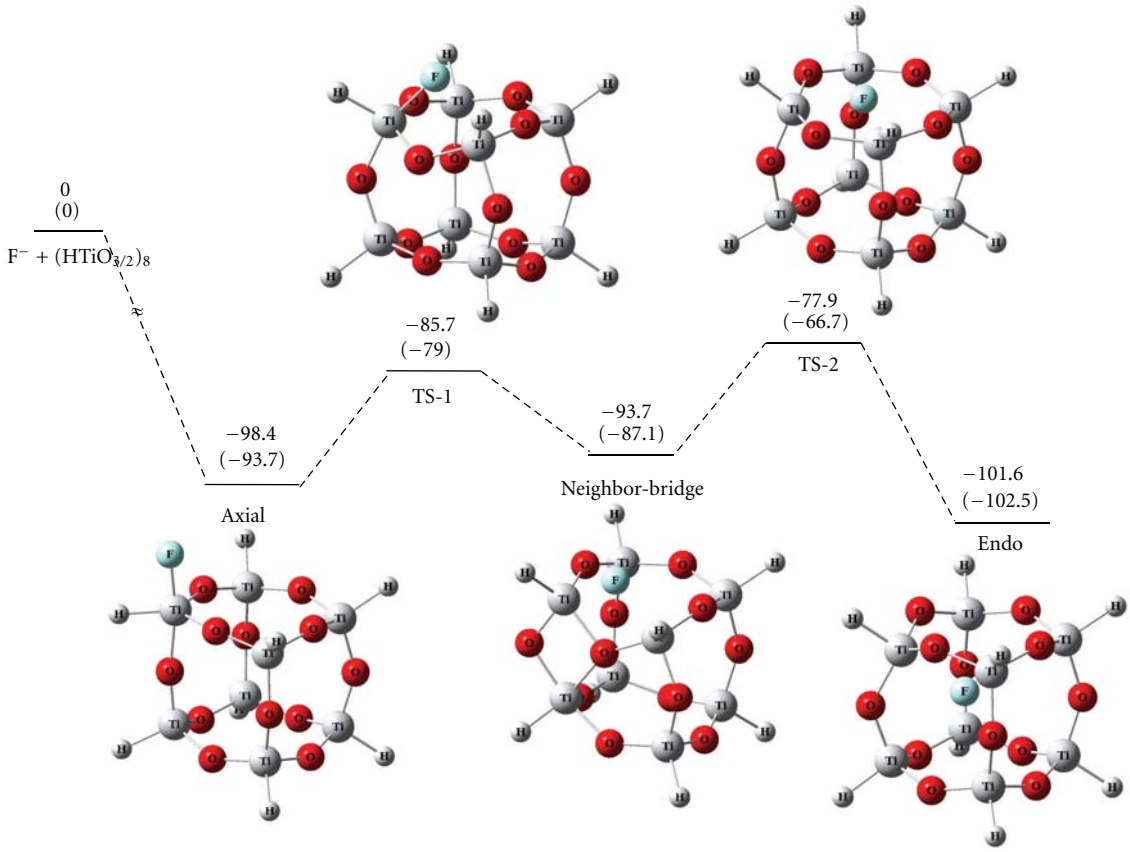

Figure 6: The potential energy surface (kcal/mol) of the insertion reaction of F^- into Ti-T_8 with the structures of some stationary points at the B3LYP/6-311+G(d)+ZPC and HF/6-311+G(d)+ZPC (in parentheses) levels.

changes. This is the same trend in the relation between Li^+ and the heavier cations (Na^+ and K^+). That is, as the element of the group is lighter (smaller), it is able to interact with specific skeletal atoms in the cage, which brings about the larger deformation of the host cage.

On the other hand, the NBO charge of Cl^- in the endohedral complex Cl^-@Ti-T_8 is −0.427 while that of F^- in F^-@Ti-T_8 is −0.688. This result suggests that the larger amount of minus charges is transferred from Cl^- to the cage compared to the case of F^- and the considerable electrostatic interaction between Cl^- and the cage because of the large ionic radius even at the center of the cage.

The last topic of this section is the reaction mechanisms of the encapsulation of the halogen anions into Ti-T_8. The potential energy surface of F^- and Cl^- is displayed in Figures 6 and 7, respectively. In both cases, the formation reaction of the exohedral complex (axial) is largely exothermic in energy. However, the following process is one-step reaction for Cl^- while two-step reaction for F^- because the "neighbor-bridge" structure exists between the exohedral and endohedral complexes for the latter as displayed in Figure 6. The "neighbor-bridge" complex has a diamond-shaped Ti_2O_2 part in the strained structure. From the complex to the second TS (TS-2), the F^- falls down into the cage with pushing out the oxygen of the flexible titanoxane (Ti–O–Ti) bond to outside of the cage. As a result, the rhombus Ti_2O_2 structure is broken down and the energy needed for the motion brings about the second energy barrier of

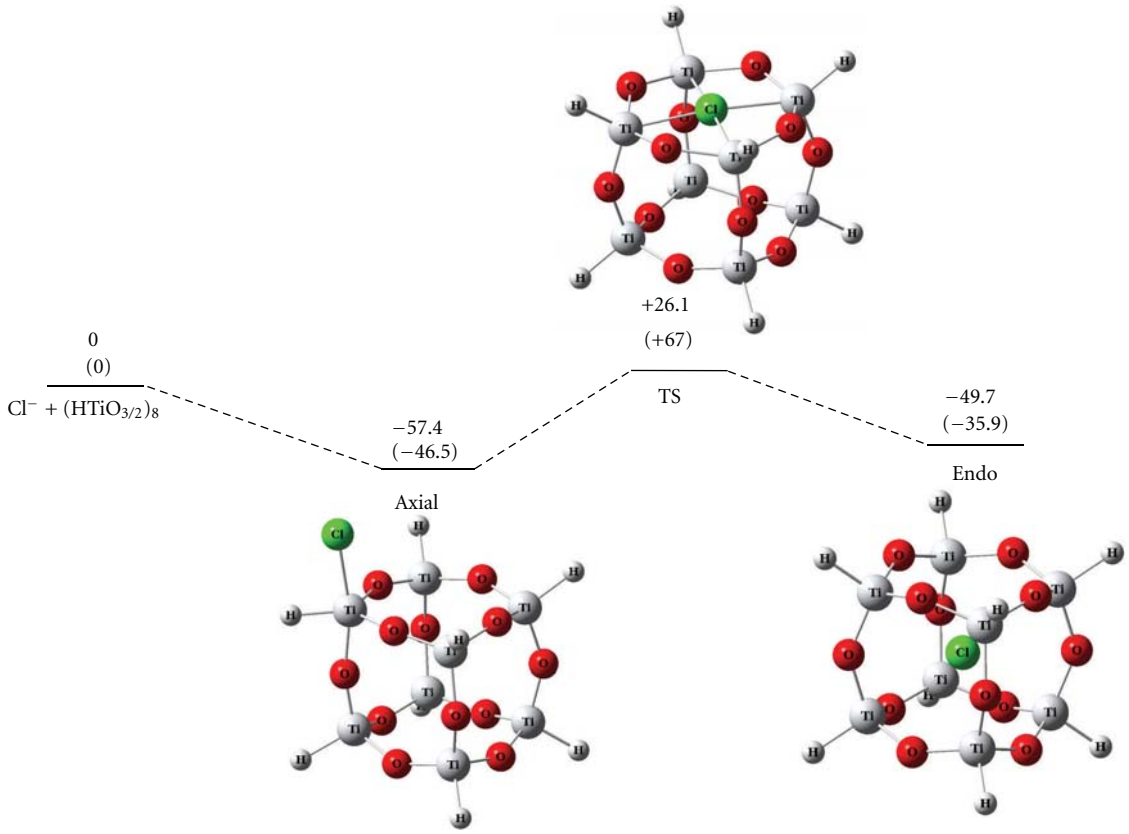

Figure 7: The potential energy surface (kcal/mol) of the insertion reaction of Cl^- into Ti-T_8 with the structures of the exohedral (Axial) and endohedral (Endo) complexes and the transition state (TS) connecting them at the B3LYP/6-311+G(d)+ZPC and HF/6-311+G(d)+ZPC (in parentheses) levels.

the reaction. All stationary points are lower than the reactants in energy. Therefore, the encapsulation of F^- into Ti-T_8 is predicted to take place rather easily. In fact, the absolute value of the ΔE_{comp} (−102.1 kcal/mol) of the endohedral complex of F^- and Ti-T_8 is largest among all species investigated in this study. In the silicon analogue, $F^-@T_8$ has already been observed experimentally so the Ti analogue may also be observed in near future.

For the encapsulation of Cl^-, the anion inserts from the center of the D_4 face as indicated from the TS structure in Figure 7. For the silicon analogue, $Cl^-@T_8$, the siloxane bond seems to be partially broken in the transition-state structure of the insertion and it could not keep the highly symmetric structure probably because of the smaller size of the cage [9]. As Figure 7 shows, the transition state "TS" for the insertion of Cl^- into Ti-T_8 is higher than the reactants in energy, which is different with the F^- case but rather resembles to the rare gas elements and Na^+ and K^+ except for the fact that the endohedral complex is lower than the reactants.

3.5. Comparison with POSS. Finally, we compare the present results for the insertion reactions with those of the Si analogues (T_8) in order to clarify the characteristics of the Ti compounds. As already mentioned frequently, the same reaction of T_8 has been investigated comprehensively by Park et al. [9] and the results are referred to in the preceding sections. Therefore, we just mention here the comparison of energetics of the reaction of Ti-T_8 and T_8 at the same level of theory in Table 7.

The trend of the binding energy (ΔE_{comp}), relative energies of the complexes, and the transition structures on the potential energy surface are similar for both compounds. The ΔE_{comp} of the exohedral complex of all elements except for Ar is minus, suggesting that these complexes are easily formed energetically. In addition, as the element becomes heavy, the relative stability of the transition state and endohedral complex becomes small probably because of their steric repulsion. Furthermore, the steric repulsion may explain that their relative energies are always larger in T_8 than in Ti-T_8 as the size of the cage of the former is smaller. Only one exception is the endohedral complex of $F^-@T_8$. The remarkable stability may be the reason why the complex has been observed experimentally. Also, the endohedral complex (endo) of $F^-@$Ti-T_8 is more stable than the exohedral (axial) complex though the relative stability is smaller than the Si analogue.

Furthermore, we should note that the considerably small release energy of the endohedral complex between Li^+ and Ti-T_8, $Li^+@$Ti-T_8. This is the same trend as the corresponding silicon complex. As already noted, therefore, the inclusion complex of Li^+ and Ti-T_8 may be hardly observed experimentally.

Table 7: The energetics (kcal/mol) of the encapsulation of X (X = He, Ne, Ar, Li^+, Na^+, K^+, F^-, and Cl^-) into A-T_8 (A = Si and Ti) at the B3LYP/6-311+G (d)+ZPC and MP2/6-311+G(d)[a] levels on the B3LYP/6-311+G(d) optimized geometries.

X	A-T_8 A	ΔE_{comp} of exo	Relative energy			Release energy
			Exo	TS	Endo	
He	Ti	−0.1	0.0	31.2	7.6	23.6
	Si	−0.1	0.0	54.3	13.2	41.1
Ne	Ti	−0.2	0.0	58.3	11.6	46.7
	Si	−0.1	0.0	109.5	24.1	85.4
Ar	Ti	0.0	0.0	145.2	46.0	99.2
	Si	0.0	0.0	252.9	95.9	157.0
Li^+	Ti	−38.1	0.0	27.8	25.8	2.0
	Si	−46.3	0.0	35.0	28.0	7.0
Na^+	Ti	−21.6	0.0	60.7	31.7	29.0
	Si	−29.3	0.0	107.2	40.3	66.9
K^+	Ti	−11.8	0.0	150.9	53.6	97.3
	Si	−17.7	0.0	237.1	85.8	151.3
F^-	Ti	−98.4	0.0 (0.0)	12.7/20.5	−3.2 (−7.6)	23.7
	Si	−58.6	0.0	65.9	−13.2	79.1
Cl^-	Ti	−57.4	0.0	83.5	7.7	75.8
	Si	−14.3	0.0	90.6	42.1	48.5

[a] The values are in parentheses.

4. Concluding Remarks

In the present work, the insertion reaction of various guest species such as rare gas, cations of the group 1, and anions of the group 17 elements, into the Ti analogue of T_8, Ti-T_8, has been investigated in comparison with the case of the Si analogue.

For rare gas elements, the mechanism of the insertion is the same as that of the Si analogue, T_8; (1) formation of the exohedral complex where the atom is above the center of a D_4 ($(HTiO)_4$) face, (2) interaction from the center of a D_4 in the transition-state structure, and (3) formation of the endohedral complex with the atom in the center of the cage. The interaction with the host is rather small for all cases, and the energy for the encapsulation (energy barrier for the isomerization of exohedral to endohedral complexes) becomes large as the element becomes heavy.

On the other hand, for the cations of the group 1 elements, the reaction mechanism between Li^+ and the heavier elements (Na^+ and K^+) is different. The latter group is rather similar to the rare gas elements in the geometries of the complexes and transition state, but Li^+ is found to interact with specific skeletal oxygen atoms and form two types of structures in both complexes as a result. Binding energy of all the complexes between Li^+ and Ti-T_8 is largely minus, suggesting that the complex of the cation and Ti-T_8 is energetically more stable than the corresponding complex between rare gas elements and Ti-T_8. Furthermore, Li^+ interacts with the skeletal oxygen strongly in the exohedral complexes and the transition state for the encapsulation, which seems to make important contribution for their stability. As a result, the final product of the reaction, an endohedral complex, Li^+@Ti-T_8, is found to be kinetically unstable so only the exohedral complex may be existable.

Finally, for the anionic species of the group 17 elements, the behavior of F^- is considerably unique. Several kinds of complexes are located for the reaction between F^- and Ti-T_8, while two types (exohedral and endohedral) of complexes are located for the case of Cl^-. It may be worth to note that especially the position of a F^- is not the center of the cage in the endohedral complex but it takes the quasitriangular bipyramidal conformation at a corner of the cage. This is in sharp contrast with the fact that F^- is in the center of the cage in the corresponding complex of the Si analogue, F^-@T_8. The same thing was also seen in the endohedral complex of F^-@Ti-T_{10}, while F^- was found to be the center of the cage in smaller Ti-T_6. Therefore, the larger room of the Ti-T_8 and Ti-T_{10} compared to the corresponding Si cages as well as the strong electrostatic interaction between F^- and Ti atom may allow the unique structure. Furthermore, this prediction can explain the observation in F^-@Si-T_{10} and F^-@Si-T_{12} where F^- is bound at the corner of the cage [11, 12].

In summary, for the present encapsulation reaction of Ti-T_8, we found quite a few similar properties with those of the silicon analogue, T_8, in spite of the considerable difference in the nature of the skeletal bond and size of the cage. This means the reaction is mainly affected by the size of the host cage and not the skeletal elements. However, for the reaction of Ti-POSS, the strong interaction between the ionic species and a part of the skeletal atoms is still expected to play an important role. As an extension of the present study, therefore, an investigation of the intra-molecular catalytic reaction inside Ti-POSS is now in progress.

The discussion for the cage effect in the F^-@Ti-T_n ($n = 8$ and 10) (Figures S1–S3 and Tables S1 and S2), see the supplementary material available online at doi: 10.1155/2012/391325.

Acknowledgment

This work was partly supported by the "Element Innovation" Project by Ministry of Education, Culture, Sports, Science and Technology in Japan.

References

[1] M. G. Voronkov and V. L. Lavrent'yev, " Polyhedral oligosilsesquioxanes and their homo derivatives," *Topics in Current Chemistry*, vol. 102, pp. 199–236, 1982.

[2] F. J. Feher, D. A. Newman, and J. F. Walzer, "Silsesquioxanes as models for silica surfaces," *Journal of the American Chemical Society*, vol. 111, no. 5, pp. 1741–1748, 1989.

[3] R. H. Baney, M. Itoh, A. Sakakibara, and T. Suzuki, "Silsesquioxanes," *Chemical Reviews*, vol. 95, no. 5, pp. 1409–1430, 1995.

[4] F. J. Feher and T. A. Budzichowski, "Silasesquioxanes as ligands in inorganic and organometallic chemistry," *Polyhedron*, vol. 14, no. 22, pp. 3239–3253, 1995.

[5] B. Tejerina and M. S. Gordon, "Insertion mechanism of N_2 and O_2 into T_n ($n = 8, 10, 12$)-silsesquioxane framework," *Journal of Physical Chemistry B*, vol. 106, no. 45, pp. 11764–11770, 2002.

[6] L. A. Villaescusa, P. Lightfoot, and R. E. Morris, "Synthesis and structure of fluoride-containing GeO_2 analogues of zeolite double four-ring building units," *Chemical Communications*, no. 19, pp. 2220–2221, 2002.

[7] A. R. Bassindale, M. Pourny, P. G. Taylor, M. B. Hursthouse, and M. E. Light, "Fluoride-Ion encapsulation within a silsesquioxane cage," *Angewandte Chemie*, vol. 42, no. 30, pp. 3488–3490, 2003.

[8] A. R. Bassindale, D. J. Parker, M. Pourny, P. G. Taylor, P. N. Horton, and M. B. Hursthouse, "Fluoride ion entrapment in octasilsesquioxane cages as models for ion entrapment in zeolites. Further examples, X-ray crystal structure studies, and investigations into how and why they may be formed," *Organometallics*, vol. 23, no. 19, pp. 4400–4405, 2004.

[9] S. S. Park, C. Xiao, F. Hagelberg, D. Hossain, C. U. Pittman Jr., and S. Saebo, "Endohedral and exohedral complexes of polyhedral double four-membered-ring (D4R) units with atomic and ionic impurities," *Journal of Physical Chemistry A*, vol. 108, no. 51, pp. 11260–11272, 2004.

[10] G. Satre, A. Pulido, and A. Corma, "Pentacoordinated germanium in AST zeolite synthesised in fluoride media. A ^{19}F NMR validated computational study ," *Chemical Communications*, vol. 2005, pp. 2357–2359, 2005.

[11] M. Pach, R. M. Macrae, and I. Carmichael, "Hydrogen and deuterium atoms in octasilsesquioxanes: experimental and computational studies," *Journal of the American Chemical Society*, vol. 128, no. 18, pp. 6111–6125, 2006.

[12] J. A. Tossell, "Calculation of ^{19}F and ^{29}Si NMR shifts and stabilities of F^- encapsulating silsesquioxanes," *The Journal of Physical Chemistry C*, vol. 111, pp. 3584–3590, 2007.

[13] D. Hossain, C. U. Pittman Jr., S. Saebo, and F. Hagelberg, "Structures, stabilities, and electronic properties of endo-And exohedral complexes of T10-polyhedral oligomeric silsesquioxane cages," *Journal of Physical Chemistry C*, vol. 111, no. 17, pp. 6199–6206, 2007.

[14] S. E. Anderson, D. J. Bodzin, T. S. Haddad et al., "Structural investigation of encapsulated fluoride in polyhedral oligomeric silsesquioxane cages using ion mobility mass spectrometry and molecular mechanics," *Chemistry of Materials*, vol. 20, no. 13, pp. 4299–4309, 2008.

[15] D. Hossain, C. U. Pittman Jr., F. Hagelberg, and S. Saebo, "Endohedral and exohedral complexes of T8-polyhedral oligomeric silsesquioxane (POSS) with transition metal atoms and ions," *Journal of Physical Chemistry C*, vol. 112, no. 41, pp. 16070–16077, 2008.

[16] D. Hossain, S. R. Gwaltney, C. U. Pittman, and S. Saebo, "Insertion of transition metal atoms and ions into the nanoscale dodecahedral silsesquioxane (T12-POSS) cage: structures, stabilities and electronic properties," *Chemical Physics Letters*, vol. 467, no. 4–6, pp. 348–353, 2009.

[17] A. R. Geoge and C. R. A. Catlow, "An investigation into the effects of ion incorporation on the electronic structure of silicate fragments via ab initio computational techniques," *Chemical Physics Letters*, vol. 247, no. 4–6, pp. 408–417, 1995.

[18] T. Kudo, M. Akasaka, and M. S. Gordon, "Ab initio molecular orbital study of the insertion of H_2 into POSS compounds," *Theoretical Chemistry Accounts*, vol. 120, no. 1–3, pp. 155–166, 2008.

[19] T. Kudo, "Ab initio molecular orbital study of the insertion of H2 into poss compounds 2: the substituent effect and larger cages," *Journal of Physical Chemistry A*, vol. 113, no. 44, pp. 12311–12321, 2009.

[20] C. McCusker, J. B. Carroll, and V. M. Rotello, "Cationic polyhedral oligomeric silsesquioxane (POSS) units as carriers for drug delivery processes," *Chemical Communications*, vol. 8, pp. 996–998, 2005.

[21] H. Yuan, K. Luo, Y. Lai et al., "A novel poly(l-glutamic acid) dendrimer based drug delivery system with both pH-sensitive and targeting functions," *Molecular Pharmaceutics*, vol. 7, no. 4, pp. 953–962, 2010.

[22] T. Kudo, T. Taketsugu, and M. S. Gordon, "Ab initio molecular dynamics study of H_2 formation inside POSS compounds," *The Journal of Physical Chemistry A*, vol. 115, pp. 2679–2791, 2011.

[23] A. Voigt, R. Murugavel, V. Chandrasekhar et al., "Facile and rational route for high-yield synthesis of titanasiloxanes from aminosilanetriols," *Organometallics*, vol. 15, no. 6, pp. 1610–1613, 1996.

[24] M. Crocker, R. H. M. Herold, A. G. Orpen, and M. T. A. Overgaag, "Synthesis and characterisation of titanium silasesquioxane complexes: soluble models for the active site in titanium silicate epoxidation catalysts," *Journal of the Chemical Society, Dalton Transactions*, no. 21, pp. 3791–3804, 1999.

[25] R. Murugavel, P. Davis, and V. S. Shete, "Reactivity studies, structural characterization, and thermolysis of cubic titanosiloxanes: precursors to titanosilicate materials which catalyze olefin epoxidation," *Inorganic Chemistry*, vol. 42, no. 15, pp. 4696–4706, 2003.

[26] K. Wada, N. Itayama, N. Watanabe, M. Bundo, T. Kondo, and T. A. Mitsudo, "Synthesis and catalytic activity of group 4 metallocene containing silsesquioxanes bearing functionalized silyl groups," *Organometallics*, vol. 23, no. 24, pp. 5824–5832, 2004.

[27] T. Kudo and M. S. Gordon, "Structures and stabilities of titanium silsesquioxanes," *The Journal of Physical Chemistry A*, vol. 105, no. 50, pp. 11276–11294, 2001.

[28] T. Kudo and M. S. Gordon, "Ab initio study of the catalytic reactivity of titanosilsesquioxanes and titanosiloxanes," *Journal of Physical Chemistry A*, vol. 107, no. 41, pp. 8756–8762, 2003.

[29] T. Kudo, M. Akasaka, and M. S. Gordon, "Ab initio molecular orbital study on the Ge^-, Sn^-, Zr^- and Si/Ge-mixed silsesquioxanes," *The Journal of Physical Chemistry A*, vol. 112, no. 21, pp. 4836–4843, 2008.

[30] A. J. M. de Man and J. Sauer, "Coordination, structure, and vibrational spectra of titanium in silicates and zeolites in comparison with related molecules. An ab initio study," *The Journal of Physical Chemistry*, vol. 100, no. 12, pp. 5025–5034, 1996.

[31] P. E. Sinclair and C. R. A. Catlow, "Quantum chemical study of the mechanism of partial oxidation reactivity in titanosilicate catalysts: active site formation, oxygen transfer, and catalyst deactivation," *The Journal of Physical Chemistry B*, vol. 103, no. 7, pp. 1084–1095, 1999.

[32] A. D. Becke, "Density-functional thermochemistry. III. The role of exact exchange," *The Journal of Chemical Physics*, vol. 98, no. 7, pp. 5648–5652, 1993.

[33] M. M. Francl, W. J. Pietro, W. J. Hehre et al., "Self-consistent molecular orbital methods. XXIII. A polarization-type basis set for second-row elements," *The Journal of Chemical Physics*, vol. 77, no. 7, pp. 3654–3665, 1982.

[34] T. Clark, J. Chandrasekhar, G. W. Spitznagel, and P. V. R. Schleyer, " Efficient diffuse function-augmented basis sets for anion calculations. III. The 3-21+G basis set for first-row elements, Li-F," *Journal of Computational Chemistry*, vol. 4, pp. 294–301, 1983.

[35] M. J. Frish, J. A. Pople, and J. S. Binkley, "Self-consistent molecular orbital methods 25. Supplementary functions for Gaussian basis sets," *The Journal of Chemical Physics*, vol. 80, pp. 3265–3269, 1984.

[36] J. A. Pople, R. Seeger, and R. Krishnann, "A semi-empirical MO theory for ionization potentials and electron affinities," *International Journal of Quantum Chemistry*, vol. 11, pp. 149–163, 1977.

[37] M. J. Frisch, G. W. Trucks, H. B. Schlegel et al., *Gaussian 03, Revision C. 02*, Gaussian, Wallingford, Conn, USA, 2004.

[38] M. W. Schmidt, K. K. Baldridge, J. A. Boatz et al., "General atomic and molecular electronic structure system," *Journal of Computational Chemistryvol*, vol. 14, pp. 1347–1363, 1993.

[39] M. S. Gordon and M. W. Schmidt, "Advances in electronic structure theory: GAMESS a decade later," in *Theory and Applications of Computational Chemistry*, C. E. Dykstra, G. Frenking, K. S. Kim, and G. E. Scuseria, Eds., chapter 41, Elsevier, San Diego, Calif, USA, 2005.

[40] J. P. Foster and F. Weinhold, "Natural hybrid orbitals," *Journal of the American Chemical Society*, vol. 102, no. 24, pp. 7211–7218, 1980.

Hindawi Publishing Corporation
International Journal of Polymer Science
Volume 2012, Article ID 984501, 6 pages
doi:10.1155/2012/984501

Research Article

Sol-Gel Preparation of Highly Water-Dispersible Silsesquioxane/Zirconium Oxide Hybrid Nanoparticles

Yoshiro Kaneko and Tomoyuki Arake

Graduate School of Science and Engineering, Kagoshima University, 1-21-40 Korimoto, Kagoshima 890-0065, Japan

Correspondence should be addressed to Yoshiro Kaneko, ykaneko@eng.kagoshima-u.ac.jp

Received 18 July 2012; Accepted 27 August 2012

Academic Editor: Kensuke Naka

Highly water-dispersible silsesquioxane/zirconium oxide hybrid nanoparticles (SQ/ZrO_2-NPs) were prepared by the following two-step reactions. First, a mixture of 3-aminopropyltrimethoxysilane (APTMOS) and zirconium tetra-*n*-butoxide (ZTB) was stirred in a mixed solvent of 0.1 mol/L methanolic hydrochloric acid and *n*-butanol at room temperature, followed by heating in an open system until the solvent was completely evaporated. Then, the aqueous solution obtained by adding water to the resulting product was heated in an open system until the water was completely reevaporated. The products (SQ/ZrO_2-NPs) obtained with a feed molar ratio of APTMOS/ZTB of more than 0.3 were dispersed well in water, and their aqueous dispersions were highly transparent, which was confirmed by UV-Vis measurements. In addition, the solid product obtained by drying its aqueous dispersion was redispersed in water. The volume-average particle sizes of SQ/ZrO_2-NPs (APTMOS/ZTB $\geq$ 0.3) were assessed to be ca. 4.6–23.8 nm by dynamic light scattering measurements in water. The theoretical refractive index of the SQ/ZrO_2-NP (APTMOS/ZTB = 0.3) was estimated to be 1.66. It was assumed that the water-dispersible property of the SQ/ZrO_2-NPs probably originated from the ZrO_2-$SiO_{1.5}(CH_2)_3NH_3^+Cl^-$ core-shell structures.

1. Introduction

The dispersion of metal oxide nanoparticles such as those of titanium oxide (TiO_2) and zirconium oxide (ZrO_2) is an important topic for their applications, particularly the formation of transparent organic-inorganic hybrid materials with high refractive indices [1–5]. To prepare transparent hybrid materials composed of polymers and metal oxide nanoparticles, metal oxides are required to disperse well (nanoscale) in various media because interface scattering between organic and inorganic components is suppressed in hybrid materials.

Among metal oxide nanoparticles, ZrO_2 nanoparticles are attractive because they offer several advantages such as chemical inertness, excellent thermal stability, high refractive index, and high hardness. Although numerous studies have focused on surface modification to disperse ZrO_2 nanoparticles, only a few examples regarding the preparation of completely homogeneous dispersions of ZrO_2 nanoparticles have been reported [6–8].

On the other hand, we have reported the preparation of water-soluble ammonium cation-containing silsesquioxane (SQ) polymers with regular structures by the sol-gel reaction of 3-aminopropyltrimethoxysilane (APTMOS) under acidic conditions [9–14]. We determined that a salt (ion pair) prepared from an amino group of APTMOS and an acid used as a catalyst probably contributes to the water-solubility and formation of regular structures of the materials. It has also been reported that highly water-dispersible SQ/silica (SiO_2) hybrid materials have been prepared by the sol-gel copolycondensation of the mixtures of APTMOS and tetramethoxysilane under the same reaction conditions as those for the aforementioned polySQs [15]. In addition, highly water-dispersible SQ/TiO_2 hybrid nanoparticles were successfully prepared by the following two-step sol-gel copolycondensation under acidic conditions [16]. First, the mixture of APTMOS and titanium tetraisopropoxide was stirred in a mixed solvent of methanolic hydrochloric acid and isopropyl alcohol at room temperature, followed by heating in an open system until the solvent was evaporated.

Then, the aqueous solution obtained by adding water to the resulting product was heated in an open system until the water was completely reevaporated. The resulting product was dispersed well in water and its aqueous dispersion was highly transparent. These synthetic approaches have motivated us to successfully obtain highly water-dispersible SQ/ZrO_2 hybrid nanoparticles (SQ/ZrO_2-NPs) because the molecular structure of titanium tetraalkoxide as a monomer is similar to that of zirconium tetraalkoxide.

Therefore, in this study, we investigated two-step sol-gel copolycondensations, that is, using alcoholic hydrochloric acid in the first step and water in the second step as solvents, for the mixtures of APTMOS and zirconium tetra-*n*-butoxide (ZTB) under various reaction conditions. As a result, highly water-dispersible SQ/ZrO_2-NPs were obtained. This paper reports on the preparation method, water-dispersible behaviors, particle sizes, refractive indices, plausible structures, and formation mechanism of the nanoparticles.

2. Experimental

2.1. Materials. All reagents (APTMOS, Tokyo Kasei Kogyo Co., Ltd., Japan and ZTB, Wako Pure Chemical Industries, Ltd., Japan) and solvents (0.5 mol/L methanolic hydrochloric acid and *n*-butanol, Wako Pure Chemical Industries, Ltd., Japan) of reagent-grade quality were commercially purchased and used without further purification.

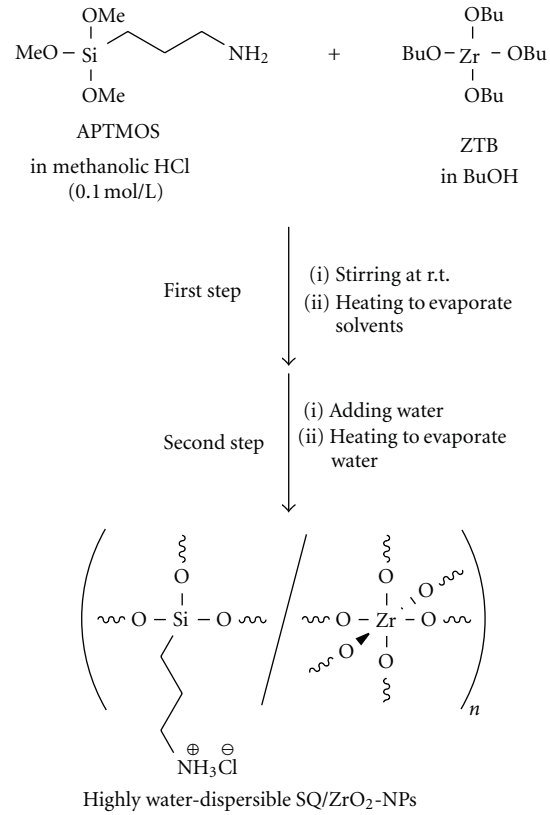

Scheme 1: Preparation of highly water-dispersible SQ/ZrO_2-NPs.

2.2. Preparation of Highly Water-Dispersible SQ/ZrO_2-NPs. A typical experiment for the preparation of highly water-dispersible SQ/ZrO_2-NPs was conducted according to the following procedure. After 0.1 mol/L methanolic hydrochloric acid (62.5 mL = 6.25 mmol) was added to APTMOS (0.269 g = 1.5 mmol), the solution was added to a solution of ZTB (85 wt% *n*-butanol solution) (2.257 g = 5.0 mmol) in *n*-butanol (125 mL). The mixture was stirred for 2 h at room temperature, followed by heating at ca. 50°C in an open system until the solvent was evaporated and further heating at 100°C for 30 min to completely remove the solvent. The obtained product was dissolved in water (100 mL) and the solution was heated at ca. 50°C in the open system until the water was reevaporated. The product was left at 100°C for 30 min and was then dispersed in water (100 mL) by stirring at room temperature for 12 h. After the resulting aqueous dispersion was filtrated to remove a slightly insoluble residue, it was heated at 50°C in an open system to evaporate water and was further heated at 100°C for 30 min to yield ca. 1.033 g of a glassy white product (SQ/ZrO_2-NPs).

2.3. Ion-Exchange Reaction of SQ/ZrO_2-NP with Sodium Laurate. SQ/ZrO_2-NP (elemental ratio of Si/Zr = 0.34, 0.173 g = 0.34 mmol of the amino group) was dispersed in 20 mL of water. This aqueous dispersion was poured into a sodium laurate aqueous solution (0.1 mol/L, 10 mL) to precipitate the product. The precipitate was collected by filtration, washed with water, and dried under reduced pressure at room temperature to yield ca. 0.252 g of a white powdered product.

2.4. Measurements. Elemental ratios of Si/Zr in the SQ/ZrO_2-NPs were estimated by energy-dispersive X-ray (EDX) spectroscopy using an XL30 scanning electron microscope (FEI Company). The UV-Vis spectra of the aqueous dispersions of the SQ/ZrO_2-NPs were recorded using a Jasco V-650 spectrophotometer (JASCO Corporation, Japan). A quartz cell (thickness 10 mm) containing water was used as a reference for UV-Vis measurements. The particle sizes of the SQ/ZrO_2-NPs were measured in water at 25°C using a Zetasizer Nano ZS (dynamic light scattering (DLS) apparatus) (Malvern Instruments, UK). The refractive indices of the aqueous dispersions of the SQ/ZrO_2-NPs were determined at 25°C using an RX-5000α refractometer (Atago Co., Ltd., Japan). The measurement wavelength was 589.3 nm (Na-D line).

3. Results and Discussion

3.1. Preparation of Highly Water-Dispersible SQ/ZrO_2-NPs. In the first step, intermediates were prepared by stirring the mixtures of APTMOS and ZTB (feed molar ratio = 0–1.0 : 1.0) in a mixed solvent of 0.1 mol/L methanolic hydrochloric acid and *n*-butanol at room temperature, followed by heating in an open system until the solvent was evaporated (Scheme 1). In the second step, after water

Table 1: Feed molar ratios of APTMOS/ZTB and elemental ratios of Si/Zr in SQ/ZrO_2-NPs.

Run	Feed molar ratio (APTMOS/ZTB)	Elemental ratio in SQ/ZrO_2-NPs[(a)] (Si/Zr)
1	1.0	1.10
2	0.8	0.99
3	0.6	0.79
4	0.3	0.34
5	0.2	0.29
6	0.1	0.22

[(a)] Estimated by EDX measurements.

was added to the resulting intermediates, these aqueous solutions were also heated in an open system until the water was completely reevaporated to obtain SQ/ZrO_2-NPs (Scheme 1). These materials were almost quantitatively obtained by this reaction system.

The values of Si/Zr elemental ratios in the SQ/ZrO_2-NPs estimated by EDX measurements are listed in Table 1. These results indicate that the Si/Zr elemental ratios were almost consistent with the feed molar ratio of APTMOS to ZTB in all cases.

3.2. Water-Dispersibility of SQ/ZrO_2-NPs. The transmittances of the 1.0 w/v% aqueous dispersions of the SQ/ZrO_2-NPs obtained with various feed molar ratios of APTMOS/ZTB were measured by UV-Vis spectroscopy (Figure 1). For the aqueous dispersions of the SQ/ZrO_2-NPs obtained with a feed molar ratio of APTMOS/ZTB greater than 0.3, high transmittances were observed in the visible wavelength region (>95%, transmitted light > 380 nm), indicating that the SQ/ZrO_2-NPs (APTMOS/ZTB ≥ 0.3) dispersed well in water and the resulting aqueous dispersions were highly transparent (Figure 1). The photographs of the aqueous dispersions also support their transparencies (Figures 2(a) and 2(b)). These high transparencies of the aqueous dispersions did not change, and precipitates were not generated even after standing for several weeks, indicating that the SQ/ZrO_2-NPs (APTMOS/ZTB ≥ 0.3) were stably maintained in water without aggregation.

On the other hand, the transmittance of the aqueous dispersion of the SQ/ZrO_2-NP (APTMOS/ZTB = 0.2, concentration = 1.0 w/v%) was lower than those of the aforementioned nanoparticles (Figure 1). In addition, those of SQ/ZrO_2-NPs (APTMOS/ZTB ≤ 0.1, concentration = 1.0 w/v%) were considerably low, indicating that these products did not disperse well in water (Figure 1). Their turbidities were also confirmed by visual observation (Figures 2(d) and 2(e)). On the basis of the aforementioned results, the products were found to be highly dispersed in water with ca. 75 mol% incorporation of the ZrO_2 component. In the case of the SQ/ZrO_2-NPs (APTMOS/ZTB ≤ 0.2), the compositional ratio of the $SiO_{1.5}(CH_2)_3NH_3^+Cl^-$ components was relatively low. Therefore, it is assumed that the

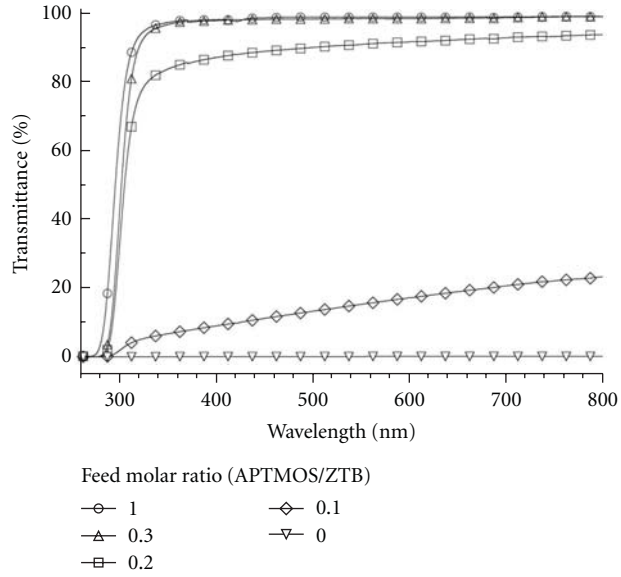

Figure 1: UV-Vis spectra of aqueous dispersions (1.0 w/v%) of SQ/ZrO_2-NPs obtained with various feed molar ratios.

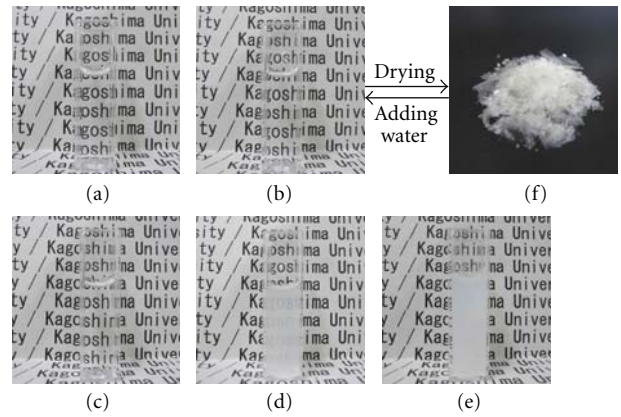

Figure 2: Photographs of aqueous dispersions (1.0 w/v%) of SQ/ZrO_2-NPs obtained with various feed molar ratios for APTMOS/ZTB: (a) 1.0, (b) 0.3, (c) 0.2, (d), 0.1, and (e) 0 and (f) solid state of SQ/ZrO_2-NP (feed molar ratio of APTMOS/ZTB = 0.3).

$SiO_{1.5}(CH_2)_3NH_3^+Cl^-$ components, which play an important role in high water-dispersibility, could not completely cover the nanoparticle surface.

The transmittances of the aqueous dispersions of the SQ/ZrO_2-NPs (APTMOS/ZTB = 0.3) with various concentrations were investigated through UV-Vis measurements (Figure 3). For the aqueous dispersions up to 5.0 w/v%, relatively higher transmittances were observed (>90%, transmitted light > 380 nm).

A solid product was recovered by the evaporation of the aforementioned aqueous dispersion (Figure 2(f), e.g., SQ/ZrO_2-NPs (APTMOS/ZTB = 0.3)), indicating that the product's water-dispersibility is not due to the decomposition of Zr−O and Si−O bonds. Even after repeating the treatment of dispersion in water and the evaporation

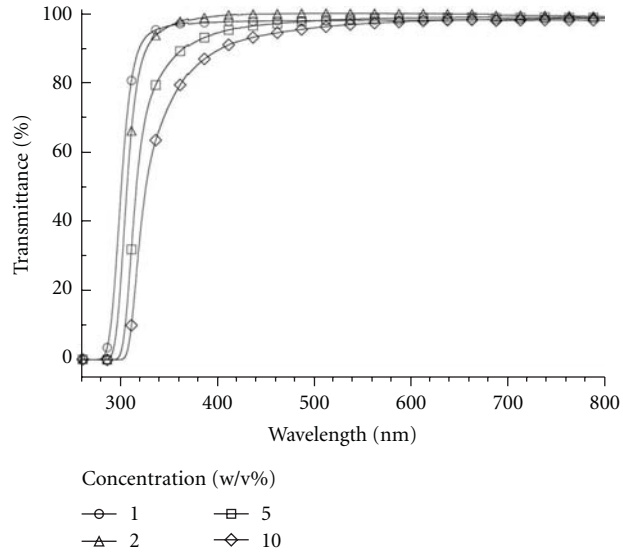

Figure 3: UV-Vis spectra of aqueous dispersions of SQ/ZrO_2-NPs (feed molar ratio of APTMOS/ZTB = 0.3) with various concentrations.

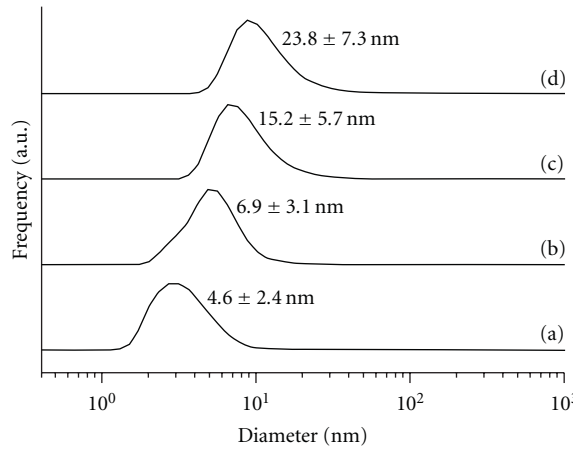

Figure 4: Volume-average particle size distributions of 2.0 w/v% aqueous dispersions of SQ/ZrO_2-NPs measured by DLS at 25°C. Feed molar ratio of APTMOS/ZTB = (a) 0.3, (b) 0.6, (c) 0.8, and (d) 1.0.

of water three times, the high transparency of the aqueous dispersion of the SQ/ZrO_2-NP was maintained, as confirmed by visual observation. Here, the dispersion treatment was performed by adding water to the SQ/ZrO_2-NP (concentration, 1.0 w/v%) and stirring at ca. 50°C. These results strongly indicate that SQ/ZrO_2-NPs exhibit high water-dispersibility and redispersion is possible.

The volume-average particle sizes of the SQ/ZrO_2-NPs (APTMOS/ZTB = 0.3, 0.6, 0.8, and 1.0) estimated by DLS measurements in water (2.0 w/v%) at 25°C were assessed to be 4.6 ± 2.4, 6.9 ± 3.1, 15.2 ± 5.7, and 23.8 ± 7.3 nm, respectively (Figure 4), indicating that the SQ/ZrO_2-NPs (APTMOS/ZTB ≥ 0.3) were well-dispersed, relatively small nanoparticles.

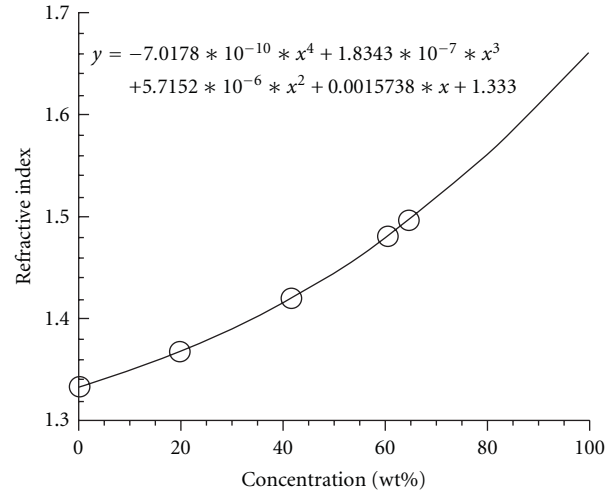

Figure 5: Correlation between refractive indices and concentrations of aqueous dispersions of SQ/ZrO_2-NPs (feed molar ratio of APTMOS/ZTB = 0.3).

3.3. Refractive Indices of SQ/ZrO_2-NP Aqueous Dispersions. To estimate the refractive indices of the SQ/ZrO_2-NP (APTMOS/ZTB = 0.3) by the Abb refractometer, we attempted to prepare a film on a flat glass substrate. However, a stable film could not be obtained. Therefore, various concentrations (0 (only water), 19.6, 41.7, 60.6, and 64.7 wt%) of the aqueous dispersions of the SQ/ZrO_2-NP were prepared, and the refractive indices of these dispersions were estimated by the Abb refractometer to be 1.333, 1.367, 1.420, 1.481, and 1.496, respectively. These values were plotted on a graph and their fitted curve was calculated as follows: [$y = -7.0178 \times 10^{-10}x^4 + 1.8343 \times 10^{-7}x^3 + 5.7152 \times 10^{-6}x^2 + 1.5738 \times 10^{-3}x + 1.333$]; y and x denote refractive indices and concentrations of the aqueous dispersions of the SQ/ZrO_2-NP (APTMOS/ZTB = 0.3), respectively (Figure 5). From this fitted curve, the theoretical refractive index of the SQ/ZrO_2-NP, that is, that for 100 wt%, was calculated to be 1.66.

3.4. Investigation of Necessity of Two-Step Sol-Gel Copolycondensation. The highly water-dispersible SQ/ZrO_2-NPs were obtained by the aforementioned two-step sol-gel copolycondensation; that is, alcoholic hydrochloric acid in the first step and water in the second step were employed as solvents. Here, to investigate the necessity of this two-step reaction, a comparative sol-gel copolycondensation experiment was performed using 0.1 mol/L aqueous hydrochloric acid as a substitute for methanolic hydrochloric acid in the first step. The Si/Zr elemental ratio of the resulting product obtained with a feed molar ratio of APTMOS/ZTB = 0.3 was estimated by EDX measurements to be ca. 0.38. The transmittance of the aqueous dispersion of this product decreased compared with that of the SQ/ZrO_2-NPs obtained by the aforementioned two-step sol-gel copolycondensation (Figure 6). Its turbidity was also confirmed by visual observation (Figure 6, inset). Use of aqueous hydrochloric acid in the first step probably resulted in the formation of

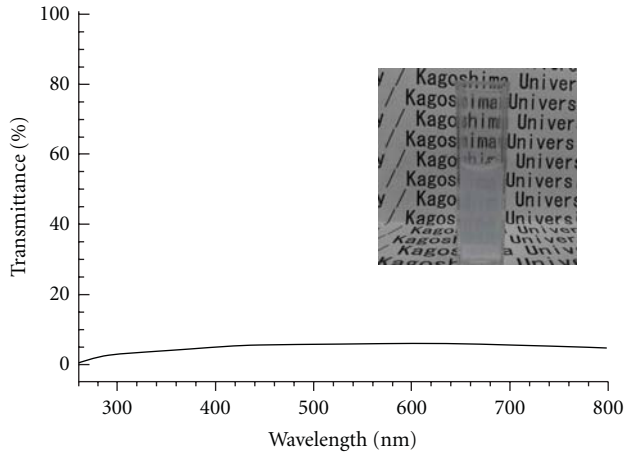

Figure 6: UV-Vis spectrum of aqueous dispersion (1.0 w/v%) of the product obtained using 0.1 mol/L aqueous hydrochloric acid as a substitute for methanolic hydrochloric acid in the first-step reaction. The inset shows a photograph of this aqueous dispersion.

Figure 7: A photograph of aqueous suspension (1.0 w/v%) of the product obtained by ion-exchange reaction of the SQ/ZrO_2-NP (feed molar ratio of APTMOS/ZTB = 0.3) with sodium laurate.

a larger particle size because the progress of the sol-gel reaction of ZTB was considerably faster than that using methanolic hydrochloric acid. These results indicate that the two-step reaction is required for the preparation of highly water-dispersible nanoparticles.

3.5. Plausible Structure of SQ/ZrO_2-NPs. We assume that the water-dispersible properties of the SQ/ZrO_2-NPs originated from the ZrO_2-$SiO_{1.5}(CH_2)$ $NH_3^+Cl^-$ core-shell structure. Therefore, to investigate the presence of ammonium cations ($-NH_3^+$) on the surface of the SQ/ZrO_2-NPs, an ion-exchange reaction of the SQ/ZrO_2-NP (APTMOS/ZTB = 0.3) was performed with sodium laurate. This was achieved by pouring the SQ/ZrO_2-NP aqueous dispersion into an aqueous solution of sodium laurate to immediately precipitate. The resulting product was not dispersed in water due to its hydrophobicity (Figure 7), although, as previously described, that with Cl^- was well dispersed. These results indicate the possibility of the ion-exchange reaction of the SQ/ZrO_2-NP, resulting in change in dispersibility in water due to the exchange of counter anions (from Cl^- to a laurate anion). Therefore, the SQ/ZrO_2-NP probably exhibits a core-shell structure with $-NH_3^+$ on its surface. Owing to charge repulsion of $-NH_3^+$ groups on the surface, SQ/ZrO_2-NPs were dispersed well in water.

3.6. Plausible Formation Mechanism of SQ/ZrO_2-NPs with Core-Shell Structures. Since ZTB is much easier to be hydrolyzed than APTMOS, a nanoaggregate composed of ZTB and oligomeric ZrO_2 components would form in the first place. Successively, hydrolysis of less reactive APTMOS probably occurred, and partially hydrolyzed material composed of $(CH_3O)_3Si(CH_2)_3NH_3^+Cl^-$ and oligomeric $SiO_{1.5}(CH_2)_3NH_3^+Cl^-$ components would stack on the surface of the ZTB/ZrO_2 aggregate. Thus, it would be assumed that the intermediate with the core-shell structure was formed (Scheme 2(a)). Subsequently, when the water was added to the intermediate and the resulting aqueous solution was heated in the open system, the reaction completely proceeded to probably prepare the final product (SQ/ZrO_2-NPs) with ZrO_2-$SiO_{1.5}(CH_2)_3NH_3^+Cl^-$ core-shell structure (Scheme 2(b)).

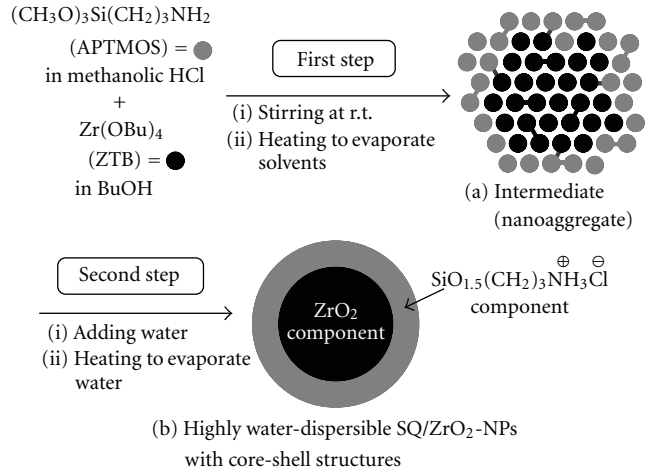

Scheme 2: Plausible formation mechanism of SQ/ZrO_2-NPs with core-shell structures.

4. Conclusions

Highly water-dispersible SQ/ZrO_2-NPs were prepared by the two-step sol-gel copolycondensation of a mixture of APTMOS and ZTB, whereby *n*-butanol and methanolic hydrochloric acid were first used as a mixed solvent, followed by water. Aqueous dispersions of SQ/ZrO_2-NPs obtained with a feed molar ratio of APTMOS/ZTB of more than 0.3 were highly transparent, and redispersion was possible. The volume-average particle sizes of the SQ/ZrO_2-NPs (APTMOS/ZTB $\geq$ 0.3) were assessed to be ca. 4.6–23.8 nm

by DLS measurements in water. The theoretical refractive index of the SQ/ZrO_2-NP (APTMOS/ZTB = 0.3) was estimated to be 1.66. It was assumed that the water-dispersible properties of the SQ/ZrO_2-NPs originated from the ZrO_2-$SiO_{1.5}(CH_2)_3NH_3^+Cl^-$ core-shell structure.

Acknowledgments

The authors thank Professor Y. Suda and Dr. M. Wakao of Graduate School of Science and Engineering, Kagoshima University (Japan), for support in DLS measurements. They also acknowledge Professor M. Higo and Dr. M. Mitsushio of Graduate School of Science and Engineering, Kagoshima University (Japan), for refractive index measurements.

References

[1] S. Lee, H. J. Shin, S. M. Yoon, D. K. Yi, J. Y. Choi, and U. Paik, "Refractive index engineering of transparent ZrO_2-polydimethylsiloxane nanocomposites," *Journal of Materials Chemistry*, vol. 18, no. 15, pp. 1751–1755, 2008.

[2] T. Otsuka and Y. Chujo, "Preparation and characterization of poly(vinylpyrrolidone)/Zirconium oxide hybrids by using inorganic nanocrystals," *Polymer Journal*, vol. 40, no. 12, pp. 1157–1163, 2008.

[3] T. Otsuka and Y. Chujo, "Synthesis of transparent poly (vinylidene fluoride) (PVdF)/zirconium oxide hybrids without crystallization of PVdF chains," *Polymer*, vol. 50, no. 14, pp. 3174–3181, 2009.

[4] M. Ochi, D. Nii, and M. Harada, "Effect of acetic acid content on in situ preparation of epoxy/zirconia hybrid materials," *Journal of Materials Science*, vol. 45, no. 22, pp. 6159–6165, 2010.

[5] Y. Hu, G. Gu, S. Zhou, and L. Wu, "Preparation and properties of transparent PMMA/ZrO_2 nanocomposites using 2-hydroxyethyl methacrylate as a coupling agent," *Polymer*, vol. 52, no. 1, pp. 122–129, 2011.

[6] M. Chatry, M. Henry, and J. Livage, "Synthesis of non-aggregated nanometric crystalline zirconia particles," *Materials Research Bulletin*, vol. 29, no. 5, pp. 517–522, 1994.

[7] J. Joo, T. Yu, Y. W. Kim et al., "Multigram scale synthesis and characterization of monodisperse tetragonal zirconia nanocrystals," *Journal of the American Chemical Society*, vol. 125, no. 21, pp. 6553–6557, 2003.

[8] W. He, Z. Guo, Y. Pu, L. Yan, and W. Si, "Polymer coating on the surface of zirconia nanoparticles by inductively coupled plasma polymerization," *Applied Physics Letters*, vol. 85, no. 6, pp. 896–898, 2004.

[9] Y. Kaneko, N. Iyi, K. Kurashima, T. Matsumoto, T. Fujita, and K. Kitamura, "Hexagonal-structured polysiloxane material prepared by sol-gel reaction of aminoalkyltrialkoxysilane without using surfactants," *Chemistry of Materials*, vol. 16, no. 18, pp. 3417–3423, 2004.

[10] Y. Kaneko, N. Iyi, T. Matsumoto, and K. Kitamura, "Synthesis of rodlike polysiloxane with hexagonal phase by sol-gel reaction of organotrialkoxysilane monomer containing two amino groups," *Polymer*, vol. 46, no. 6, pp. 1828–1833, 2005.

[11] Y. Kaneko and N. Iyi, "Sol-gel synthesis of rodlike polysilsesquioxanes forming regular higher-ordered nanostructure," *Zeitschrift für Kristallographie*, vol. 222, no. 11, pp. 656–662, 2007.

[12] Y. Kaneko and N. Iyi, "Sol-gel synthesis of water-soluble polysilsesquloxanes with regular structures," *Kobunshi Ronbunshu*, vol. 67, no. 5, pp. 280–287, 2010.

[13] Y. Kaneko, M. Shoiriki, and T. Mizumo, "Preparation of cage-like octa(3-aminopropyl)silsesquioxane trifluoromethanesulfonate in higher yield with a shorter reaction time," *Journal of Materials Chemistry*, vol. 22, no. 29, pp. 14475–14478, 2012.

[14] Y. Kaneko, H. Toyodome, M. Shoiriki, and N. Iyi, "Preparation of ionic silsesquioxanes with regular structures and their hybridization," *International Journal of Polymer Science*. In press.

[15] Y. Kaneko, N. Iyi, T. Matsumoto, and H. Usami, "Synthesis of water-soluble silicon oxide material by sol-gel reaction in tetraalkoxysilane-aminoalkyltrialkoxysilane binary system," *Journal of Materials Research*, vol. 20, no. 8, pp. 2199–2204, 2005.

[16] Y. Kaneko, "Preparation of highly water-dispersible titanium-silicon binary oxide materials by sol-gel method," *Journal of Nanoscience and Nanotechnology*, vol. 11, no. 3, pp. 2458–2464, 2011.

Hindawi Publishing Corporation
International Journal of Polymer Science
Volume 2012, Article ID 173624, 17 pages
doi:10.1155/2012/173624

Review Article

Design and Synthesis of Functional Silsesquioxane-Based Hybrids by Hydrolytic Condensation of Bulky Triethoxysilanes

Hideharu Mori

Department of Polymer Science and Engineering, Graduate School of Science and Engineering, Yamagata University, 4-3-16, Jonan, Yonezawa 992-8510, Japan

Correspondence should be addressed to Hideharu Mori, h.mori@yz.yamagata-u.ac.jp

Received 12 July 2012; Accepted 15 September 2012

Academic Editor: Kimihiro Matsukawa

This paper presents a short overview of recent advances in the design and synthesis of organic-inorganic hybrids using silsesquioxane-based nanoparticles having nanometer size, relatively narrow size distribution, high functionalities, and various characteristic features, mainly focusing on our recent researches related to the subject. A highlight of this paper is the water-soluble silsesquioxane-based nanoparticles, including hydroxyl-functionalized and cationic silsesquioxanes, which were synthesized via the one-step condensation of the bulky triethoxysilane precursors. The design and synthesis of R-$SiO_{1.5}$/SiO_2 and R-$SiO_{1.5}$/TiO_2 hybrids by hydrolytic cocondensation of a triethoxysilane precursor and metal alkoxides are briefly introduced. This paper also deals with recent results in stimuli-responsive hybrids based on the water-soluble silsesquioxane nanoparticles and fluorinated and amphiphilic silsesquioxane hybrids.

1. Introduction

The silsesquioxane family is now recognized to have an enormous potential as a building block for various advanced materials, and their applications can be found in the areas of catalysis, coordination chemistry, and material science, such as organic-inorganic nanocomposites [1–9]. Silsesquioxane is a family of compounds characterized by a ratio of 1.5 between the silicon and oxygen atoms [4], and the structures can be expressed in the general formula: $(R–SiO_{1.5})_n$ (n = even number) [1]. In particular, much interest has been paid to cubic T_8 silsesquioxane $(R–SiO_{1.5})_8$, consisting of a rigid, crystalline silica-like core that is perfectly defined spatially (0.5–0.7 nm) and that can be linked covalently to eight R groups [10, 11], because of their possible applications in optics, electronics, engineering, and biosciences.

Although some T_8 compounds are commercially available, the synthesis of polyhedral oligomeric silsesquioxane (also known as T_8 silsesquioxane or POSS) is plagued by relatively low yields of multistage syntheses and time-consuming procedures. One alternative to exploit them for practical applications is to use a more easily accessible mixture of silsesquioxanes. The hydrolysis and polycondensation of substituted alkoxysilanes, $R–Si(OR')_3$, containing a nonhydrolyzable Si–C bond or chlorosilanes are known to be a representative method to afford a variety of silsesquioxanes with various substituent groups and cage structures [2–4]. In the synthesis of silsesquioxanes via hydrolytic condensation of $R–Si(OR')_3$, it is known that the reactions and the resulting structures are influenced by many factors, such as the nature of the R′ and R groups, solvent, concentration, addition rate, quality of water, temperature, pH, and reaction time [3, 4]. Among them, water related with the hydrolysis reaction to give trisilanol and the solvent related with the solubilities of a precursor and resulting hybrid may play a relevant role in influencing the synthesis.

A variety of silsesquioxanes having various functional groups, different numbers of substituent groups, and cage structures has been developed. Completely condensed silsesquioxanes, $(R–SiO_{1.5})_n$ with $n = 4, 6, 8, 10$, and 12, have been synthesized and characterized [4]. Completely condensed structures, $(R–SiO_{1.5})_n$ with $n > 12$, are not so common, but some examples have been reported [3, 12, 13]. In addition to the fully condensed structures, $(R–SiO_{1.5})_n$,

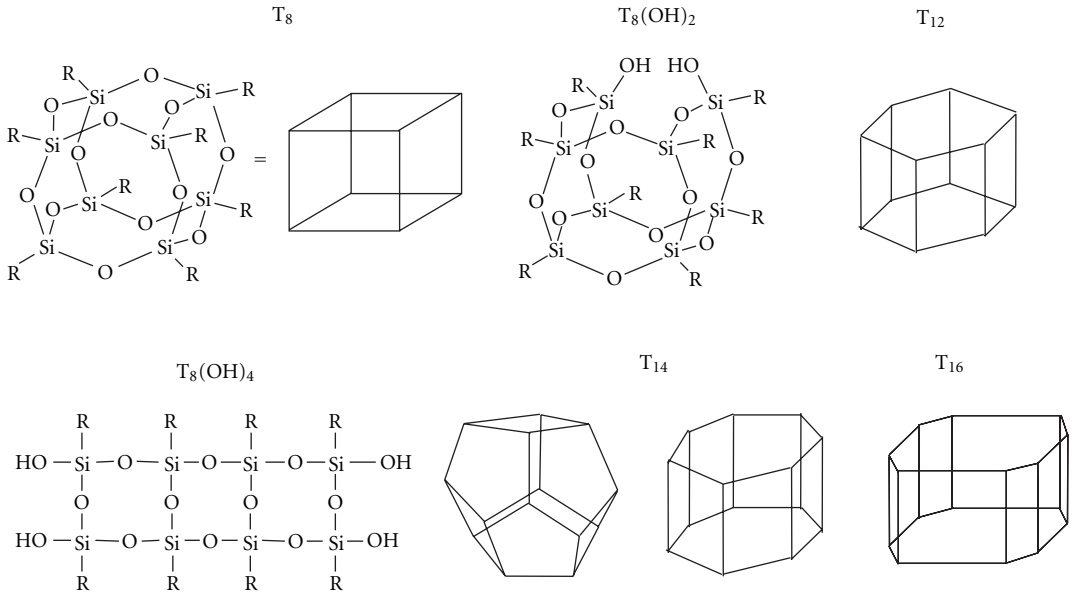

Figure 1: Schematic representation of various structures, ladder ($T_8(OH)_4$), partially cage ($T_8(OH)_2$), and cage (T_8–T_{16}) structures.

which is denoted as T_n (n = even number), incompletely condensed structures containing Si–OH groups are known, which have generic formula; $[R\text{–}SiO_{1.5-x}(OH)_{2x}]_n$ or $T_n(OH)_m$ [1, 4, 14]. The structures include perfect polyhedra, incompletely condensed polyhedra (species with 1–3 OH per molecule), ladder-type structure (species with 4 OH per molecule), open structure (species with more than 5 OH per molecule), linear structure, and all their possible combinations. Examples of possible structures are shown in Figure 1.

Preferable formation of cubic T_8 species over the T_{10}, T_{12}, and other fully condensed species is known to be due to the stability of the Si_4O_4 ring structures. Even if a variety of cubic silsesquioxanes having various functional groups has been developed by the hydrolysis/condensation process, it does have certain inherent disadvantages, such as long reaction times, up to three months in some cases, and low yields less than 50% [5]. The low yield is one of the most important problems to afford cubic T_8 species by the hydrolysis/condensation. This is mainly attributed to the formation of the mixtures of the fully condensed products with byproducts of ladder and other nonpolyhedral silsesquioxanes and formation of oligomeric products having higher contents of silicon atoms, such as T_{10}, T_{12}. The difficulty in the separation of the desired cubic T_8 species from the byproducts is another reason for low yields.

Organic-inorganic hybrid nanoparticles have attracted a great deal of attention due to their potential applications in a wide range of fields. Further advances of such organic-inorganic nanocomposite materials require fine-tuning of the sizes, structures, compositions, topologies, and spatial assembly of individual constitutes and their interfaces. Several efforts have been directed at the preparation of novel colloids and nanoparticles based on the hydrolytic condensation of monosilanes, and the resulting products are often called polysilsesquioxanes colloids or polyorganosiloxane nanoparticles. For example, Bronstein et al. reported the synthesis of a new family of polysilsesquioxanes colloids based by hydrolytic condensation of N-(6-aminohexyl)aminopropyltrimethoxysilane [15]. They claimed that the well-defined colloids (30–50 nm) were obtained at neutral initial pH. The synthesis of nanoparticles of poly(phenyl/methylsilsesquioxane) was conducted by polymerization of the cohydrolyzate from a mixture of trichlorophenylsilane and trichloromethylsilane in aqueous solution [16]. By changing the initial conditions, the average size of the resultant particles could be controlled from 30 to 250 nm in diameter. Other examples involve the syntheses of poly(phenylsilsesquioxane)s with particle sizes from 30 to 110 nm by polycondensation of phenylsilanetriol formed in aqueous solution [17] and polyorganosiloxane nanoparticles by using alkylalkoxysilanes, in which methyltrimethoxysilane was used as a network-forming monomer and diethoxydimethylsilane was employed as a chain-forming monomer in the presence of the surfactant [18].

This paper highlights recent developments in the design and synthesis of organic-inorganic hybrids using silsesquioxane-based nanoparticles having nanometer size, relatively narrow size distribution, high functionalities, and various characteristic features (Figure 2). Because the synthesis of T_8 silsesquioxane requires complicated and time-consuming procedures, much attention has been paid in developing facile synthetic methods for silsesquioxane-based nano-objects having uniform size and characteristic properties. This paper initially deals with the water-soluble silsesquioxane-based nanoparticles, including hydroxyl-functionalized silsesquioxanes (Figure 2(a)) and cationic silsesquioxanes (Figure 2(c)), which were synthesized via the one-step condensation of the bulky triethoxysilane precursors. An attractive feature of this system is that it makes it feasible to create a variety of hybrid materials

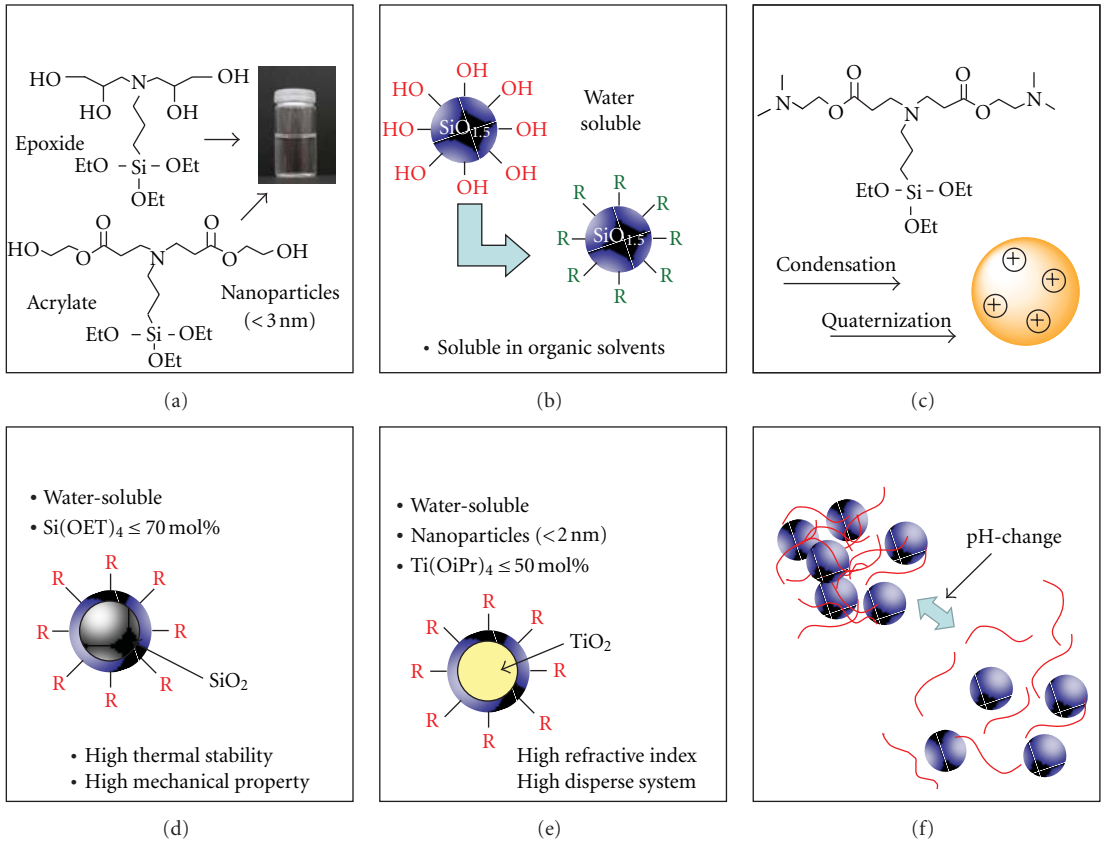

Figure 2: Summary of water-soluble silsesquioxane-based nanoparticles. (a) Water-soluble hybrids synthesized by hydrolytic condensation of hydroxyl-functionalized triethoxysilanes; (b) end-group modifications of the hydroxyl groups of the water-soluble hybrids; (c) cationic hybrids obtained by hydrolytic condensation, followed by quaternization; (d) R–$SiO_{1.5}$/SiO_2 hybrids; (e) R–$SiO_{1.5}$/TiO_2 hybrids prepared by hydrolytic cocondensation of the hydroxyl-functionalized triethoxysilane and metal alkoxides; (f) smart hybrids based on the complexation of the silsesquioxane nanoparticles and weak polyelectrolyte.

having different functional organic components through the design of appropriate triethoxysilane precursors, because various epoxy compounds and vinyl monomers can be employed as starting materials. A facile synthetic method with short synthetic steps of high yield is another advantage of this approach, an advantage which is a crucial in practical applications. Other examples involve the synthesis of R–$SiO_{1.5}$/SiO_2 hybrids (Figure 2(d)) and R–$SiO_{1.5}$/TiO_2 hybrids (Figure 2(e)) by hydrolytic cocondensation of the hydroxyl-functionalized triethoxysilane precursor and metal alkoxides. The design and synthesis of stimuli-responsive hybrids based on the silsesquioxane nanoparticles (Figure 2(f)) are briefly introduced. Examples of fluorinated and amphiphilic silsesquioxane hybrids are also given (Figure 3).

2. Hydroxyl-Functionalized Silsesquioxane-Based Hybrids

Research on water-soluble metal/metal oxide nanoparticles with narrow size distributions and characteristic properties has been extensively conducted, due to their potential applications, particularly in biorelated fields. Effective use of water-soluble nanoparticles in a given application requires fine-tuning of two factors; the physical properties of the particles itself (size, topology, composition, and nature of the particle itself) and the chemical properties of their interfaces to avoid unfavorable aggregation of individual nanoparticle and to promote specific interactions with target molecules. During recent years, there has been increasing attention paid to water-soluble silsesquioxane-based materials with tunable properties and well-defined multidimensional architectures [19–23].

Water-soluble silsesquioxane-based nanoparticles (diameter < 3.0 nm) were synthesized by hydrolytic condensation of hydroxyl-functionalized triethoxysilanes under mild conditions (Figure 2(a)). The first example is the synthesis of water-soluble nanoparticles by hydrolytic condensation of a functionalized precursor, *N*,*N*-di(2,3-dihydroxypropyl)aminopropyltriethoxysilane, which was prepared by addition reaction of (3-aminopropyl)triethoxysilane and glycidol (Figure 4(a)) [24, 25]. After the solvents (methanol and ethanol) were evaporated in vacuum, the product was obtained as a glassy solid at room temperature. In addition to tertiary amino groups, the resulting nanoparticle should have hydroxyl groups on the outermost surface, which lead to water-soluble property. The resulting silsesquioxane-based nanoparticle is soluble directly in water, methanol,

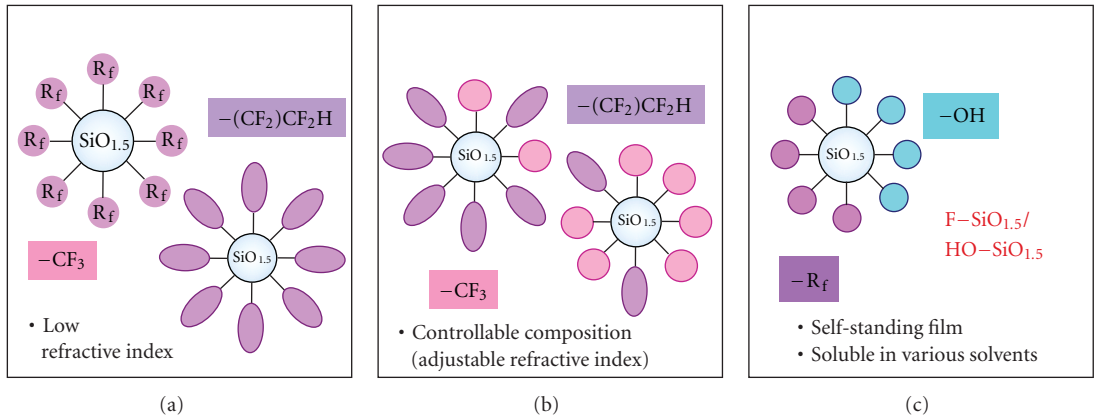

FIGURE 3: Summary of fluorinated silsesquioxane-based nanoparticles. (a) Fluorinated hybrids prepared by hydrolytic condensation of triethoxysilane precursors derived from fluoroalkyl acrylates; (b) cocondensation products obtained by hydrolytic cocondensation of TFEA-based and OFPA-based triethoxysilane precursors; (c) amphiphilic hybrids based on hydrolytic cocondensation of the hydroxyl-functionalized triethoxysilane precursor and fluorinated triethoxysilane precursors.

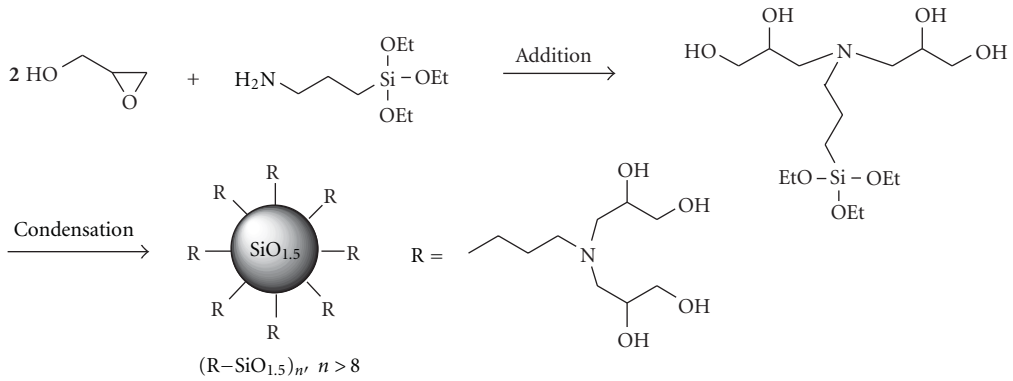

(a) Condensation of a triethoxysilane derived from glycidol

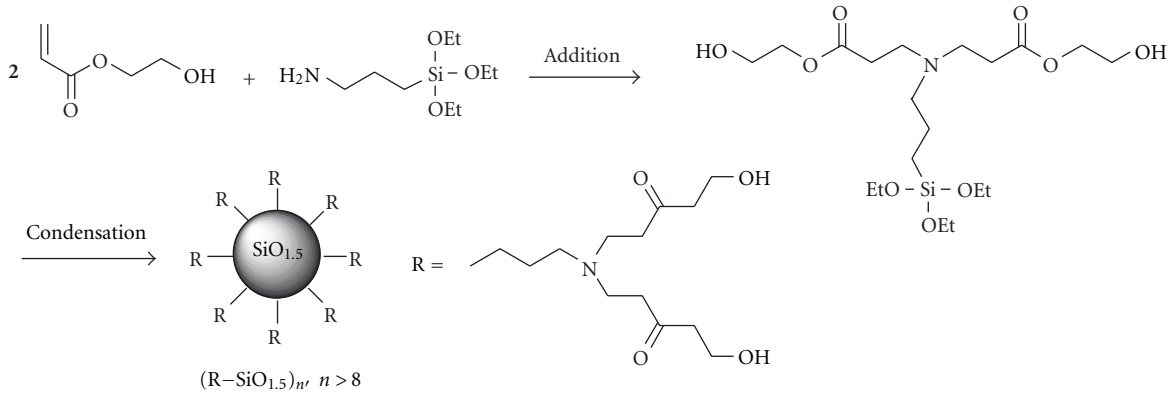

(b) Condensation of a triethoxysilane derived from 2-hydroxyethyl acrylate

FIGURE 4: Synthesis of water-soluble silsesquioxane-based nanoparticles by hydrolytic condensation of hydroxyl-functionalized triethoxysilanes.

DMF, and DMSO, while insoluble in most organic solvents, such as dichloromethane, acetone, and dioxane, and so forth. The resulting particles have relatively narrow size distribution with average particle diameter less than 3.0 nm, as confirmed by transmission electron microscopy (TEM) and scanning force microscopy (SFM). Due to the tiny size and high functionality, the nanoparticles can be uniformly dispersed in water and behave as single dissolved molecules to form a transparent colloidal solution. MALDI-TOF MS analysis indicated that the product consists of

many species having 12–18 Si atoms with different numbers of intramolecular cyclizations, and the Si–O–C bonds are formed through the reaction of SiOH (or SiOEt) groups with the hydroxyl functionalities of an organic moiety bonded to a Si atom. The species having high number of intermolecular cyclization were predominantly detected, suggesting that product mainly consists of complete and incomplete cage-like structures. Note that most of functional groups are considered to exist on the surface of the silsesquioxane-based materials, there is a possibility for some functional groups to exist within the materials. Nevertheless, this facile synthetic method with short synthetic steps with high yield endowed the nanoparticles with characteristic properties such as high functionalities, good solubility in aqueous media, nanometer size, and narrow size distribution. The silsesquioxane-based nanoparticles with a high density of hydroxyl groups on the surface were used as functional cores for the syntheses of organic/inorganic hybrid stars via "grafting from" polymerization methods [26, 27], amphiphilic silsesquioxanes having various molar ratios of hydrophilic and hydrophobic terminal groups [28], smart nanohybrid based on the complexation with amphiphilic block copolymer micelles [29], and polyurethane-silsesquioxane hybrids [30].

Although the mechanism of the formation is not yet fully understood, the feasibility to create the nanoparticles having narrow size distribution by one step condensation of the organotriethoxysilane is of interest, as it offers the possibility of large-scale production without tedious and time-consuming process. Similar behavior was also reported by another group, in which hydrolytic condensation of triethoxysilanes bearing bulky organic substituents with hydroxyl groups produced cage-type silsesquioxane having a sharp distribution with 8, 9, and 10 Si atoms [31, 32]. They demonstrated that the formation of the closed structures seems to be originated by the presence of (β-hydroxyl) tertiary amine groups in the starting organotrialkoxysilanes, in addition to the bulkiness of the organic group attached to silicon atoms [33, 34].

A bulky functionalized triethoxysilane precursor prepared by addition reaction of (3-aminopropyl)triethoxysilane and 2-hydroxyethyl acrylate (HEA) could be also employed for the preparation of water-soluble nanoparticles (Figure 4(b)) [35]. This can be regarded as the synthesis of a new family of the silsesquioxane-based nanoparticles having uniform size distribution and characteristic water-soluble property by hydrolytic condensation of the hydroxyl-functionalized triethoxysilane precursor. As shown in Figure 4(b), the first step is the addition reaction of aminopropyltriethoxysilane and HEA, followed by acidic condensation of the addition product to afford silsesquioxane-based nanoparticles. The condensation of the triethoxysilane precursor proceeded as a homogeneous system in methanol in the presence of HF (3.2%) at ambient temperature for 2 h to afford the water-soluble hybrids quantitatively. In addition to tertiary amino groups, the resulting silsesquioxane-based nanoparticles should have hydroxyl groups on the outermost surface, which leads to water soluble property. The size distribution was relatively small, and the average particle size was less than 2 nm, as confirmed by X-ray diffraction (XRD) and SFM measurements (Figure 5). The narrow polydispersity (M_w/M_n = 1.08) and a reasonable molecular weight (M_n = 3300), corresponding to species having 6–12 silicon atoms, were also confirmed by size-exclusion chromatography (SEC) measurements. For SEC measurement, the hydroxyl groups of the water-soluble silsesquioxane-based nanoparticles were converted into isobutyl ester form by esterification reaction (Figure 2(b)). The investigation of the hydrolytic condensation under various conditions suggested that the presence of the hydroxyl groups in the alkyl chain facilitates the internal cyclization, and the homogeneous reaction systems in alcohol may be prerequisite for the nanoparticle formation. In this system, the triethoxysilane precursor, R–Si$(OCH_2CH_3)_3$, R = –$CH_2CH_2CH_2N(CH_2CH_2COOCH_2CH_2OH)_2$, has a bulky organic group attached to a silicon atom, but the position of the hydroxyl group is far from the tertiary amino group. The bulkiness of the organic group and the distance between the hydroxyl group and the tertiary amino group may have some influence on the internal cyclization, resulting in the formation of closed structures and avoidance of gelation.

In this synthetic procedure, the reaction system is homogeneous during the hydrolysis/condensation reaction, since both the precursor and the resulting silsesquioxane hybrid are soluble in methanol in the presence of a small amount of HF aqueous solution used as acidic catalyst. This is a quite different feature from conventional systems, in which the reaction is heterogeneous, because precursors containing a H or an alkyl chain bonded to a Si atom are only soluble in organic solvents. In this system, the usage of the functional triethoxysilane precursor having two hydroxyl groups and ester groups may support the formation of the functionalized silsesquioxane hybrid that has nanometer size, uniform size distribution, and good solubility in many solvents. These results suggest the feasibility of creating the silsesquioxane hybrid having a high density of chemically bonded peripheral hydroxyl groups on the outermost surface, via the one-step condensation of the bulky triethoxysilane precursor, which can be achieved through the careful choice of the organic structure and condensation conditions.

3. Water-Soluble R–$SiO_{1.5}$/SiO_2 Hybrid Nanoparticles by Cocondensation

Cocondensation of a trialkoxysilane and a tetraalkoxysilane compound provides organic-inorganic hybrid materials, in which thermal and mechanical properties can be manipulated by the tetraalkoxysilane content. The increase in a tetraalkoxysilane compound in the feed may lead to the formation of glassy hybrids with higher inorganic component. Further, the cocondensation can be regarded as a convenient and promising process to produce novel functional hybrids, which have inorganic silica-like properties and exhibit characteristic solubility in appropriate solvents, if the presence of a particular trialkoxysilane prevents the gelation effectively during the hydrolytic cocondensation of the mixtures.

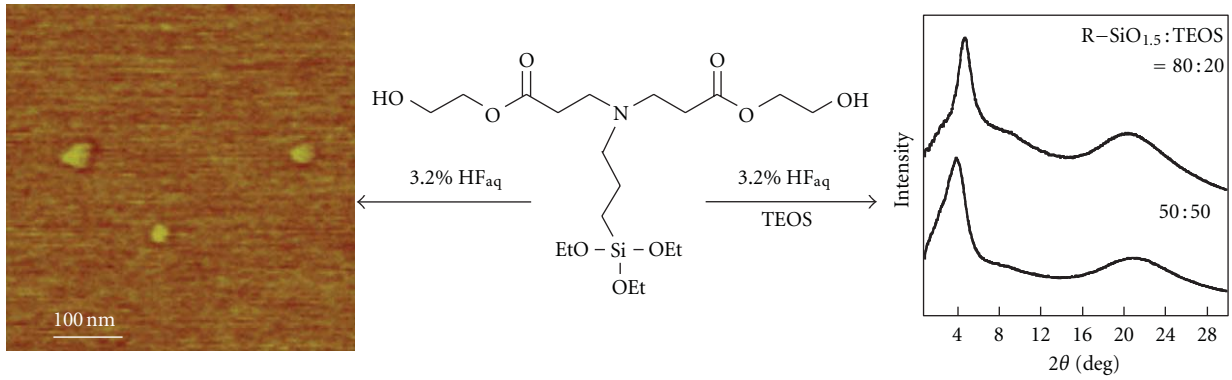

Figure 5: SFM height image and XRD spectra of water-soluble silsesquioxane-based nanoparticles synthesized by hydrolytic (co-)condensation of the hydroxyl-functionalized triethoxysilane precursor derived from 2-hydroxyethyl acrylate (HEA). Reprinted with permission from [35]. Copyright 2007 American Chemical Society.

The cocondensation of tetraethoxysilane (TEOS) with the hydroxyl-functionalized triethoxysilane precursor provided water-soluble nanoparticles having similar sizes (ca, 2 nm) with higher thermal property, depending on the composition in the feed (Figure 6(a)) [35]. Cocondensation was carried out under different feed ratios in methanol at room temperature, and the water-soluble products were obtained in the cases of TEOS molar ratio up to 70% (Figure 2(d)). Thermal stability and the char yield were found to increase with increasing the TEOS content in the feed, as determined by thermogravimetric analysis. The isolated nanoparticles distributed homogeneously without any aggregation were visualized by SFM, when the product was prepared at TEOS/the triethoxysilane = 50/50 mol%. The formation of the nanoparticles by hydrolytic cocondensation was also confirmed by the XRD studies (Figure 5). In the cocondensation process, the content of inorganic component, solubility, thermal stability, and size of the hybrid materials could be manipulated, depending on the triethoxysilane precursor/tetraethoxysilane ratio in the feed. Another attractive feature of this system is the feasibility to create a variety of hybrid materials, because various metal alkoxides can be employed as starting materials.

4. Water-Soluble R–$SiO_{1.5}$/TiO_2 Hybrid Nanoparticles by Cocondensation

Titania-silica mixed oxides have attracted significant research interest, because of their wide range of applications, such as glasses with a low thermal coefficient [36] or high strength [37], super-hydrophilic surfaces [38, 39], implant coatings for direct tissue attachment [40, 41], high-k dielectric materials [42], optical sensors [43–45], antireflection coating for solar cells [46], optical planar waveguide [47–49], and heterogeneous catalysts [50–54]. Various kinds of TiO_2–SiO_2 composites have been developed, which involve spherical particles [55, 56], thin films [39, 44, 46], fibers [57, 58], and porous materials [50, 54, 59]. Manipulation of the size, shape, microstructures, and surface area is crucial to improve characteristic properties, such as catalytic activity, photoactivity, chemical durability, and optical and thermal properties.

Novel water-soluble R–$SiO_{1.5}$/TiO_2 hybrid nanoparticles were synthesized by hydrolytic cocondensation of titanium alkoxides ($Ti(OR')_4$ R′ = ethyl, isopropyl, and butyl) with the hydroxyl-functionalized triethoxysilane precursor (Figure 2(e)) [60]. Cocondensation of a titanium alkoxide with the triethoxysilane precursor was investigated at different feed ratios, suggesting that water-soluble nanoparticles were obtained only at less than 30% of $Ti(OEt)_4$ molar ratio in the feed. In contrast, the cocondensation of titanium tetraisopropoxide, $Ti(O^iPr)_4$, with the triethoxysilane precursor in the presence of acetylacetone proceeded as a homogeneous system until 70% of $Ti(O^iPr)_4$ molar ratio to afford water-soluble organic-inorganic hybrid nanoparticles containing titania-silica mixed oxides (Figure 6(b)), as confirmed by NMR, FT-IR, elemental, and ICP analyses. SFM measurements of the product prepared at $Ti(O^iPr)_4$/the triethoxysilane = 50/50 mol% with acetylacetone indicated the formation of the nanoparticles having relatively narrow size distribution with average particle diameter less than 2.0 nm without aggregation. The refractive index of the hybrid nanoparticle was 1.571. The isolated nanoparticles distributed homogeneously were visualized by TEM, and the size of the hybrid nanoparticle (1.9 nm) was determined by XRD.

5. Cationic Hybrid Nanoparticles

Cationic silsesquioxane-based materials with tunable properties and well-defined multidimensional architectures have become of special interest, because of their industrial importance and scientifically interesting properties. The potential applications involve biocompatible drug carrier [61], detection of conformation transformation of double-stranded DNA [62], probe for the detection of DNA [63], light-harvesting unimolecular nanoparticle for fluorescence amplification in cellular imaging [64], modification of montmorillonite [65], and preparation of nanocomposite thin

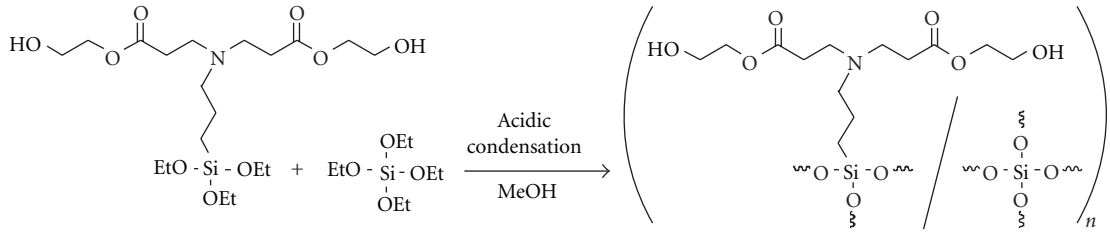

(a) Cocondensation of $Si(OEt)_4$ with the triethoxysilane precursor

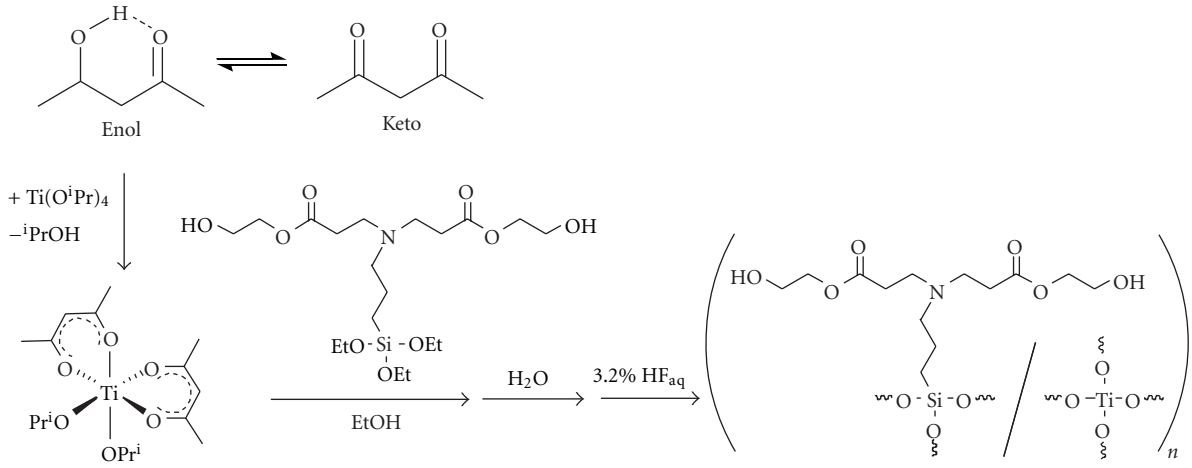

(b) Cocondensation of $Ti(O^iPr)_4$ with the triethoxysilane in the presence of acetylacetone

Figure 6: Synthesis of hybrid nanoparticles by cocondensation of the hydroxyl-functionalized triethoxysilane precursor derived from 2-hydroxyethyl acrylate (HEA).

films via layer-by-layer electrostatic self-assembly [22, 66]. Most of these cationic silsesquioxanes have been prepared from octafunctional polyhedral oligomeric silsesquioxanes, consisting of a rigid, crystalline silica-like core that is perfectly defined spatially (0.5–0.7 nm) and that can be linked covalently to eight R groups, such as octavinyl- and octaamino-substituted ones.

Recently, the synthesis of novel cationic silsesquioxane hybrids having uniform size distribution and characteristic water-soluble property by hydrolytic condensation of a triethoxysilane precursor derived from 2-(dimethylamino)ethyl acrylate (DMAEA) was reported, as shown in Figure 2(c) [67]. The development of an easily accessible mixture of silsesquioxanes with ionic or ionizable groups is one option for their exploitation in practical applications. As shown in Figure 7(a), the first step is the addition reaction of aminopropyltriethoxysilane and DMAEA, followed by hydrolytic condensation of the addition product to afford silsesquioxane hybrid. Acidic condensation of the DMAEA-based triethoxysilane precursor proceeded as a homogeneous system in methanol at room temperature to afford the water-soluble hybrid almost quantitatively. In addition to the ester groups, the resulting silsesquioxane hybrid exhibits a high density of chemically bonded peripheral tertiary amino groups on the outermost surface, which leads to water-solubility and various characteristic properties. The relatively low polydispersity (M_w/M_n = 1.33) and a reasonable molecular weight (M_n = 2700) were confirmed by SEC measurement. The size of the silsesquioxane hybrid (1.7 nm) was also determined by XRD. Quaternization reaction of the tertiary amine-containing hybrids with methyl iodide led to cationic silsesquioxane hybrids containing quaternized amine functionalities, which showed good solubility in polar solvents. SFM measurements indicated the formation of the cationic silsesquioxane hybrids having relatively narrow size distribution with average particle diameter (about 2.0 nm) without aggregation. Hence, it is entirely fair to say that the product obtained by the hydrolytic condensation of the functional precursor derived from DMAEA is a mixture of silsesquioxanes having different silicon atoms, which can be called silsesquioxane-based nanoparticles, because their structures are topologically equivalent to a sphere. Note that polyhedral silsesquioxanes are often referred to as spherosiloxanes, since polyhedral structures are topologically equivalent to a sphere. Cocondensation of TEOS with the triethoxysilane precursor was carried out under different feed ratios, and water-soluble products were obtained in the cases of TEOS molar ratio up to 40% (Figure 7(b)). This convenient synthetic approach may lead to further development of novel organic-inorganic hybrids, because of the characteristic properties of the cationic silsesquioxane hybrid, such as high functionalities, solubility in aqueous medium, nanometer size, and narrow size distribution.

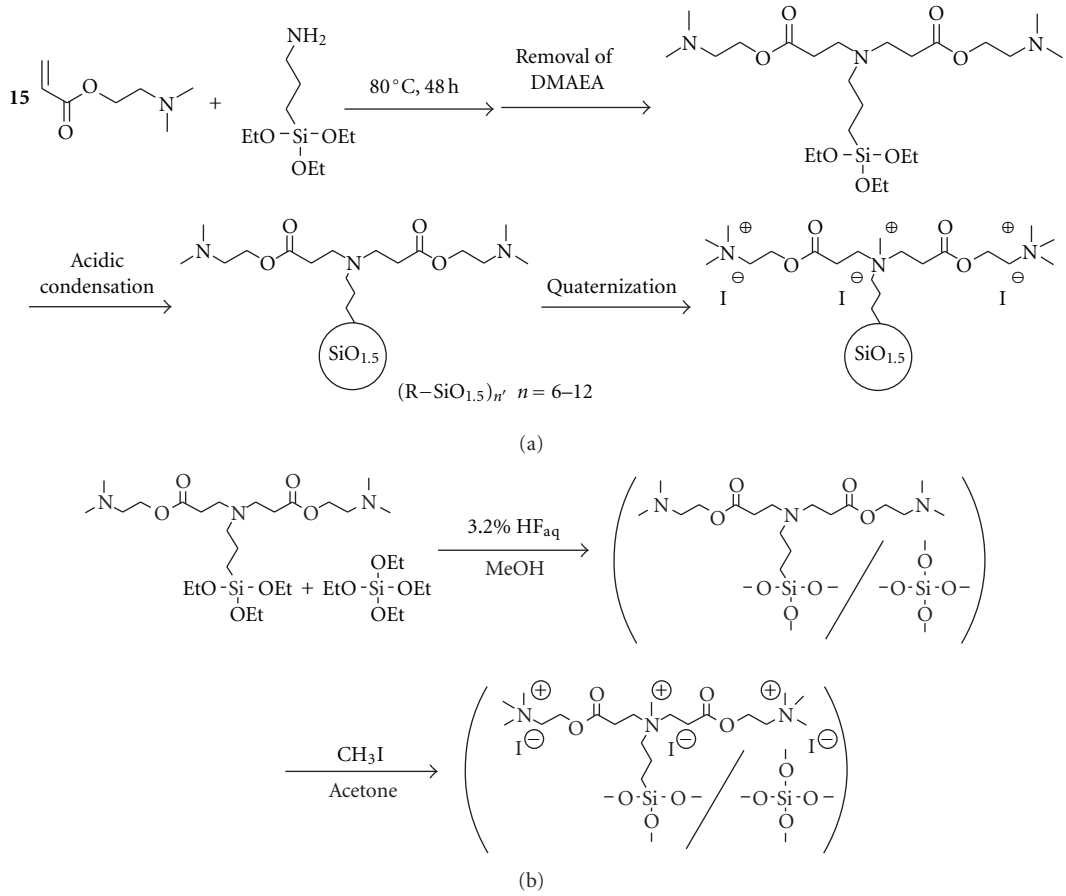

Figure 7: Synthetic routes for cationic silsesquioxane hybrids by (a) hydrolytic condensation of a functionalized precursor derived from 2-(dimethylamino)ethyl acrylate (DMAEA), followed by quaternization, and (b) hydrolytic cocondensation of tetraethoxysilane (TEOS) with the DMAEA-based triethoxysilane precursor.

6. Fluorinated Silsesquioxane-Based Hybrids

In recent years, increasing attention has been paid to fluorinated silsesquioxanes, which consist of a silicon-oxygen core framework and a fluoroalkyl shell. For example, fluorinated polyhedral oligomeric silsesquioxane molecules, in which the rigid cage is surrounded by perfluoroalkyl groups, were employed in the design of superoleophobic surfaces [68]. In this system, the fluorinated silsesquioxanes exhibited limited solubility because they were synthesized by basic condensation of triethoxysilane derivatives having hydrophobic and oleophobic fluoroalkyl groups such as 1*H*,1*H*,2*H*,2*H*-heptadecafluorodecyl and 1*H*,1*H*,2*H*,2*H*-tridecafluorooctyl groups [68, 69]. A number of fluorinated polyhedral oligomeric silsesquioxane structures possessing a high degree of hydrophobicity has been prepared via a facile corner-capping methodology using various fluoroalkyl trichlorosilanes [70, 71]. A fluorinated polyhedral oligomeric silsesquioxane was also prepared by hydrosilylation of octakis(dimethylsiloxy)silsesquioxane with a fluorinated allyl ether derivative [72]. Another example is the synthesis of a heteroleptic silsesquioxane consisting of perfluoro, isooctyl, and amino (or alkoxy) groups by basic hydrolysis of the corresponding trialkoxysilane precursors [73, 74]. Fluorinated silsesquioxane/polymer hybrids have recently inspired additional research efforts in which the silsesquioxane component has been either blended or covalently linked with a polymer [75–79]. Various fluorinated silsesquioxane/polymer hybrids have been also employed for modification of surface dewettability [80–82] and in lithography [83, 84].

Recently, the synthesis of novel low-refractive-index fluorinated silsesquioxane-based hybrids that have uniform size distribution, good solubility, and a tunable refractive index by hydrolytic condensation of triethoxysilane precursors derived from fluoroalkyl acrylates was demonstrated (Figure 3(a)) [85]. As shown in Figure 8(a), the first step is the addition reaction of aminopropyltriethoxysilane and fluoroalkyl acrylates, followed by acidic condensation of the addition products. Two acrylates having different fluoroalkyl chains—1*H*,1*H*,5*H*-octafluoropentyl acrylate (OFPA) and 2,2,2-trifluoroethyl acrylate (TFEA)—were employed for the preparation of the fluorinated triethoxysilane precursors ($R–Si(OCH_2CH_3)_3$). The condensation of the fluorinated triethoxysilane precursors in the presence of a small amount of HF aqueous solution proceeded as a homogeneous system

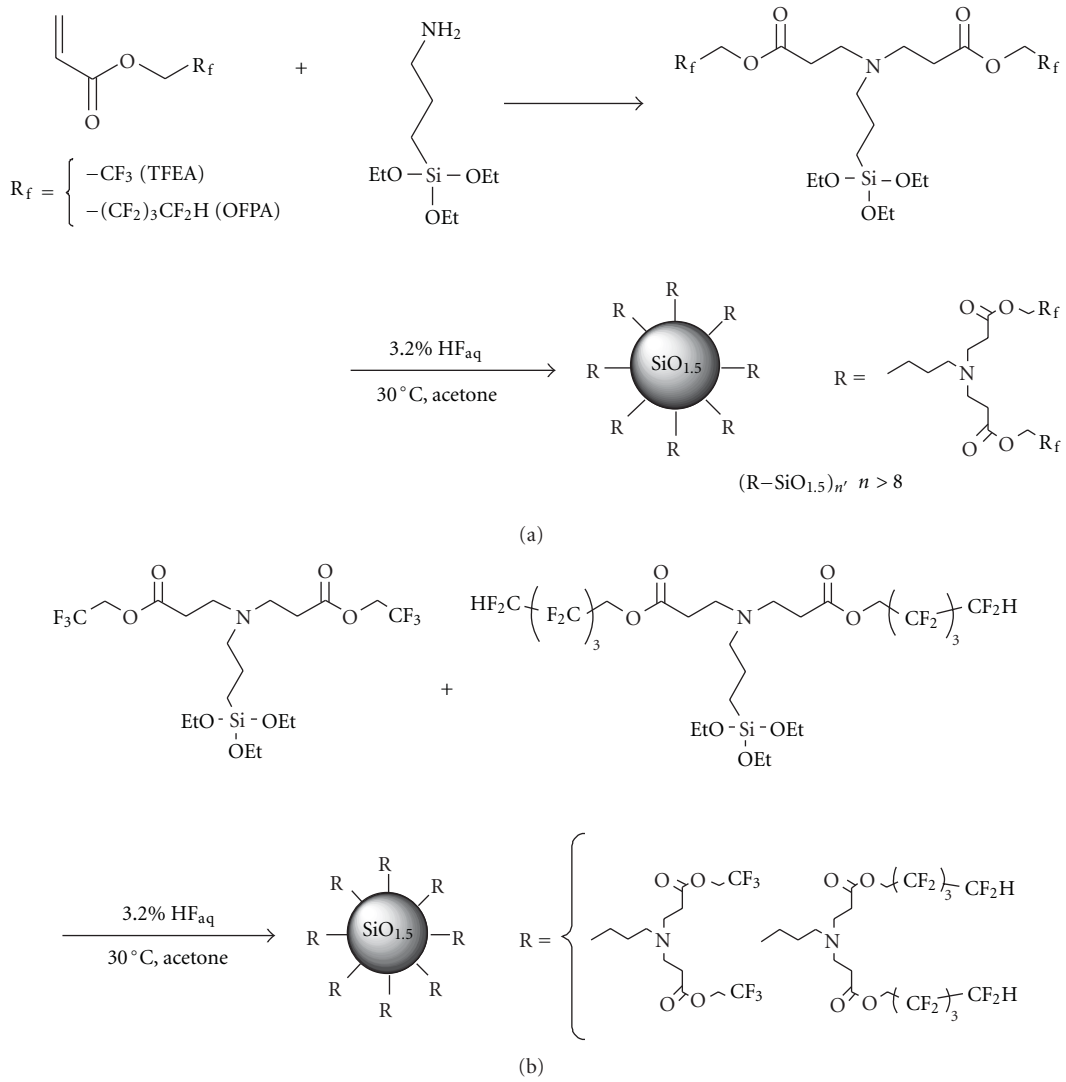

Figure 8: Synthetic routes for fluorinated silsesquioxane-based hybrids obtained via (a) hydrolytic condensation of triethoxysilane precursors derived from fluoroalkyl acrylates, and (b) hydrolytic cocondensation of TFEA-based and OFPA-based triethoxysilane precursors.

in acetone at 30°C until the end of the reaction. After the solvents (acetone and ethanol) were evaporated in a vacuum, the products were obtained quantitatively. The products were soluble in a variety of organic solvents, including $CHCl_3$, THF, and acetone, but were insoluble in hexane and water. The resulting silsesquioxane-based hybrids exhibited a high density of chemically bonded peripheral fluoroalkyl groups, which led to various characteristic properties, including a low refractive index. The low polydispersities and reasonable molecular weights of the resulting fluorinated silsesquioxanes (M_n = 4800, M_w/M_n = 1.01; and M_n = 4300, M_w/M_n = 1.07 for the OFPA- and TFEA-based products, resp.) were confirmed by SEC. The formation of spherical hybrids having relatively narrow size distributions (average particle diameter < 3.0 nm) without aggregation was confirmed by SFM measurements. The XRD and DSC measurements indicated that the fluorinated silsesquioxane hybrids can be regarded as amorphous glass having low glass transition temperatures. Different from the cubic silsesquioxane crystals, some silsesquioxanes having long and/or specific substituent groups were amorphous, which showed broad XRD peaks [86–88]. Similar to such amorphous silsesquioxanes, the fluorinated silsesquioxane hybrids [85], hydroxyl-functionalized silsesquioxane hybrids [35], and cationic silsesquioxane hybrids [67] synthesized via the one-step condensation of the bulky triethoxysilane precursors can be regarded as amorphous glasses, which are mainly due to the long alkyl groups. The refractive indexes of the TFEA- and OFPA-based silsesquioxane hybrids were 1.43 and 1.40, respectively.

Cocondensation of the TFEA- and OFPA-based triethoxysilane precursors afforded a series of fluorinated hybrids whose refractive index and various other properties can be manipulated by varying the composition of the feed (Figure 8(b)). The formation of hybrids having spherical structures via hydrolytic cocondensation was also confirmed

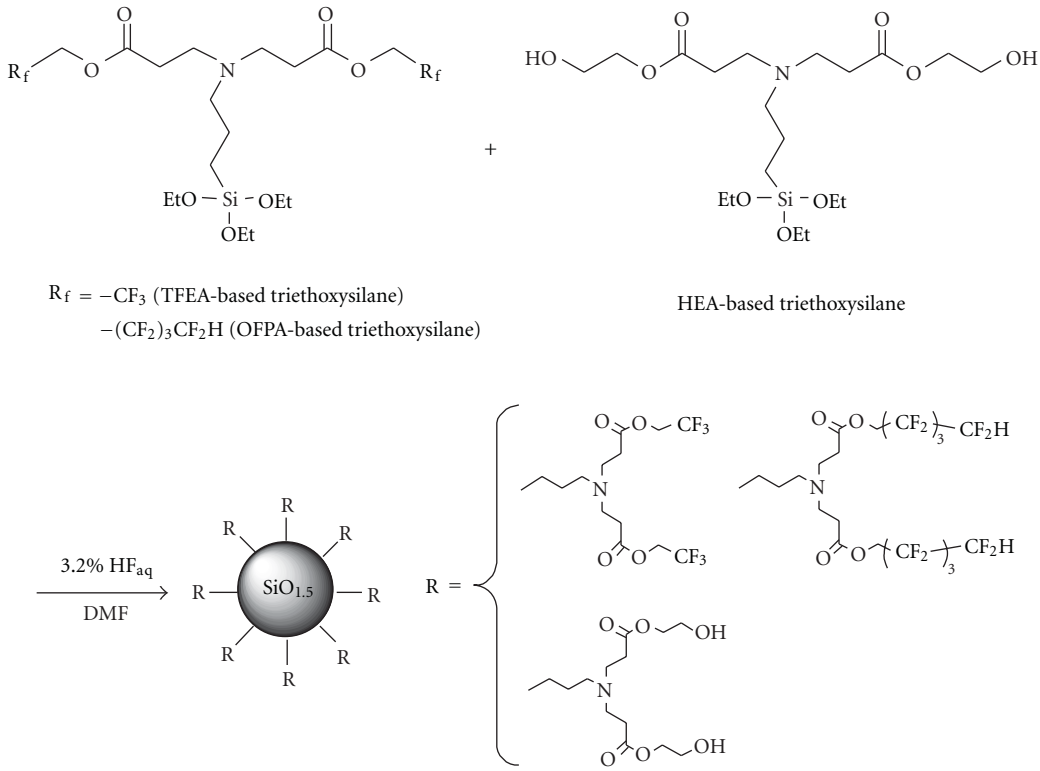

Figure 9: Synthetic route for the amphiphilic silsesquioxane-based hybrids based on hydrolytic cocondensation of the hydroxyl-functionalized triethoxysilane precursor and fluorinated triethoxysilane precursors.

by XRD and SFM measurements. Low refractive indexes of the fluorinated silsesquioxane-based hybrids could be tuned by adjusting the feed ratio of the TFEA-based and OFPA-based triethoxysilane precursors in the cocondensation (Figure 3(b)).

7. Amphiphilic Silsesquioxane-Based Hybrids

Silsesquioxanes having two or more different organic groups immobilized to an inorganic core have recently attracted considerable attention, because of their intriguing phase behavior and enormous potential as a building block for various advanced materials [5]. For example, Gunawidjaja et al. reported bulk and surface assembly of amphiphilic silsesquioxane compounds with various hydrophilic and hydrophobic terminal group compositions [28]. For the synthesis of silsesquioxanes having different substituent groups, several methods have been employed, which involve cohydrolysis/cocondensation of chlorosilanes and alkoxysilanes, corner-capping method, and synthetic modification of a preexisting silsesquioxane compound [5]. During recent years, there has been increasing attention paid to silsesquioxanes having fluoroalkyl chain as a hydrophobic component and another organic group. The synthesis of heteroleptic silsesquioxane consisting of perfluoro, isooctyl, and amino (or alkoxy) groups was conducted by basic hydrolysis of corresponding trialkoxysilane precursors [73, 74]. A number of fluorinated polyhedral oligomeric silsesquioxanes structures possessing another organic group has been prepared via a facile corner-capping methodology [70, 71]. Additionally, fluorinated polyhedral oligomeric silsesquioxanes possessing one reactive functional group by the corner-capping method were employed for preparation of various fluorinated silsesquioxanes/polymer hybrids [89–91].

Amphiphilic silsesquioxanes-based hybrids were synthesized by hydrolytic cocondensation of a hydroxyl-functionalized triethoxysilane precursor derived from 2-hydroxyethyl acrylate (HEA) and fluorinated triethoxysilane precursors derived from 1*H*,1*H*,5*H*-octafluoropentyl acrylate (OFPA) and 2,2,2-trifluoroethyl acrylate (TFEA), as shown in Figure 9 [92]. The OFPA-based triethoxysilane precursor has a bulky fluoroalkyl group attached to a silicon atom, whereas the TFEA-based precursor has a shorter fluoroalkyl group. The bulkiness of the fluoroalkyl group may have some influence on the internal cyclization, resulting in the formation of closed structures and avoidance of gelation. On the basis of the preparation method (hydrolytic cocondensation of two different triethoxysilanes, R_f–$Si(OEt)_3$ and R_{OH}–$Si(OEt)_3$), the general structure of the hybrids is expected to be $([R_f\text{–}co\text{–}R_{OH}]-SiO_{1.5})_n$, where each silicon atom is bound to an average of one-and-a-half oxygens and to one alkyl chain involving the fluoroalkyl groups or hydroxyalkyl groups. The resulting amphiphilic silsesquioxane hybrids should have fluoroalkyl groups and hydroxyalkyl groups on the outermost surface, in addition to the tertiary amino groups and ester groups, which lead to various characteristic properties.

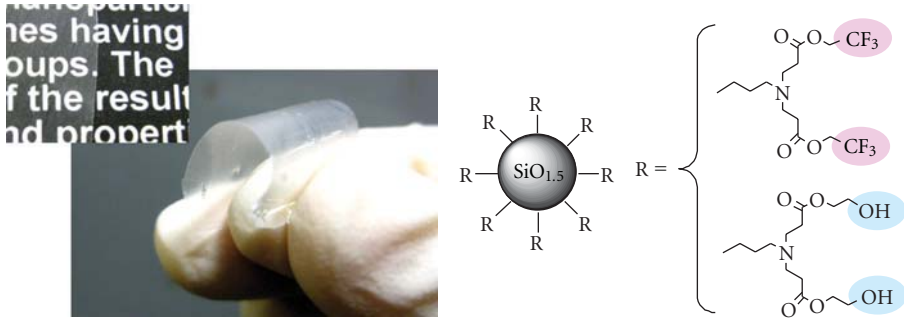

Figure 10: Photograph of flexible film of the TFEA-*co*-HEA silsesquioxane hybrid prepared by hydrolytic cocondensations. Reprinted with permission from [92]. Copyright 2012 Elsevier.

Hydrolytic cocondensations of two functionalized triethoxysilane precursors proceeded as homogeneous systems in *N*,*N*-dimethylformamide (DMF) to afford amphiphilic silsesquioxanes hybrids, which were soluble in a variety of solvents, depending on the composition. The structure of the constitutional unit of the hybrids was confirmed by the results of NMR and FT-IR measurements. SFM and XRD measurements indicated the formation of spherical hybrids having relatively narrow size distributions (average particle diameter < 3.0 nm) without aggregation. Cocondensation of the hydroxyl-functionalized precursor (HEA-based triethoxysilane) and fluorinated precursors (OFPA-based and TFEA-based triethoxysilane) provided amphiphilic hybrid materials, in which solubility, amphiphilicity, refractive index, film forming, and various properties could be manipulated by the composition in the feed (Figure 3(c)). As can be seen in Figure 10, flexible semitransparent films were obtained from the amphiphilic silsesquioxane hybrids having hydrophilic and hydrophobic chains connected chemically to an inorganic core, which were prepared by hydrolytic cocondensations at suitable feed ratios [92]. Note that self-standing hybrid films were obtained from the amphiphilic silsesquioxane hybrids in this system without any addition of cross-linker and polymer, although most of film-forming nanocomposites were prepared from organic-inorganic hybrid systems comprising of polymer chains and inorganic particles. In the systems, the formation of the flexible semitransparent films would be the result of specific interactions between the hydroxyl groups, tertiary amino groups, fluoroalkyl groups, and ester groups in the amphiphilic silsesquioxane hybrids. The presence of intermolecular interactions between these functional groups of the hybrids may contribute to achieving good film-forming property, in which physically cross-linked polymer-like materials can be easily fabricated into the self-standing hybrid films.

8. Stimuli-Responsive Organic-Inorganic Hybrids

Stimuli-responsive organic-inorganic hybrids have recently attracted considerable interest, because combination with inorganic materials offers the opportunity to develop new nanosized "intelligent" or "smart" hybrids [25, 93–97]. Manipulation of specific intermolecular interactions, such as hydrogen-bonding, acid-base interactions, and oppositely charged ionic interactions, is crucial for the design and development of stimuli-responsive organic-inorganic hybrid structures with nanometer dimensions [98–101]. The water soluble silsesquioxane-based nanoparticles obtained from glycidol (Figure 4(a)) could be used as a component for characteristic intelligent colloidal hybrids, in which the complexation of tertiary amine-containing nanoparticles and a weak anionic polyelectrolyte can be manipulated simply by pH change in aqueous solution (Figure 2(f)) [25, 97]. Poly(acrylic acid), PAA, was selected as a weak polyelectrolyte, because the degree of ionization of carboxylic acids can be easily controlled by the pH value. In this system, both PAA and the silsesquioxane nanoparticles formed visually transparent solutions in water, while a white turbid dispersion was obtained just after mixing the two solutions at room temperature. The complex formation in water was strongly affected by the pH value, and the pH-induced association-dissociation behavior was a reversible and rapid process. The reversible pH-induced colloid formation due to the complexation of the inorganic-organic nanomaterials can provide a viable route to the production of tailored materials with unique properties for various applications.

The nature of the interaction of biomolecules, such as proteins, peptides, and amino acids, with inorganic materials is a subject of extraordinary relevance due to increasing interest in biointerfaces for medical, diagnostic, and biotechnology applications. In recent years, increasing attention has also been paid to developing silsesquioxane/biomolecule hybrids [102–109]. A series of researches in the design and synthesis of amino acid-based polymers including stimuli-responsive polymers, such as pH-responsive, thermoresponsive, and dual-stimuli-responsive block copolymers, and self-assembled block copolymers having tunable chiroptical properties, have been reported, which were obtained by reversible addition-fragmentation chain transfer (RAFT) polymerization [110].

Recently, smart amino acid-based polymer/silsesquioxane hybrids was developed, in which the complexation of water-soluble silsesquioxane nanoparticles [35], derived from HEA-based triethoxysilane (Figure 11(a)), and amino

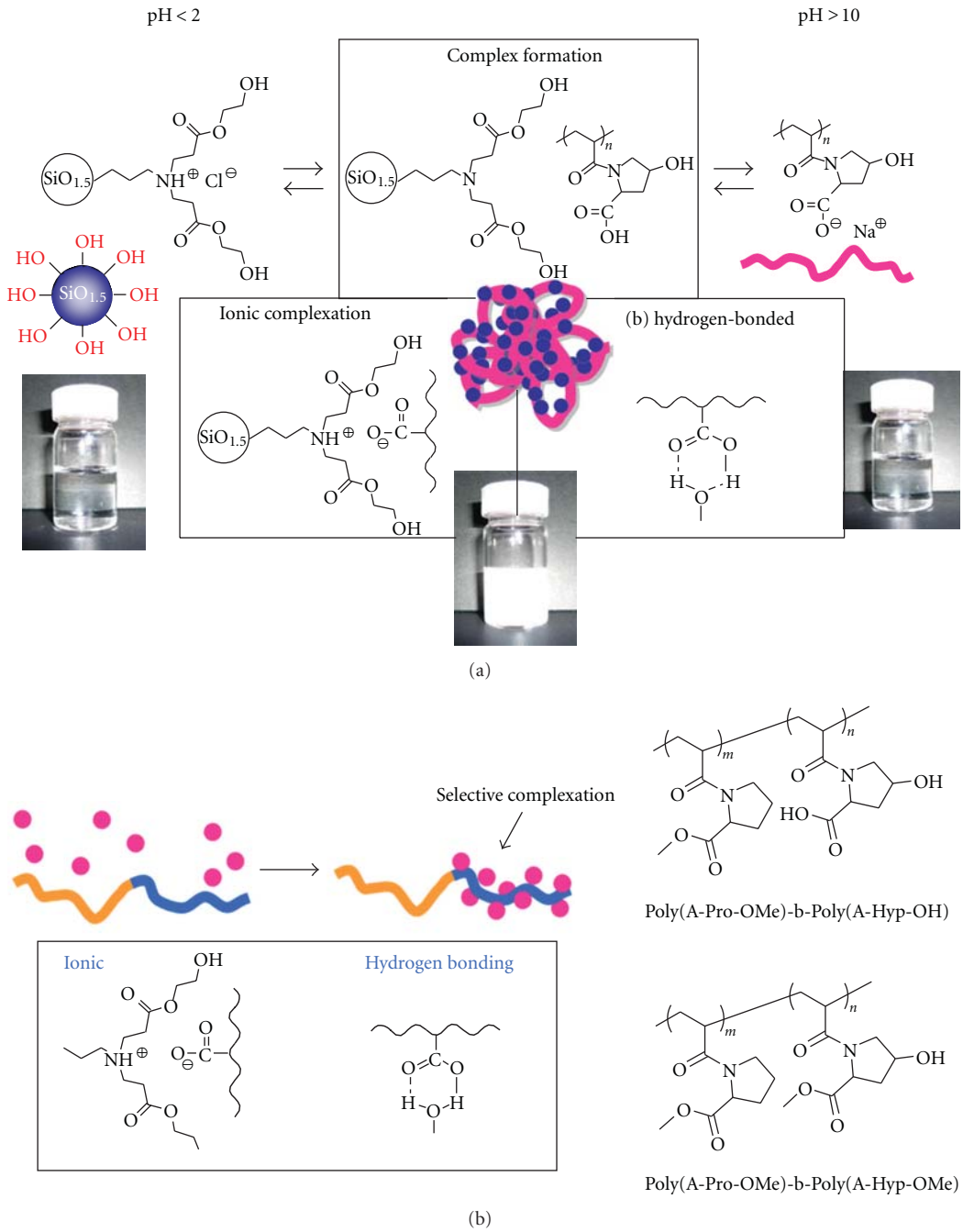

Figure 11: Smart organic-inorganic hybrids based on (a) complexation of amino acid-based polymer and water-soluble silsesquioxane nanoparticles, and (b) selective complexation of the silsesquioxane nanoparticles and block copolymer.

acid-based polymer, can be manipulated by pH changes in aqueous media [111]. The nanoparticles obtained from HEA-based triethoxysilane should have many ester groups on the surface, which may contribute hydrogen bond and therefore affect stimuli-responsive complexation of tertiary amine-containing nanoparticles and a weak anionic polyelectrolyte. Simple mixing of aqueous solutions of the amino acid-based polymer obtained from *N*-acryloyl-4-*trans*-hydroxy-l-proline (A-Hyp-OH) [112] and the silsesquioxane nanoparticles led to the straightforward formation of the pH-responsive hybrids, in which a white turbid dispersion was observed at pH = 5–8, whereas transparent solutions were obtained at pH = 2 and 10 (Figure 11(a)). The methylated sample, poly(A-Hyp-OMe), exhibited a characteristic soluble-insoluble transition at around 49.5°C [112], and thermoresponsive hybrids were obtained by complexation of the silsesquioxane nanoparticles with poly(A-Hyp-OMe) [111]. In contrast, poly(*N*-acryloyl-l-proline methyl ester) and poly(A-Pro-OMe), exhibited a relatively lower phase-separation temperature (around 18°C) in neutral water

(pH = 7) [113–115], and the thermoresponsive polymer showed no specific interaction with the silsesquioxane nanoparticles [111].

Self-assembly of block copolymer/nanoparticle hybrids has also generated significant research interest, because the nanoparticles can be spatially organized in the formed aggregates [29, 116–120]. Depending on the chemical nature of the functional segments and their composition, the block copolymers afford a great opportunity for tuning chemical and physical properties as well as assembled structures. Additionally, the size, shape, and nature of the inorganic nanoparticles and specific interactions between the organic and inorganic components act as crucial elements to provide an effective route for the controlled self-ordering of nanoparticles with polymers and for the endowment of characteristic properties. Smart organic-inorganic hybrids were prepared using noncovalent interactions between water-soluble silsesquioxane nanoparticles containing tertiary amine moieties and two amino acid-based block copolymers prepared by RAFT polymerization (Figure 11(b)) [121]. A dual thermoresponsive block copolymer displaying LCST and UCST was employed, in which only the poly(A-Hyp-OH) segment could interact with the silsesquioxane nanoparticles, whereas another poly(A-Pro-OMe) segment showed a characteristic thermoresponsive property without any interaction with the nanoparticles. The simple mixing procedure of two transparent aqueous solutions led to the formation of smart organic-inorganic hybrids through the selective complexation of the silsesquioxane nanoparticles and the poly(A-Hyp-OH) segment in the block copolymer.

9. Conclusion

This paper has summarized recent development of the silsesquioxanes-based nanoparticles prepared by hydrolytic condensation of bulky triethoxysilane precursors derived from functional acrylate derivatives. The addition reaction of aminopropyltriethoxysilane with 2-hydroxyethyl acrylate (HEA), 2-(dimethylamino)ethyl acrylate (DMAEA), 1*H*,1*H*,5*H*-octafluoropentyl acrylate (OFPA), and 2,2,2-trifluoroethyl acrylate (TFEA) afforded functional triethoxysilane precursors. The hydrolytic condensation of the addition products proceeded as homogeneous systems under suitable conditions to afford the functional silsesquioxane hybrids almost quantitatively. The development of an easily accessible mixture of silsesquioxanes with a variety of functional groups is one option for their exploitation in practical applications. This convenient synthetic approach have allowed great advances in the further development of novel organic-inorganic hybrids, because of the characteristic properties of the functional silsesquioxane hybrid, such as high functionalities, solubility in aqueous medium, nanometer size, and narrow size distribution. Depending on the chemical nature of the functional trietoxysilane precursors, additional component (trialkoxysilanes and metal alkoxides used for the cocondensation), and their composition, the silsesquioxane hybrids afforded great flexibility for tuning functional groups in the organic part, components of the inorganic parts, and various properties as well as size and shape of the hybrids. The manipulation of noncovalent interactions such as hydrogen bonding and interelectrolyte interaction was also crucial for providing organic-inorganic smart hybrids having characteristic stimuli-responsive properties. The multiscale ordering of such functional nanomaterials is a powerful technique for the creation of tailored hybrid materials with unique properties for various applications.

Acknowledgments

The author acknowledges Professor Takeshi Endo (Director of Molecular Engineering Institute, Kinki University and Vice President of Kinki University) and Professor Koichiro Yonetake (Yamagata University) for helpful suggestions, discussions, and collaborations.

References

[1] P. Eisenberg, R. Erra-Balsells, Y. Ishikawa et al., "Cagelike precursors of high-molar-mass silsesquioxanes formed by the hydrolytic condensation of trialkoxysilanes," *Macromolecules*, vol. 33, no. 6, pp. 1940–1947, 2000.

[2] F. J. Feher and T. A. Budzichowski, "Silasesquioxanes as ligands in inorganic and organometallic chemistry," *Polyhedron*, vol. 14, no. 22, pp. 3239–3253, 1995.

[3] M. G. Voronkov and V. I. Lavrent'yev, "Polyhedral oligosilsesquioxanes and their homo derivatives," *Topics in Current Chemistry*, vol. 102, pp. 199–236, 1982.

[4] P. P. Pescarmona and T. Maschmeyer, "Oligomeric silsesquioxanes: synthesis, characterization and selected applications," *Australian Journal of Chemistry*, vol. 54, no. 9-10, pp. 583–596, 2001.

[5] D. B. Cordes, P. D. Lickiss, and F. Rataboul, "Recent developments in the chemistry of cubic polyhedral oligosilsesquioxanes," *Chemical Reviews*, vol. 110, no. 4, pp. 2081–2173, 2010.

[6] S. Sulaiman, A. Bhaskar, J. Zhang, R. Guda, T. Goodson III, and R. M. Laine, "Molecules with perfect cubic symmetry as nanobuilding blocks for 3-D assemblies. Elaboration of octavinylsilsesquioxane. Unusual luminescence shifts may indicate extended conjugation involving the silsesquioxane core," *Chemistry of Materials*, vol. 20, no. 17, pp. 5563–5573, 2008.

[7] R. Y. Kannan, H. J. Salacinski, P. E. Butler, and A. M. Seifalian, "Polyhedral oligomeric silsesquioxane nanocomposites: the next generation material for biomedical applications," *Accounts of Chemical Research*, vol. 38, no. 11, pp. 879–884, 2005.

[8] R. M. Laine, "Nanobuilding blocks based on the $[OSiO_{1.5}]_x$ (x = 6, 8, 10) octasilsesquioxanes," *Journal of Materials Chemistry*, vol. 15, no. 35-36, pp. 3725–3744, 2005.

[9] P. D. Lickiss and F. Rataboul, "Chapter 1 fully condensed polyhedral oligosilsesquioxanes (POSS): from synthesis to application," *Advances in Organometallic Chemistry*, vol. 57, pp. 1–116, 2008.

[10] A. Provatas and J. G. Matisons, "Silsesquioxanes: synthesis and applications," *Trends in Polymer Science*, vol. 5, pp. 327–332, 1997.

[11] C. Zhang and R. M. Laine, "Hydrosilylation of allyl alcohol with $[HSiMe_2OSiO_{1.5}]_8$: octa(3-hydroxypropyldimethylsiloxy)octasilsesquioxane and its octamethacrylate derivative as potential precursors to hybrid nanocomposites,"

Journal of the American Chemical Society, vol. 122, no. 29, pp. 6979–6988, 2000.

[12] P. A. Agaskar, V. W. Day, and W. G. Klemperer, "A new route to trimethylsilylated spherosilicates: synthesis and structure of $[Si_{12}O_{18}](OSiMe_3)_{12}$, D_{3h}-$[Si_{14}O_{21}](OSiMe_3)_{14}$, and C_{2v}-$[Si_{14}O_{21}](OSiMe_3)_{14}$," *Journal of the American Chemical Society*, vol. 109, no. 18, pp. 5554–5556, 1987.

[13] C. L. Frye and W. T. Collins, "The oligomeric silsesquioxanes, $(HSiO_{3/2})_n$," *Journal of the American Chemical Society*, vol. 92, no. 19, pp. 5586–5588, 1970.

[14] R. J. J. Williams, R. Erra-Balsells, Y. Ishikawa, H. Nonami, A. N. Mauri, and C. C. Riccardi, "UV-MALDI-TOF and ESI-TOF mass spectrometry characterization of silsesquioxanes obtained by the hydrolytic condensation of (3-glycidoxypropyl)-trimethoxysilane in an epoxidized solvent," *Macromolecular Chemistry and Physics*, vol. 202, no. 11, pp. 2425–2433, 2001.

[15] L. M. Bronstein, C. N. Linton, R. Karlinsey et al., "Controlled synthesis of novel metalated poly(aminohexyl)-(aminopropyl)silsesquioxane colloids," *Langmuir*, vol. 19, no. 17, pp. 7071–7083, 2003.

[16] C. Ma, I. Taniguchi, M. Miyamoto, and Y. Kimura, "Formation of stable nanoparticles of poly(phenyl/methylsilsesquioxane) in aqueous solution," *Polymer Journal*, vol. 35, no. 3, pp. 270–275, 2003.

[17] C. Ma and Y. Kimura, "Preparation of nano-particles of poly(phenylsilsesquioxane)s by emulsion polycondensation of phenylsilanetriol formed in aqueous solution," *Polymer Journal*, vol. 34, no. 9, pp. 709–713, 2002.

[18] N. Jungmann, M. Schmidt, and M. Maskos, "Characterization of polyorganosiloxane nanoparticles in aqueous dispersion by asymmetrical flow field-flow fractionation," *Macromolecules*, vol. 34, no. 23, pp. 8347–8353, 2001.

[19] P. Maitra and S. L. Wunder, "Oligomeric poly(ethylene oxide)-functionalized silsesquioxanes: interfacial effects on Tg, Tm, and δHm," *Chemistry of Materials*, vol. 14, no. 11, pp. 4494–4497, 2002.

[20] R. Knischka, F. Dietsche, R. Hanselmann, H. Frey, R. Mülhaupt, and P. J. Lutz, "Silsesquioxane-based amphiphiles," *Langmuir*, vol. 15, no. 14, pp. 4752–4756, 1999.

[21] K. Y. Mya, X. Li, L. Chen, X. Ni, J. Li, and C. He, "Core-corona structure of cubic silsesquioxane-poly(ethylene oxide) in aqueous solution: fluorescence, light scattering, and TEM studies," *Journal of Physical Chemistry B*, vol. 109, no. 19, pp. 9455–9462, 2005.

[22] G. Wu and Z. Su, "Polyhedral oligomeric silsesquioxane nanocomposite thin films via layer-by-layer electrostatic self-assembly," *Chemistry of Materials*, vol. 18, no. 16, pp. 3726–3732, 2006.

[23] B. L. Frankamp, N. O. Fischer, R. Hong, S. Srivastava, and V. M. Rotello, "Surface modification using cubic silsesquioxane ligands. facile synthesis of water-soluble metal oxide nanoparticles," *Chemistry of Materials*, vol. 18, no. 4, pp. 956–959, 2006.

[24] H. Mori, M. G. Lanzendörfer, A. H. E. Müller, and J. E. Klee, "Silsesquioxane-based nanoparticles formed via hydrolytic condensation of organotriethoxysilane containing hydroxy groups," *Macromolecules*, vol. 37, no. 14, pp. 5228–5238, 2004.

[25] H. Mori, A. H. E. Müller, and J. E. Klee, "Intelligent colloidal hybrids via reversible pH-induced complexation of polyelectrolyte and silica nanoparticles," *Journal of the American Chemical Society*, vol. 125, no. 13, pp. 3712–3713, 2003.

[26] S. Muthukrishnan, F. Plamper, H. Mori, and A. H. E. Müller, "Synthesis and characterization of glycomethacrylate hybrid stars from silsesquioxane nanoparticles," *Macromolecules*, vol. 38, no. 26, pp. 10631–10642, 2005.

[27] J. Xu and W. Shi, "Synthesis and crystallization kinetics of silsesquioxane-based hybrid star poly(ελunate-caprolactone)," *Polymer*, vol. 47, no. 14, pp. 5161–5173, 2006.

[28] R. Gunawidjaja, F. Huang, M. Gumenna et al., "Bulk and surface assembly of branched amphiphilic polyhedral oligomer silsesquioxane compounds," *Langmuir*, vol. 25, no. 2, pp. 1196–1209, 2009.

[29] M. Schumacher, M. Ruppel, J. Yuan et al., "Smart organic-inorganic nanohybrids based on amphiphilic block copolymer micelles and functional silsesquioxane nanoparticles," *Langmuir*, vol. 25, no. 6, pp. 3407–3417, 2009.

[30] V. N. Bliznyuk, T. A. Tereshchenko, M. A. Gumenna et al., "Structure of segmented poly(ether urethane)s containing amino and hydroxyl functionalized polyhedral oligomeric silsesquioxanes (POSS)," *Polymer*, vol. 49, no. 9, pp. 2298–2305, 2008.

[31] D. P. Fasce, R. J. J. Williams, F. Méchin, J. P. Pascault, M. F. Llauro, and R. Pétiaud, "Synthesis and characterization of polyhedral silsesquioxanes bearing bulky functionalized substituents," *Macromolecules*, vol. 32, no. 15, pp. 4757–4763, 1999.

[32] D. P. Fasce, R. J. J. Williams, R. Erra-Balsells, Y. Ishikawa, and H. Nonami, "One-step synthesis of polyhedral silsesquioxanes bearing bulky substituents: UV-MALDI-TOF and ESI-TOF mass spectrometry characterization of reaction products," *Macromolecules*, vol. 34, no. 11, pp. 3534–3539, 2001.

[33] I. E. dell'Erba, D. P. Fasce, R. J. J. Williams, R. Erra-Balsells, Y. Fukuyama, and H. Nonami, "Poly(silsesquioxanes) derived from the hydrolytic condensation of organotrialkoxysilanes containing hydroxyl groups," *Journal of Organometallic Chemistry*, vol. 686, no. 1-2, pp. 42–51, 2003.

[34] D. P. Fasce, I. E. Dell'Erba, and R. J. J. Williams, "Synthesis of a soluble functionalized-silica by the hydrolysis and condensation of organotrialkoxysilanes bearing (β-hydroxy) tertiary amine groups with tetraethoxysilane," *Polymer*, vol. 46, no. 17, pp. 6649–6656, 2005.

[35] H. Mori, Y. Miyamura, and T. Endo, "Synthesis and characterization of water-soluble silsesquioxane-based nanoparticles by hydrolytic condensation of triethoxysilane derived from 2-hydroxyethyl acrylate," *Langmuir*, vol. 23, no. 17, pp. 9014–9023, 2007.

[36] Z. Deng, E. Breval, and C. G. Pantano, "Colloidal sol/gel processing of ultra-low expansion TiO_2/SiO_2 glasses," *Journal of Non-Crystalline Solids*, vol. 100, no. 1–3, pp. 364–370, 1988.

[37] S. Kirtay, E. Oktay, and V. Gunay, "Glass strengthening by SiO_2-TiO_2 organically modified silica coating," *Thin Solid Films*, vol. 515, no. 4, pp. 2145–2152, 2006.

[38] M. Houmard, D. Riassetto, F. Roussel et al., "Morphology and natural wettability properties of sol-gel derived TiO_2-SiO_2 composite thin films," *Applied Surface Science*, vol. 254, no. 5, pp. 1405–1414, 2007.

[39] S. Permpoon, M. Houmard, D. Riassetto et al., "Natural and persistent superhydrophilicity of SiO_2/TiO_2 and TiO_2/SiO_2 bi-layer films," *Thin Solid Films*, vol. 516, no. 6, pp. 957–966, 2008.

[40] V. Ääritalo, S. Areva, M. Jokinen, M. Lindén, and T. Peltola, "Sol-gel-derived TiO_2-SiO_2 implant coatings for direct tissue attachment. Part I: Design, preparation and

characterization," *Journal of Materials Science*, vol. 18, no. 9, pp. 1863–1873, 2007.

[41] S. Areva, V. Ääritalo, S. Tuusa, M. Jokinen, M. Lindén, and T. Peltola, "Sol-Gel-derived TiO_2-SiO_2 implant coatings for direct tissue attachment. Part II: Evaluation of cell response," *Journal of Materials Science*, vol. 18, no. 8, pp. 1633–1642, 2007.

[42] D. K. Sarkar, D. Brassard, M. A. E. Khakani, and L. Ouellet, "Dielectric properties of sol-gel derived high-k titanium silicate thin films," *Thin Solid Films*, vol. 515, no. 11, pp. 4788–4793, 2007.

[43] M. Zaharescu, A. Barau, L. Predoana et al., "TiO_2-SiO_2 sol-gel hybrid films and their sensitivity to gaseous toluene," *Journal of Non-Crystalline Solids*, vol. 354, no. 2–9, pp. 693–699, 2008.

[44] A. Łukowiak, R. Dylewicz, S. Patela, W. Stręk, and K. Maruszewski, "Optical properties of SiO_2-TiO_2 thin film waveguides obtained by the sol-gel method and their applications for sensing purposes," *Optical Materials*, vol. 27, no. 9, pp. 1501–1505, 2005.

[45] X. Shu, Y. Chen, H. Yuan, S. Gao, and D. Xiao, "H_2O_2 sensor based on the room-temperature phosphorescence of nano TiO_2/SiO_2 composite," *Analytical Chemistry*, vol. 79, no. 10, pp. 3695–3702, 2007.

[46] S. Y. Lien, D. S. Wuu, W. C. Yeh, and J. C. Liu, "Tri-layer antireflection coatings (SiO_2/SiO_2-TiO_2/TiO_2) for silicon solar cells using a sol-gel technique," *Solar Energy Materials and Solar Cells*, vol. 90, no. 16, pp. 2710–2719, 2006.

[47] W. Chen, X. Tao, J. Zhang, Q. Fang, and J. Yang, "Sol-gel-processed SiO_2/TiO_2/methylcellulose composite materials for optical waveguides," *Journal of the American Ceramic Society*, vol. 88, no. 11, pp. 2998–3002, 2005.

[48] N. D. Afify, R. Grisenti, G. Dalba et al., "Short-range order around Er^{3+} in silica waveguides containing aluminium, titanium and hafnium," *Optical Materials*, vol. 28, no. 6-7, pp. 864–867, 2006.

[49] A. C. Marques and R. M. Almeida, "Raman spectra and structure of multicomponent oxide planar waveguides prepared by sol-gel," *Journal of Sol-Gel Science and Technology*, vol. 40, no. 2-3, pp. 371–378, 2006.

[50] W. Dong, Y. Sun, C. W. Lee et al., "Controllable and repeatable synthesis of thermally stable anatase nanocrystal-silica composites with highly ordered hexagonal mesostructures," *Journal of the American Chemical Society*, vol. 129, no. 45, pp. 13894–13904, 2007.

[51] A. O. Bouh, G. L. Rice, and S. L. Scott, "Mono- and dinuclear silica-supported titanium(IV) complexes and the effect of TiOTi connectivity on reactivity," *Journal of the American Chemical Society*, vol. 121, no. 31, pp. 7201–7210, 1999.

[52] J. Jarupatrakorn and T. D. Tilley, "Silica-supported, single-site titanium catalysts for olefin epoxidation. A molecular precursor strategy for control of catalyst structure," *Journal of the American Chemical Society*, vol. 124, no. 28, pp. 8380–8388, 2002.

[53] M. Fujiwara, H. Wessel, H. S. Park, and H. W. Roesky, "A sol-gel method using tetraethoxysilane and acetic anhydride: immobilization of cubic μ-oxo Si-Ti complex in a silica matrix," *Chemistry of Materials*, vol. 14, no. 12, pp. 4975–4981, 2002.

[54] A. R. Oki, Q. Xu, B. Shpeizer et al., "Synthesis, characterization and activity in cyclohexene epoxidation of mesoporous TiO_2-SiO_2 mixed oxides," *Catalysis Communications*, vol. 8, no. 6, pp. 950–956, 2007.

[55] A. Matsuda, Y. Higashi, K. Tadanaga, and M. Tatsumisago, "Hot-water treatment of sol-gel derived SiO_2-TiO_2 microparticles and application to electrophoretic deposition for thick films," *Journal of Materials Science*, vol. 41, no. 24, pp. 8101–8108, 2006.

[56] J. W. Lee, S. Kong, W. S. Kim, and J. Kim, "Preparation and characterization of SiO_2/TiO_2 core-shell particles with controlled shell thickness," *Materials Chemistry and Physics*, vol. 106, no. 1, pp. 39–44, 2007.

[57] S. W. Lee, Y. U. Kim, S. S. Choi, T. Y. Park, Y. L. Joo, and S. G. Lee, "Preparation of SiO_2/TiO_2 composite fibers by sol-gel reaction and electrospinning," *Materials Letters*, vol. 61, no. 3, pp. 889–893, 2007.

[58] S. Zhan, D. Chen, X. Jiao, and Y. Song, "Mesoporous TiO_2/SiO_2 composite nanofibers with selective photocatalytic properties," *Chemical Communications*, no. 20, pp. 2043–2045, 2007.

[59] J. Jiao, Q. Xu, and L. Li, "Porous TiO_2/SiO_2 composite prepared using PEG as template direction reagent with assistance of supercritical CO_2," *Journal of Colloid and Interface Science*, vol. 316, no. 2, pp. 596–603, 2007.

[60] H. Mori, Y. Miyamura, and T. Endo, "Synthesis and characterization of water-soluble $SiO_{1.5}$/TiO_2 hybrid nanoparticles by hydrolytic co-condensation of triethoxysilane containing hydroxyl groups," *Materials Chemistry and Physics*, vol. 115, no. 1, pp. 287–295, 2009.

[61] C. McCusker, J. B. Carroll, and V. M. Rotelo, "Cationic polyhedral oligomeric silsesquioxane (POSS) units as carriers for drug delivery processes," *Chemical Communications*, no. 8, pp. 996–998, 2005.

[62] L. Cui, D. Chen, and L. Zhu, "Conformation transformation determined by different self-assembled phases in a DNA complex with cationic polyhedral oligomeric silsesquioxane lipid," *ACS Nano*, vol. 2, no. 5, pp. 921–927, 2008.

[63] Q. C. Zou, Q. J. Yan, G. W. Song, S. L. Zhang, and L. M. Wu, "Detection of DNA using cationic polyhedral oligomeric silsesquioxane nanoparticles as the probe by resonance light scattering technique," *Biosensors and Bioelectronics*, vol. 22, no. 7, pp. 1461–1465, 2007.

[64] K. Y. Pu, K. Li, and B. Liu, "Cationic oligofluorene-substituted polyhedral oligomeric silsesquioxane as light-harvesting unimolecular nanoparticle for fluorescence amplification in cellular imaging," *Advanced Materials*, vol. 22, no. 5, pp. 643–646, 2010.

[65] F. Zhao, C. Wan, X. Bao, and B. Kandasubramanian, "Modification of montmorillonite with aminopropylisooctyl polyhedral oligomeric silsequioxane," *Journal of Colloid and Interface Science*, vol. 333, no. 1, pp. 164–170, 2009.

[66] Y. C. Li, S. Mannen, J. Schulz, and J. C. Grunlan, "Growth and fire protection behavior of POSS-based multilayer thin films," *Journal of Materials Chemistry*, vol. 21, no. 9, pp. 3060–3069, 2011.

[67] H. Mori and M. Yamada, "Synthesis and characterization of cationic silsesquioxane hybrids by hydrolytic condensation of triethoxysilane derived from 2-(dimethylamino)ethylacrylate," *Colloid and Polymer Science*. In press.

[68] A. Tuteja, W. Choi, M. Ma et al., "Designing superoleophobic surfaces," *Science*, vol. 318, no. 5856, pp. 1618–1622, 2007.

[69] J. M. Mabry, A. Vij, S. T. Iacono, and B. D. Viers, "Fluorinated polyhedral oligomeric silsesquioxanes (F-POSS)," *Angewandte Chemie*, vol. 47, no. 22, pp. 4137–4140, 2008.

[70] S. T. Iacono, A. Vij, W. Grabow, D. W. Smith Jr., and J. M. Mabry, "Facile synthesis of hydrophobic fluoroalkyl

functionalized silsesquioxane nanostructures," *Chemical Communications*, no. 47, pp. 4992–4994, 2007.

[71] K. Koh, S. Sugiyama, T. Morinaga et al., "Precision synthesis of a fluorinated polyhedral oligomeric silsesquioxane-terminated polymer and surface characterization of its blend film with poly(methyl methacrylate)," *Macromolecules*, vol. 38, no. 4, pp. 1264–1270, 2005.

[72] Y. S. Ye, Y. C. Yen, W. Y. Chen, C. C. Cheng, and F. C. Chang, "A simple approach toward low-dielectric polyimide nanocomposites: blending the polyimide precursor with a fluorinated polyhedral oligomeric silsesquioxane," *Journal of Polymer Science A*, vol. 46, no. 18, pp. 6296–6304, 2008.

[73] I. Jerman, M. Koželj, and B. Orel, "The effect of polyhedral oligomeric silsesquioxane dispersant and low surface energy additives on spectrally selective paint coatings with self-cleaning properties," *Solar Energy Materials and Solar Cells*, vol. 94, no. 2, pp. 232–245, 2010.

[74] I. Jerman, B. Orel, A. S. Vuk, M. Koželj, and J. Kovač, "A structural and corrosion study of triethoxysilyl and perfluorooctyl functionalized polyhedral silsesquioxane nanocomposite films on AA 2024 alloy," *Thin Solid Films*, vol. 518, no. 10, pp. 2710–2721, 2010.

[75] S. T. Iacono, S. M. Budy, J. M. Mabry, and D. W. Smith Jr., "Synthesis, characterization, and surface morphology of pendant polyhedral oligomeric silsesquioxane perfluorocyclobutyl aryl ether copolymers," *Macromolecules*, vol. 40, no. 26, pp. 9517–9522, 2007.

[76] H. Hussain, B. H. Tan, C. S. Gudipati et al., "Synthesis and characterization of organic/inorganic hybrid star polymers of 2,2,3,4,4,4-hexafluorobutyl methacrylate and octa(aminophenyl)silsesquioxane nano-cage made via atom transfer radical polymerization," *Journal of Polymer Science A*, vol. 46, no. 22, pp. 7287–7298, 2008.

[77] H. Hussain, B. H. Tan, K. Y. Mya, Y. Liu, C. B. He, and T. P. Davis, "Synthesis, micelle formation and bulk properties of poly(ethylene glycol)b-poly(pentafluorostyrene)-g-polyhedral oligomeric silsesquioxane amphiphilic hybrid copolymers," *Journal of Polymer Science A*, vol. 48, no. 1, pp. 152–163, 2010.

[78] A. G. Kannan, N. R. Choudhury, and N. Dutta, "Fluoro-silsesquioxane-urethane hybrid for thin film applications," *ACS Applied Materials & Interfaces*, vol. 1, no. 2, pp. 336–347, 2009.

[79] H. Fujiwara, T. Narita, and H. Hamana, "Novel fluorinated hybrid polymer preparation from silsesquioxanes by radical polyaddition," *Journal of Fluorine Chemistry*, vol. 125, no. 9, pp. 1279–1285, 2004.

[80] S. T. Iacono, S. M. Budy, D. W. Smith, and J. M. Mabry, "Preparation of composite fluoropolymers with enhanced dewetting using fluorinated silsesquioxanes as drop-in modifiers," *Journal of Materials Chemistry*, vol. 20, no. 15, pp. 2979–2984, 2010.

[81] R. Misra, R. D. Cook, and S. E. Morgan, "Nonwetting, nonrolling, stain resistant polyhedral oligomeric silsesquioxane coated textiles," *Journal of Applied Polymer Science*, vol. 115, no. 4, pp. 2322–2331, 2010.

[82] K. Zeng and S. Zheng, "Nanostructures and surface dewettability of epoxy thermosets containing hepta(3,3,3-trifluoropropyl) polyhedral oligomeric silsesquioxane-capped polyethylene oxide," *Journal of Physical Chemistry B*, vol. 111, no. 50, pp. 13919–13928, 2007.

[83] A. M. Douvas, F. Van Roey, M. Goethals et al., "Partially fluorinated, polyhedral oligomeric silsesquioxane-functionalized (meth)acrylate resists for 193 nm bilayer lithography," *Chemistry of Materials*, vol. 18, no. 17, pp. 4040–4048, 2006.

[84] C. Pina-Hernandez, P. F. Fu, and L. J. Guo, "Easy duplication of stamps using UV-cured fluoro-silsesquioxane for nanoimprint lithography," *Journal of Vacuum Science and Technology B*, vol. 26, no. 6, pp. 2426–2429, 2008.

[85] H. Mori, C. Sada, T. Konno, and K. Yonetake, "Synthesis and characterization of low-refractive-index fluorinated silsesquioxane-based hybrids," *Polymer*, vol. 52, pp. 5452–5463, 2011.

[86] Y. C. Sheen, C. H. Lu, C. F. Huang, S. W. Kuo, and F. C. Chang, "Synthesis and characterization of amorphous octakis-functionalized polyhedral oligomeric silsesquioxanes for polymer nanocomposites," *Polymer*, vol. 49, no. 18, pp. 4017–4024, 2008.

[87] R. M. Laine and M. F. Roll, "Polyhedral phenylsilsesquioxanes," *Macromolecules*, vol. 44, no. 5, pp. 1073–1109, 2011.

[88] C. Liu, Y. Liu, Z. Shen, P. Xie, D. Dai, R. Zhang et al., "Synthesis and characterization of novel alcohol-soluble ladderlike poly(silsesquioxane)s containing side-chain hydroxy groups," *Macromolecular Chemistry and Physics*, vol. 202, pp. 1576–1580, 2001.

[89] K. Zeng, L. Wang, S. Zheng, and X. Qian, "Self-assembly behavior of hepta(3,3,3-trifluoropropyl) polyhedral oligomeric silsesquioxane-capped poly(ε-caprolactone) in epoxy resin: nanostructures and surface properties," *Polymer*, vol. 50, no. 2, pp. 685–695, 2009.

[90] K. Zeng, Y. Liu, and S. Zheng, "Poly(ethylene imine) hybrids containing polyhedral oligomeric silsesquioxanes: preparation, structure and properties," *European Polymer Journal*, vol. 44, no. 12, pp. 3946–3956, 2008.

[91] K. Zeng and S. Zheng, "Synthesis and characterization of organic/inorganic Polyrotaxanes from Polyhedral oligomeric silsesquioxane and poly(ethylene oxide)/α- cyclodextrin polypseudorotaxanes via click chemistry," *Macromolecular Chemistry and Physics*, vol. 210, no. 9, pp. 783–791, 2009.

[92] H. Mori, C. Sada, T. Konno, R. Koizumi, and K. Yonetake, "Film-forming amphiphilic silsesquioxane hybrids prepared by hydrolytic co-condensation of hydroxyl-functionalized and fluorinated triethoxysilanes," *Polymer*, vol. 53, pp. 3849–3860, 2012.

[93] J. Rodríguez-Hernández, F. Chécot, Y. Gnanou, and S. Lecommandoux, "Toward 'smart' nano-objects by self-assembly of block copolymers in solution," *Progress in Polymer Science*, vol. 30, no. 7, pp. 691–724, 2005.

[94] H. Mori and A. H. E. Müller, "New polymeric architectures with (meth)acrylic acid segments," *Progress in Polymer Science*, vol. 28, no. 10, pp. 1403–1439, 2003.

[95] S. Förster, V. Abetz, and A. H. E. Müller, "Polyelectrolyte block copolymer micelles," *Advances in Polymer Science*, vol. 166, pp. 173–210, 2004.

[96] A. O. Moughton and R. K. O'Reilly, "Using metallo-supramolecular block copolymers for the synthesis of higher order nanostructured assemblies," *Macromolecular Rapid Communications*, vol. 31, no. 1, pp. 37–52, 2010.

[97] H. Mori, M. G. Lanzendörfer, A. H. E. Müller, and J. E. Klee, "Organic-inorganic nanoassembly based on complexation of cationic silica nanoparticles and weak anionic polyelectrolytes in aqueous and alcohol media," *Langmuir*, vol. 20, no. 5, pp. 1934–1944, 2004.

[98] A. K. Boal, F. Ilhan, J. E. Derouchey, T. Thurn-Albrecht, T. P. Russell, and V. M. Rotello, "Self-assembly of nanoparticles into structured spherical and network aggregates," *Nature*, vol. 404, no. 6779, pp. 746–748, 2000.

[99] B. L. Frankamp, O. Uzun, F. Ilhan, A. K. Boal, and V. M. Rotello, "Recognition-mediated assembly of nanoparticles into micellar structures with diblock copolymers," *Journal of the American Chemical Society*, vol. 124, no. 6, pp. 892–893, 2002.

[100] M. Hara, J. T. Lean, and T. E. Mallouk, "Photocatalytic oxidation of water by silica-supported tris(4,4′-dialkyl-2,2′-bipyridyl)ruthenium polymeric sensitizers and colloidal iridium oxide," *Chemistry of Materials*, vol. 13, no. 12, pp. 4668–4675, 2001.

[101] R. Tamaki and Y. Chujo, "Synthesis of polystyrene and silica gel polymer hybrids utilizing ionic interactions," *Chemistry of Materials*, vol. 11, no. 7, pp. 1719–1726, 1999.

[102] A. R. Bassindale, A. Codina-Barrios, N. Frascione, and P. G. Taylor, "The use of silsesquioxane cages and phage display technology to probe silicone-protein interactions," *New Journal of Chemistry*, vol. 32, no. 2, pp. 240–246, 2008.

[103] N. Alobaid, H. J. Salacinski, K. M. Sales et al., "Nanocomposite containing bioactive peptides promote endothelialisation by circulating progenitor cells: an in vitro evaluation," *European Journal of Vascular and Endovascular Surgery*, vol. 32, no. 1, pp. 76–83, 2006.

[104] A. De Mel, G. Punshon, B. Ramesh et al., "In situ endothelialisation potential of a biofunctionalised nanocomposite biomaterial-based small diameter bypass graft," *Bio-Medical Materials and Engineering*, vol. 19, no. 4-5, pp. 317–331, 2009.

[105] T. L. Kaneshiro, X. Wang, and Z. R. Lu, "Synthesis, characterization, and gene delivery of poly-L-iysine octa(3-aminopropyl)silsesquioxane dendrimers: nanoglobular drug carriers with precisely defined molecular architectures," *Molecular Pharmaceutics*, vol. 4, no. 5, pp. 759–768, 2007.

[106] T. L. Kaneshiro and Z. R. Lu, "Targeted intracellular codelivery of chemotherapeutics and nucleic acid with a well-defined dendrimer-based nanoglobular carrier," *Biomaterials*, vol. 30, no. 29, pp. 5660–5666, 2009.

[107] S. W. Kuo, H. F. Lee, W. J. Huang, K. U. Jeong, and F. C. Chang, "Solid state and solution self-assembly of helical polypeptides tethered to polyhedral oligomeric silsesquioxanes," *Macromolecules*, vol. 42, no. 5, pp. 1619–1626, 2009.

[108] S. W. Kuo and H. T. Tsai, "Control of peptide secondary structure on star shape polypeptides tethered to polyhedral oligomeric silsesquioxane nanoparticle through click chemistry," *Polymer*, vol. 51, no. 24, pp. 5695–5704, 2010.

[109] S. Fabritz, D. Heyl, V. Bagutski et al., "Towards click bioconjugations on cube-octameric silsesquioxane scaffolds," *Organic & Biomolecular Chemistry*, vol. 8, no. 9, pp. 2212–2218, 2010.

[110] H. Mori and T. Endo, "Amino acid-based block copolymers by RAFT polymerization," *Macromolecular Rapid Communications*, vol. 33, pp. 1090–1107, 2012.

[111] H. Mori and S. Saito, "Smart organic-inorganic hybrids based on the complexation of amino acid-based polymers and water-soluble silsesquioxane nanoparticles," *Reactive and Functional Polymers*, vol. 71, no. 10, pp. 1023–1032, 2011.

[112] H. Mori, I. Kato, M. Matsuyama, and T. Endo, "RAFT polymerization of acrylamides containing proline and hydroxyproline moiety: controlled synthesis of water-soluble and thermoresponsive polymers," *Macromolecules*, vol. 41, no. 15, pp. 5604–5615, 2008.

[113] H. Mori, H. Iwaya, A. Nagai, and T. Endo, "Controlled synthesis of thermoresponsive polymers derived from L-proline via RAFT polymerization," *Chemical Communications*, no. 38, pp. 4872–4874, 2005.

[114] H. Mori, H. Iwaya, and T. Endo, "Controlled synthesis of thermoresponsive polymer via RAFT polymerization of an acrylamide containing l-proline moiety," *Reactive and Functional Polymers*, vol. 67, no. 10, pp. 916–927, 2007.

[115] H. Mori, H. Iwaya, and T. Endo, "Structures and chiroptical properties of thermoresponsive block copolymers containing L-proline moieties," *Macromolecular Chemistry and Physics*, vol. 208, no. 17, pp. 1908–1918, 2007.

[116] S. Luo, J. Xu, Y. Zhang, S. Liu, and C. Wu, "Double hydrophilic block copolymer monolayer protected hybrid gold nanoparticles and their shell cross-linking," *Journal of Physical Chemistry B*, vol. 109, no. 47, pp. 22159–22166, 2005.

[117] B. J. Kim, J. J. Chiu, G. R. Yi, D. J. Pine, and E. J. Kramer, "Nanoparticle-induced phase transitions in diblock-copolymer films," *Advanced Materials*, vol. 17, no. 21, pp. 2618–2622, 2005.

[118] Y. Kang and T. A. Taton, "Controlling shell thickness in core-shell gold nanoparticles via surface-templated adsorption of block copolymer surfactants," *Macromolecules*, vol. 38, no. 14, pp. 6115–6121, 2005.

[119] B. S. Kim and T. A. Taton, "Multicomponent nanoparticles via self-assembly with cross-linked block copolymer surfactants," *Langmuir*, vol. 23, no. 4, pp. 2198–2202, 2007.

[120] Y. Kang and T. A. Taton, "Core/shell gold nanoparticles by self-assembly and crosslinking of micellar, block-copolymer shells," *Angewandte Chemie*, vol. 44, no. 3, pp. 409–412, 2005.

[121] H. Mori, S. Saito, and K. Shoji, "Complexation of amino-acid-based block copolymers with dual-thermoresponsive properties and water-soluble silsesquioxane nanoparticles," *Macromolecular Chemistry and Physics*, vol. 212, pp. 2558–2572, 2011.

Hindawi Publishing Corporation
International Journal of Polymer Science
Volume 2012, Article ID 526795, 17 pages
doi:10.1155/2012/526795

Research Article

Characterization and Some Insights into the Reaction Chemistry of Polymethylsilsesquioxane or Methyl Silicone Resins

Maki Itoh,[1] Fukuyo Oka,[1] Michitaka Suto,[1] Simon D. Cook,[2] and Norbert Auner[3]

[1] *Electronics Solutions S&T, Dow Corning Toray Co., Ltd., 2-2 Chigusa-Kaigan, Chiba Ichihara 299-0108, Japan*
[2] *Analytical Sciences, Dow Corning Corporation, 2200 W. Salzburg Road, Midland, MI 48686-0994, USA*
[3] *Institute for Inorganic and Analytical Chemistry, Goethe University Frankfurt, Max-von-Laue-Straße 7, 60438 Frankfurt am Main, Germany*

Correspondence should be addressed to Maki Itoh, maki.itoh@dowcorning.com

Received 15 June 2012; Accepted 17 August 2012

Academic Editor: Takahiro Gunji

Structural characterization of a polymethylsilsesquioxane (PMSQ) and a DT-type methyl silicone resin (MeDT) has been carried out by various instrumental analyses including GPC, NMR, gas chromatography, and gas chromatography-mass spectrometry. Although the PMSQ had a *Mw* around 5000, the resin contained a significant amount of low molecular weight species consisting of T^2 [$MeSi(OH)O_{2/2}$] and T^3 [$MeSiO_{3/2}$] units, ranging from $T^3{}_4T^2{}_3$ to $T^3{}_8T^2{}_2$ including many isomers. One isomer of $T^3{}_6T^2{}_2$ was isolated of which structure was determined as a cage structure. The species are supposed to consist mainly of cyclotetra- and cyclopentasiloxanes, but presence of strained rings such as cyclotrisiloxane rings also was suggested. In MeDT, species in which the T^2 units in the molecules from PMSQ is replaced with D^2 [$Me_2SiO_{2/2}$] were found, for example, $T^3{}_6D^2{}_2$, suggesting that general silicone resins consist of similar structures as silsesquioxanes. The Mark-Houwink exponent for these methyl resins was ~0.3, indicating the molecular shape to be compact. Investigation on the formation chemistry of the cubic octamers indicates that siloxane bond rearrangement is an important mechanism in the molecule build-up process.

1. Introduction

Silicone resins are a class of polysiloxane material primarily built from T ($RSiO_{3/2}$) and Q ($SiO_{4/2}$) units, thus have much higher crosslink density than elastomers that mainly consist of D unit ($R_2SiO_{2/2}$) [1, 2]. The M ($R_3SiO_{1/2}$) and D units are also used as components in silicone resins but usually at much lower concentrations. In silicone industry, silicone resins are defined as solvent-soluble materials that are stable at room temperature and have functionalities for further crosslinking to give insoluble materials in the final application forms like coatings. In this sense, silicone resins can be differentiated from sol-gel materials in which the final insoluble materials are formed in many cases directly from monomers, although the synthetic chemistry is essentially the same. One of the forms of silicone resins that consists exclusively from T units is called silsesquioxanes or polysilsesquioxanes [2–6]. Silicone resins or silsesquioxanes are known since the beginning of silicone industry in the 1930s [7], but traditionally these materials have been captured via simple parameters including the molar ratio of substituents to the silicon atom, R/Si ratio (1.0–1.7), molar ratio of phenyl substituent to methyl, and molecular weight. However, little has been known on what structural features are responsible for which property as well as what reaction mechanism results in what structure.

Polyphenylsilsesquioxane (PPSQ) has been often referred to as a ladder polymer since Brown Jr. et al. reported the polymer to have *cis*-syndiotactic conformation [8, 9]. They assigned the structure by X-ray diffractometry (XRD), IR, UV, bond angle calculation, and the exponent *a* value in the Mark-Houwink equation. However, these data do not appear to be sufficient to claim such a defined structure. The XRD pattern is reported by Andrianov et al., which is questionable for a *cis*-syndiotactic structure [10, 11]. Some papers refer to the material as ladder polymers if there are no silanols left or simply by the IR spectra showing two bands at ~1150 and ~1050 cm^{-1} [2], but these data cannot always be

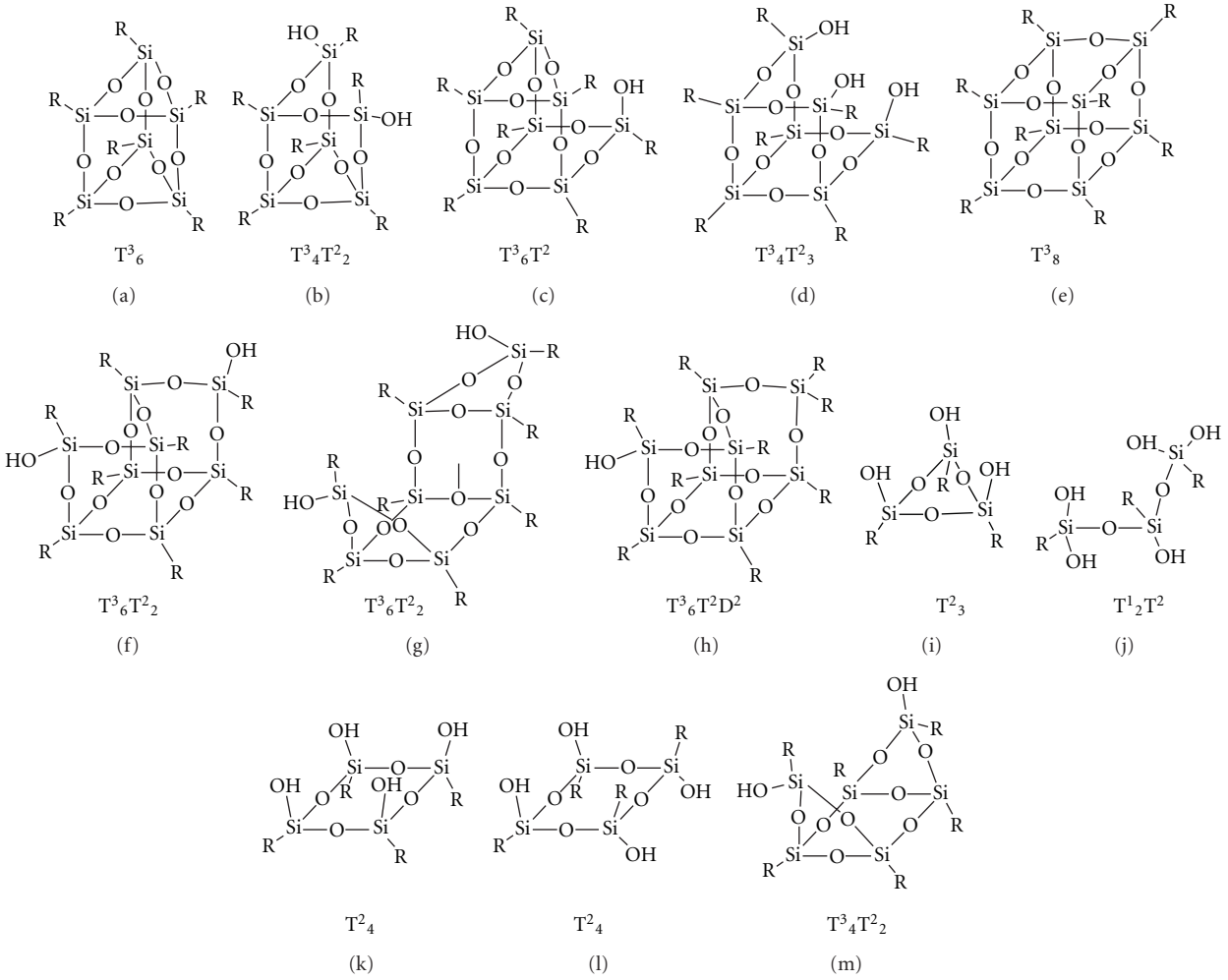

Figure 1: Possible structures of silsesquioxanes or silicone resins. Structure (f) was identified in the present study; (a), (e), and (i) have most probably no choice other than these structures; (b), (d), and (j) are identified with other substituents (see the text below); the presence of (h), (k), and (h) are likely; (c), (g), and (l) is possible structures from the chemical formulae.

evidence for a ladder structure. Park and coworkers indicated by calculation that the IR band around 1150 cm^{-1} is derived from the parallel asymmetric Si–O–Si stretch vibration mode while the lower-frequency band around 1050 cm^{-1} is the asymmetric Si–O–Si stretch; thus incompletely condensed cages or T^3_6 cage shown in Figure 1(a) can show these two bands [12]. Among these characterization techniques, the *a* value in the Mark-Houwink equation is repeatedly reported to give values around 1 [13–15], implying that PPSQ has random coil to rod-like shapes. In their dilute solution study, Helminiak and Berry concluded that the conformation of PPSQ can be represented with a worm-like chain model with a persistence length of 75 Å [16]. Frye and Klosowski strongly opposed the ladder structure and suggested a more or less randomly linked array of polycyclic cages [17]. Real ladder structures can be found only for low molecular weight oligomers, up to heptacyclic ladder structures with isopropyl substituent as prepared by a stepwise synthesis [18–21] or by oxidation of ladder oligosilanes [22]. Preparation of ladder-like polymethylsilsesquioxanes (PMSQs) by spontaneous condensation of *cis-trans-cis*-tetrabromotetramethylcyclotetrasiloxane is suggested by Chang and coworkers [21]. It does not appear that the material is ultimately proven to have a ladder structure or it may not be known how one can prove a resin having a ladder structure, but an interesting observation in this work is that the IR spectrum of this PMSQ exhibits two absorption bands at 1130 and 1030 cm^{-1}, while tri- or pentacyclic ladder oligomers or a T^3_6 cage (all isopropyl substituted) does not show such clear pair of the two bands. Seki et al. reported the preparation of ladder-like PMSQs by the hydrolytic polycondensation of an isocyanate-functional cyclic tetramer of methyl T^2 having the structure of Figure 1(l) [23]. The triple-detector GPC gave a *Mw* of 285,000 and a *Mn* of 110,000 with the Mark-Houwink *a* value of 0.53. This *a* value is much lower than what can be claimed as a rigid rod

molecule, but is higher than common PMSQ (*vide infra*), suggesting that this PMSQ may have somewhat extended molecular shape. Another PMSQ with a *Mw* of 214,000 and a *Mn* of 71,000 prepared from a hydridofunctional cyclic tetramer showed the *a* value of 0.38. Both these two PMSQs showed the distinct two bands at 1150 and 1130 cm^{-1} in the IR spectra, indicating that the two IR bands are not directly associated with a ladder structure.

In contrast to more uncertain ladder structures, cage structures are identified in many reports. For instance, completely condensed cages around the cubic octamers with various substituents including methyl, n-hexyl, and phenyl are reported in old and new papers [3–6, 24, 25]. For a hydrogen silsesquioxane (HSQ) synthesized by the toluene-sulfuric acid method [26], Agaskar and Klemperer carefully fractionated cages [27]. They identified completely condensed $^{H}T^{3}_{8}$, $^{H}T^{3}_{10}$, $^{H}T^{3}_{12}$, $^{H}T^{3}_{14}$, and $^{H}T^{3}_{16}$ cage molecules using gas chromatography, ^{1}H and ^{29}Si NMR, elemental analysis, and mass spectrometry. Synthesis and identification of compounds with the structures of Figures 1(a), 1(c), 1(d), and 1(f) having cyclohexyl group as the substituent are presented by Feher and coworkers [28]. Most of these molecules consist of cycloterta- and cyclopentasiloxane rings, but the presence of strained cyclotrisiloxane rings in the structures of Figures 1(a) and 1(c) is also reported.

Methyltrichlorosilane is the most abundant low cost starting material in silicone industry as compared to phenyltrichlorosilane or trichlorosilane. Thus PMSQ or methyl silicone resins are one of the most important materials among silicone resins. In this work, structural characterization of a PMSQ will be described with some insight into the reaction chemistry. The materials were prepared by a simple hydrolytic polycondensation with excess water, which is not a very specific synthetic procedure to form characteristic structures. The interpretation of the ^{29}Si NMR spectra was revisited by trimethylsilyl-(Me_3Si-) capping of the silanol. The presence of low molecular weight compounds was then studied by gas chromatograph (GC) and GC-mass spectrometry (MS) analyses for Me_3Si-capped species. Isolation of a compound was tried to identify the structure by X-ray crystallography. The understanding of the chemistry for the formation of such molecules was explored by analyzing the reaction species at earlier stage of the hydrolytic polycondensation and by reacting the isolated molecule of known structure in a similar reaction condition trying to uncover the development of the structures during the course of the reaction.

In addition to the PMSQ, a DT-type methyl silicone resin, denoted as MeDT, having a small amount of D unit in addition to the T unit, was studied to compare with the PMSQ. This will show the structural characteristics of a more typical industrial silicone resin and will help verifying the generality of the findings for the PMSQ.

As usually practiced in silicone industry, the term "T" in this paper denotes species derived from $RSiX_3$ (X denotes Cl or OR) by hydrolytic condensation. Consequently, structures in the resin denoted as a T unit could contain $RSi(OH)_3$, $RSi(OH)_2O_{1/2}$, $RSi(OH)O_{2/2}$, and $RSiO_{3/2}$. These four structures are described as T^0, T^1, T^2, and T^3, respectively (the numbers in superscript denote the number of siloxane bonding). Likewise, a D unit represents those species derived from R_2SiCl_2 containing $R_2Si(OH)_2$, $R_2Si(OH)O_{1/2}$, and $R_2SiO_{2/2}$, abbreviated as D^0, D^1, and D^2, respectively.

2. Experimental

2.1. Materials. Methyltrichlorosilane (Kanto Chemical), dimethyldichlorosilane, octamethylcyclotetrasiloxane (D_4) (Shin-Etsu Chemical), N,O-bis(trimethylsilyl)trifluoroacetamide (BSTFA), methyl isobutyl ketone (MIBK, 4-methyl-2-pentanone), dichloromethane, 2-methylpentane, chloroform, distilled water, magnesium sulfate (Wako Pure Chemical), deuterated chloroform ($CDCl_3$), and tetrahydrofuran (THF) (Aldrich) were used without further purification.

2.2. Analytical Techniques. GPC curves were obtained using a Tosoh HLC-8020 gel permeation chromatograph equipped with a refractive index detector and two Tosoh TSKgel GMH_{XL}-L columns eluted by chloroform at the flow rate of 1.0 mL/min. The molecular weight was determined relative to polystyrene standards. The calibration curve was corrected for each run from the difference in the retention time of cyclohexane as the internal standard assuming that the retention times of the polystyrene standards and the resin molecules are proportional to the shift of the retention time of the internal standard.

The chromatographic equipment for the GPC with triple detector (light scattering, viscometric, and refractive index detectors) using THF was equipped with a Viscotek T60A light scattering/viscometric detector, a Waters 2410 refractive index detector, and two Polymer Laboratories Mixed E columns, programmed to run at 1.0 mL/min. Instrument calibration was based on polystyrene standard and the sample concentration was 0.5–1 wt%. The sample was prepared four times to verify reproducibility.

^{29}Si NMR spectra were recorded on a Bruker ACP-300 spectrometer in $CDCl_3$. The sample concentration was ~ 600 mg in 2.4 mL of the solvent for a 10 mm tube. Chromium acetylacetonate was used as a relaxation agent in ~32 mg quantity. A gated decoupling in which protons were irradiated only during the acquisition of FID (free induction decay) was employed with the pulse angle of 45° and the pulse delay of 7 s. The number of scans was >1000 and the line broadening of 2.0 Hz was employed on plotting. The chemical shift was adjusted using tetramethylsilane as either an internal or an external standard.

Gas chromatography-mass spectrometry (GC-MS) study was conducted using a Shimadzu gas chromatograph-quadrupole mass spectrometer, model QP-5050A, utilizing an electron impact ionization source with an ionizing electron energy of 70 eV. The interfacial temperature was 300°C and the ion source temperature was 250°C. The GC was a Shimadzu GC-17A gas chromatograph equipped with a capillary column (J&W Scientific, 30 m × 0.250 mm, coated with DB-5 in 0.10 mm thickness). The GC temperature

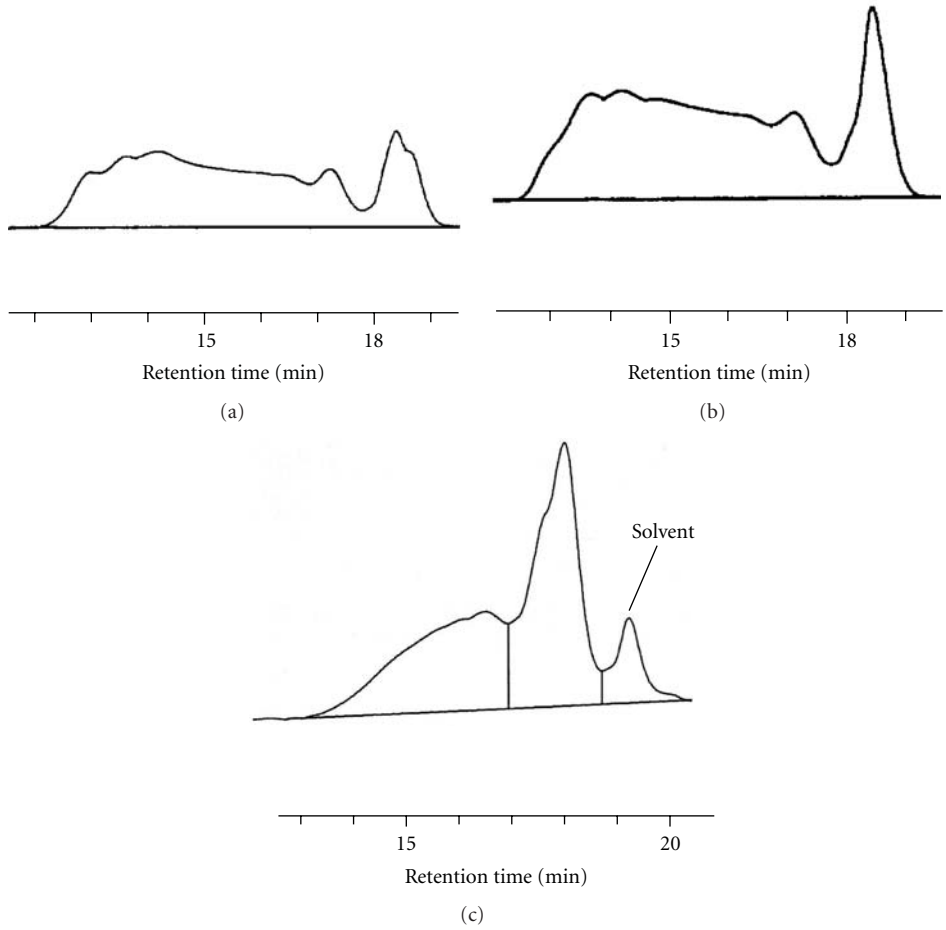

Figure 2: GPC curves for (a) PMSQ-1, (b) MeDT-1, and (c) PMSQ-NA.

program used was: initial temperature, 60°C; initial time, 2.00 minutes; program rate, 40°C/min; final temperature, 280°C; injection temperature, 280°C; detector temperature, 300°C. Helium was used as a carrier gas with its pressure of 150 kPa. A sample of ~25 wt% solution containing D_4 as an internal standard was injected in 0.1 μL amount. A Shimadzu GC-14A gas chromatograph equipped with the same capillary column as installed in the GC-MS and a flame ionization detector (FID) was used. The same carrier gas pressure, temperature program, and injection amount as in the GC-MS studies were employed for exactly the same sample. For PMSQ at earlier reaction stage, the following temperature program was used both for GC and GC-MS analyses: initial temperature, 60°C; initial time, 2.00 minutes; program rate, 10°C/min; final temperature, 280°C; He pressure of 100 kPa.

XRD study was performed with a JEOL JDX-3530 diffractometer using Ni-filtered Cu-K_α radiation. The intensity distribution ($2^\circ < 2\theta < 35^\circ$) was observed in the reflecting mode using a goniometer equipped with a monochromator. The crystallinity was determined by the known method from the crystalline peaks and amorphous halo.

X-ray single crystal analysis was performed on a SIEMENS SMART diffractometer at a temperature of about −120°C. The structure was determined by direct methods using program SHELXS.

2.3. Preparation of PMSQ. Using the method described in a previous paper [29], the PMSQ was synthesized from 1196 g (8.00 mol) of methyltrichlorosilane in 3.20 L each of MIBK and water and heat aging at 50°C for 2 h 50 min. The PMSQ (PMSQ-1) was obtained as a white solid in 528 g quantity. Another batch, PMSQ-2, was synthesized in a 9 mol scale heat aging at 50°C for 4 h, providing 562 g of the material. To obtain a PMSQ without the heat aging, 74.7 g (0.500 mol) of methyltrichlorosilane was reacted by the same method using 200 mL each of MIBK and water, and the product was recovered immediately after the completion of the dropwise addition of methyltrichlorosilane to the mixture of MIBL and water with the maximum temperature during the addition over 26 min of 20.0°C (PMSQ-NA).

2.4. Preparation of MeDT. The MeDT resin was prepared in a similar manner using a mixture of 1155 g (7.7 mol) of methyltrichlorosilane and 165 g (1.3 mol) of dimethyldichlorosilane, and 4.00 L of MIBK and 3.42 L water. The heat aging after the hydrolysis was performed at 60°C for 2 h, giving a solid MeDT in 580 g yield. Another lot, MeDT-2, was

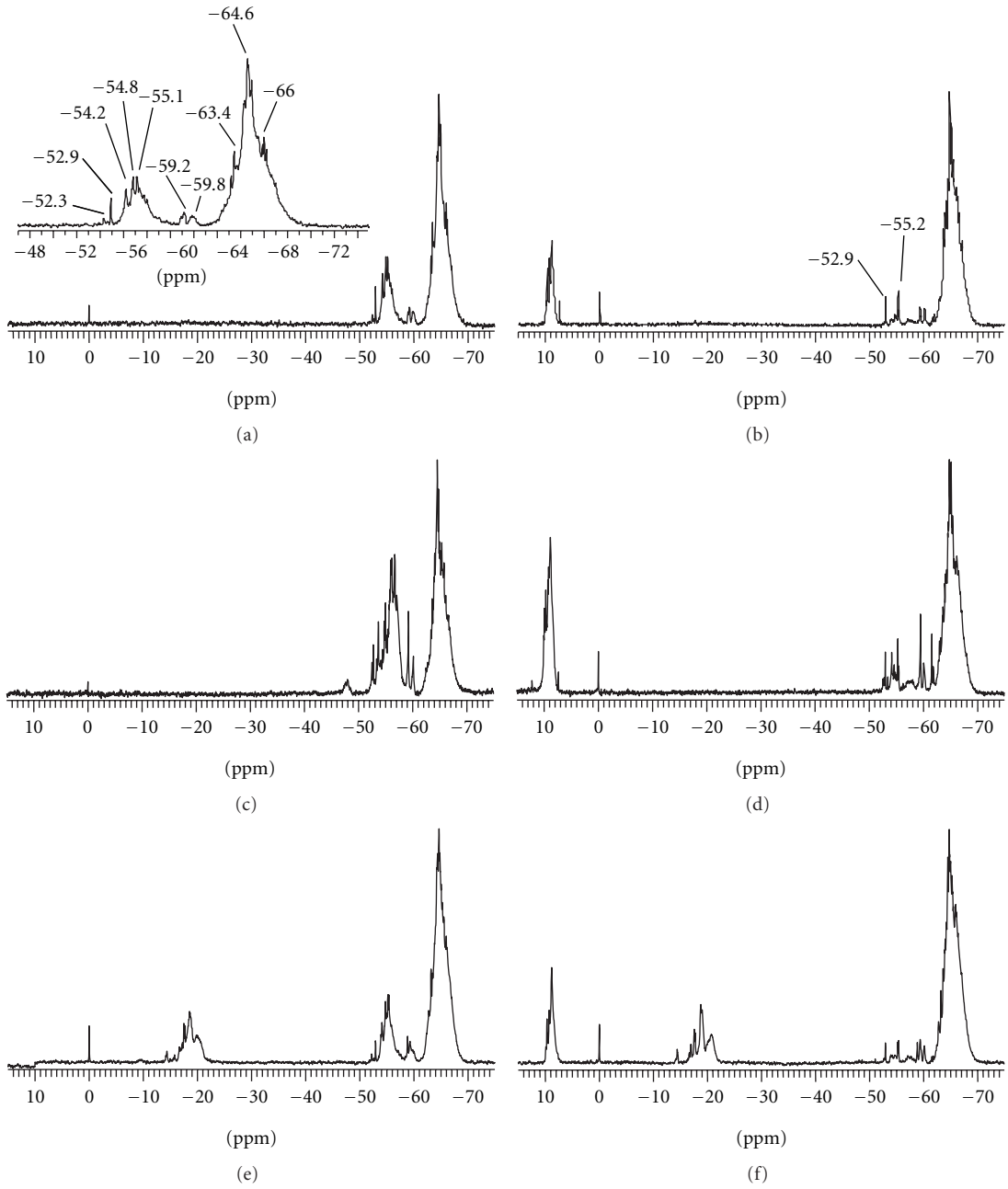

Figure 3: ^{29}Si NMR spectra of (a) PMSQ-1, (b) Me_3Si-capped PMSQ-1, (c) PPMSQ-NA, (d) Me_3Si-capped PMSQ-NA, (e) MeDT-1, and (f) Me_3Si-capped MeDT-1.

synthesized in the same scale with the heat aging at 60°C for 3 h.

2.5. Isolation of a Molecule. To 100 g of PMSQ-1, a mixture of 1400 mL of hexane and 600 mL of chloroform, was added. After stirring for 30 min, the mixture was allowed to stand for 20 min, followed by decanting the supernatant solution. By stripping the solvent, Fraction 1, the lower molecular weight fraction, was obtained in 31% yield. Fraction 1 (19.99 g) was dissolved in 204 mL of acetone (0.098 g/mL). While stirring, 54 mL of distilled water was added to the solution, and the mixture was allowed to stand overnight, giving two separated layers. The top layer was separated by decantation, and 14 mL of water was added, which again gave two layers. The solvent in the top layer was stripped off, followed by redissolving in 77 mL of acetone (resin/acetone ratio of 0.098 g/mL). Removing the solvent from the supernatant solution gave the lowest molecular weight fraction, Fraction 4, as a solid (5.204 g). To 2.00 g of Fraction 4, 11.4 g of chloroform was added (15 wt%) and the solution was allowed to stand overnight at room temperature. Insoluble material remained in the solution, the amount of which increased by

standing overnight. A crude cage material, Fraction 4-P1, was obtained by collecting the precipitates by filtration (0.068 g). By concentrating the filtrate followed by standing overnight, 0.067 g of a crude product (Fraction 4-P2) was isolated by filtration. Further concentration of the filtrate afforded a crude product, Fraction 4-P3, in a very small amount (0.008 g). Similarly, 0.10 g of a crude material (Fraction 4-P4 and 5) was obtained from 1.74 g of Fraction 4 and 0.48 g of a crude product (Fraction 4-P6 and 7) was obtained from 9.58 g of another Fraction 4. Recrystallization of 0.64 g of the crude products (**1**: mixture of Fraction 4-P1, 4, 5, 6, and 7) from an acetone/chloroform mixture gave crystals (**X1**, 0.43 g). Needle crystals, **X2**, were obtained from **X1** by slow evaporation of the solution (acetone/chloroform = 3/1) covered with a heptane layer.

2.6. Trimethylsilyl-(Me_3Si-) Capping of Silanol in the Methyl Silicone Resins. A 25 mL three-neck flask with a septum, a three-way stopcock, a glass stopper, and a magnetic stir bar was charged with 3.01 g of PMSQ-1, followed by purging with nitrogen through the stopcock. After dissolving in 9.0 mL of dichloromethane, 1.7 mL of BSTFA was added using a syringe through the septum over 2 min while cooling on an ice-water bath. The amount of BSTFA was set at ~1.2 times of the SiOH present in the resin simply calculated from the T^2 region (−50 to −58 ppm) in the ^{29}Si NMR spectrum and the theoretical amount of water in the dichloromethane as calculated by the solubility of water of 0.198 wt%. After stirring at room temperature for ~10 minutes, ~10 mL of water was added, followed by washing the slightly basic organic phase with water to neutral. The organic phase was dried over magnesium sulfate and the solvent was stripped off under vacuum. Me_3Si-capping of the OH in MeDT was carried out in the same way.

2.7. Quantification Method of GC Peaks. The quantification procedure for the Me_3Si-capped PMSQ-1 is described below. Me_3Si-capped PMSQ-1 (73.8 mg) was dissolved in 0.17 mL of chloroform. A stock solution of D_4 was prepared by dissolving 31.7 mg of D_4 in 157.7 mg of chloroform. The stock solution (23.8 mg, 30 μL) was added to the solution of Me_3Si-capped PMSQ as an internal standard, which made the amount of D_4 in the PMSQ solution 3.98 mg (0.0134 mmol). The PMSQ solution was subjected to both the GC-MS and the GC analyses. After assigning the GC peaks from the GC-MS assignment, quantification was made assuming that the GC peak area with a FID detector was proportional to the number of methyl groups. The following shows an example taking peak **x** in Figure 4 for $T^3{}_6T^2{}_2$: Dividing the GC area for D_4 by the number of methyl group, 8, gives mole equivalent area for the D_4. In the present case, the D_4 GC peak at 3.372 min had an area of 7217; thus the mole equivalent area was 902.1. Since the amount of D_4 was 0.0134 mmole, the GC peak area for 1 mmol of D_4 is 67320 (902.1/0.0134). The peak **x** at 6.826 min for $T^3{}_6T^2{}_2$ had the peak area of 1478. Since the number of methyl group for a *trimethylsilyl-capped* $T^3{}_6T^2{}_2$ is 14, the mole equivalent area for this molecule was 105.6 (1478/14). From this value and the molar equivalent

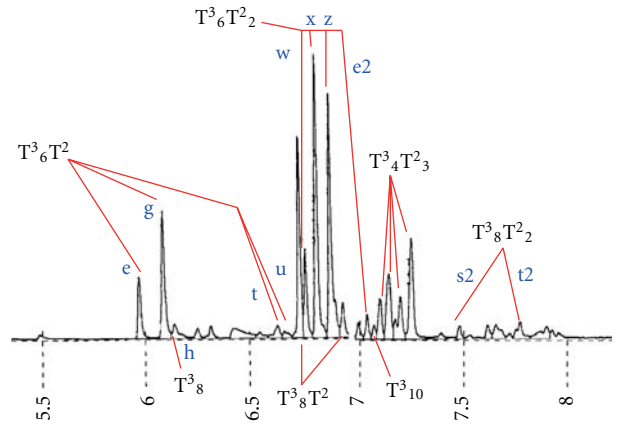

Figure 4: Gas chromatograph of Me_3Si-capped PMSQ with the peak assignment by the GC-MS. The molecular compositions are described as uncapped PMSQ.

peak area for D_4, the amount of this molecule is calculated as 0.00157 mmole (105.6/67320). By multiplying the molecular weight of *uncapped* $T^3{}_6T^2{}_2$, 554, the amount of this molecule is calculated as 0.872 mg. Since the amount of the entire resin, 73.8 mg, was based on the Me_3Si-capped PMSQ, the weight of the uncapped resin was calculated by the ^{29}Si NMR data. The average molecular formula of PMSQ-1 was determined as $T^{2(OH)}{}_{0.045}T^{3(OSiMe3)}{}_{0.150}T^3{}_{0.805}$ by simply assigning the resonances around 10 ppm as the M unit, those between −51 and −58 ppm as the T^2 unit, and those at −58 to −71 ppm as the T^3 unit. This gives the average formula weight of 79.70, from which that for the uncapped resin was calculated as 68.88. From these values, the amount of the resin used for the GC quantification on uncapped basis was calculated as 63.8 mg (73.8 × 68.88/79.70). Thus the amount of the molecule of peak **x** is 1.37 wt% of the entire PMSQ. (The residual resonances in the T^2 region after the capping was assigned to T^3 in strained rings as shown below, but in this calculation, the integration in the T^2 region was simply used as T^2 silicon, which will not cause major impact on the calculation.)

2.8. Quench Capping of Early Reaction Intermediates (PMSQ-QC). A D_4 stock solution was prepared by dissolving 30.2 mg of D_4 in 294.5 mg of MIBK. In a 20 mL vial was placed 2.2 mL of 2-methylpentane and 0.8 mL (~0.78 g, ~3.0 mmol) of BSTFA, and the vial was placed in a dry ice-acetone bath of −70°C. In a 10 mL vial with a magnetic stir bar and a digital thermocouple thermometer, 0.7 mL of water, 0.35 mL of MIBK, and 30 μL (23.7 mg) of the D_4 stock solution (2.20 mg of D_4) were stirred vigorously in an ice-water bath. After the temperature of the mixture in the 10 mL vial reached 1.2°C, 0.1 mL (0.178 g, 1.19 mmol) of methyltrichlorosilane was added dropwise using a 1.0 mL syringe in 140 s (the maximum reaction temperature during the addition was 9.2°C), and the mixture was stirred another 35 s. The relative amount of MIBK to methyltrichlorosilane was the same as the above PMSQ synthesis, but the amount of water was twice the standard condition. The content of

Table 1: GPC data for PMSQs and MeDT resins.

Material	*Mw*	*Mn*	18 min peak area
PMSQ-1	6370	1140	19.0%
PMSQ-NA	790	500	53.0%
MeDT-1	4220	1040	22.9%

the reaction vial was then dumped into the 20 mL vial. The organic phase was separated from the frozen water phase and was washed with 3-4 mL of water 4 times to neutral. The 2-methylpentane was stripped off to obtain a solid product which was subjected to GC and GC-MS analyses in the same way as the Me_3Si-capped PMSQ. However, one difference was that the amount of the entire resin is not known. Thus, firstly the amount of a molecule was determined in mmol relative to the amount of D_4 (0.00742 mmol), which was multiplied by the number of silicon atoms in that molecule. This amount was expressed as percent of the feed methyltrichlorosilane (1.19 mmol) as Si mol% in Table 4.

2.9. Quantification of $T^3{}_8$ Cubic Octamer. To a mixture of 45 mL of MIBK and 60 mL of water on an ice bath, 22.4 g (0.15 mol) of methyltrichlorosilane dissolved in 15 mL of MIBK was added dropwise. The reaction temperature was kept at 5–9°C during the addition over 1 h. After the completion of the addition, the reaction mixture was heated on an oil bath. It took 23 min for the reaction temperature to increase to 50°C, after which the heating was continued at 50°C for 3 h. After the MIBK phase was washed to neutral, the insoluble materials were collected from the MIBK phase by centrifugation (6000 rpm, 15 min). The precipitate was washed by dispersing in MIBK followed by centrifugation. The MIBK used for washing was combined with the MIBK phase. The precipitate was further washed with acetone and dried under vacuum for 3 h (284.4 mg). The water phase and the water used for this washing were combined and subjected to centrifugation. The precipitate was washed with acetone twice and dried. All the precipitates obtained were combined. The solvent was removed from the MIBK phase after removing the precipitate, giving a resin as a solid (10.2 g). The resin was Me_3Si-capped by the method described above and subjected to GC analysis using D_4 as an internal standard. In other two runs, the products were recovered immediately after the completion of the addition of the chlorosilane (0 h aging) and after 17 h aging at 50°C.

2.10. Reaction of the Isolated $T^3{}_6T^2{}_2$. The crude isolated $T^3{}_6T^2{}_2$ cage, **1**, (50.0 mg, 0.0901 mmol) was dissolved in 0.864 mL of MIBK (the amount of MIBK relative to Si was three time of the PMSQ synthesis due to the solubility of $T^3{}_6T^2{}_2$). After adding 0.30 mL of 24 wt% hydrochloric acid, the mixture was heated at 50°C for 3 h. The MIBK phase was washed with water to neutral before recovering the precipitate by centrifugation. The amount of the precipitates was 9.7 mg (19 wt% of the starting material). From the MIBK phase, 37.5 mg of a resin was obtained by removing the solvent (**1-R**, 75 wt% of the starting material). The content of the $T^3{}_8$ cage in the precipitated was determined by XRD crystallinity and that in the resin was determined by the aforementioned GC/GC-MS method after Me_3Si-capping.

3. Results and Discussion

3.1. GPC Analysis. Figure 2 represents the GPC curves for PMSQ-1 and MeDT-1 with the molecular weight data listed in Table 1. Both materials showed multimodal curves. The weight average molecular weight, *Mw*, were 6370 for PMSQ-1 and 4370 for MeDT-1. Both materials contained low molecular weight species, the peak at 17.9 min for PMSQ-1, 19.0% peak area with the *Mw* of 390, and the peak at 18.5 min for MeDT-1, 22.9% peak area with the *Mw* of 410. For PMSQ-2 and MeDT-2, GPC using coupled refractive index, viscosity, and light scattering detectors was conducted. Because the light scattering signal was too weak for realistic measurement, the universal calibration method was used as an alternative and the results are summarized in Table 2. The relationship between molecular weight M and intrinsic viscosity $[\eta]$ is typically represented by the Mark-Houwink equation:

$$[\eta] = KM^a, \tag{1}$$

where the coefficient K and the exponent a depend on the solute-solvent pair and temperature. The Mark-Houwink exponent can provide information with respect to molecular shape, where the limits are 0 for spheres and 2 for rod-like molecules. The a values around 0.3 mean that the molecule is far from rigid-rod shapes.

3.2. NMR Spectroscopy. Figure 3(a) shows the ^{29}Si NMR spectrum of PMSQ-1 together with the T unit region magnified. The integration data are summarized in Table 3. The spectrum consists of three major envelopes: (i) −51 to −58 ppm, (ii) −58 to −60.5 ppm, and (iii) −60.5 to −70 ppm. Region (i) will be assigned to T^2 silicon and (ii) and (iii) to T^3 silicon [30–32]. These broad resonances suggest the presence of a variety of environments. At the same time, sharp peaks are observed at −52.3, −52.9, −54.2, −54.8, −55.1, −63.2, −63.4, −64.3, −64.6, −64.9, −66.0 ppm, and so forth, indicating that specific environments are heavily populated or preferred. Figure 3(b) illustrates the ^{29}Si NMR spectrum of Me_3Si-capped PMSQ-1. The resonances in the T^2 region decreased and a new resonance appeared around 9 ppm for the vinyl dimethyl-M unit. The NMR integration for the M region, the decrease in the T^2 region, and the increase in the T^3 region indicated that no condensation essentially took place during the capping reaction. However, the resonances including the two sharp peaks at −52.9 and −55.2 ppm remained in the −51 to −58 ppm region. A deuteration technique in IR spectroscopy by Lipp to detect trace silanol in PDMS revealed that the silanol content of the Me_3Si-capped PMSQ was 0.12 wt%, implying that the capping efficiency was around 95% [33]. Feher and coworkers reported that an incompletely condensed cyclohexylsilsesquioxane of the structure (b) in Figure 1 showed the ^{29}Si NMR peaks at

Table 2: Universal GPC data.

	Mn	Mw	$[\eta]_n$	$[\eta]_w$	Rg_n	Rg_w	M-H a	M-H Log K
PMSQ-2	3640	17400	0.025	0.028	1.66	2.33	0.329	−2.845
MeDT-2	3700	24600	0.024	0.028	1.68	2.46	0.293	−2.752

Table 3: ^{29}Si NMR data for PMSQ-1 and MeDT-1.

Materials	M	D^1 (−12/−15)	D^2-a (−15/−19.2)	D^2-b (−19.2/−23)	T^1 (−46/−49)	T^2 (−50/−58)	T^3-a (−58/−60.5)	T^3-b (−60.5/−70)
PMSQ-1	—	—	—	—	—	0.194	0.034	0.772
—cap[a]	0.150	—	—	—	—	0.045	0.024	0.931
PMSQ-NA	—	—	—	—	0.015	0.378	0.039	0.568
—cap[a]	0.292	—	—	0	—	0.102	0.045	0.854
MeDT-1	—	0.004	0.093	0.047	—	0.142	0.027	0.688
—cap[a]	0.111	0.005	0.088	0.053	—	0.035	0.023	0.797

[a]The sum of the D and the T region integration is standardized as unity excluding the M unit.

−55.57, −56.94, −57.11, and −66.40 ppm in the intensity ratio of 1 : 2 : 2 : 1 [34]. Since there are only two T^2 silicon atoms among the six, this clearly indicates that the T^3 silicon in the strained cyclotrisiloxane ring gives resonances around −56 ppm for this silsesquioxane structure with an aliphatic substituent. Unno and coworkers reported the chemical shift for hexasilsesquioxane (Figure 1(a)) with substituents of 1,1,2-trimethylpropyl and t-butyl giving peaks at −55.1 and −54.3 ppm, respectively [35]. All these pieces of information imply that an aliphatic substituted T^3 silicon in a cyclotrisiloxane ring gives ∼10 ppm downfield shift. Therefore it is highly likely that the major part of the residual resonances in the −51 to −58 ppm region for the Me_3Si-capped PMSQ represent silicon atoms of T^3 in strained rings. It is safe to say that only 75–80 mol% of the silicon in the −51 to −58 ppm region can be assigned to T^2. In other words, the T^2/T^3 molar ratio of the PMSQ from traditional ^{29}Si NMR assignment is 0.19/0.81, but the actual composition is roughly $T^2_{0.15}T^3_{0.85}$.

Table 3 and Figures 3(e) and 3(f) show the data and spectra for the ^{29}Si NMR spectrum of MeDT-1. Essentially the same phenomenon that there are residual resonances in the −51 to −58 ppm region after Me_3Si-capping was seen. However, the integration of the D silicon region around −20 ppm is not affected by the capping, indicating that there is no D^1 silicon in MeDT-1. Usually D^2 silicon, represented by those in polydimethylsiloxane, appears around −22 ppm [36]. Those in −15 to −19 ppm region denoted as D^2-a in Table 3 will be D^2 silicon next to a T unit. The sharp peak at −14.4 ppm which was not affected by the capping could be a D^2 silicon in strained ring structures. In a similar manner to the PMSQ, the composition of MeDT-1 could be described as $D^2_{0.15}T^2_{0.10}T^3_{0.75}$.

3.3. GC-MS and GC Analysis. PMSQ-1 was subjected to GC and GC-MS analyses using the Me_3Si-capped material to avoid silanol condensation in the high-temperature GC injection port and the detector. Figure 4 shows the GC chart using an FID detector. GC-MS analysis was carried out using the same capillary column as the GC in which molecular weights of 18 peaks were identified. The molecular weights are assigned based upon the common knowledge that a methyl radical (molecular mass of 15) is readily cleaved from neutral species [37] which are subjected to 70 eV electron ionization. As a reference data, T^3_8 was directly placed in the ionization chamber of the GC-MS instrument, which gave the expected $[M\text{-}Me]^+$ ion at 521 daltons, arising from the loss of a CH_3 radical from the odd electron molecular ion of the neutral (nominal mass = 536 Daltons). As can be seen in Figure 4, seven species with their isomers were detected. Mass spectrometry of PMSQ materials is reported for matrix-assisted laser desorption/ionization time-of-flight (MALDI) MS [38], graphite plate laser desorption/ionization time-of-flight (GPLDI-TOF) MS [39, 40], and electrospray ionization Fourier transform ion cyclotron resonance (ESI-FTICR) MS [38]. These mass spectroscopic methods can directly analyze silanol-functional PMSQs without the Me_3Si-capping, but the GC-MS method can identify the presence of isomers and quantify the identified material in combination with a GC. As described in the experimental section, the peaks in Figure 4 were quantified using D_4 as an internal standard as listed in Table 4. The molecular weight observed in the GC-MS is for the capped species. For instance, $[MeSiO_{3/2}]_6[MeSi(OSiMe_3)_{2/2}]_2$ was actually observed instead of the original $T^3_6T^2_2$, but the amount of each species shown in Table 4 was calculated on the uncapped molecules as described in the experimental section. The sum of the seven types of species, 18 compounds all together including isomers, was 7.9 wt% of the entire PMSQ, in which the most abundant compound was $T^3_6T^2_2$.

The GC-MS and GC study of MeDT-1 was carried out by the same method. For the PMSQ, one molecular weight detected by the GC-MS corresponded to one combination of T^3 and T^2. For MeDT, however, there were multiple compositions which corresponded to a given molecular weight for the capped resin. The molecular weight of 550 could

Table 4: QR-ES-Metflex GC quantification summary.

Composition	Number	FW w/o cap	FW w/cap	PMSQ-1 wt% w/o cap	PMSQ-NA wt% w/o cap	PMSQ-QC Si mol% w/o cap
T^0	a	94	310	—	—	0.02
T^3_6	b	402	402	—	0.18	0
T^2_3	c	228	444	—	—	0.01
T^1_2	d	170	454	—	—	0.03
$T^3_6T^2$	e	478	550	0.37	1.12	0.32
$T^3_6T^2$	f	478	550	—	0.09	0.07
$T^3_6T^2$	g	478	550	0.81	2.13	0.48
$T^3_4T^2_2$	h	420	564	—	1.64	0.55
$T^3_4T^2_2$	j	420	564	—	1.92	1.80
T^3_8	k	536	536	0.11	—	—
$T^3_2T^2_3$	l	362	578	—	—	0.28
$T^3_4T^2$	m	344	416	—	—	0.33
$T^3_2T^2_3$	n	362	578	—	—	0.25
T^2_4	o	304	592	—	—	0.41
$T^3_2T^2_3$	p	362	578	—	—	0.30
T^2_4	q	304	592	—	—	0.36
$T^3_2T^2_3$	r	362	578	—	0.31	0.87
$T^3_2T^2_3$	s	362	578	—	—	0.20
$T^3_6T^2$	t	478	550	0.13	trace?	—
$T^3_6T^2$	u	478	550	0.07	trace?	—
$T^3_8T^2$	v	612	684	1.20	0.47	0.12
$T^3_6T^2_2$	w	554	698	0.41	0.38	0.32
$T^3_6T^2_2$	x	554	698	1.37	1.28	0.35
$T^3_6T^2_2$	y	554	698	—	0.35	0.20
$T^3_6T^2_2$	z	554	698	1.33	1.19	0.31
$T^3_8T^2$	a2	612	684	0.26	0.22	0.13
$T^3_6T^2_2$	b2	554	698	—	—	0.11
$T^3_8T^2$	c2	612	684	—	0.22	0.13
$T^3_8T^2$	d2	612	684	—	0.21	0.11
$T^3_6T^2_2$	e2	554	698	0.12	0.65	0.31
T^3_{10}	f2	670	670	0.12	—	—
$T^3_4T^2_3$	g2	496	712	0.17	0.79	0.60
$T^3_4T^2_3$	h2	496	712	0.37	1.19	0.75
$T^3_4T^2_3$	i2	496	712	—	0.25	0.23
$T^3_4T^2_3$	j2	496	712	0.26	0.94	0.44
$T^3_4T^2_3$	k2	496	712	—	—	0.20
$T^3_4T^2_3$	l2	496	712	0.52	2.22	1.11
$T^3_2T^2_4$	m2	438	726	—	0.82	1.67
$T^3_2T^2_4$	n2	438	726	—	0.51	1.24
$T^3_2T^2_4$	o2	438	726	—	0.29	0.66
$T^3_2T^2_4$	p2	438	726	—	0.17	0.44
T^2_5	q2	380	740	—	—	0.29
T^2_5	r2	380	740	—	—	0.20
$T^3_8T^2_2$	s2	688	832	0.08	—	—
$T^3_8T^2_2$	t2	688	832	0.18	—	—
Total				7.87	19.57	16.36

Table 5: GC quantification of assignable low molecular weight species in MeDT-1.

GC time	Structure[a]	FE w/cap	FW w/o cap	wt% w/o cap
4.896	$T^3{}_4T^2{}_2$	416	416	0.16
5.474	$T^3{}_4T^2{}_2$	490	490	0.13
5.513	$T^3{}_6D^2$	476	476	0.84
5.606	$T^3{}_4D^2{}_3$	490	490	0.16
5.749	$T^3{}_6D^2{}_2$[a]	550	550	0.62
5.832	$T^3{}_6D^2{}_2$[a]	550	550	0.30
6.011	$T^3{}_6D^2{}_2$[a]	550	550	0.11
6.075-1	$T^3{}_4T^2D^2{}_2$[b]	564	492	0.15
6.075-2	$T^3{}_6D^2{}_2$[a]	550	550	0.31
6.118-1	$T^3{}_4T^2D^2{}_2$[b]	564	492	0.32
6.118-2	$T^3{}_4T^2D^2{}_2$[b]	564	492	0.46
6.149	$T^3{}_4T^2D^2{}_2$[b]	564	492	0.15
6.189	$T^3{}_4T^2D^2{}_2$[b]	564	492	0.45
6.278	$T^3{}_6T^2D^2$	624	552	0.63
6.338-1	$T^3{}_8D^2$	610	610	0.286
6.338-2	$T^3{}_6T^2D^2$	624	552	1.30
6.446	$T^3{}_8D^2$	610	610	0.10
6.566	$T^3{}_6T^2D^2$	624	552	0.28
6.647	$T^3{}_8T^2$	684	612	1.41
6.748-2	$T^3{}_8T^2$	684	612	0.37
	Total	—	—	8.53

[a]This molecule is most possibly $T^3{}_6D^2{}_2$ but could be $T^3{}_6T^2$.
[b]This molecule is most possibly $T^3{}_4T^2D^2{}_2$ but could be $T^3{}_4T^2{}_2$.

be interpreted as a capped $T^3{}_6T^2$ or a $T^3{}_6D^2{}_2$ (not capped being completely condensed), and the molecular weight of 564 could be a capped $T^3{}_4T^2{}_2$ or a capped $T^3{}_4T^2D^2{}_2$. To help determine which composition was the correct assignment to the GC-MS molecular weight, an uncapped resin was subjected to GC-MS, which gave the same peaks of molecular weight of 550 (m/e of 535) as the capped material. Thus the molecular weight of 550 for the capped species was assigned as $T^3{}_6D^2{}_2$, not $T^3{}_6T^2$. Based upon the appearance in electrospray mass spectrometry, the capped molecular weight of 564 could be $T^3{}_4T^2D^2{}_2$ [41]. Based on these considerations, the assignment and quantification were made as summarized in Table 5. Eight species ranging from $T^3{}_4D^2{}_2$ to $T^3{}_8T^2$ (20 compounds all together including isomers) were detected with their sum of 8.5 wt% on an uncapped resin basis.

Comparing the PMSQ and the MeDT resin, the number of the species detected by GC and GC-MS and their sum were similar. But it is noted that many of the T^2 units $[CH_3Si(OH)O_{2/2}]$ in the PMSQ are replaced with D^2 unit $[(CH_3)_2SiO_{2/2}]$, the units with two siloxane bonds and two substituents. While $T^3{}_6T^2{}_2$ was the most abundant species in the PMSQ, $T^3{}_6T^2D^2$ (exemplified in Figure 1(h)) was the most abundant in the methyl-DT resin. Most of the molecules in the PMSQ were incompletely condensed silsesquioxanes, but 35% of the molecules were completely condensed in the MeDT. It should be noted that these

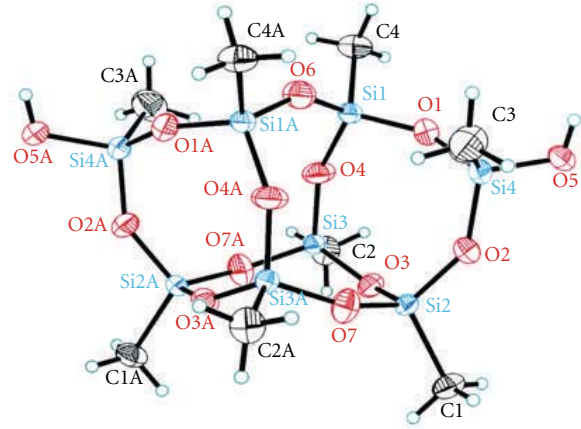

Figure 5: The structure of **X2**.

structures are not specific to silsesquioxanes, but common to silicone resins.

3.4. Isolation of a Compound and Consideration for the Structures. One compound **1** was able to be isolated from PMSQ-1 by solvent fractionation and recrystallization as described in the experimental section. GC analysis of the Me_3Si-capped material showed that crude crystal of **1** mainly consisted of peak **z** in Figure 4 with the relative GC peak area of 90%. The GC purity increased to 98% after recrystallization (**X1**). Figure 5 shows the X-ray single crystal structure of **X2** which proves that the molecule is $T^3{}_6T^2{}_2$. The molecule consisted of two identical parts related by a crystallographic twofold axis passing through atom O6. Schematically, this compound is described as shown in Figure 1(f). Tables 6 and 7 show the bond distances and the bond angles, respectively. The Si–O bond lengths range from 1.601(3) to 1.630(3) Å, which are comparable to values found in the other Si–O ring systems [28, 42]. Figure 6 shows the unit cell structure of **X2**. The molecules showed no short intramolecular contact distances and were connected by intermolecular hydrogen bonding between the hydroxyl groups. Four neighboring hydroxyl groups were arranged about a crystallographic fourfold axis. There were no other significant intermolecular interactions, but a chloroform molecule was statically distributed over four symmetry equivalent positions.

Figure 7(a) shows the ^{29}Si NMR spectrum of crude **1** mainly consisting of four sharp resonances at −55.7, −63.6, −64.5, and −65.1 ppm with the integration ratio of 1 : 1 : 1 : 1. The peak at −55.7 ppm is of the T^2 silicon and the other three peaks are of the T^3 silicon atoms. The pattern was similar to that of the cyclohexylsilsesquioxane of the same structure (pyridine/C_6D_6, −58.46, −65.66, −67.51, −68.58 ppm, 1 : 1 : 1 : 1) [28]. The spectrum verifies that T^3 silicon atoms in a cyclotetrasiloxane or a cyclopentasiloxane ring, not in a strained cyclotrisiloxane, appear in the −65 ppm region, not in the −55 ppm region. The ^{29}Si NMR peak assignment was further verified by Me_3Si-capping as shown in Figure 7(b). The spectrum shows four resonances at –64.0, −64.1, −64.8, and −65.4 ppm with the integration ratio of 1 : 1 : 1 : 1,

Table 6: Bond distances for **1**, **X2**.

Atom 1	Atom 2	Distance (Å)
Si1	O1	1.609 (3)
Si1	O4	1.626 (3)
Si1	O6	1.615 (2)
Si1	C4	1.828 (5)
Si2	O2	1.614 (3)
Si2	O3	1.630 (3)
Si2	O7	1.620 (3)
Si2	C1	1.840 (4)
Si3	O3	1.621 (3)
Si3	O4	1.601 (3)
Si3	O7	1.608 (3)
Si4	O1	1.612 (3)
Si4	O2	1.620 (3)
Si4	O5	1.611 (3)
Si4	C3	1.848 (5)
Si3	C2	1.819 (4)

Table 7: Bond angles for **1**, **X2**.

Atom 1	Atom 2	Atom 3	Angle (deg)
O1	Si1	O4	109.0 (2)
O1	Si1	O6	108.6 (1)
O1	Si1	C4	110.5 (2)
O4	Si1	O6	108.7 (2)
O4	Si1	C4	110.9 (2)
O6	Si1	C4	109.1 (2)
O2	Si2	O3	108.9 (2)
O2	Si2	O7	109.1 (2)
O2	Si2	C1	109.7 (2)
O3	Si2	O7	108.6 (1)
O3	Si2	C1	110.0 (2)
O7	Si2	C1	110.4 (2)
O3	Si3	O4	109.2 (1)
O3	Si3	O7	109.4 (1)
O3	Si3	C2	110.0 (2)
O4	Si3	O7	107.9 (2)
O4	Si3	C2	111.2 (2)
O7	Si3	C2	109.2 (2)
O1	Si4	O2	109.0 (2)
O1	Si4	O5	109.0 (2)
O1	Si4	C3	109.8 (2)
O2	Si4	O5	105.3 (2)
O2	Si4	C3	112.1 (2)
O5	Si4	C3	111.4 (2)
Si1	O1	Si4	151.5 (2)
Si2	O2	Si4	144.1 (2)
Si2	O3	Si3	145.5 (2)
Si1	O4	Si3	153.9 (2)
Si1	O6	Si1	146.8 (3)
Si2	O7	Si3	153.3 (2)

reflecting the conversion of the T^2 silicon to T^3 by the capping. The M/T ratio was 1/4 as expected.

The isolation of this molecule and the identification of the structure clarify the presence of cage molecules in the

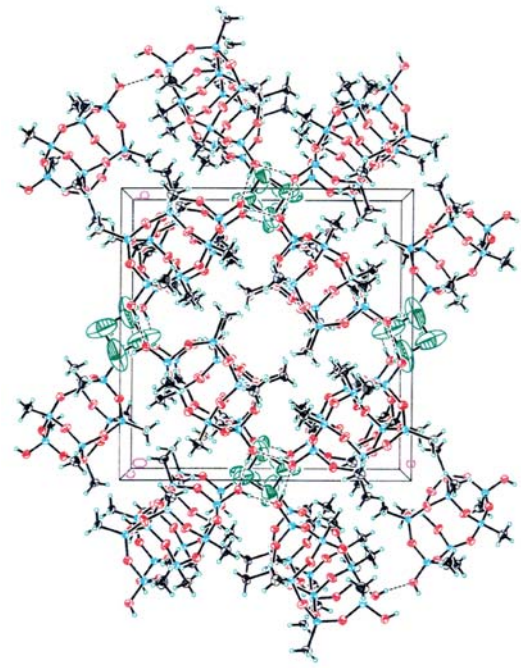

Figure 6: The unit cell structure of **X2**.

PMSQ. As shown in Figure 4 and Table 4, there are three other isomers for the composition of $T^3{}_6T^2{}_2$, peaks w, x, and e2. Since the structure of these species is unknown, it is possible to draw a ladder-like structure shown in Figure 1(g). For the chemical formulae like $T^3{}_6T^2$ or $T^3{}_8T^2$, however, one cannot draw such ladder-like structures. $T^3{}_8$ and $T^3{}_{10}$ are surely cage structures. Thus it is safe to say that the presence of cage molecules in the PMSQ is evident. Since Feher and coworkers reported spontaneous formation of structures (a), (d), and (f) for cyclohexyl substituent [28], the major structure of $T^3{}_4T^2{}_3$ could be (d) in Figure 1. The presence of cage molecules may be in line with the low Mark-Houwink exponent values. Another observation is that the structure of $T^3{}_6T^2$ cannot be drawn without including at least one cyclotrisiloxane ring as shown in Figure 1(c) as an example. This structure was reported by Feher and coworkers as the dehydration product from the material having the structure of Figure 1(d) for a cyclohexylsilsesquioxane. If a ladder structure as in Figure 1(g) exists, that also contains cyclotrisiloxane rings. The presence of $T^3{}_6T^2$ and the residual resonance in the −55 ppm region after Me_3Si-capping in the ^{29}Si NMR spectrum verifies the presence of strained cyclotrisiloxane rings.

3.5. Early Stage of the Reaction. To obtain insight into the formation of these low molecular weight species in PMSQ-1, reaction intermediates at much earlier reaction stage were captured. PMSQ-1 was prepared by adding 8.00 mol (~1200 g) of methyltrichlorosilane to a mixture of water and MIBK over 3 h 4 min allowing the reaction temperature to increase to 23°C, followed by heating up to 50°C taking

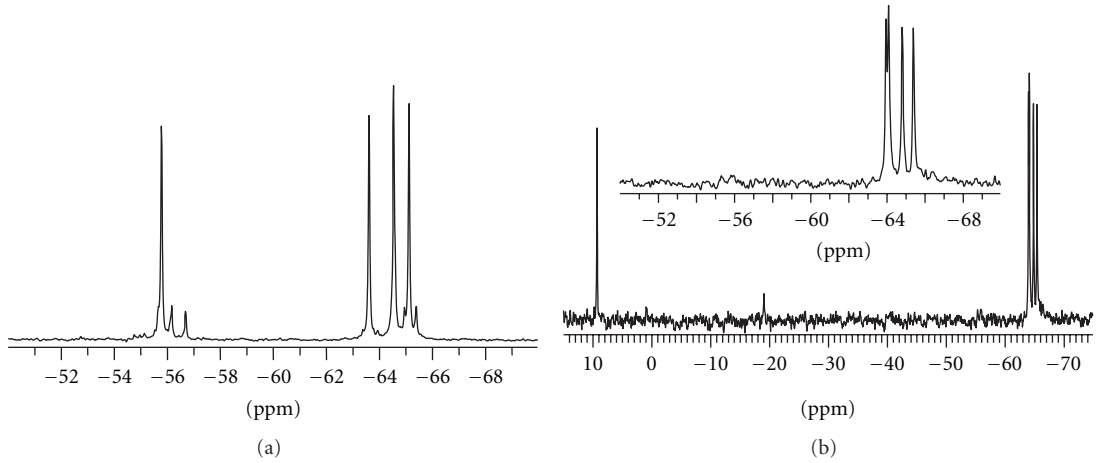

Figure 7: ^{29}Si NMR spectrum of (a) crude **1** and (b) Me_3Si-capped **X1**.

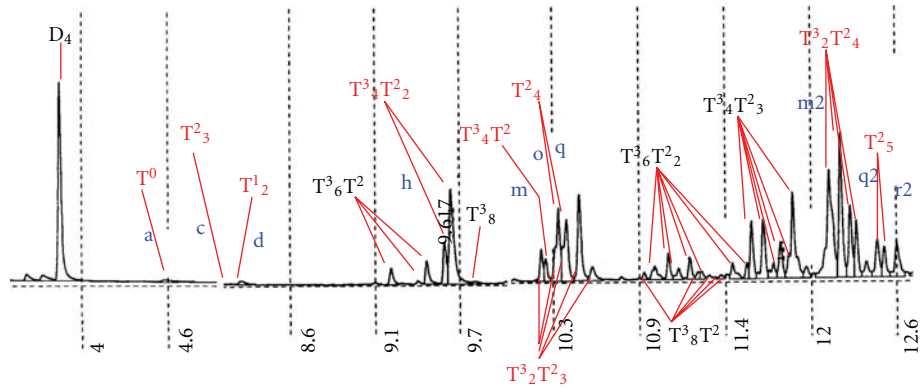

Figure 8: Gas chromatograph of PMSQ-QC with the peak assignment by the GC-MS. The molecular compositions are described as uncapped PMSQ.

53 min and aging at 50°C for ~3 h. In contrast, to capture the reaction intermediates at earlier stage, firstly a quench capping approach was carried out. Methyltrichlorosilane (0.2 g) was added to a stirred mixture of water and MIBK over 140 s suppressing the reaction temperature only up to 9°C. After stirring for 35 s, the reaction mixture was poured into 2-methylpentane containing BSTFA in a dry ice-acetone bath to freeze the acid-water phase and cap the silanol by trimethylsilyl group. The reaction product, PMSQ-QC, was subjected to GC and GC-MS analyses in a similar way to the analysis of the Me_3Si-capped PMSQ-1.

Figure 8 shows the FID-GC chart with the peak assignment from GC-MS for PMSQ-QC. The GC quantitative analysis data are summarized in Table 4. Since the amount of the entire resin is not known for PMSQ-QC, the amount of each species relative to the entire resin on the uncapped basis was calculated as silicon mol% (see the Experimental section), which is close to weight percent. Many species that were not present in PMSQ-1 were observed: T^0 [$CH_3Si(OH)_3$], $T^1{}_2$ [$HO(CH_3)_2Si\text{-}O\text{-}Si(CH_3)_2OH$], $T^2{}_3$ [cyclic trimer of $CH_3Si(OH)O_{2/2}$], $T^2{}_4$ [cyclic tetramer, two isomers], $T^2{}_5$ [cyclic pentamer, two isomers], $T^2{}_4T^2$ [one isomer], $T^2{}_2T^2{}_3$ [five isomers], $T^2{}_2T^2{}_4$ [four isomers], and $T^2{}_4T^2{}_2$ [three isomers]. Including those common with the PMSQ, which are $T^2{}_6T^2$, $T^2{}_6T^2{}_2$, and $T^2{}_4T^2{}_3$, the sum of the identified species was 16.4%, indicating that more than 80% of the silicon is already in higher molecular weight species. Most of the cage structures found in PMSQ-1 or in the literature [3–6, 27, 28] consist of cyclotetra- or cyclopentasiloxanes. The abundance of $T^2{}_4$ and $T^2{}_5$ in PMSQ-QC may be in line with this. The amount of the cyclic trimer, $T^2{}_3$ exemplified in Figure 1(i), was very small but clearly identified, while a linear trimer, $T^1{}_2T^2$ illustrated in Figure 1(j), was not detected. Thus the formation of strained cyclic trimer was evidenced. In a computer simulation of condensation of $HSi(OH)_3$ and trisilanol with other substituents under excess water condition [43, 44], Kudo and Gordon suggested that the energy for the formation of cyclic trimer is not very much higher than that for cyclic tetramer. For the formation mechanism of cyclic tetramer, they indicated that insertion of T^0 to cyclic trimer is even more favored than the condensation of two $T^1{}_2$ molecules or T^0 and a linear trimer. Kelts and Armstrong observed the formation of cyclic trimers of Q^2, [$Si(OH)_2O_{2/2}$], by ^{29}Si NMR spectroscopy for the hydrolytic polycondensation of tetraethyl orthosilicate [45]. Brunet reported the formation

of cyclic trimers by the acidic sol-gel reaction of methyltriethoxysilane as observed by DEPT ^{29}Si NMR spectroscopy [46]. Among the detected species in the present study, the structures of $T^2{}_2T^2{}_3$ and $T^2{}_4T^2{}_2$ also cannot be drawn without including cyclotrisiloxane rings as exemplified in Figure 1(m) (the structures represent one possible isomer but it is not verified that these exact structures are real). All these observations imply that the condensation favors the formation of such strained rings at this stage of the reaction. For cyclic tetramer, $T^2{}_4$, all *cis* isomer shown in Figure 1(k) is reported for phenyl [47] and isopropyl [18] substituents. Kudo and Gordon simulated that the formation of the all *cis* isomer is most favored due to hydrogen bonding among the silanols in the transition state [43]. They calculated that the next stable isomer is the structure of Figure 1(l).

As the reaction stage in between PMSQ-1 and PMSQ-QC, a PMSQ was recovered immediately after the completion of the addition of methyltrichlorosilane (0.500 mol) to a mixture of water and MIBK without heat aging, PMSQ-NA. Figure 2(c) shows the GPC curve. The low molecular weight end overlaps with the solvent peak and the relative area of the peak around 18 min reached 53%. The *Mw* and the *Mn* are much lower than those of PMSQ-1. Figure 3(c) represents the ^{29}Si NMR spectrum. As summarized in Table 3, the resonance in the T^1 region (−46 to −49 ppm) was present and the resonances in the T^1 and the T^2 region were twice of those in the T^2 region in PMSQ-1. By Me_3Si-capping as shown in Figure 3(d), the resonances in the T^2 region again remained of which relative area was greater than that for PMSQ-1.

The GC and the GC-MS data for PMSQ-NA by the same method described before are listed in Table 4. The change in PMSQ-QC, PMSQ-NA, and PMSQ-1 can be summarized as follows.

(1) Species present in PMSQ-QC but reduced or extinct in PMSQ-NA and extinct in PMSQ-1 are T^0, $T^2{}_3$, $T^1{}_2$, $T^2{}_4$ (both 2 isomers), $T^2{}_5$ (both 2 isomers), $T^3{}_2T^2{}_3$ (all the 5 isomers), $T^3{}_4T^2$, $T^3{}_2T^2{}_4$ (all the 4 isomers), $T^3{}_4T^2{}_3$ (1 out of the 6 isomers), and $T^3{}_6T^2{}_2$ (1 out of the 6 isomers).

(2) Species that increase monotonously (including those not present in PMSQ-QC and PMSQ-NA) are $T^3{}_8$, $T^3{}_{10}$, $T^3{}_6T^2$ (2 out of the 5 isomers), $T^3{}_8T^2$ (2 out of the 4 isomers), and $T^3{}_6T^2{}_2$ (3 out of the 6 isomers). The isolated isomer of $T^3{}_6T^2{}_2$, *z*, is one of these.

(3) Species that increase from PMSQ-QC to PMSQ-NA, but then decrease or become extinct in PMSQ-1, are $T^3{}_6T^2$ (3 out of the 5 isomers), $T^3{}_4T^2{}_2$ (both 2 isomers), $T^3{}_6T^2{}_2$ (2 out of the 6 isomers), $T^3{}_8T^2$ (2 out of the 4 isomers), and $T^3{}_4T^2{}_3$ (5 out of the 6 isomers). Many of the species of which structures cannot be drawn without a cyclotrisiloxane ring are in this category.

It should be noted that the sum of the material detected by the GC-MS analysis increased from 16.4% in PMSQ-QC to 19.6% in PMSQ-NA. This suggests that the buildup of the molecules during the course of the reaction is not simply proceeding by continued condensation.

Table 8: The amount of $T^3{}_8$ formed during the hydrolytic polycondensation of $MeSiCl_3$.

Aging time (h)	Yield (wt%)		
	In precipitates	In soluble PMSQ	Total
0	1.06	—	(1.06)
3.0	2.92	0.41	3.33
17.0	4.54	0.17	4.71

3.6. Reaction Chemistry for the Formation of the $T^3{}_8$ Cubic Octamer. In an effort to obtain insights into the chemistry for the structure buildup in silsesquioxanes or silicone resins, formation of $T^3{}_8$ cubic octamers was pursued. Three separate runs were carried out: after completing the dropwise addition of methyltrichlorosilane to a mixture of MIBK and water, (i) the product was immediately recovered (0 h aging), (ii) aged at 50°C for 3 h, and (iii) aged at 50°C for 17 h. For each run, precipitates were collected both from the MIBK and the water phases, followed by determining the amount of $T^3{}_8$ by X-ray diffraction crystallinity, which was around 80%. The soluble resins were subjected to Me_3Si-capping by BSTFA, for which the GC quantification was carried out in the same way as mentioned above. The amounts of $T^3{}_8$ by these methods are listed in Table 8. The amount of $T^3{}_8$ in the resin at 0 h aging was not able to be determined because the GC peak of $T^3{}_8$ overlapped with that of $T^3{}_4T^2{}_2$, preventing from the quantitative analysis. However, it is safe to say that the amount of $T^3{}_8$ increased with increasing aging time, because the major part of the material is found in the precipitate.

Figure 9 illustrates various potential routes for the formation of $T^3{}_8$. The natural thought would be simple condensation of precursor molecules, represented by routes (i)–(iv). The species T^0, $T^1{}_2$, $T^2{}_4$, and $T^2{}_2T^2{}_4$ appearing in routes (i), (ii), and (iv) are present at the very early stage exemplified by PMSQ-QC. However, T^0, $T^1{}_2$, and $T^2{}_4$ are extinct in PMSQ-NA (0 h aging) and in PMSQ-1 (3 h aging) and $T^2{}_2T^2{}_4$ decreased in PMSQ-NA and is extinct in PMSQ-1. Considering the fact that the amount of $T^3{}_8$ continues to increase during the 17-hour aging, there appear to be no clear evidence that routes (i), (ii), and (iv) are the major mechanism of $T^3{}_8$ formation. Route (iii) does not require such early reaction stage intermediates, but there is no evidence of the presence of this structure among the isomers of $T^3{}_6T^2{}_2$.

To investigate if siloxane bond rearrangement was involved in forming $T^3{}_8$, aging of the isolated $T^3{}_6T^2{}_2$, crude **1**, was conducted at 50°C for 3 h in MIBK with hydrochloric acid of a similar concentration as the PMSQ synthesis. The solution after the reaction was cloudy, for which centrifugation was carried out after washing the MIBK phase with water. WAXD analysis of the precipitates showed that they were $T^3{}_8$ with the crystallinity of 82%. The amount of the precipitates was 19 wt% of the starting material; hence the amount of $T^3{}_8$ was 16 wt%. From the MIBK phase

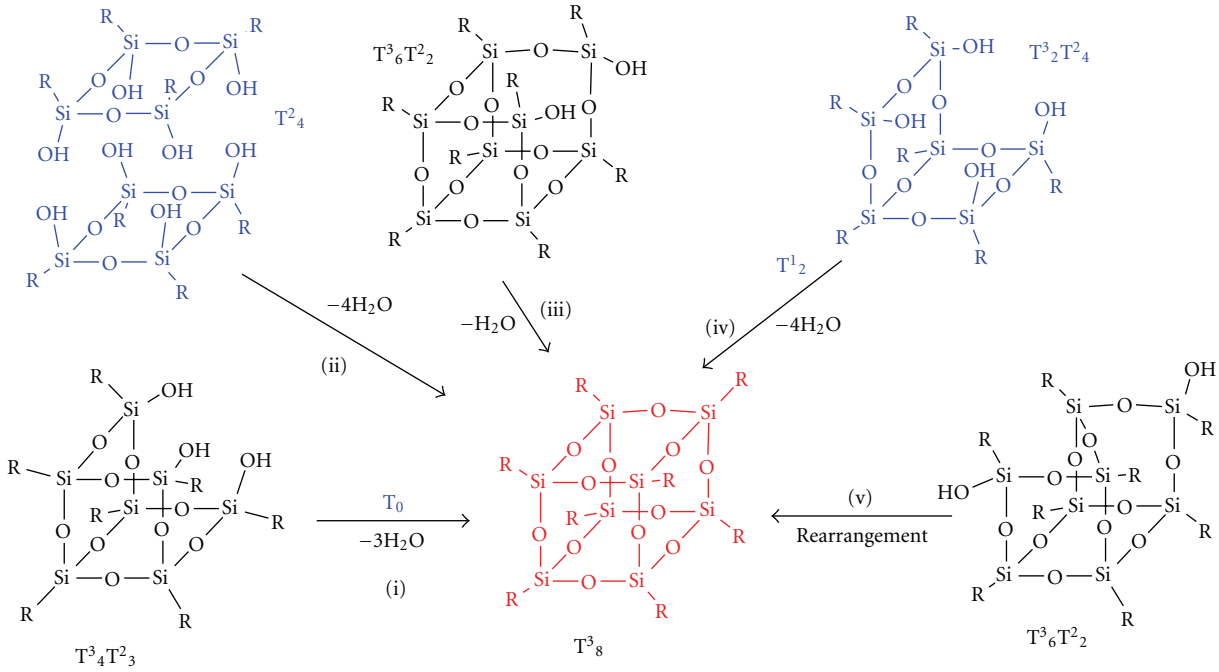

Figure 9: Potential routes for the formation of the T^3_8 cubic octamer.

Table 9: Formation of T^3_8 from $T^3_6T^2_2$ Cage 1 compound.

Composition	GC time (min)	wt% w/o capping	
		Before aging 1	After aging 1 − *R*
$T^3_6T^2_2$	10.8	—	5
$T^3_6T^2_2$	10.9	0.3	20
$T^3_6T^2_2$	11.1	90	17
T^3_8	—	0	16[a]

[a]Determined by WAXD of the precipitate.

after centrifugation, a resin was obtained by removing the solvent (1-R, 75 wt% of the starting material), which was subjected to GC analysis after Me_3Si-capping (1-R-cap). As summarized in Table 9, the amount of the starting material decreased to 17 wt%, while two other isomers of $T^3_6T^2_2$ formed in 5 and 20 wt% yields by the reaction. $T^3_6T^2$ and $T^3_4T^2_3$ were also detected but the amounts of these molecules were much smaller compared with that of the $T^3_6T^2_2$ isomers. GPC of 1-R-cap revealed the formation of higher molecular weight species too. These findings prove that siloxane bond rearrangement of low molecular weight molecules is one of the mechanisms for T^3_8 formation, route (v) in Figure 9. We can speculate that such reaction mechanism can be applied to molecules other than T^3_8. In the hydrolytic polycondensation of phenyltrimethoxysilane in alkaline media, Lee and Kawakami reported that the $T^3_4T^2_3$ structure, Figure 1(d), is first formed, which was then consumed to provide the so-called double-decker structure, $T^3_4T^2_4$, that need siloxane bond rearrangement [48].

4. Concluding Remarks

The present study focused on the characterization of a PMSQ and a methyl-DT silicone resin that were synthesized by hydrolytic polycondensation of chlorosilanes without specific control of the reaction. The key findings can be summarized as follows.

Firstly, as opposed to the proposal by Brown and coworkers that PPSQs have ladder structures [8, 9], the PMSQ was found to contain cage molecules. Presence of intense low molecular weight peak in the GPC curve, several sharp peaks on the broad envelope of resonances in the ^{29}Si NMR spectrum, and low Mark-Houwink exponent value are the indirect evidences. More direct proof was obtained by the GC and GC-MS study which revealed the presence of ~20 low molecular weight species with their sum of ~8 wt%. Isolated $T^3_6T^2_2$ molecule, Presence of T^3_8 and T^3_{10} cage molecules, and some species of which structures can be drawn only as cages from the chemical formulae determined by the GC-MS clarified the presence of cage structures. Cyclization plays a critical role in the formation of these materials to deviate from Flory's random branching theory as pointed out by McCormick and coworkers for the sol-gel reaction of tetraethyl orthosilicate [49] and methyltriethoxysilane [50].

Secondly substantial evidences for the presence of strained cyclotrisiloxane rings were found. Among the chemical formulae identified by the GC-MS analysis, the structures of $T^3_6T^2$ cannot be drawn without including at least one cyclotrisiloxane ring (see Figure 1(c)). The ^{29}Si NMR spectrum of the PMSQ of which silanols were capped by trimethylsilyl group suggested the presence of strained T^3

structure by the residual resonances in the classical T^2 region, −50 to −58 ppm. A cyclic trimer of T^2 was directly observed at the very early stage of the reaction (PMSQ-QC). In addition, 2 out of the 5 isomers of $T^3{}_6T^2$ increased monotonously from PMSQ-QC to the PMSQ, and the other 3 isomers increased from PMSQ-QC to PMSQ-NA, then decreased in the PMSQ. This suggests that the cyclotrisiloxane rings are not always unstable species.

In the study to clarify the formation mechanism of $T^3{}_8$ cubic octamer, no clear evidence was identified that $T^3{}_8$ was formed by simple condensation of precursor molecules. In contrast, when the isolated $T^3{}_6T^2{}_2$ (90% purity) was subjected to the same heat aging condition in acidic media as the synthesis of the PMSQ, the amount of the starting material was reduced to 17%, and $T^3{}_8$ and two other isomers of $T^3{}_6T^2{}_2$ were found in 16, 20, and 5% amounts, respectively. Thus, siloxane bond rearrangement is an important mechanism in the formation of cage molecules or low molecular weight species. The amount of the species detected by the GC-MS analysis in PMSQ-QC and PMSQ-NA could be in line with this observation. Some species increased from PMSQ-QC to PMSQ-NA then decreased in the PMSQ, and some molecules monotonously increased from PMSQ-QC to the PMSQ. This could be indicating that the reaction is not proceeding only by simple continuation of condensation.

Finally the methyl-DT resin containing 15 mol% of a D^2 unit $[(CH_3)_2SiO_{2/2}]$ showed essentially the same tendency as the PMSQ, showing the presence of cage molecules as analyzed by GPC, ^{29}Si NMR spectroscopy, and GC/GC-MS studies (the reaction chemistry was not pursued). One feature was that many of the T^2 unit $[CH_3Si(OH)O_{2/2}]$ in the PMSQ were replaced with D^2 unit $[(CH_3)_2SiO_{2/2}]$ in the methyl-DT resin. Thus the form of the molecule as an incompletely condensed cage in the PMSQ, for example, $T^3{}_6T^2{}_2$, was a completely condensed cage, for example, $T^3{}_6D^2{}_2$. The presence of cyclotrisiloxane rings was suggested in a similar manner by the residual resonance in the −50 to −58 ppm region in the ^{29}Si NMR spectrum after trimethylsilyl-capping and the presence of species that one cannot draw a structure without including a cyclotrisiloxane ring, for example, $T^3{}_6D$. This has clarified that a methyl-DT resin, which is a more common industrial silicone resin, consists of similar structures as silsesquioxanes and the generality of the trend found in the PMSQ.

Disclaimer

The information provided in this paper does not constitute a contractual commitment by Dow Corning. While Dow Corning has tried to assure that information contained in this paper is accurate and fully up to date, Dow Corning does not guarantee or warranty the accuracy or completeness of information provided herein. Dow Corning reserves the right to make improvements, corrections, and/or changes to this paper in the future. To the full extent permitted by law, Dow Corning disclaims any and all liability with respect to your use of, or reliance upon, this paper. You have the sole obligation to decide whether information provided by Dow Corning will work in your processes or will be safe and efficacious in your applications. It is your sole responsibility to determine the suitability of the information provided to you. Dow corning does not make any warranty or representation, express or implied with respect to the utility or completeness of the information provided herein, and specifically disclaims the implied warranties of merchantability and fitness for a particular purpose.

Acknowledgments

The authors thank Drs. Akihito Saito of Dow Corning (currently Canon Inc.), Ronald Tecklenburg, Elmer Lipp, Larry Wood, Russel King, Katsuya Eguchi, Gregg Zank, and Dimitris Katsoulis of Dow Corning for their great support and helpful discussions.

References

[1] L. H. Brown, "Silicones in protective coatings," in *Treatise on Coatings*, R. Myers and J. S. Long, Eds., vol. 1, part 3, chapter 13, pp. 513–563, Marcel Dekker, New York, NY, USA, 1972.

[2] R. H. Baney, M. Itoh, A. Sakakibara, and T. Suzuki, "Silsesquioxanes," *Chemical Reviews*, vol. 95, no. 5, pp. 1409–1430, 1995.

[3] M. G. Voronkov and V. I. Lavrent'yev, "Polyhedral oligosilsesquioxanes and their homo delivatives," *Topics in Current Chemistry*, vol. 102, pp. 199–236, 1982.

[4] P. G. Harrison, "Silicate cages: precursors to new materials," *Journal of Organometallic Chemistry*, vol. 542, no. 2, pp. 141–183, 1997.

[5] V. Chandrasekhar, R. Boomishankar, and S. Nagendran, "Recent developments in the synthesis and structure of organosilanols," *Chemical Reviews*, vol. 104, no. 12, pp. 5847–5910, 2004.

[6] D. B. Cordes, P. D. Lickiss, and F. Rataboul, "Recent developments in the chemistry of cubic polyhedral oligosilsesquioxanes," *Chemical Reviews*, vol. 110, no. 4, pp. 2081–2173, 2010.

[7] E. L. Warrick, *Forty Years of Firsts: The Recollections of a Dow Corning Pioneer*, chapter 1, McGraw-Hill, New York, NY, USA, 1990.

[8] J. F. Brown Jr., J. H. Vogt Jr., A. Katchman, J. W. Eustance, K. M. Kiser, and K. W. Krantz, "Double chain polymers of phenylsilsesquioxane," *Journal of the American Chemical Society*, vol. 82, no. 23, pp. 6194–6195, 1960.

[9] J. F. Brown, "Double chain polymers and nonrandom crosslinking," *Journal of Polymer Science C*, vol. 1, no. 1, pp. 83–97, 1963.

[10] K. A. Andrianov, A. A. Zhdanov, and V. Yu Levin, "Some physical properties of organosilicon ladder polymers," *Annual Review of Materials Science*, vol. 8, pp. 313–326, 1978.

[11] D. Ya Tsvankin, V. Yu Levin, V. S. Pankov, V. P. Zhukov, A. A. Zhdanov, and K. A. Andrianov, "New type of temperature variation of X-ray diffraction from a number of polymers," *Polymer Science U.S.S.R.*, vol. 21, no. 9, pp. 2348–2358, 1979.

[12] E. S. Park, H. W. Ro, C. V. Nguyen, R. L. Jaffe, and D. Y. Yoon, "Infrared spectroscopy study of microstructures of poly(silsesquioxane)s," *Chemistry of Materials*, vol. 20, no. 4, pp. 1548–1554, 2008.

[13] T. E. Helminiak, C. L. Benner, and W. E. Gibbs, "Some solution properties of the ladder polymer cis-syndiotactic

poly-phenylsilsesquioxane," *ACS Polymer Preprints*, vol. 8, pp. 284–291, 1967.

[14] V. N. Tsvetkov, K. A. Andrianov, G. I. Okhrimenko, and M. G. Vitovskaya, "Conformation and rigidity of ladder polymer molecules," *European Polymer Journal*, vol. 7, no. 9, pp. 1215–1230, 1971.

[15] L. Shi, X. Zhang, Y. Si, M. Ye, and D. Li, "Solution properties of ladder-like polymer polyphenylsilsesquioxanes," *Chinese Journal of Polymer Science*, vol. 5, no. 4, pp. 359–365, 1987.

[16] T. E. Helminiak and G. C. Berry, "Properties of the ladder polymer cis-syndiotactic poly(phenylsilsesquioxane) in solution," *Journal of Polymer Science*, vol. 65, no. 1, pp. 107–123, 1978.

[17] C. L. Frye and J. M. Klosowski, "Concerning the so-called "ladder structure" of equilibrated phenylsilsesquioxane," *Journal of the American Chemical Society*, vol. 93, no. 18, pp. 4599–4601, 1971.

[18] M. Unno, A. Suto, K. Takada, and H. Matsumoto, "Synthesis of ladder and cage silsesquioxanes from 1,2,3,4- tetrahydroxycyclotetrasiloxane," *Bulletin of the Chemical Society of Japan*, vol. 73, no. 1, pp. 215–220, 2000.

[19] M. Unno, A. Suto, and H. Matsumoto, "Pentacyclic laddersiloxane," *Journal of the American Chemical Society*, vol. 124, no. 8, pp. 1574–1575, 2002.

[20] M. Unno, T. Matsumoto, and H. Matsumoto, "Synthesis of laddersiloxanes by novel stereocontrolled approach," *Journal of Organometallic Chemistry*, vol. 692, no. 1–3, pp. 307–312, 2007.

[21] S. Chang, T. Matsumoto, H. Matsumoto, and M. Unno, "Synthesis and characterization of heptacyclic laddersiloxanes and ladder polysilsesquioxane," *Applied Organometallic Chemistry*, vol. 24, no. 3, pp. 241–246, 2010.

[22] S. Kyushin, R. Tanaka, K. Arai, A. Sakamoto, and H. Matsumoto, "Domino oxidation of ladder oligosilanes: formation of novel ladder frameworks containing oligosiloxane and oligosilane chains," *Chemistry Letters*, no. 12, pp. 1297–1298, 1999.

[23] H. Seki, T. Kajiwara, Y. Abe, and T. Gunji, "Synthesis and structure of ladder polymethylsilsesquioxanes from silafunctionalized cyclotetrasiloxanes," *Journal of Organometallic Chemistry*, vol. 695, no. 9, pp. 1363–1369, 2010.

[24] A. J. Barry, W. H. Daudt, J. J. Domicone, and J. W. Gilkey, "Crystalline organosilsesquioxanes," *Journal of the American Chemical Society*, vol. 77, no. 16, pp. 4248–4252, 1955.

[25] K. A. Andrianov and B. A. Lzmaylov, "Hydrolytic polycondensation of higher alkyltrichlorosilanes," *Journal of Organometallic Chemistry*, vol. 8, no. 3, pp. 435–441, 1967.

[26] C. L. Frye and W. T. Collins, "The oligomeric silsesquioxanes, $(HSiO_{3/2})_n$," *Journal of the American Chemical Society*, vol. 92, no. 19, pp. 5586–5588, 1970.

[27] P. A. Agaskar and W. G. Klemperer, "The higher hydridospherosiloxanes: synthesis and structures of $H_nSi_nO_{1.5n}$ (n = 12, 14, 16, 18)," *Inorganica Chimica Acta*, vol. 229, no. 1-2, pp. 355–364, 1995.

[28] F. J. Feher, D. A. Newman, and J. F. Walzer, "Silsesquioxanes as models for silica surfaces," *Journal of the American Chemical Society*, vol. 111, no. 5, pp. 1741–1748, 1989.

[29] T. Kondo, K. Yoshii, K. Horie, and M. Itoh, "Photoprobe study of siloxane polymers. 3. Local free volume of polymethylsilsesquioxane probed by photoisomerization of azobenzene," *Macromolecules*, vol. 33, no. 10, pp. 3650–3658, 2000.

[30] Z. Xie, Z. He, D. Dai, and R. Zhang, "Study on the synthesis and characterization of the soluble, high molecular weight and ladderlike polymethylsilsesquioxane," *Chinese Journal of Polymer Science*, vol. 7, no. 2, pp. 183–188, 1989.

[31] G. E. Maciel, M. J. Sullivan, and D. W. Sindorf, "Carbon-13 and silicon-29 nuclear magnetic resonance spectra of solid poly(methylsiloxane) polymers," *Macromolecules*, vol. 14, no. 5, pp. 1607–1608, 1981.

[32] G. Engelhardt, H. Jancke, E. Lippmaa, and A. Samoson, "Structure investigations of solid organosilicon polymers by high resolution solid state ^{29}Si NMR," *Journal of Organometallic Chemistry*, vol. 210, no. 3, pp. 295–301, 1981.

[33] E. D. Lipp, "Deuteration technique to detect trace silanol by IR spectroscopy," Personal communication to M. Itoh, March 2000.

[34] F. J. Feher, D. Soulivong, and G. T. Lewis, "Facile framework cleavage reactions of a completely condensed silesquioxane framework," *Journal of the American Chemical Society*, vol. 119, no. 46, pp. 11323–11324, 1997.

[35] M. Unno, S. B. Alias, H. Saito, and H. Matsumoto, "Synthesis of hexasilsesquioxanes bearing bulky substituents: hexakis((1,1,2-trimethylpropyl)silsesquioxane) and hexakis (tert-butylsilsesquioxane)," *Organometallics*, vol. 15, no. 9, pp. 2413–2414, 1996.

[36] R. B. Taylor, B. Parbhoo, and D. M. Fillmore, "Muclear magnetic resonance spectroscopy," in *The Analytical Chemistry of Silicones*, A. Lee Smith, Ed., pp. 382–383, John Wiley & Sons, New York, NY, USA, 1991.

[37] I. Hasegawa, S. Sakka, K. Kuroda, and C. Kato, "Trimethylsilylation of the hydrolysed and polycondensed products of methyltriethoxysilane," *Journal of Chromatography A*, vol. 410, pp. 137–143, 1987.

[38] R. E. Tecklenburg, W. E. Wallace, and H. Chen, "Characterization of a $[(O_{3/2}SiMe)\times(OSi(OH)Me)_y(OSiMe2)_z]$ silsesquioxane copolymer resin by mass spectrometry," *Rapid Communications in Mass Spectrometry*, vol. 15, no. 22, pp. 2176–2185, 2001.

[39] H.-J. Kim, J.-K. Lee, S.-J. Park, H. W. Ro, D. Y. Yoo, and D. Y. Yoon, "Observation of low molecular weight poly(methylsilsesquioxane)s by graphite plate laser desorption/ionization time-of-flight mass spectrometry," *Analytical Chemistry*, vol. 72, no. 22, pp. 5673–5678, 2000.

[40] H. W. Ro, E. S. Park, C. L. Soles, and D. Y. Yoon, "Structure-property relationships for methylsilsesquioxanes," *Chemistry of Materials*, vol. 22, no. 4, pp. 1330–1339, 2010.

[41] R. E. Tecklenburg, "Electrospray mass spectrometry data," Personal communication to M. Itoh, March 2000.

[42] N. Auner, B. Ziemer, B. Herrschaft, W. Ziche, P. John, and J. Weis, "Structural studies of novel siloxysilsesquioxanes," *European Journal of Inorganic Chemistry*, vol. 1999, no. 7, pp. 1087–1094, 1999.

[43] T. Kudo and M. S. Gordon, "Theoretical studies of the mechanism for the synthesis of silsesquioxanes. 2. Cyclosiloxanes (D_3 and D_4)," *The Journal of Physical Chemistry A*, vol. 104, no. 17, pp. 4058–4063, 2000.

[44] T. Kudo and M. S. Gordon, "Exploring the mechanism for the synthesis of silsesquioxanes. 3. The effect of substituents and water," *The Journal of Physical Chemistry A*, vol. 106, no. 46, pp. 11347–11353, 2002.

[45] L. W. Kelts and N. J. Armstrong, "A silicon-29 NMR study of the structural intermediates in low pH sol-gel reactions," *Journal of Materials Research*, vol. 4, no. 2, pp. 423–433, 1989.

[46] F. Brunet, "Polymerization reactions in methyltriethoxysilane studied through ^{29}Si NMR with polarization transfer," *Journal of Non-Crystalline Solids*, vol. 231, no. 1-2, pp. 58–77, 1998.

[47] J. F. Brown Jr., "The polycondensation of phenylsilanetriol," *Journal of the American Chemical Society*, vol. 87, no. 19, pp. 4317–4324, 1965.

[48] D. W. Lee and Y. Kawakam, "Incompletely condensed silsesquioxanes: formation and reactivity," *Polymer Journal*, vol. 39, no. 3, pp. 230–238, 2007.

[49] L. V. Ng, P. Thompson, J. Sanchez, C. W. Macosko, and A. V. McCormick, "Formation of cagelike intermediates from nonrandom cyclization during acid-catalyzed sol-gel polymerization of tetraethyl orthosilicate," *Macromolecules*, vol. 28, no. 19, pp. 6471–6476, 1995.

[50] S. E. Rankin, C. W. Macosko, and A. V. McCormick, "Importance of cyclization during the condensation of hydrolyzed alkoxysilanes," *Chemistry of Materials*, vol. 10, no. 8, pp. 2037–2040, 1998.

Hindawi Publishing Corporation
International Journal of Polymer Science
Volume 2012, Article ID 723892, 4 pages
doi:10.1155/2012/723892

Research Article

Nonacyclic Ladder Silsesquioxanes and Spectral Features of Ladder Polysilsesquioxanes

Masafumi Unno, Tomoe Matsumoto, and Hideyuki Matsumoto

Department of Chemistry and Chemical Biology and International Education and Research Center for Silicon Science, Graduate School of Engineering, Gunma University, Kiryu 376-8515, Japan

Correspondence should be addressed to Masafumi Unno, unno@gunma-u.ac.jp

Received 29 June 2012; Accepted 24 August 2012

Academic Editor: Kimihiro Matsukawa

Laddersiloxanes, that is, ladder silsesquioxanes with defined structures, could be obtained by stepwise synthesis starting from cyclic silanols. These compounds were shown to have high thermal stability. As an extension of the previous work, the first nonacyclic ladder silsesquioxanes were synthesized by the reaction of bicyclic silanol with tricyclic tetrachloride, which were obtained from cyclic silanols. The structure was confirmed by spectral measurements, and the spectral features of a series of ladder polysilsesquioxanes with determined structures were analyzed.

1. Introduction

Recently, the interest in ladder silsesquioxanes has been growing mainly because of their high thermal stability and their application to functional materials [1–3]. To study the relationship between the structure and properties, we prepared ladder silsesquioxanes, determined their structures, and investigated the properties. We referred to these ladder silsesquioxanes as "laddersiloxanes," and we reported the syntheses and crystallographic analysis of tricyclic laddersiloxanes [4, 5]; pentacyclic laddersiloxanes [6]; bi-, tri-, tetra-, and pentacyclic laddersiloxanes with an all *anti* conformation [7]; extendible pentacyclic laddersiloxanes [8] and heptacyclic laddersiloxanes by a stereocontrolled approach [9]. As an extension, herein, we report the synthesis of the first nonacyclic ladder silsesquioxanes.

2. Experiments

Preparative recycle-type high-performance liquid chromatography (HPLC) was carried out by using a JAI LC-908 HPLC with a Chemco 7-ODS-H column (20 × 250 mm). The Fourier-transform nuclear magnetic resonance (NMR) spectra were obtained by using a JEOL model Λ-500 (^{1}H NMR at 500.00 MHz, ^{13}C NMR at 125.65 MHz, and ^{29}Si NMR at 99.25 MHz). The chemical shifts were reported as δ units (ppm) relative to $SiMe_4$, and the residual solvent peaks were considered as the standard. Electron impact mass spectrometry was performed with a JEOL JMS-DX302. The infrared spectra were measured with a Shimadzu FTIR-8700.

*2.1. Preparation of Bicyclic Ladder Silanol (**4**).* A solution of $(i\text{-PrPhSiCl})_2O$ [6] (1.02 g, 2.66 mmol) in pyridine (8 mL) was added dropwise to $[i\text{-Pr(OH)SiO}]_4$ (1.02 g, 2.45 mmol) [10–12] in pyridine (8 mL) for 3 h at 0°C. The mixture was stirred for an additional 20 min at 0°C. The reaction mixture was added to saturated aqueous NH_4Cl and hexane, and two phases were separated. The aqueous phase was extracted with hexane. The organic phase was then washed with saturated aqueous NH_4Cl, then dried over anhydrous magnesium sulfate, and concentrated. The crude product was separated by dry column chromatography (eluent: hexane/Et_2O = 9 : 1), followed by the separation using recycle-type HPLC (eluent: MeOH/THF = 9 : 1) to give bicyclic ladder silanols (**4**, 1.00 g, 56%) (isomeric mixture). They were identified by the comparison with authentic sample [4, 5].

2.2. Reaction of Tricyclic Laddersiloxanes Tetrachloride with Bicyclic Ladder Silanols. A solution of bicyclic ladder silanols

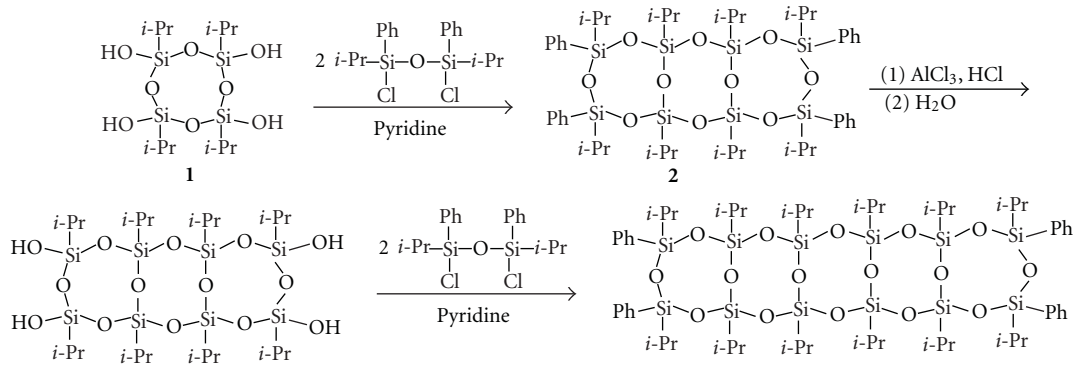

Scheme 1: Synthesis of pentacyclic laddersiloxanes.

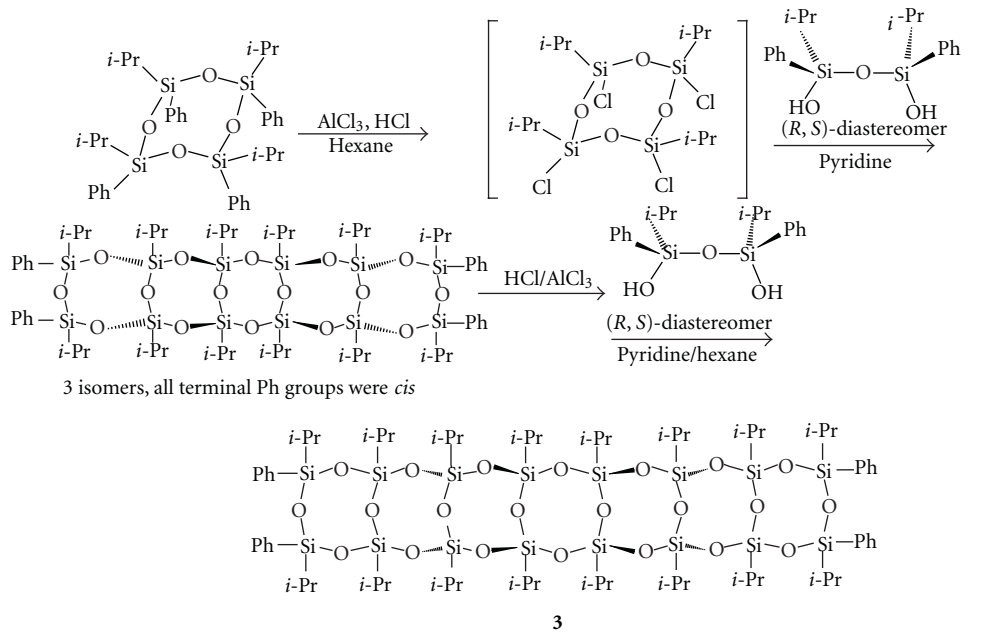

Scheme 2: Synthesis of heptacyclic laddersiloxanes.

(**4**) (1.00 g, 1.38 mmol) in pyridine (4 mL) was added dropwise to a solution of tetrachloro-tricyclic laddersiloxanes (**5**) [6] (0.552 g, 0.600 mmol) in pyridine (6 mL) for 13 min at room temperature. The mixture was stirred for 5 d at 100°C. The reaction mixture was added to saturated aqueous NH_4Cl and hexane, and two phases were separated. The aqueous phase was extracted with hexane. The combined organic phase was washed with saturated aqueous NH_4Cl, then dried over anhydrous magnesium sulfate, and concentrated. Ethanol was added to the concentrate, and the resulting $(i\text{-}PrSiO_{1.5})_8$ (26 mg, 6%) was obtained by filtration. The filtrate was separated by dry column chromatography (eluent: hexane/Et_2O = 9 : 1), followed by separation with recycle-type gel permeation chromatography (GPC) (eluent: THF) to give nonacyclic ladder silsesquioxanes (isomeric mixture) (**6**) (98 mg, 7%). **6**: MS (70 eV) *m/z* (%) 2134 (M^+-*i*-Pr, 5), 28 (100). IR (NaCl) ν 3072, 3051, 2947, 2895, 2868, 1593, 1466, 1429, 1387, 1366, 1259, 1115, 1034, 999, 920, 889, 719, 702 cm^{-1}.

3. Results and Discussions

3.1. Synthesis of Nonacyclic Ladder Silsesquioxanes. Our strategy for constructing a real ladder structure is based on the reaction of cyclotetrasiloxane units [10–12]. Recently, Gunji's group reported the synthesis of ladder polysilsesquioxane starting from cyclotetrasiloxane units [13], showing that this unit is essential to obtain the real ladder structure. As can be seen from Scheme 1, all *cis*-cyclotetrasiloxanetetraol **1** was treated with dichlorodisiloxane to give tricyclic laddersiloxanes **2**. Dephenylchlorination that was followed by hydrolysis afforded tricyclic tetraols, and then, a similar procedure could be applied again to extend ladder [6]. The obtained pentacyclic laddersiloxanes (mixture of isomers) were isolated by recycle-type reverse-phase HPLC, and the structure of one of the isomers was determined by X-ray crystallography. In this synthesis, tricyclic laddersiloxanes **2** were obtained in a good yield (85%), but the yield of pentacyclic laddersiloxane was not satisfactory (47%,

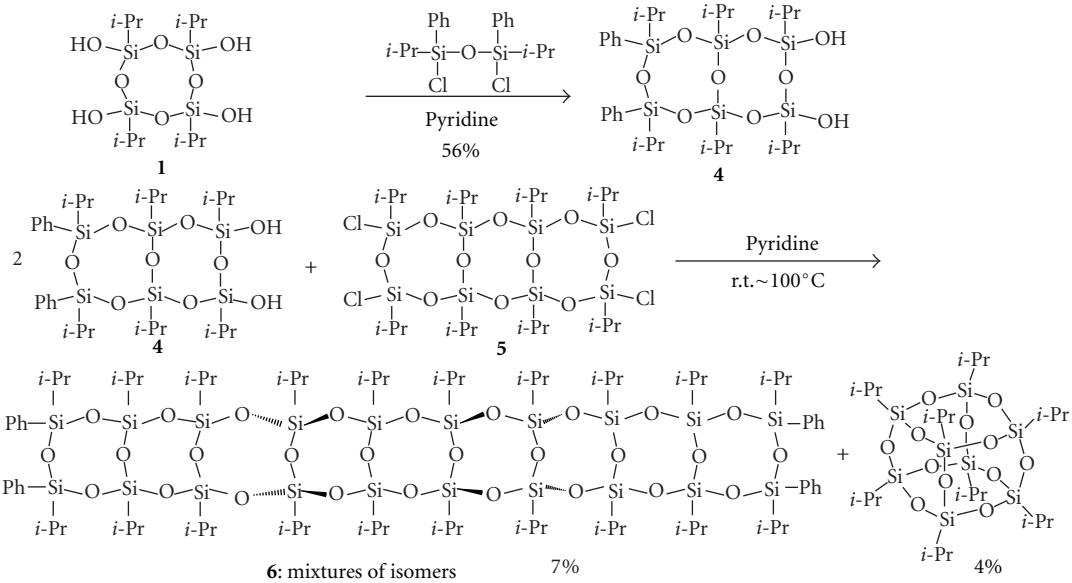

Scheme 3: Synthesis of nonacyclic ladder silsesquioxanes.

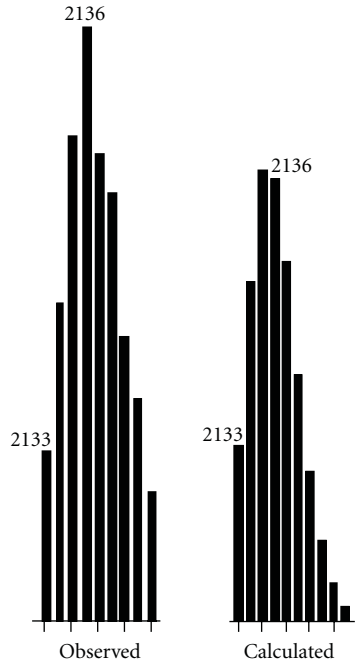

Figure 1: Observed and calculated mass spectra of nonacyclic ladder silsesquioxanes **6.**

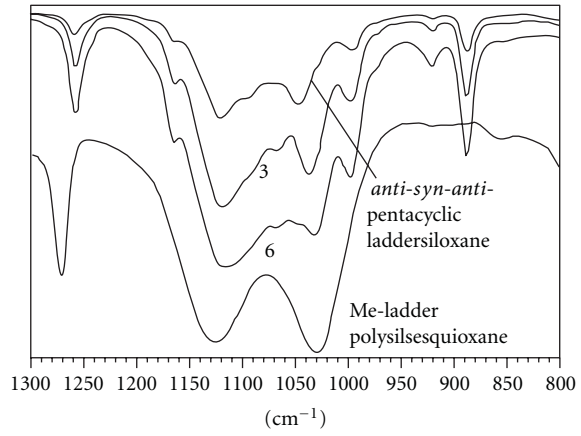

Figure 2: IR spectra of pentacyclic, heptacyclic, nonacyclic laddersiloxanes and ladder polysilsesquioxanes.

mixture of five stereoisomers). This can be attributed to the generation of disadaptive isomers. Additional rings can be formed when the terminal hydroxyl groups are in the *cis* position. However, when two hydroxyl groups are in *trans* position, laddersiloxanes cannot be obtained. This explains why the yield of pentacyclic laddersiloxanes was not high.

Therefore, in the case of heptacyclic laddersiloxanes **3**, we separated and utilized (1R,3S)-disiloxanediol in order to obtain extendible products [8] (Scheme 2). By the reaction with (R,S)-disiloxanediol, only *cis*-diphenyl pentacyclic laddersiloxanes were obtained. These laddersiloxanes enabled us to obtain **3**.

Although the obtained heptacyclic laddersiloxanes **3** could be theoretically extendible, synthesis of nonacyclic laddersiloxanes from heptacyclic laddersiloxanes was unsuccessful because of the lack of enough supply of starting heptacyclic laddersiloxanes. Therefore, we devised alternative approach.

During the preparation of tricyclic laddersiloxane **2**, we observed the generation of bicyclic diol **4** as a by-product. To obtain **4** in a higher yield, we treated **1** with 1 equiv. of dichlorodisiloxane. As shown in Scheme 3, the desired diol **4** was obtained in 56% yield. When we reacted **4** with tricyclic tetrachloride **5**, which was prepared in the synthesis of pentacyclic laddersiloxanes [6], target nonacyclic ladder silsesquioxanes **6** were obtained as a mixture of isomers

Table 1: ^{29}Si NMR chemical shift of laddersiloxanes.

Compounds	^{29}Si NMR chemical shift/ppm
syn-Tricyclic laddersiloxane [4, 5]	−67.2
anti-Tricyclic laddersiloxane [4, 5]	−66.8
All *anti*-Pentacyclic laddersiloxane [7]	−65.8, −65.2
anti-syn-syn-Pentacyclic laddersiloxane [6]	−66.5, −65.9
Heptacyclic laddersiloxane (isomeric mixture) **3** [8]	−66.2 to −64.9
Nonacyclic ladder silsesquioxanes (isomeric mixture) **6**	−66.5 to −65.5
Methyl ladder polysilsesquioxane (solid state) [9]	−64.5

(7%) with octasilsesquioxane (6%). As in the case of heptacyclic laddersiloxanes, nonacyclic ladder silsesquioxanes were obtained as a viscous oil, and X-ray crystallographic analysis was impossible. Therefore, we determined the structure of **6** by spectroscopic analysis.

The ^{29}Si NMR spectrum of **6** in $CDCl_3$ showed multiple peaks between −66.52 and −65.45 ppm and between −34.53 and −32.80 ppm. The peaks around −65 ppm were attributed to the internal silicon atom, and those around –34 ppm were attributed to the terminal Si(–Ph) atom. The chemical shifts of silicon (*T*) atoms in laddersiloxanes, whose structures were determined by X-ray analysis, are summarized in Table 1. The ^{29}Si NMR value of **6** was in good agreement with those of other laddersiloxanes. In addition, the mass spectrum showed a peak at 2133 (M^+–C_3H_6), and the isotope pattern was similar to the calculated one (Figure 1). From these results, the obtained product was identified as a nonacyclic ladder silsesquioxanes.

3.2. Spectral Features of Ladder Silsesquioxanes. The ^{29}Si NMR chemical shifts of internal silicon atoms of laddersiloxanes are summarized in Table 1. The results indicate that ^{29}Si NMR peaks of laddersiloxanes and ladder polysilsesquioxanes are observed in a narrow area and are independent of the number of rings, stereostructures, and terminal substituents.

The IR spectra are very useful for the characterization of ladder silsesquioxanes. As Yoon's group has shown in their theoretical IR studies [14], ladder silsesquioxanes are characterized by two peaks around 1150 cm^{-1} and 1050 cm^{-1}, while IR spectra of cage silsesquioxanes do not have a peak at 1050 cm^{-1} [14]. As shown in Figure 2, two peaks were detected in that region for all laddersiloxanes. Because heptacyclic and nonacyclic laddersiloxanes are a mixture of stereoisomers, these two peaks are rather broad and are comprised of several peaks. On the other hand, absorption peaks of ladder polysilsesquioxanes were sharp and symmetrical, showing the highly organized structure.

Acknowledgments

The authors acknowledge the generous gift of silicon compounds by Shin-Etsu Chemical, Momentive Performance Materials, and Azumax.

References

[1] S. S. Choi, A. S. Lee, H. S. Lee et al., "Synthesis and characterization of UV-curable ladder-like polysilsesquioxane," *Journal of Polymer Science Part A*, vol. 49, no. 23, pp. 5012–5018, 2011.

[2] M. Handke, B. Handke, A. Kowalewska, and W. Jastrzebski, "New polysilsesquioxane materials of ladder-like structure," *Journal of Molecular Structure*, vol. 924–926, pp. 254–263, 2009.

[3] H. Seki, N. Abe, Y. Abe, and T. Gunji, "Synthesis and structure of syn,anti,syn-pentacyclic ladder oligomethylsilsesquioxane," *Chemistry Letters*, vol. 40, no. 7, pp. 722–723, 2011.

[4] M. Unno, B. A. Shamsul, M. Arai, K. Takada, R. Tanaka, and H. Matsumoto, "Synthesis and characterization of cage and bicyclic silsesquioxanes via dehydration of silanols," *Applied Organometallic Chemistry*, vol. 13, no. 4, pp. 303–310, 1999.

[5] M. Unno, A. Suto, K. Takada, and H. Matsumoto, "Synthesis of ladder and cage silsesquioxanes from 1,2,3,4-tetrahydroxycyclotetrasiloxane," *Bulletin of the Chemical Society of Japan*, vol. 73, no. 1, pp. 215–220, 2000.

[6] M. Unno, A. Suto, and H. Matsumoto, "Pentacyclic laddersiloxane," *Journal of the American Chemical Society*, vol. 124, no. 8, pp. 1574–1575, 2002.

[7] M. Unno, R. Tanaka, S. Tanaka, T. Takeuchi, S. Kyushin, and H. Matsumoto, "Oligocyclic ladder polysiloxanes: alternative synthesis by oxidation," *Organometallics*, vol. 24, no. 4, pp. 765–768, 2005.

[8] M. Unno, T. Matsumoto, and H. Matsumoto, "Synthesis of laddersiloxanes by novel stereocontrolled approach," *Journal of Organometallic Chemistry*, vol. 692, no. 1-3, pp. 307–312, 2007.

[9] S. Chang, T. Matsumoto, H. Matsumoto, and M. Unno, "Synthesis and characterization of heptacyclic laddersiloxanes and ladder polysilsesquioxane," *Applied Organometallic Chemistry*, vol. 24, no. 3, pp. 241–246, 2010.

[10] M. Unno, K. Takada, and H. Matsumoto, "Synthesis, structure, and reaction of the tetrahydroxycyclotetrasiloxane, [(i-Pr)(OH)SiO]$_4$," *Chemistry Letters*, no. 6, pp. 489–490, 1998.

[11] M. Unno, K. Takada, and H. Matsumoto, "Formation of supermolecule by assembling of two different silanols," *Chemistry Letters*, no. 3, pp. 242–243, 2000.

[12] M. Unno, Y. Kawaguchi, Y. Kishimoto, and H. Matsumoto, "Stereoisomers of 1,3,5,7-tetrahydroxy-1,3,5,7-tetraisopropylcyclotetrasiloxane: synthesis and structures in the crystal," *Journal of the American Chemical Society*, vol. 127, no. 7, pp. 2256–2263, 2005.

[13] H. Seki, T. Kajiwara, Y. Abe, and T. Gunji, "Synthesis and structure of ladder polymethylsilsesquioxanes from silafunctionalized cyclotetrasiloxanes," *Journal of Organometallic Chemistry*, vol. 695, no. 9, pp. 1363–1369, 2010.

[14] E. S. Park, H. W. Ro, C. V. Nguyen, R. L. Jaffe, and D. Y. R. Yoon, "Infrared spectroscopy study of microstructures of poly(silsesquioxane)s," *Chemistry of Materials*, vol. 20, no. 4, pp. 1548–1554, 2008.

Hindawi Publishing Corporation
International Journal of Polymer Science
Volume 2012, Article ID 460835, 6 pages
doi:10.1155/2012/460835

Research Article

Evolution of Mesopores in Monolithic Macroporous Ethylene-Bridged Polysilsesquioxane Gels Incorporated with Nonionic Surfactant

Atsushi Mushiake, Kazuyoshi Kanamori, and Kazuki Nakanishi

Department of Chemistry, Graduate School of Science, Kyoto University, Kitashirakawa, Sakyo-ku, Kyoto 606-8502, Japan

Correspondence should be addressed to Kazuki Nakanishi, kazuki@kuchem.kyoto-u.ac.jp

Received 11 July 2012; Accepted 4 September 2012

Academic Editor: Takahiro Gunji

By combining the micellar templating in nanometer scale with the polymerization-induced phase separation in micrometer scale, ethylene-bridged polysilsesquioxane gels with hierarchical macropores and mesopores are prepared. The difference of mesopore structures depending on the method of the solvent removal has been observed by the X-ray diffraction and the nitrogen adsorption-desorption measurements. During the hydrothermal treatment under the basic condition, the reorganization of the polysilsesquioxane gel network occurred differently depending on the alkoxy group contained in the precursors. From ^{29}Si CP/MAS NMR measurements, it was revealed that the crosslinking density of the hydrothermally treated gels was increased so that the highly ordered mesostructure of the wet gel could be preserved even after the evaporative drying of solvent.

1. Introduction

Synthesis of solids with surfactant-templated mesopores is an established procedure where various precursors can be used to produce metal oxides and metalloxane-based organic-inorganic hybrid materials [1–3]. It has been reported that monolithic ethane-silica gels with well-defined cocontinuous macropores and highly ordered mesopores has been synthesized via spontaneous route from the ethylene bridged silicon alkoxide with the aid of a structure-directing agent [4, 5]. These materials have higher alkaline resistance than pure silica gels due to their Si–C bond, so they can favorably be applied to catalyst supports, adsorbents, and separation media. The synthesis process is based upon alkoxy-derived sol-gel reactions in the presence of water-soluble organic polymers, such as poly(ethylene oxide). During the polymerization reaction of silicon alkoxides in an acidic condition, spinodal decomposition-type phase separation occurs concurrently with gelation, resulting in the formation of bicontinuous gel-rich and solvent-rich phases on the length scale of micrometers. In the pure silica system, subsequent solvent exchange with a basic aqueous solution and aging treatment generates the mesopores in the gel-rich phase via a process of dissolution/reprecipitation (Ostwald ripening) [6]. Upon evaporation drying, the gel-rich phase becomes mesoporous gel skeletons, and the solvent-rich phase turns into macropores that serve as flow-through pores. The macropores allow facile transport of fluid, while the mesopores offer extended surface area that facilitates the contacts between fluid and the solid surface [7].

In contrast to the pure silica system, the dissolution/reprecipitation hardly occurs in the bridged polysilsesquioxane system due to higher resistance of siloxane bonds against nucleophilic attacks. It is thus difficult to form mesopores in the gel skeletons just by solvent exchange with a basic solution. It is reported, however, that the relatively strong hydrothermal treatment of macroporous wet titania (TiO_2) gels which have negligible solubility in water results in the development of mesoporous structure [8]. It is therefore expected that mesopores in bridged polysilsesquioxane gels are also developed by appropriate hydrothermal treatments even if the structural evolution does not occur by dissolution/reprecipitation process. Although there are some reports on the formation of micropores in bridged

polysilsesquioxanes [9–11], almost nothing is known on the development of mesopores. In this paper, we investigate the effect on the mesostructure of the mode of solvent removal and conditions of hydrothermal treatments under weakly basic conditions. We also compare the difference between ethylene-bridged precursors: one with methoxy and the other ethoxy groups as hydrolysable ligands.

2. Experimental

2.1. Chemicals. The 1,2-bis(trimethoxysilyl)ethane, BTME, and 1,2-bis(triethoxysilyl)ethane, BTEE, purchased from Sigma-Aldrich, were used as precursors for silsesquioxane network. As structure-directing agents, poly(ethylene glycol)$_{20}$-*block*-poly(propylene glycol)$_{70}$-*block*-poly(ethylene glycol)$_{20}$, with average molecular mass of 5800, and poly(ethylene glycol)$_{106}$-*block*-poly(propylene glycol)$_{70}$-*block*-poly(ethylene glycol)$_{106}$, with average molecular mass of 12600, obtained from Sigma-Aldrich (equivalent to Pluronic P123 and F127, BASF) were used. Acetic acid (HOAc, 99.7 wt%), a product of Kishida Chemical Co., Ltd., and nitric acid (HNO_3, 60 wt%), a product of Hayashi Pure Chemical Industry Co., Ltd., were used as acid catalysts. Urea, a product of Hayashi Pure Chemical Industry Co., Ltd., was adopted for the purpose of raising solution pH homogeneously within a wet gel by the gradual generation of ammonia due to its hydrolysis. All reagents were used as received.

2.2. Synthesis Procedure. In the BTME-HOAc-P123-Urea system, BTME (2.14 g) was added to the homogeneous solution of P123 (2.2 g), urea (1.0 g), and 0.01 M acetic acid (15 g) under vigorous stirring at 0°C for hydrolysis. After 10 min of stirring, the resultant solution was kept at 60°C for gelation/aging. After 48 h, the solvent was removed by evaporative drying method or supercritical drying method. Hereinafter, we denote the samples prepared by these methods as ME-EvD and ME-SCD, respectively. Also, the hydrothermal treatment was conducted at 150°C using aged gels for 20 h in an autoclave under a weakly basic condition. Then, the wet gel was evaporatively dried. Obtained sample is denoted as ME-HyT.

In the BTEE-HNO_3-P123 system, BTEE (1.92 g) was added to the homogeneous solution of P123 (1.6 g) and 0.1 M nitric acid (16 g) under vigorous stirring at 0°C for hydrolysis. Due to considerably low reactivity of ethoxy ligands towards hydrolysis, the use of nitric acid was mandatory. After 20 min of stirring, the resultant solution was kept at 60°C for 24 h. After gelation/aging, the solvent was removed by evaporative drying method or supercritical drying method, and we denote the samples prepared in these method as EE-EvD and EE-SCD, respectively. The hydrothermal treatment was conducted at 150°C using aged gels for 20 h in an autoclave after the solvent exchange with 1.0 M aqueous solution of urea. The exchange of solvent with 1.0 M urea solution is necessary to ensure the weakly basic condition during the hydrothermal treatment. Samples obtained by the evaporative drying of the hydrothermally treated gels are denoted as EE-HyT. Some of dried gels were heat-treated at 250°C for 2 h to remove organic components. The heat-treatment condition was selected so as not to decompose the bridging hydrocarbon chain while removing other organic constituents as completely as possible.

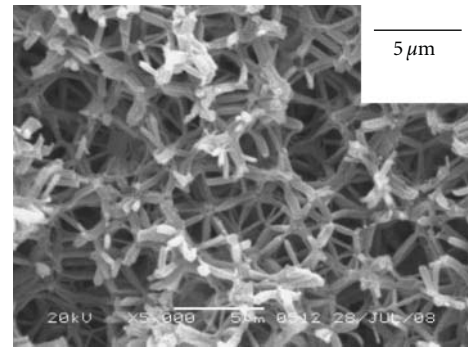

Figure 1: SEM image of the ME-EvD sample.

2.3. Characterization. The morphology of dried gels was observed by a scanning electron microscope (SEM, JSM-6060S, JEOL Ltd., Japan). X-ray diffraction (XRD) analysis with Ni-filtered Cu Kα radiation (RINT Ultima III, Rigaku Co., Japan) for heat-treated gels was performed at room temperature. Nitrogen sorption measurements for heat-treated gels were performed to obtain mesopore size distribution with BELSORP-mini II (BEL JAPAN, Japan). Samples were outgassed under vacuum at 80°C for 24 h prior to measurements. The adsorption branch was used for the calculation of pore size distribution by BJH method. An NMR spectrometer Chemagnetics CMX-400 has been operated for dried gels under a static magnetic field of 9.4 T. The contact time for the cross polarization was fixed at 5.0 ms and the rate of sample spinning was set to 6 kHz. The ^{29}Si chemical shifts were expressed as values relative to tetramethylsilane (Me_4Si) by using the resonance line at −34 ppm for PDMS crystals as an external reference.

3. Results and Discussion

3.1. BTME-HOAc-P123-Urea System

3.1.1. Macromorphology. Figure 1 shows the typical SEM image of the ME-EvD sample. Thin columnar gel skeletons are fully connected at nodes comprising co-continuous and high-porosity structure. The macropore size is a few micrometers and the macroporosity reaches ca. 90%. The columnar skeletons contain cylindrical mesopores which are 2D hexagonally ordered along with the long axes as shown below in detail.

3.1.2. X-Ray Diffraction. Figure 2 shows XRD patterns of the ME-EvD, the ME-SCD, and the ME-HyT samples. The ME-EvD sample shows only single broad peak at higher scattering angle than the other two samples. On the other hand, in addition to the sharp (10) peak, the (11) and

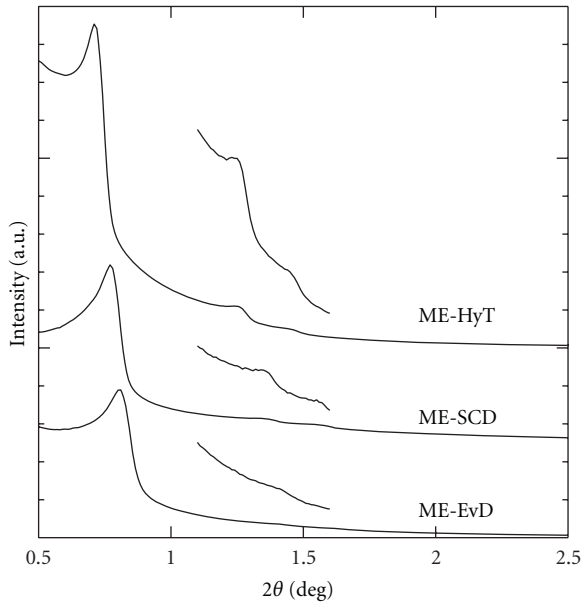

Figure 2: XRD patterns of the ME-EvD, the ME-SCD, and the ME-HyT samples.

(20) peaks are observed for the ME-SCD and the ME-HyT gels. This indicates that the periodicity of 2D hexagonal symmetry in an extended length scale is preserved after the solvent removal. In the process of evaporative drying, the large shrinkage occurs on the ME-EvD sample, and ordered mesostructure of the wet gels is collapsed. The robust ME-HyT sample maintains the mesostructure of the wet gel due to the highly cross-linked structure during the hydrothermal treatment. The ME-SCD sample also shows higher-order peaks with weaker intensity than those of ME-HyT. This result is expected because the capillary force should not work on the gel networks during the supercritical drying process. In addition, the intensity of the ME-HyT sample increases around $2\theta = 0.5^\circ$. This suggests that additional heterogeneity, pores for example, on a longer length scale than that of template pores is present in the ME-HyT sample.

3.1.3. Nitrogen Sorption Measurements. The nitrogen adsorption-desorption isotherms and differential pore size distributions calculated by BJH method of respective gel samples are shown in Figure 3. The isotherms for three samples are classified to type IV with type H1 hysteresis of IUPAC classification, which show the presence of cylindrical mesopores. The mesopore size and the pore volume of ME-EvD sample are smaller than the others due to the larger drying shrinkage. The pore volume of ME-SCD sample is larger than that of ME-EvD sample due to the limited shrinkage. In addition, the mesopore size of ME-HyT is much larger than those of others. This is presumably because some of the adjacent mesopores were merged to form larger mesopores during the hydrothermal treatment. Unlike the pure silica system, a process of dissolution/reprecipitation (Ostwald ripening) hardly occurs in bridged polysilsesquioxane gels under the basic condition. This is

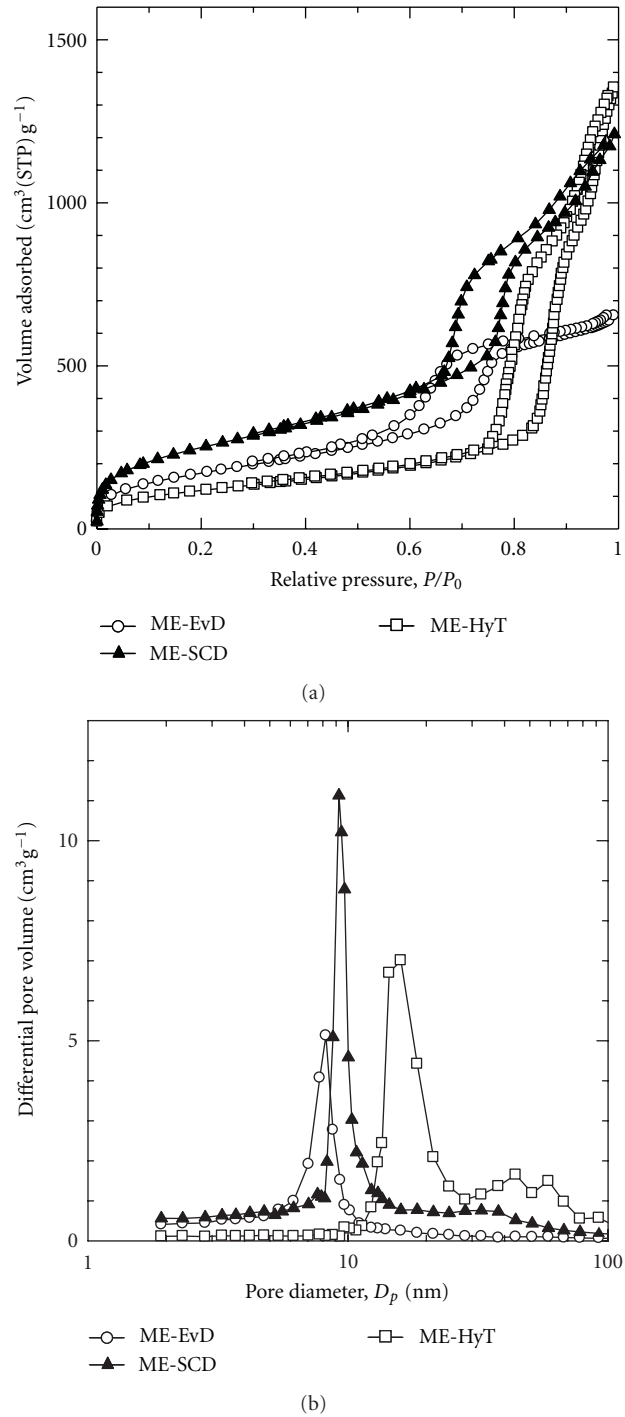

Figure 3: Adsorption-desorption isotherms (a) and differential pore size distributions (b) of the ME-EvD, the ME-SCD, and the ME-HyT samples.

mainly due to the limited solubility of polysilsesquioxane network owing to the Si–ethylene bond that suppresses the cleavage of Si–O bonds by nucleophilic attacks [12]. The drastic reorganization of siloxane network should necessarily be accompanied by significant change in connectivity of Si–O network.

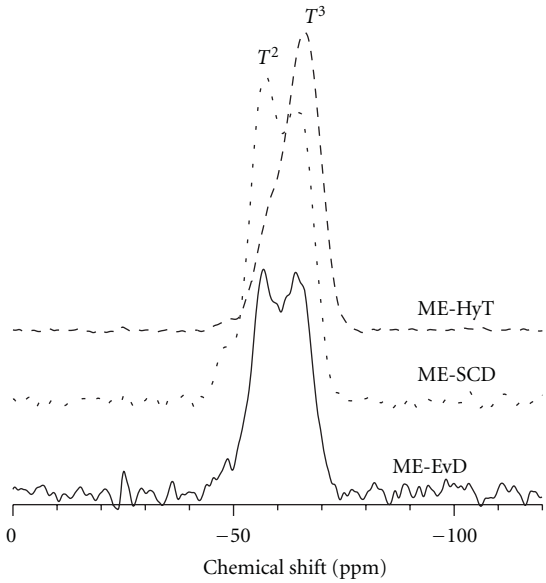

Figure 4: ^{29}Si CP/MAS NMR spectra of the ME-EvD, the ME-SCD, and the ME-HyT samples.

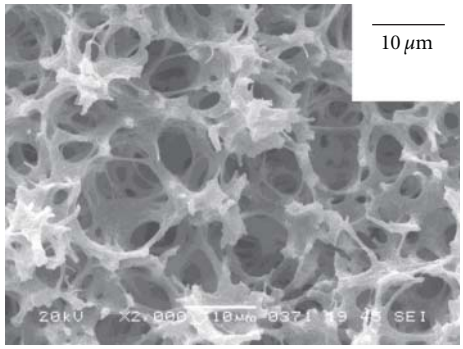

Figure 5: SEM image of the EE-EvD sample.

3.1.4. ^{29}Si CP/MAS NMR Measurements. The ^{29}Si CP/MAS NMR spectraofrespective gel samples are shown in Figure 4. The peaks at −48, −57, and −64 ppm are assigned to T^1, T^2, and T^3 Si, respectively. T^n indicates the Si in the formula of $R'\underline{Si}(OSi)_n(OR)_{3-n}$ where R′ is ethylene bridge and R is methyl group or proton. In the ME-EvD and the ME-SCD samples, the T^2 peak is the largest. On the other hand, the NMR spectrum drastically changes in the ME-HyT sample: T^3 becomes the largest, and T^2 decreases instead. This indicates that the hydrothermal treatment induces reorganization of gel network in such a way that crosslink density is increased. The change confirmed by ^{29}Si CP/MAS NMR is in good agreement with the development of coarser mesopores and increased porosity where rigid frameworks are developed by consuming finer structures.

3.2. BTEE-HNO_3-P123 System

3.2.1. Macro-Morphology. Figure 5 shows the SEM image of the EE-EvD. sample. The structure is coarser co-continuous than the ME-EvD sample. The average macropore size of the EE-EvD sample is 3 μm in contrast to 1 μm of the ME-EvD sample, and columnar skeletons are not observed. This suggests mesopores of the EE-EvD sample are not as highly ordered as those of the ME-EvD sample. The main reason is ethanol generated by the hydrolysis of BTEE that hinders the micelle formation more strongly than the case of methanol generated after hydrolysis of BTME.

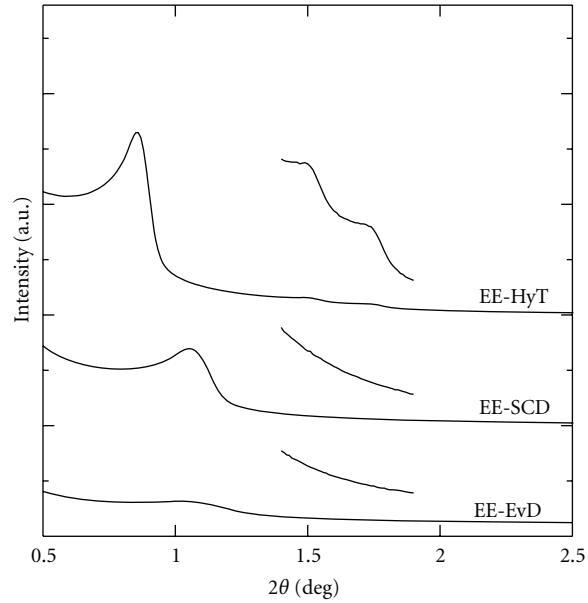

Figure 6: XRD patterns of the EE-EvD, the EE-SCD, and the EE-HyT samples.

3.2.2. X-Ray Diffraction. Figure 6 shows XRD patterns of the EE-EvD, the EE-SCD, and the EE-HyT samples. Not only the EE-EvD sample, but also the EE-SCD sample shows only single broad peak at higher scattering angle compared with the ME-EvD and the ME-SCD samples. The EE-HyT sample, however, shows highly ordered peak of 2D hexagonal symmetry due to the robust macroframework. In the EE-SCD sample, highly ordered mesostructure of the wet gel is collapsed and shrinkage occurs due to the high pressure during supercritical drying. On the other hand, the highly ordered mesostructure of the ME-SCD sample is preserved after supercritical drying. It can be reasonably assumed that the crosslink density of the gels prepared in the BTEE-HNO_3-P123 system is lower and the gels are more fragile than the gels prepared in the BTME-HOAc-P123-Urea system. In the BTME-HOAc-Urea system, the hydrolysis is conducted in a weakly acidic condition, and the following gelation process occurs in neutral or weakly basic condition. Hydrolysis of starting alkoxides are complete and high probability of crosslinking is available in the polycondensation stage. The BTEE-HNO_3 system, on the other hand, is crosslinked in an acidic condition where less branching and crosslinking density is expected.

3.2.3. Nitrogen Sorption Measurements. The nitrogen adsorption-desorption isotherms and differential pore

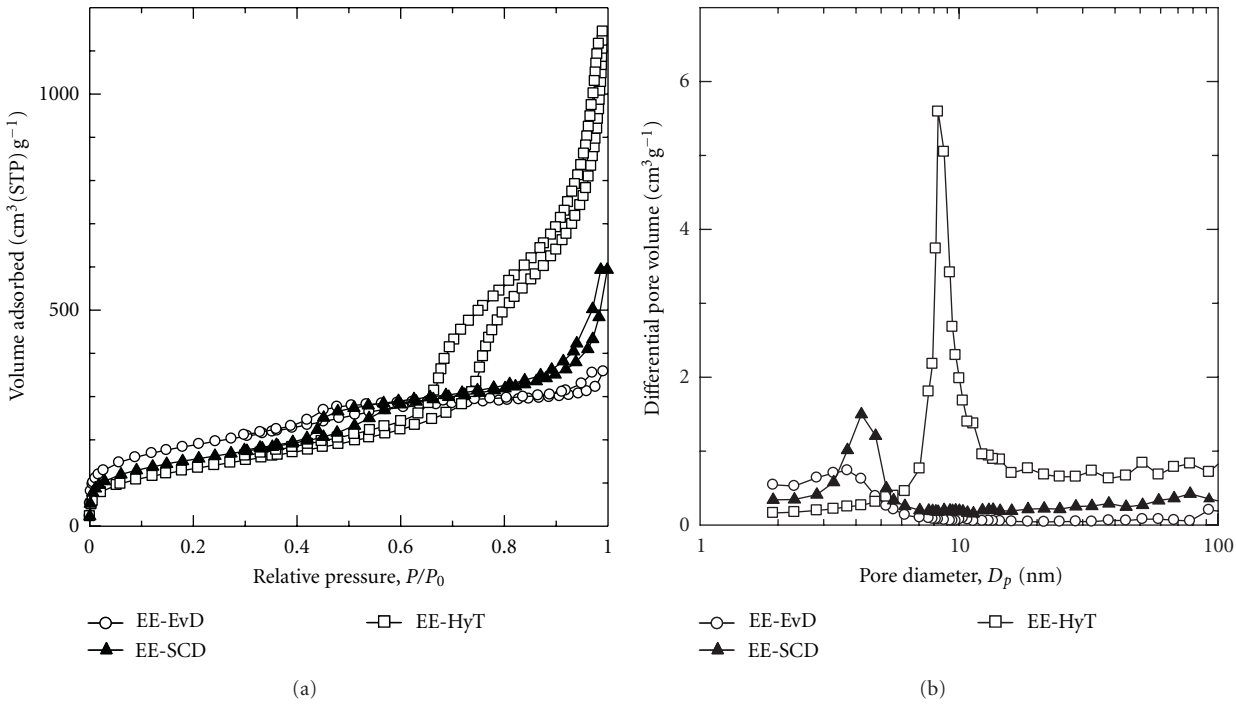

Figure 7: Adsorption-desorption isotherms (a) and differential pore size distributions (b) of the EE-EvD, the EE-SCD and the EE-HyT samples.

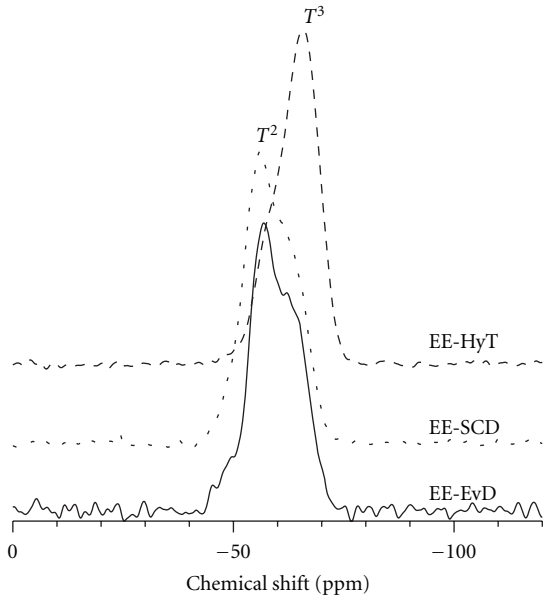

Figure 8: ^{29}Si CP/MAS NMR spectra of the EE-EvD, the EE-SCD and the EE-HyT samples.

size distributions calculated by BJH method of respective samples are shown in Figure 7. Only the isotherm for the EE-HyT sample shows H1 hysteresis and the pore volume is much higher than those of the other two samples. By contrast, the pore volume and the mesopore size of the EE-SCD sample are very small due to the shrinkage during supercritical drying even though those of the ME-SCD sample are large. This coincides with the fact of disordered pore structure evidence by the XRD measurement. The difference also suggests that gel networks prepared in the BTEE-HNO_3-P123 system are more fragile than the gels prepared in the BTME-HOAc-P123-Urea system.

3.2.4. ^{29}Si CP/MAS NMR Measurements. The ^{29}Si CP/MAS NMR spectra of respective samples are shown in Figure 8. T^n indicates the Si in the formula of $R'Si(OSi)_n(OR)_{3-n}$ where R' is ethylene bridge and R is ethyl group or proton. In the EE-EvD and the EE-SCD samples, the T^2 peak is the largest, and small T^1 and T^3 are observed. As with the BTME-HOAc-P123-Urea system, T^3 becomes the largest, and T^2 decrease their intensity in the EE-HyT sample. This again indicates the reorganization of gel network in BTEE-HNO_3-P123 system occurs and crosslinking is enhanced during the hydrothermal treatment. As a result, EE-HyT sample maintains their mesostructure of wet gel after evaporative drying. The peak ratio, T^2/T^3 in the EE-EvD and the EE-SCD, samples is much higher than that in the ME-EvD and the ME-SCD samples reflecting that the overall flexibility of the network is higher in BTEE systems. Consequently, the EE-EvD sample shows broader single peak than the ME-EvD sample in the XRD measurements due to larger shrinkage during the evaporative drying process. The collapse of highly ordered mesostructure of the EE-SCD sample during the supercritical drying process can also be explained by the difference in crosslinking density.

4. Conclusions

Mesopore structure of ethylene-bridged polysilsesquioxane changed depending on the precursor and method of the solvent removal. By the hydrothermal treatment, reorganization of gel network occurred and crosslink density was increased. As a result, the highly ordered mesostructure was maintained after evaporative drying. The crosslink density of the gels prepared in the BTEE-HNO_3-P123 system was lower and the gels were more fragile than the gels prepared in BTME-HOAc-P123-Urea system, and highly ordered mesostructure of the wet gels was collapsed during drying process without hydrothermal treatment. Gelation in higher pH conditions coupled with appropriate hydrothermal conditions are necessary to prepare well-defined hierarchically porous ethylene-bridged polysilsesquioxane monoliths.

Acknowledgment

This work was partly supported by JST, ALCA Project.

References

[1] Yanagisawa, T. Shimizu, T. Kuroda, and K. Kato C, "The preparation of alkyltriinethylaininonium-kaneinite complexes and their conversion to microporous materials," *Bulletin of the Chemical Society of Japan*, vol. 63, no. 4, pp. 988–992, 1990.

[2] C. T. Kresge, M. E. Leonowicz, W. J. Roth, J. C. Vartuli, and J. S. Beck, "Ordered mesoporous molecular sieves synthesized by a liquid-crystal template mechanism," *Nature*, vol. 359, no. 6397, pp. 710–712, 1992.

[3] S. Inagaki, Y. Fukushima, and K. Kuroda, "Synthesis of highly ordered mesoporous materials from a layered polysilicate," *Journal of the Chemical Society, Chemical Communications*, no. 8, pp. 680–682, 1993.

[4] K. Nakanishi, Y. Kobayashi, T. Amatani, K. Hirao, and T. Kodaira, "Spontaneous formation of hierarchical macro-mesoporous ethane-silica monolith," *Chemistry of Materials*, vol. 16, no. 19, pp. 3652–3658, 2004.

[5] K. Nakanishi, T. Amatani, S. Yano, and T. Kodaira, "Multiscale templating of siloxane gels via polymerization-induced phase separation," *Chemistry of Materials*, vol. 20, no. 3, pp. 1108–1115, 2008.

[6] R. Takahashi, K. Nakanishi, and N. Soga, "Insight on structural change in sol-gel-derived silica gel with aging under basic conditions for mesopore control," *Journal of Sol-Gel Science and Technology*, vol. 33, no. 2, pp. 159–167, 2005.

[7] K. Nakanishi and N. Tanaka, "Sol-gel with phase separation. Hierarchically porous materials optimized for high-performance liquid chromatography separations," *Accounts of Chemical Research*, vol. 40, no. 9, pp. 863–873, 2007.

[8] J. Konishi, K. Fujita, K. Nakanishi et al., "Sol-gel synthesis of macro-mesoporous titania monoliths and their applications to chromatographic separation media for organophosphate compounds," *Journal of Chromatography A*, vol. 1216, no. 44, pp. 7375–7383, 2009.

[9] H. W. Oviatt Jr., K. J. Shea, and J. H. Small, "Alkylene-bridged silsesquioxane sol-gel synthesis and xerogel characterization. Molecular requirements for porosity," *Chemistry of Materials*, vol. 5, no. 7, pp. 943–950, 1993.

[10] D. A. Loy, J. P. Carpenter, T. M. Alam et al., "Cyclization phenomena in the sol-gel polymerization of α,ω- bis(triethoxysilyl)alkanes and incorporation of the cyclic structures into network silsesquioxane polymers," *Journal of the American Chemical Society*, vol. 121, no. 23, pp. 5413–5425, 1999.

[11] B. Boury and R. J. P. Corriu, "Adjusting the porosity of a silica-based hybrid material," *Advanced Materials*, vol. 12, no. 13, pp. 989–992, 2000.

[12] K. D. Wyndham, J. E. O'Gara, T. H. Walter et al., "Characterization and evaluation of C_{18} HPLC stationary phases based on ethyl-bridged hybrid organic/inorganic particles," *Analytical Chemistry*, vol. 75, no. 24, pp. 6781–6788, 2003.

Hindawi Publishing Corporation
International Journal of Polymer Science
Volume 2012, Article ID 568301, 5 pages
doi:10.1155/2012/568301

Research Article

Synthesis and Properties of Polysilsesquioxanes Having Ethoxysulfonyl Group as a Side Chain

Takahiro Gunji, Kazuki Yamamoto, Akira Tomobe, Noritaka Abe, and Yoshimoto Abe

Department of Pure and Applied Chemistry, Faculty of Science and Technology, Tokyo University of Science, 2641 Yamazaki, Noda, Chiba 278-8510, Japan

Correspondence should be addressed to Takahiro Gunji, gunji@rs.noda.tus.ac.jp

Received 29 June 2012; Accepted 20 August 2012

Academic Editor: Yoshiro Kaneko

Polysilsesquioxane having an ethoxysulfonyl group as a side chain was synthesized to prepare a proton-conductive film composed of a main chain of siloxane. At first, sodium 4-(2-methylallyloxy)benzenesulfonate was chlorinated with thionyl chloride. Next, hydrosilylation with trichlorosilane was carried out in the presence of platinum catalyst followed by treatment with ethanol. Finally, the hydrolytic polycondensation was carried out to provide poly(3-(4-ethoxysulfonylphenoxy)-2-methylpropyl)silsesquioxane. This polysilsesquioxane was heated to form a free-standing film that was brittle and brown in color.

1. Introduction

Fuel cells, which generate power using hydrogen and oxygen gases, have been a focus of recent interest due to their potential for resolving both energy and environmental problems, as they produce very little pollution and have a high power generation efficiency. In particular, polymer electrolyte fuel cells (PEFCs), which are fuel cells that utilize a proton conductive membrane as an electrolyte, are expected to have a high potential, as PEFCs can generate power at low temperature with high energy density. PEFCs are therefore suitable for miniaturization to make them suitable for home use, for portable devices, or for car batteries. The proton-conducting membrane most commonly used is a fluorine-containing polyelectrolyte film that works under moderate moisture to improve proton conductivity. PEFCs are, however, difficult to operate at high temperatures, which can lower the power-generation efficiency due to the low heat resistance of the electrolyte film.

In the previous works, a proton-conducting membrane utilizing a siloxane bond as a main chain with high heat resistance was utilized: polysilsesquioxanes having an acid group in the side chain were prepared by a sol-gel method [1–5] and then mixed with polyketone [6, 7], fluorine-containing polymer [8], or phosphor-containing polymer [9]. The film prepared showed high proton conductivity of approximately 10^{-2} S/cm [1–3, 5, 7, 9], which is higher than the perfluoro-type polymer electrolyte [10]. The degradation or phase separation of organic and inorganic components is a demerit in the use of these membranes over the long term.

In our previous report, film formation was carried out by hydrolytic polycondensation and subsequent oxidation of a silane-coupling agent, which resulted in the degradation of polysiloxanes by a sulfonic acid group to give a broken film [11]. In contrast, copolymerization of a silane coupling agent having a mercapto group with 1,2-trimethoxysilylethane provided a proton-conducting film with a heat resistivity to 150°C.

Polysilsesquioxane is useful as a framework in organic-inorganic polymer hybrid material because of its high heat-resistivity, high mechanical properties, and easy introduction of functional groups in the side chain. The application of polysilsesquioxanes as a PEFC membrane is limited by the degradation of the siloxane chain and gel formation by the acid groups. In order to improve this problem, a polysilsesquioxane having an arylsulfonic acid as a side chain was examined. The side chain is expected to form a stacking structure by the steric hindrance and interaction of pi electrons of an aryl group to depress the degradation of siloxane bonding by sulfonic acid. In this work, therefore, the

synthesis of polysilsesquioxane having a sulfonic acid group from an arylsulfonic ester derivative as well as formation of the membrane was investigated according to the Scheme 1.

2. Experimental

2.1. Reagents. Thionyl chloride, toluene, pyridine, acetone, sodium hydroxide, and 6 mol/L hydrochloric acid (Wako Pure Chemical Industries Ltd., reagent grade) were used as received.

Trichlorosilane (Shin-Etsu Chemical Industry, Co., Ltd.) was used as received.

Ethanol and hexane (Kanto Chemical, Co., Ltd.) were dried over calcium oxide and distilled before use.

Sodium 4-hydroxybenzenesulfonate dihydrate, 3-chloro-2-methyl-1-propene, and chloroplatinic (IV) acid (Tokyo Chemical Industry Co., Ltd.) were used as received.

2.2. Synthesis of Sodium 4-(2-Methyl-2-propenoxy)benzenesulfonate. Sodium 4-(2-methyl-2-propenoxy)benzenesulfonate was synthesized according to the procedure shown in the literature [12]. Sodium 4-hydroxybenzenesulfonate dihydrate 174 g (0.75 mol) was mixed with water 375 mL, acetone 375 mL, and sodium hydroxide 30.8 g (0.77 mol) and heated to reflux for 10 min. 3-Chloro-2-methyl-1-propene was added slowly and subjected to reflux for 24 h, followed by recrystallization.

Yield: 104 g (80%). White crystal. ^{1}H NMR [δ/ppm] (300 MHz, $CDCl_3$) 1.84 (s, 3H), 4.55 (s, 2H), 5.07 (d, 1H), 5.09 (d, 1H), 7.06 (d, 2H, J = 9.0 Hz), 7.99 (d, 2H, J = 9.0 Hz). MS (ESI) m/z = 246[M^+], 211[M-Cl]$^+$.

2.3. Synthesis of 4-(2-Methyl-2-propenoxy)benzenesulfonyl Chloride. 4-(2-methyl-2-propenoxy)benzenesulfonyl chloride was synthesized according to a previously reported procedure [12]. First, 25 g (0.1 mol) of sodium 4-(2-methyl-2-propenoxy)benzenesulfonate was mixed with thionyl chloride 11 mL (0.15 mol), dimethylformamide 0.1 mL, and toluene 100 mL and heated to 100°C for 12 h. The reaction mixture was washed with water three times, followed by drying and condensation.

Yield: 23 g (80%). Colorless liquid. ^{1}H NMR [δ/ppm] (300 MHz, $CDCl_3$) 1.84 (s, 3H), 4.55 (s, 2H), 5.07 (d, 1H), 5.09 (d, 1H), 7.06 (d, 2H, J = 9.0 Hz), 7.99 (d, 2H, J = 9.0 Hz). MS (ESI) m/z = 246[M^+], 211[M-Cl]$^+$.

2.4. Synthesis of 4-(2-Methyl-3-trichlorosilylpropoxy)benzenesulfonyl Chloride. 3.0 g (13 mmol) of 7 was mixed with trichlorosilane 12 mL (0.15 mol) and 5% 2-propanol solution of chloroplatinic acid dihydrate 0.1 mL and heated at 50°C for 12 h to complete the hydrosilylation. Product was recovered by condensation under reduced pressure.

Yield: 3.2 g (69%). Yellow liquid. ^{1}H NMR [δ/ppm] (300 MHz, $CDCl_3$) 1.26 (d, 3H), 1.50 (dd, 1H), 1.77 (dd, 1H), 2.49 (m, 1H), 3.80 (d, 2H), 7.50 (d, 2H), 7.80 (d, 2H). ^{13}C NMR [δ/ppm] (75 MHz, $CDCl_3$) 19.1, 28.9, 29.2, 73.9, 115.2, 129.5, 136.2, 163.9. ^{29}Si NMR [δ/ppm] (100 MHz, $CDCl_3$) −14.24.

2.5. Synthesis of Ethyl 4-(2-Methyl-3-triethoxysilylpropoxy)benzenesulfonate (STES). 3.2 g (6 mmol) of 4-(2-methyl-3-trichlorosilylpropoxy)benzenesulfonyl chloride, ethanol 1.6 g (0.35 mmol), and pyridine 2.0 g (0.25 mol) were added to hexane 50 mL and heated at 50°C for 6 h. Hydrogen chloride pyridine salt was filtered, and the filtrate was subjected to condensation. Ethyl 4-(2-methyl-3-triethoxysilylpropoxy)benzenesulfonate (STES) was isolated by short silica gel column chromatography using chloroform as an eluent.

Yield: 2.5 g (61%). Slightly yellow liquid. ^{1}H NMR [δ/ppm] (300 MHz, $CDCl_3$) 0.75 (m, 2H), 1.12 (d, 3H, J = 6.9 Hz), 1.22 (t, 9H, J = 6.9 Hz), 1.29 (t, 3H, J = 7.2 Hz), 2.22 (m, 1H), 3.86 (q, 6H), 3.92 (d, 2H), 4.08 (q, 2H), 7.00 (d, 2H, J = 9.0 Hz), 7.82 (d, 2H, J = 9.0 Hz). ^{13}C NMR [δ/ppm] (75 MHz, $CDCl_3$). ^{29}Si NMR [δ/ppm] (100 MHz, $CDCl_3$) −46.37. MS (ESI) m/z = 420[M^+], 375[(M-C_2H_5O)$^+$.

2.6. Synthesis of Poly(3-(4-ethoxysulfonylphenoxy)-2-methylpropyl)silsesquioxane (SPES). Into a 100 mL four-necked flask, STES 2.10 g (5 mmol) and ethanol 0.46 g were charged. After cooling for 10 min using an ice bath, water and 6 mol/L hydrochloric acid were added in the molar ratio of HCl/SPES = 0.1 and stirred for 10 min. After removing the ice bath, the solution was stirred for 10 min at room temperature. The flask was then heated at 80°C for 4 h with stirring to provide poly(3-(4-ethoxysulfonylphenoxy)-2-methylpropyl)silsesquioxane (SPES) as a highly viscous liquid.

2.7. Formation of Films. A 33% THF solution of SPES was poured into a scale made from polytetrafluoroethylene and heated at 80°C for 3 days.

2.8. Measurement. ^{1}H, ^{13}C, and ^{29}Si nuclear magnetic resonance (NMR) spectra were recorded by JEOL NM ECP-300 or JNM ECP-500. Chloroform-*d* was used as a solvent, and tetramethylsilane was used as an internal standard of chemical shift.

Fourier transformation infrared (FT-IR) spectra were acquired by JASCO FT/IR410. The KBr disk method and CCl_4 solution method were utilized for solid and liquid samples, respectively.

Gas chromatography (GC) was performed by Shimadzu GC-14B. Injection temperature: 250°C. Column temperature: 50–250°C (+20°C/min). TCD temperature: 250°C. Carrier gas: helium.

Gas chromatograph/mass spectroscopy (GC/MS) was performed by JEOL GCMate.

High-performance liquid chromatography (HPLC) was performed with a Shimadzu LC-6AD attached to a YMC guard column ODS-A (50 × 20 mm) and two YMC ODS-A5 μm. Acetonitrile (7 mL/min) was used as an eluent. Detector: RID-10A.

Gel-permeation chromatography (GPC) was performed with a Shimadzu LC-6AD attached to a Polymer Laboratory PL gel 5 μ Mixed-D column. Tetrahydrofuran was used as an eluent. Detector: RID-10A.

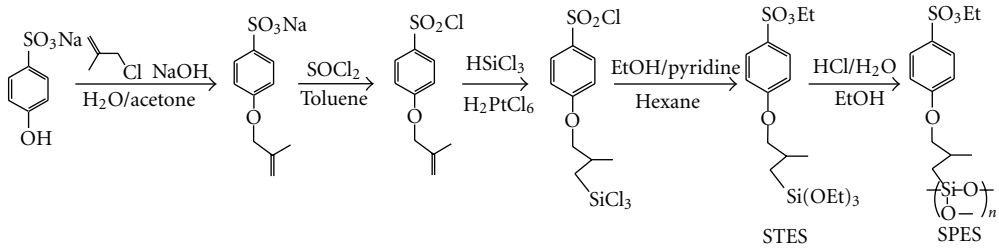

Scheme 1: Schematic figure for the synthesis of SPES.

Table 1: Results for the synthesis of SPES[a].

Number	r (molar ratio of H_2O/Si)	Yield (g)	GPC[b]		Percentage[c] of sulfonic acid/%
			M_w	M_w/M_n	
1	1.0	1.77	2.000	1.2	—
2	2.0	1.64	3.200	1.1	—
3	3.0	1.51	4.500	1.1	7
4	5.0	1.50	5.200	1.2	18
5	6.0	1.54	5.800	1.5	32
6	8.0	1.54	4.800	1.5	55
7	10.0	1.50	4.400	1.3	61
8	12.0	1.50	4.600	1.1	79

[a] Scale in operation: STES 2.10 g (5 mmol). EtOH 0.46 g (10 mmol). Molar ratio: HCl/Si = 0.10.
[b] Calculated based on standard polystyrene.
[c] Calculated based on the integral ratio of signals in ^{1}H NMR spectrum.

3. Results and Discussion

3.1. Synthesis of SPES. The synthesis of polysilsesquioxane having an arylsulfonate group as a side chain was planned by the hydrolytic polycondensation of trialkoxysilane. First, we planned the synthesis of ethyl 4-(2-triethoxysilylethyl)benzenesulfonate by the hydrosilylation of ethyl 4-vinylbenzenesulfonate and triethoxysilane, which resulted in the formation of a mixture of ethyl 4-(2-triethoxysilylethyl)benzenesulfonate and ethyl 4-(1-triethoxysilylethyl)benzenesulfonate. We therefore designed the structure of ethyl 4-(2-methyl-3-triethoxysilylpropoxy)benzenesulfonate as a target compound.

The synthesis of ethyl 4-(2-methyl-3-triethoxysilylpropoxy)benzenesulfonate was established by a four-step reaction from sodium 4-hydroxybenzenesulfonate dihydrate.

4-(2-Methyl-3-trichlorosilylpropoxy)benzenesulfonyl chloride was synthesized by the hydrosilylation of 4-(2-methyl-2-propenoxy)benzenesulfonyl chloride with trichlorosilane in the presence of chloroplatinic acid. This reaction proceeded gently to provide a unique product, 4-(2-methyl-3-trichlorosilylpropoxy)benzenesulfonyl chloride. This product was isolated by distillation under reduced pressure as a colorless liquid of high hydrolyzability. The formation of this compound was confirmed by the disappearance of signals corresponding to a vinylidene group in the ^{1}H and ^{13}C NMR spectra.

STES was synthesized by the reaction of 4-(2-methyl-3-trichlorosilylpropoxy)benzenesulfonyl chloride with ethanol. This reaction is one of the general procedures for replacing a chloro group with an ethoxy group: both chloro groups on silicon and sulfur were replaced with an ethoxy group in a one-step reaction. The formation of STES was confirmed by NMR and MASS analyses.

SPES was synthesized by the hydrolysis of STES in the presence of hydrochloric acid under a nitrogen stream. The results for the synthesis of SPES are summarized in Table 1 including the molecular weight and the percentage of sulfonic acid which were calculated based on the GPC analysis and the integral ratio of signals in the ^{1}H NMR spectrum of SPES, respectively. The progress of hydrolytic polycondensation of STES was confirmed by the increasing viscosity of the hydrolysis product. The yield of SPES decreased with an increase in the molar ratio of water to STES, which suggests the formation of SPES with high molecular weight. In addition, the molecular weight and the percentage of sulfonic acid of SPES increased with the increase of the molar ratio of water to STES. When the molar ratio of water to STES was set to be more than 6, the molecular weight of SPES decreased in accordance with the degradation of the siloxane linkage by the sulfonic acid. SPES (number 2) was soluble in acetone, tetrahydrofuran, diethyl ether, and chloroform, and the solubility was independent of the molecular weight of SPES.

The ^{1}H NMR spectrum of SPES (number 2) is shown in Figure 1. The intensity of signals due to the ethoxy group in the ethoxysulfonyl group was decreased compared to that of the 2-methylpropyl group, which suggests the

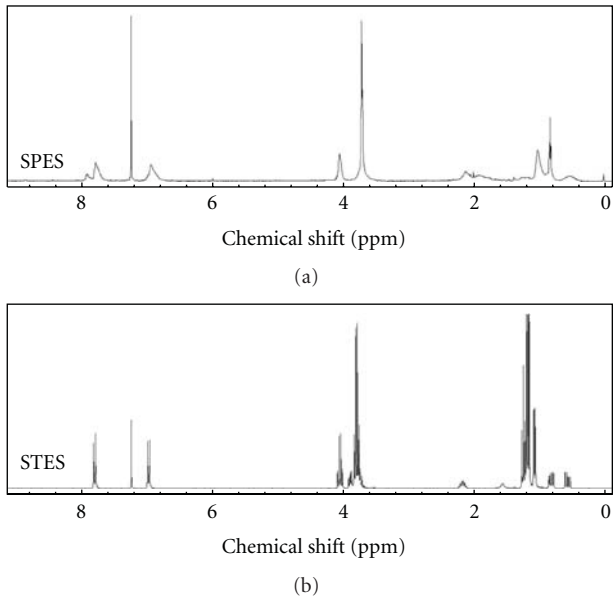

Figure 1: ^{1}H NMR spectra of STES and SPES (number 2).

hydrolysis of the ethoxysulfonyl group to form sulfonic acid. Additionally, the appearance of new signals due to a phenylene group at the lower field suggests the formation of sulfuric acid. The ^{29}Si NMR spectra of SPES (number 2) and SPTS are shown in Figure 2. The signal due to STES disappeared in the spectrum of SPES, and new signals appeared in the chemical shift areas ascribed to T^1, T^2, and T^3 unit structures. (The symbol T^n denotes the unit structure as $RSi(OSi)_n(OEt)_{3-n}$ (n = 1, 2, 3; R: 3-(4-ethoxysulfonylphenoxy)-2-methylpropyl group).) The appearance of signals due to T^1, T^2, and T^3 unit structures supports the formation of polysilsesquioxane. The degree of condensation was calculated based on the equation $AT^3/(AT^1 + AT^2 + AT^3)$, with AT^n denoting the peak area of the unit structure T^n, as 46%. Approximately half of the silicon atoms in SPES condensed to form the silsesquioxane structure.

3.2. Film Formation of SPES. SPES film was prepared by aging SPES (number 2) at 80°C for several days. A photograph of the SPES film is shown in Figure 3. SPES was a colorless liquid, and its film became brown with heating, which may have been due to the formation of a sulfonic acid group from the ethoxysulfonyl group. The thickness was approximately 0.1 mm, and the film was brittle, easily broken into pieces when bended. The relatively low molecular weight and degree of crosslinking of SPES would cause this decrease in the film strength.

The film was colored by using an acid-functional dye: methyl red. The film was uniformly colored in red, which supports the formation of a sulfonic acid group by heating.

The thermogravimetric differential thermal analysis of thin film is shown in Figure 4. Exothermic peaks were found at 200–240°C and 600–640°C with weight loss and were

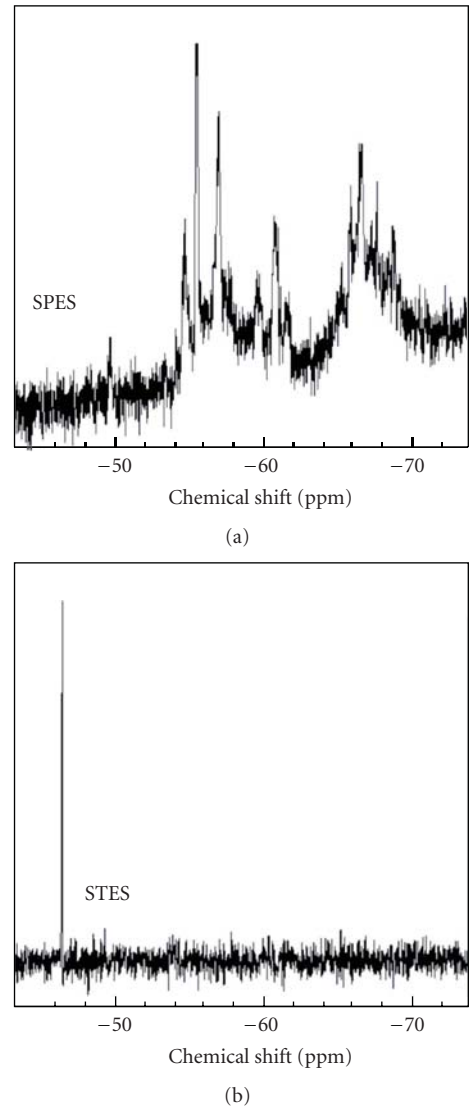

Figure 2: ^{29}Si NMR spectra of STES and SPES (number 2).

ascribed to the degradation of an ethoxysulfonyl group and organic component, respectively. The SPES film showed thermoresistivity up to 200°C.

The film showed proton conductivity of 2×10^{-2} S/cm at room temperature.

4. Conclusion

Poly(3-(4-ethoxysulfonylphenoxy)-2-methylpropyl)silsesquioxane (SPES) was synthesized from sodium 4-(2-methyl-2-propenoxy)benzenesulfonate by a five-step reaction. The molecular weight of SPES was 2000–5200, reaching a maximum when the molar ratio of water was 6.0. The ethoxysulfonyl group was hydrolyzed when the molar ratio of water was greater than 3.0. The ratio of the T^3 unit was 46% when the molecular weight of SPES was 3200. SPES film was prepared by heating SPES at 80°C for 3 days. The film

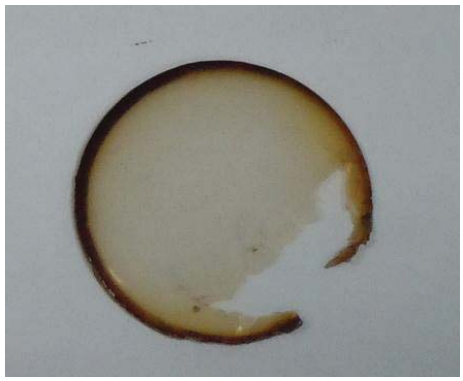

Figure 3: A photograph of the SPES film.

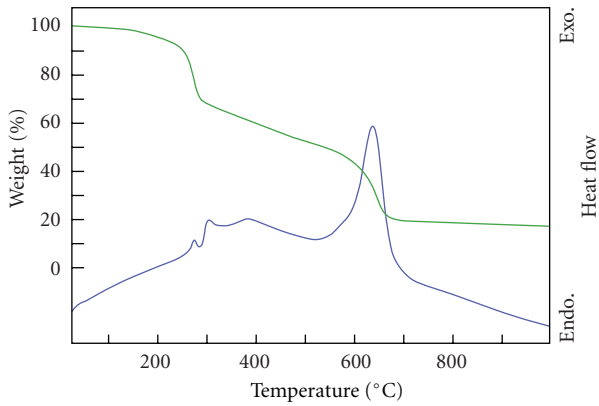

Figure 4: Thermogravimetric differential thermal analysis of SPES film.

was brown and brittle and showed thermal resistivity up to 200°C.

Acknowledgment

This work was supported by a Grant-in-Aid for Scientific Research on Innovative Areas "New Polymeric Materials Based on Element-Blocks (no. 2401)" (24102008A02) of The Ministry of Education, Culture, Sports, Science and Technology, Japan.

References

[1] G. J. D. Kalaw, Z. Yang, I. H. Musselman, D. J. Yang, K. J. Balkus, and J. P. Ferraris, "Novel polysilsesquioxane hybrid membranes for proton exchange membrane fuel cell (PEMFC) applications," *Separation Science and Technology*, vol. 43, no. 16, pp. 3981–4008, 2008.

[2] T. Tezuka, K. Tadanaga, A. Hayashi, and M. Tatsumisago, "Proton-conductive inorganic-organic hybrid membrane prepared from 3-(2-aminoethylaminopropyl)triethoxysilane and sulfuric acid by the sol-gel method," *Journal of the Electrochemical Society*, vol. 156, no. 1, pp. B174–B177, 2009.

[3] M. Khiterer, D. A. Loy, C. J. Cornelius et al., "Hybrid poly electrolyte materials for fuel cell applications: design, synthesis, and evaluation of proton-conducting bridged polysilsesquioxanes," *Chemistry of Materials*, vol. 18, no. 16, pp. 3665–3673, 2006.

[4] K. Miyatake, T. Tombe, Y. Chikashige, H. Uchida, and M. Watanabe, "Enhanced proton conduction in polymer electrolyte membranes with acid-functionalized polysilsesquioxane," *Angewandte Chemie*, vol. 46, no. 35, pp. 6646–6649, 2007.

[5] C. S. Karthikeyan, S. P. Nunes, and K. Schulte, "Permeability and conductivity studies on Ionomer-polysilsesquioxane hybrid materials," *Macromolecular Chemistry and Physics*, vol. 207, no. 3, pp. 336–341, 2006.

[6] X. Li, Y. Song, M. Zhu, B. Liu, and Z. Jiang, "Preparation and properties of the POSS-containing composites as proton exchange membranes," *Gaodeng Xuexiao Huaxue Xuebao*, vol. 32, no. 8, pp. 1670–1672, 2011.

[7] S. H. Pezzin, N. Stock, S. Shishatskiy, and S. P. Nunes, "Modification of proton conductive polymer membranes with phosphonated polysilsesquioxanes," *Journal of Membrane Science*, vol. 325, no. 2, pp. 559–569, 2008.

[8] C. Chanthad, K. Xu, H. Huang, and Q. Wang, "Proton-conductive polymer nanocomposite membranes prepared from telechelic fluorinated polymers containing perfluorosulfonic acid side chains," *Journal of Polymer Science, Part A*, vol. 48, no. 21, pp. 4800–4810, 2010.

[9] B. J. Liu, X. F. Li, M. M. Guo, C. Liu, L. Li, and Z. H. Jiang, "Synthesis and hybrid of a(4-phosphonic acid)phenylated poly(arylene ether sulfone)," *Gaodeng Xuexiao Huaxue Xuebao*, vol. 31, no. 6, pp. 1081–1083, 2010.

[10] T. Gunji, Y. Suetaka, Y. Abe, S. Inagaki, and S. Fujita, "Synthesis of organic-inorganic hybrids from benzene-bridged polysiloxane," *Kobunshi Ronbunshu*, vol. 65, no. 6, pp. 416–420, 2008.

[11] T. Gunji, Y. Shigematsu, T. Kajiwara, and Y. Abe, "Preparation of free-standing films with sulfonyl group from 3-mercaptopropyl(trimethoxy)silane/1,2-bis(triethoxysilyl)ethane copolymer," *Polymer Journal*, vol. 42, no. 8, pp. 684–688, 2010.

[12] A. B. Claryton, US Patent, 4897144.

Hindawi Publishing Corporation
International Journal of Polymer Science
Volume 2012, Article ID 586594, 9 pages
doi:10.1155/2012/586594

Research Article

A Synthetic Route to Quaternary Pyridinium Salt-Functionalized Silsesquioxanes

Nataliya Kostenko,[1] Jochen Gottfriedsen,[2] Liane Hilfert,[2] and Frank T. Edelmann[2]

[1] *Department of Chemistry, University of Tromsø, Hansine Hansens veg, 9037 Tromsø, Norway*
[2] *Chemisches Institut, Otto-von-Guericke-Universität, Universitätsplatz 2, 39106 Magdeburg, Germany*

Correspondence should be addressed to Frank T. Edelmann, frank.edelmann@ovgu.de

Received 5 June 2012; Accepted 12 August 2012

Academic Editor: Yoshiro Kaneko

A synthetic route to potentially biocidal silsesquioxanes functionalized by quaternary pyridinium functionalities has been developed. *N*-Alkylation reactions of the precursor compounds 4-(2-(trimethoxysilyl)ethyl)-pyridine (**5**) and 4-(2-trichlorosilylethyl)pyridine (**6**) with iodomethane, *n*-hexylbromide, and *n*-hexadecylbromide cleanly afforded the corresponding *N*-alkylpyridinium salts (**7**–**10**). The synthesis of a 4-(2-ethyl)pyridine POSS derivative (**2**) was achieved by capping of the silsesquioxane trisilanol $Cy_7Si_7O_9(OH)_3$ (**1**) via two different preparative routes. Attempts to use compound **2** as precursor for quaternary pyridinium salt-functionalized POSS derivatives were met with only partial success. Only the reaction with iodomethane cleanly afforded the new *N*-methylpyridinium salt **12** in high yield, whereas *n*-hexylbromide and *n*-hexadecylbromide failed to react with **2** even under forcing conditions.

1. Introduction

Over the past fifty years a broad variety of new classes of polymers have been prepared and studied which should provide advances in developing a new family of compounds for antibacterial surface treatments [1]. Such polymeric materials or films which kill or inactivate microorganisms upon their direct contact are known as *biocidal (antimicrobial) polymers* or also *polymeric biocides*. During the 1990s the interest in biocidal polymers arose rapidly due to their potential ability to keep surfaces and materials *permanently* antiseptic. This continues to be of current importance for a wide range of applications. Biocidal polymers are used, for example, in cartridge filters for the disinfection of potable and recreational water supplies, in filter units for air disinfection, as sterile bandages, clothing, surgical gloves for medical uses, as biocidal polymeric coatings on surfaces of ship hulls, shower walls and many other kinds of tubing. The ideal biocidal polymer should possess at least the following characteristics: (1) it should be easily and inexpensively synthesized; (2) it should be stable in long-term usage and storage at the temperature of its intended application; (3) it should be not soluble in water in the case of water disinfection applications; (4) it should not decompose to and emit toxic products; (5) it should not be toxic or irritating to those handling it; (6) it should be regenerable upon loss of activity; and (7) it should be biocidal to a broad spectrum of pathogenic microorganisms in brief times of contact [1–4].

By now various biocidal polymers have been produced and tested in different fields, but the achievement of a polymer which combines all of these characteristics continues to be elusive. In accordance with literature reviews there are several classes of biocides which possess great potential for the development of the ideal biocidal polymers for their sufficiently high activity against the two major classes of bacteria and fungi, Gram-positive and Gram-negative. They will not be removed from surfaces on washing, they remain capable of continually acting against the bacteria, they are not toxic or irritating, and one of the very attractive advantages is that they cause no antibiotic resistance [1–4]. Their approximate composition is represented in Scheme 1.

Such biocidal polymers always comprise three essential structural parts: the *carrying surface*, usually the

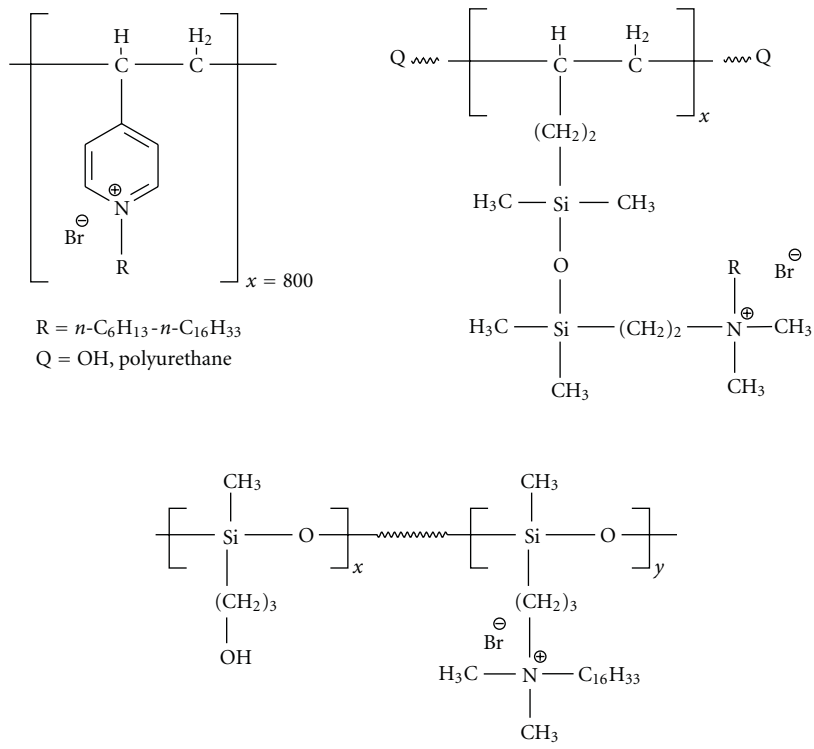

Scheme 1

carbohydrate-base (cotton cloth, wood, paper, or bulk cellulose, etc.), and also glasses and silica, and the *polymer films* (in Scheme 1 polyethylene, polyurethane, and polysiloxane) which contain anchored *polyquat moieties* (the quaternary nitrogen) and which directly contact to a cell membrane and cause its disruption. It has been experimentally proven that low antiseptic activity already reveals for the moieties with *N*-alkyl chains from three to eight carbon units in length and is very high for the moieties containing a 16-carbon lipophilic chain [1–4].

Polyhedral oligomeric silsesquioxanes (POSS) form an exciting class of hybrid organic-inorganic filler materials receiving considerable attention in recent years [5–17]. They represent several elements of novelty, for example, molecular diameters between 1 and 3 nm, low density, high thermal stability, and an array of side-chain functionalities [18] which accounts for compatibility with various host polymers. Thus is seemed of interest to synthesize and characterize a new class of biocidal materials based on polyhedral oligomeric silsesquioxanes by attaching distant quaternary ammonium functional groups to the POSS cage. In this contribution, we report the first synthetic approach eventually leading to POSS derivatives comprising a pendant quaternized 4-(2-ethyl)pyridyl group.

The key precursor **1** and the target molecules **2** and **3** are illustrated in Scheme 2. Trisilanol **1** was chosen as the best model for silica that has been developed to date for its close-range geometric similarity to known SiO_2 structures. It is a very useful model for both spectroscopic comparisons and chemical reactivity studies for it structurally resembles specific surface structures that occur on silica [19–23]. Alkylated quaternary 4-(2-ethyl)pyridyl groups containing 6- and 16-carbon chains are of considerable interest for their significant activity against a wide range of bacteria (**3a, b**, Scheme 2). The intended synthetic route involved capping of **1** with either 4-(2-(trimethoxysilyl)ethyl)-pyridine and 4-(2-trichlorosilylethyl)pyridine to give the 4-(pyridine)ethyl derivative **2** which could then be alkylated by treatment with appropriate alkyl halides to give the target compounds **3a** and **3b**.

2. Results and Discussion

2.1. Preparation of the Starting Materials 4-(2-Trichlorosilylethyl)pyridine (5) and 4-(2-(Trimethoxysilyl)ethyl)-pyridine (6). The envisaged synthetic route for functionalizing the trisilanol precursor **1** first required the availability of the starting materials 4-(2-trichlorosilylethyl)pyridine (**5**) and 4-(2-(trimethoxysilyl)ethyl)pyridine (**6**). Both of them had been reported in the literature [24, 25]. The reported synthesis of **5** involves hydrosilylation of 4-vinylpyridine (**4**) with trichlorosilane according to Scheme 3. Through a slight modification of the original preparation reported in [25] the yield of **5** could be increased from 52% to 81%, making this compound readily available in large quantities.

The original preparation of 4-(2-(trimethoxysilyl)ethyl) pyridine (**6**) calls for treatment of the trichlorosilyl precursor **5** with trimethyl orthoformate in the presence of catalytic amounts of aluminum trichloride according to Scheme 4 [25].

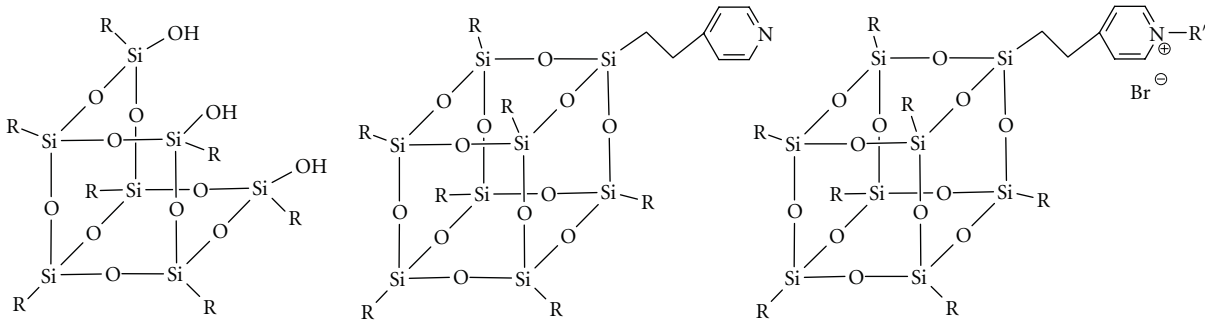

Scheme 2

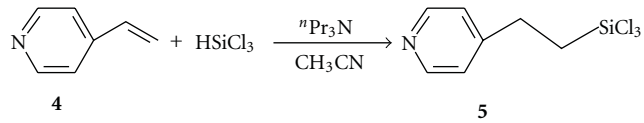

Scheme 3

Although the reaction outlined in Scheme 4 had been described only on a 1 g-scale, we found that by employing longer heating times up to *ca.* 10 g of **6** could be prepared without difficulties. As an alternative route to **6**, the direct hydrosilylation of vinylpyridine (**4**) with trimethoxysilane, $HSi(OMe)_3$, has also been investigated (Scheme 5). Such reactions of unsaturated substrates with trialkoxysilanes have been shown to work well in the presence of suitable hydrosilylation catalysts such as $H_2PtCl_6 \times H_2O$ (Speier's catalyst) or Karstedt's catalyst (= $Pt(LL)_2$, LL = $(CH_2{=}CHSiMe_2)_2O$) [26–31]. Reactions were carried out under various conditions (e.g., without solvent or in acetonitrile solution, without catalyst or in the presence of Speier's catalyst or Karstedt's catalyst), but surprisingly all these reactions failed to produce appreciable amounts of **6**. Thus the original preparation (Scheme 4) remains the best access to the trimethoxysilyl derivative **6**.

*2.2. Quaternization of 4-(2-Trichlorosilylethyl)pyridine (**5**) and 4-(2-(Trimethoxysilyl)ethyl)-pyridine (**6**) with Different Alkyl Halides.* Next, quaternization reactions of the precursors **5** and **6** with different alkyl halides were studied. In quaternization reactions of tertiary amines with alkyl halides the reactivity of the latter generally decreases in the series RI > RBr > RCl, for example, MeBr > EtBr > *n*-$C_6H_{13}Br$ > C_{16} $H_{33}Br$. Although for application reasons we were particularly interested in the reactivity of alkyl halides with longer chains, for example, with six or sixteen carbon atoms, reactions with methyl iodide as the simplest and most reactive alkyl halide were also included. Usually *N*-alkylation reactions of tertiary amines are performed in polar solvents (acetonitrile, methanol, ethanol, etc.). The highest reaction rates are normally observed in bipolar aprotic solvents (DMF, DMSO), but when using these solvents difficulties in product isolation and purification can became apparent. Quaternization reactions of **5** and **6** were carried out in anhydrous organic solvents (e.g., methanol, acetonitrile, THF) as illustrated in Scheme 6. Owing to the very high solubility of 4-(2-trichlorosilylethyl)pyridine (**5**) and iodomethane in all organic solvents, the *N*-alkylation with iodomethane was possible to perform in pentane, diethyl ether, THF, DMSO, acetonitrile, ethanol, and methanol. The highest reaction rates were observed in the more polar solvents and the slowest in nonpolar solvents. The pure product, the *N*-methylpyridinium salt **7**, was isolated as a white solid after recrystallization from diethyl ether in nearly quantitative yield (98%).

As expected, the analogous quaternization reactions with *n*-hexyl and *n*-hexadecyl bromide (Scheme 7) were much slower than the CH_3I reactions. *N*-alkylation of **6** with *n*-hexylbromide could readily be performed in those polar solvents (acetonitrile, methanol) in which the highest reaction rates were observed for iodomethane, but the *N*-alkylation with *n*-hexadecylbromide could only be carried out in diethyl ether or THF because of its poor miscibility with the more polar solvents. Accordingly, in both cases the reaction rates and isolated yields were so low that even after 5–7 days of refluxing the reactions were less than 30% completed.

Much better yields (69–78%) were obtained in a second series of *N*-alkylation experiments which were performed under solvent-free conditions by just stirring a mixture of the reagents at temperatures of 100–130°C for 48–72 h. Under these conditions the pure *N*-*n*-hexylpyridinium salt **9** was isolated from diethyl ether as a pale greenish oil and the *N*-*n*-hexadecylpyridinium salt **10** as a very pale greenish solid. The structures of all prepared pyridinium salts **7**–**10** were confirmed by ^1H and ^{13}C NMR data. In particular, *N*-alkylpyridinium salt formation was proven by the long range

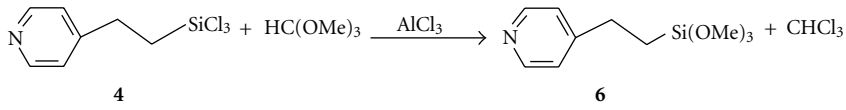

Scheme 4

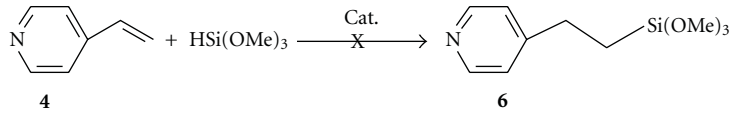

Scheme 5

coupling between the protons in the positions 1,1′ and 4 in the HQBC NMR experiment (Scheme 8).

2.3. Capping of Trisilanol ***1*** *with the Pyridine-4-ethyl Functionality.* For the preparation of the 4-(2-ethyl)pyridine derivative of silsesquioxane trisilanol **1** two different synthetic procedures have been developed. The first route, illustrated in Scheme 9, first involved *in situ* preparation of $Cy_7Si_7O_9(OLi)_3$ (**11**) by deprotonation of **1** with 3 equivelant of $LiN(SiMe_3)_2$ according to the literature [32, 33]. This was immediately followed by treatment with equimolar amounts of 4-(2-trichlorosilylethyl)pyridine (**5**). This method was highly efficient and gave the highest yields of the target product **2** (up to 92–96%).

The second route was performed in toluene and involved the reaction of **1** with **4** in the presence of triethylamine (Scheme 10). This method was also found to be quite straightforward and afforded the desired compound **2** in good yields around 68–72%.

The pure product **2** was isolated as a white solid by the recrystallization from a toluene/acetonitrile mixture. The crystalline material is moderately soluble in pentane, toluene, diethyl ether and highly soluble in THF, but insoluble in DMSO, acetonitrile, methanol, and water. The constitution of **2** was confirmed by its ^{1}H, ^{13}C, and ^{29}Si NMR spectra and elemental analysis.

2.4. Attempted Quaternization Reactions of Compound ***2****.* As mentioned above, the final step towards the target compounds **3a** and **3b** would be the quaternization reaction of **2** with the appropriate alkyl bromides. While such reactions using the model compounds **5** and **6** were successful (*cf.* Section 2.2), nearly all attempts to carry out *N*-alkylation reactions with the pyridine-4-ethyl-functionalized POSS derivative **2** failed. Only with iodomethane it was possible to isolate the new N-methylpyridinium iodide **12**. Since compound **2** is insoluble in DMSO, acetonitrile and methanol, its *N*-alkylation with iodomethane (Scheme 11) could not be carried out in these very polar solvents which would have been desirable. While in less polar THF and nonpolar toluene solubility of **2** is very high, the quaternization rates with iodomethane were so low that even under reflux conditions over 5–7 days the product (methylpyridinium salt **12**) content in the reaction mixture did not exceed 5–8%. It was, however, found that the yield of **12** could be drastically improved (up to 92%) by prolonged heating of the precursor **2** in neat iodomethane. The resulting white solid was characterized by NMR spectroscopy. It dissolves in $CDCl_3$ but is insoluble in diethyl ether and hydrocarbons. Unfortunately, *n*-hexyl bromide and *n*-hexadecylbromide did not react with **2** even under forcing reaction conditions (e.g., extended heating of **2** in the neat alkylbromide). Thus the target compounds **3a** and **3b** thus far remain elusive. It also remains to be examined in the course of a future study if compounds like **12** exhibit biocidal properties.

3. Conclusions

In summarizing the results reported here, a possible synthetic route to new quaternary pyridinium salt-functionalized silsesquioxane (POSS) derivatives has been outlined. Such compounds could be of interest as potential POSS-based biocides. Judging from the initial results reported here it appears that the proposed synthetic route to *N*-alkylpyridinium-functionalized POSS derivatives such as **3a** and **3b** is principally feasible. Thus far, however, only with iodomethane a clean reaction to give the quaternized product **12** has been achieved, while under the chosen reaction conditions *n*-hexyl bromide and *n*-hexadecylbromide failed to react with **2** to give the corresponding *N*-alkylpyridinium salts.

4. Experimental

4.1. General Information. All reactions were carried out in an atmosphere of dry nitrogen with the use of standard Schlenk techniques or in a dry box (M. Braun, Labmaster 130 and MB 150B-G). NMR spectra were recorded on a Bruker DPX-NMR spectrometer (^{1}H 400 MHz, ^{13}C{^{1}H} 101 MHz, ^{29}Si{^{1}H} 79.5 MHz). Chemical shifts are reported in ppm and referenced to residual solvent resonances (^{1}H, ^{13}C) or an internal standard (^{1}H, ^{29}Si: TMS = 0 ppm). 4-Vinylpyridine (**4**), iodomethane, trimethylorthoformate, trichlorosilane, hexachloroplatinic acid (Speier's catalyst), and platinum(0)-1,3-divinyl-1,1,3,3-tetramethyl-disiloxane complex (Karstedt's catalyst) were obtained commercially (Aldrich or Acros) and used as received. The silsesquioxane precursor **1** was prepared in our laboratory according to the published procedure [19]. *n*-Pentane, *n*-hexane, toluene, diethyl ether, and THF were dried over sodium/benzophenone and freshly distilled under nitrogen prior to use. The other solvents and

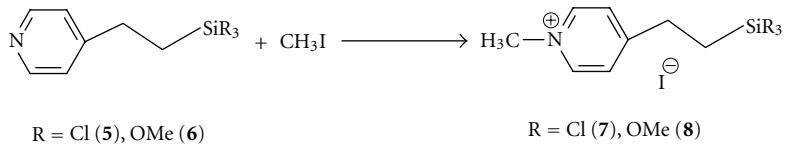

R = Cl (**5**), OMe (**6**)

R = Cl (**7**), OMe (**8**)

Scheme 6

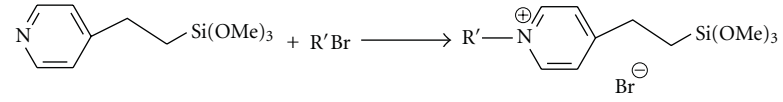

6

R′ = $^{n}C_6H_{13}$ (**9**), $^{n}C_{16}H_{33}$ (**10**)

Scheme 7

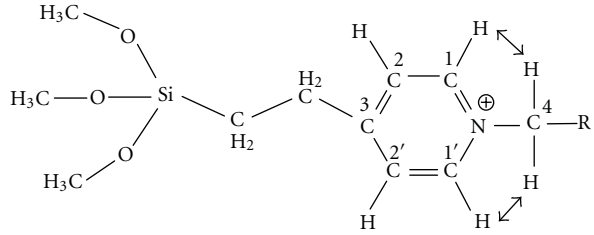

Scheme 8

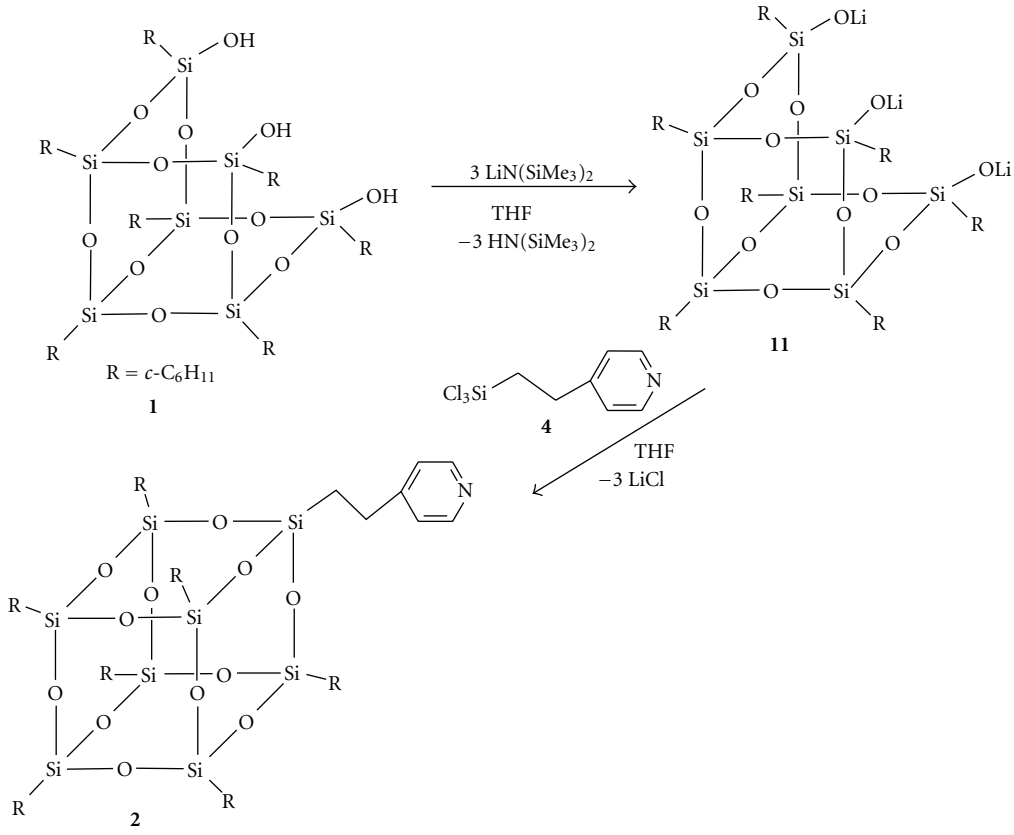

Scheme 9

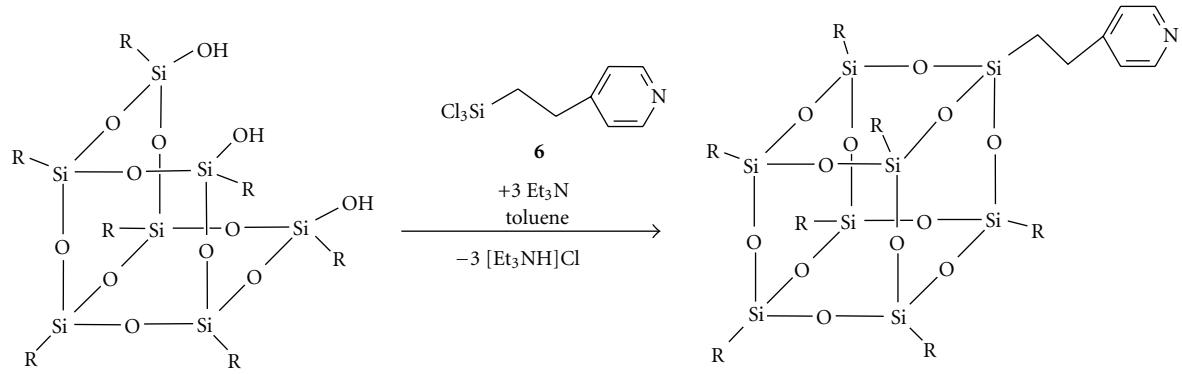

1 **2**

Scheme 10

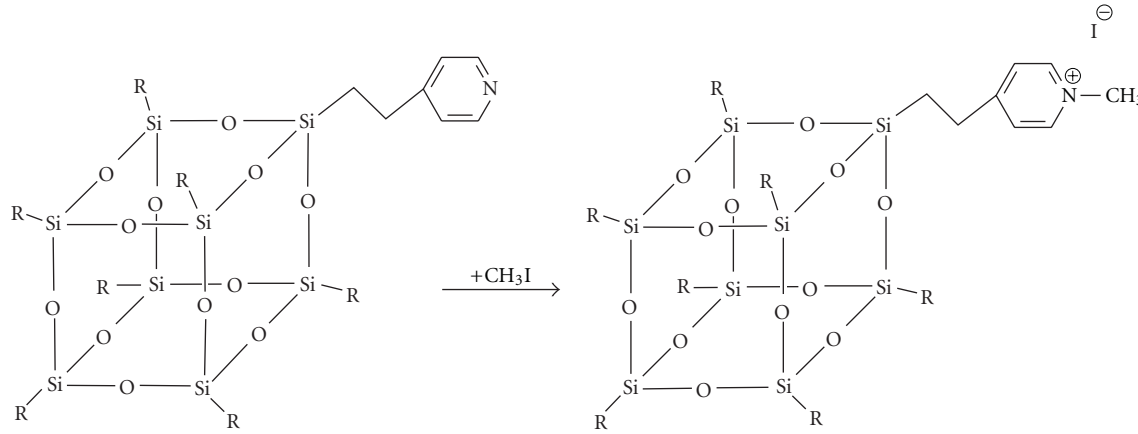

2 **12**

Scheme 11

reagents were first dried over the appropriate drying agent, then distilled and kept in the refrigerator. Chloroform was dried over phosphorus pentoxide (P_2O_5), acetone over boric anhydride (B_2O_3), acetonitrile over potassium carbonate (K_2CO_3), and triethylamine and tri-*n*-propylamine over calcium hydride (CaH_2). It was found that commercially available 4-vinylpyridine (**4**) had to be fractionally distilled under reduced pressure (5 mbar, b.p. 35-36°C) prior to use in order to achieve a reasonable purity and to remove polymeric material.

4.2. Preparation of 4-(2-(Trichlorosilyl)ethyl)pyridine (5) (Modified from [25]). In a 100 mL round-bottom Schlenk flask with a stirring bar, trichlorosilane (10.0 mL, 12.56 g, 92.6 mmol) was mixed with tri-*n*-propylamine (0.9 mL, 0.66 g, 4.6 mmol). Then, 4-vinylpyridine (**4**, 10.0 mL, 9.75 g, 92.7 mmol) was added very slowly and dropwise, waiting every time until heat evolution had ceased. At the end of adding the 4-vinylpyridine the reaction mixture completely turned into white solid and mixing was not possible. Then, *ca.* 20 mL of acetonitrile were added and the reaction mixture was refluxed at 60°C with the cooling condenser held at −26°C for 36 h until the white solid completely turned into a yellow-orange solution. This solution was fractionally distilled under reduced pressure (2 mbar), collecting the fraction boiling at 105–110°C as a colorless, slightly hazy liquid which on standing at r.t. reversibly tended to crystallize into a white solid with a light green tint. During purification of the product by distillation, gentle warming of the distillation bridge with a heating gun was necessary in order to avoid clogging. Yield 17.02 g (81%). Analysis calcd. for $C_7H_8Cl_3NSi$ (240.59): C 34.95, H 3.35, N 5.82; found: C 35.66, H 3.30, N 6.22%. ^{1}H NMR (400.13 MHz, $CDCl_3$, 25°C) δ 8.52-8.51 (m, 2H-*pyr*), 7.14-7.13 (m, 2H-*pyr*), 2.87 (m, 2H, $-CH_2-$py), 1.74 (m, 2H, $-CH_2-Si(OMe)_3$); $^{13}C\{^1H\}$NMR (100.61 MHz, $CDCl_3$, 25°C) δ 149.52 (s, C), 149.50, 122.78 (s, CH), 27.09, 24.12 (s, CH_2). MS (relative intensity) *m/e* 239 (M^+, 28%), 203 (M^+–Cl, 12%), 106 (M^+–Cl−$SiCl_2$, 100%), 92 (M^+–Cl−$SiCl_2$–CH_2, 24%).

4.3. Preparation of 4-(2-(Trimethoxysilyl)ethyl)pyridine (6) (Modified from [25]). A 100 mL Schlenk-flask was charged with a small amount (*ca.* 20 mg) of powdered anhydrous $AlCl_3$ and a stirring bar. Then, 4-(2-(trichlorosilyl)ethyl)-pyridine (**5**, 12.39 g, 51.5 mmol) was added. Trimethylorthoformate (22.5 mL, 21.86 g, 0.206 mol) was then added in

small portions of 3–5 mL, each time waiting 25–30 min until the vigorous gas evolution had stopped and the reaction mixture had cooled down to room temperature. (*Caution*: a more rapid addition of trimethylorthoformate causes intensive warming of the system which could lead to instantaneous splashing). At first, the yellow reaction mixture developed a pink and then an orange-brown color. After that the reaction mixture was refluxed at +80°C (oil bath) for 24–36 h until the refluxing stopped and the color had changed to deep green. The reaction mixture was fractionally distilled under reduced pressure (2 mbar), collecting the colorless fraction boiling at 118–120°C. When the product was distilling it was also necessary to gently heat the distillation bridge with a heating gun. Yield 8.43 g (72%). Analysis calcd. for $C_{10}H_{17}NO_3Si$ (227.34): C 52.83, H 7.54, N 6.16; found: C 51.31, H 7.45, N 5.73%. ^{1}H NMR (400.13 MHz, $CDCl_3$, 25°C) δ 8.48-8.47 (m, 2H-*pyr*), 7.13-7.12 (m, 2H-*pyr*), 3.55 (s, 9H, $-OCH_3$), 2.70 (m, 2H, $-CH_2-$py), 0.97 (m, 2H, $-CH_2-Si(OMe)_3$); ^{13}C{^{1}H}NMR (100.61 MHz, $CDCl_3$, 25°C): δ 152.25 (s, C), 148.91, 122.48 (s, CH), 49.62 (s, CH_3), 27.36, 9.36 (s, CH_2); ^{15}N {^{1}H} NMR (40.56 MHz, $CDCl_3$, 25°C): $\delta-152.65$ (s). MS (relative intensity): *m/e* 226 (M^+, 100%), 121 ($M^+-Si(OMe)_3$, 51%), 91 ($M^+-Si(OMe)_3-CH_2$, 21%).

4.4. Preparation of N-Methyl-4-(2-(Trichlorosilyl)ethyl) pyridinium Iodide ***(7)***. In a 100 mL Schlenk flask equipped with a stirring bar, 4-(2-(trichlorosilyl)ethyl)pyridine (**5**, 1.0 g, 4.4 mmol) was dissolved in 5 mL of acetonitrile and iodomethane (0.5 mL, 0.63 g, 4.4 mmol) was added. The reaction mixture was stirred at room temperature for 1 h, the solvent was removed under vacuum, and the powdery yellow residue was twice washed with 10 mL of diethyl ether to give the pure product. Yield 1.66 g (98%). Analysis calcd. for $C_8H_{11}Cl_3INSi$ (382.53): C 25.12, H 2.90, N 3.66; found: C 24.12, H 3.31, N 3.50%. ^{1}H NMR (400.13 MHz, $CDCl_3$, 25°C) δ 9.22-9.21 (m, 2H-pyr^+), 7.99–7.97 (m, 2H-pyr^+), 4.67 (s, 3H, $-CH_3$), 3.20 (m, 2H, $-CH_2-py^+$), 1.89 (m, 2H, $-CH_2-SiCl_3$); ^{13}C{^{1}H}NMR (100.61 MHz, $CDCl_3$, 25°C) δ 161.21 (s, C), 145.36, 127.67 (s, CH), 49.08 (s, CH_3), 28.51, 23.42 (s, CH_2).

4.5. Preparation of N-Methyl-4-(2-(Trimethoxysilyl)ethyl)pyridine Iodide ***(8)***. In a 100 mL Schlenk flask with a stirring bar 4-(2-(trimethoxysilyl)ethyl)pyridine (**6**, 1.0 mL, 1.23 g, 5.411 mmol) was dissolved in 5 mL of acetonitrile, and iodomethane (0.34 mL, 0.77 g, 5.411 mmol) was added at room temperature. The reaction mixture was stirred at r.t for 1 h. Then the solvent was removed under vacuum and the yellow oily residue was washed with 5 mL of diethyl ether under stirring at room temperature until the oil turned into yellow solid. The solid was washed with 5 mL of diethyl ether once again and dried *in vacuo* giving the pure product. Yield 1.18 g (98%). The pure compound could be isolated as colorless thin needles by recrystallization from boiling diethyl ether. Analysis calcd. for $C_{11}H_{20}INO_3Si$ (240.59): C 34.95, H 3.35, N 5.82; found: C 35.66, H 3.30, N 6.22%. ^{1}H NMR (400.13 MHz, $CDCl_3$, 25°C) δ 9.26-9.24 (m, 2H-pyr^+), 7.89–7.87 (m, 2H-pyr^+), 4.66 (s, 3H, $-CH_3$), 3.59 (s, 9H, $-OCH_3$), 2.99 (m, 2H, $-CH_2-py^+$), 1.02 (m, 2H, $-CH_2-Si(OMe)_3$); ^{13}C{^{1}H}NMR (100.61 MHz, $CDCl_3$, 25°C) δ 164.30 (s, C), 144.86, 127.27 (s, CH), 50.63, 48.59 (s, CH_3), 29.14, 9.28 (s, CH_2); ^{15}N {^{1}H} NMR (40.56 MHz, $CDCl_3$, 25°C) δ 28.00 (s).

4.6. Preparation of N-n-Hexyl-4-(2-(Trimethoxysilyl)ethyl) pyridine Bromide ***(9)***. In a 50 mL Schlenk flask with a stirring bar 4-(2-(trimethoxysilyl)ethyl)pyridine (**6**, 1.0 mL, 1.23 g, 5.4 mmol) was mixed with *n*-hexylbromide (5% excess, 0.79 mL, 0.93 g, 5.7 mmol). The reaction mixture was stirred at 80°C (oil bath) for 48 h. When the reaction mixture changed its color from deep green to orange-brown, the heating was stopped. The formed deep green oil was washed with 5 mL of diethyl ether and then dried under vacuum at +40°C to give **9** as a pale green oil. Yield 2.02 g (96%). Analysis calcd. for $C_{16}H_{30}BrNO_3Si$ (392,41): C 48.97, H 7.71, N 3.57; found: C 48.88, H 7.30, N 4.05%. ^{1}H NMR (400.13 MHz, $CDCl_3$, 25°C): δ 9.59–9.57 (m, 2H-pyr^+), 7.95–7.93 (m, 2H-pyr^+), 4.92 (t, 2H, py^+-CH_2-*hexyl*), 3.59 (s, 9H, $-OCH_3$), 2.98 (m, 2H, $-CH_2-py^+$), 2.06 (m, 2H, $-CH_2-$*hexyl*), 1.40 (m, 2H, $-CH_2-$*hexyl*), 1.37–1.23 (m, 4H, $-(CH_2)_2-$*hexyl*), 1.02 (m, 2H, $-CH_2-Si(OMe)_3$), 0.86 (t, 3H, $-CH_3-$*hexyl*); ^{13}C{^{1}H}NMR (100.61 MHz, $CDCl_3$, 25°C): δ 163.72 (s, C), 144.32, 127.18 (s, CH), 60.60 (s, CH_2), 50.39 (s, CH_3), 31.48, 30.76, 28.83, 25.28, 21.98 (s, CH_2), 13.55 (s, CH_3), 9.11 (s, CH_2).

4.7. Preparation of N-n-Hexadecyl-4-(2-(Trimethoxysilyl) ethyl)pyridine Bromide ***(10)***. In a 50 mL Schlenk-flask with a stirring bar 4-(2-(trimethoxysilyl)ethyl)pyridine (1.0 mL, 1.23 g, 5.4 mmol) was mixed with *n*-hexadecylbromide (5% excess, 1.74 mL, 1.74 g, 5.7 mmol). The reaction mixture was stirred at 80°C (oil bath) for 72 h. The formed oily mixture when cooled down to room temperature turned into a deep green solid. The pure product could be isolated as colorless thin needles by the recrystallization from methanol. Yield 2.91 g (96%). Analysis calcd. for $C_{26}H_{40}BrNO_3Si$ (522.60): C 59.76, H 7.71, N 2.68; found: C 57.95, H 7.33, N 2.23%. ^{1}H NMR (400.13 MHz, $CDCl_3$, 25°C) δ 9.36–9.34 (m, 2H-pyr^+), 7.87-7.86 (m, 2H-pyr^+), 4.94 (t, 2H, py^+-CH_2-*hexadec*), 3.58 (s, 9H, $-OCH_3$), 2.98 (m, 2H, $-CH_2-py^+$), 1.99 (m, 2H, $-CH_2-$*hexadec*), 1.33 (m, 2H, $-CH_2-$*hexadec*), 1.29–1.17 (m, 22H, $-(CH_2)_{11}-$*hexadec*), 1.01 (m, 2H, $-CH_2-Si(OMe)_3$), 0.88 (t, 3H, $-CH_3-$*hexadec*); ^{13}C{^{1}H}NMR (100.61 MHz, $CDCl_3$, 25°C) δ 164.25 (s, C), 144.32, 127.39 (s, CH), 61.22 (s, CH_2), 50.75 (s, CH_3), 29.63 (m, 6 CH_2), 29.60, 29.55, 29.47, 29.30, 29.22, 29.05, 26.01, 22.63 (s, CH_2), 14.07 (s, CH_3), 9.42 (s, CH_2); ^{15}N {^{1}H} NMR (40.56 MHz, $CDCl_3$, 25°C) δ 53.20 (s).

4.8. Preparation of $Cy_7Si_8O_{12}(CH_2)_2C_5H_4N$ ***(2)***. Freshly distilled hexamethyldisilazane $HN(SiMe_3)_2$ (1.96 mL, 9.2 mmol) was diluted with 5 mL of freshly distilled hexane. 5.78 mL of 1.6 M *n*-BuLi (9.2 mmol) solution were added dropwise at −35°C (2-propanol/liquid nitrogen mixture). The reaction mixture was stirred for 0.5 h. The thus prepared cold solution of $LiN(SiMe_3)_2$ was added slowly *via* a double-ended needle to the stirred solution of $Cy_7Si_8O_9(OH)_3$ (**1**,

3.0 g, 3.1 mmol) in 300 mL of freshly distilled THF at −35°C. The reaction mixture was stirred for 1-2 h allowing warming up slowly and then another 0.5 h at room temperature. Then the solvents were removed completely *in vacuo*. The white residue was washed twice with *n*-pentane. The solid was dried *in vacuo* once again and then dissolved in 300 mL of THF. Now 24.2 mL of a toluene solution (20 mL) of 4-(2-(trichlorosilyl)ethyl)-pyridine (0.74 g, 3.1 mmol) was added dropwise *via* a double-ended needle. The reaction mixture was stirred at room temperature for 6 h and 1 h at 60°C (oil bath) until a small amount of white solid started precipitating. Then the reaction mixture was concentrated to 150 mL, the solution was filtered from white sediment (LiCl) and the sediment was washed twice with 100 mL of THF. The solvent from the filtrate was removed completely and the white residue was dried *in vacuo* at +40°C. Yield 3.35 g (98%). Analysis calcd. for $C_{49}H_{85}NO_{12}Si_8$ (1104.90): C 53.27, H 7.75, N 1.27; found: C 53.01, H 7.29, N 2.12%. ^{1}H NMR (400.13 MHz, $CDCl_3$, 25°C) δ 8.49-8.48 (m, 2H-*pyr*), 7.16-7.15 (m, 2H-*pyr*), 2.74 (m, 2H-*pyr*), 1.96–1.48 (complex m, 35H-*cycl*), 1.37–1.04 (complex m, 35H-*cycl*), 0.97 (m, 2H-*pyr*), 0.82–0.67 (complex m, 7H-*cycl*); ^{13}C{^{1}H}NMR (100.61 MHz, $CDCl_3$, 25°C) δ 153.60 (s, C-*pyr*), 149.27, 123.45 (s, CH-*pyr*), 28.61 (s, CH_2-*pyr*), 27.53, 27.44, 27.39, 26.85, 26.80, 26.63, 26.59 (s, CH_2-*cycl*), 23.08, 23.04 (s, 4 : 3 for CH-*cycl*), 12.81 (s, CH_2-*pyr*); ^{15}N {^{1}H} NMR (40.56 MHz, $CDCl_3$, 25°C) δ −158.81 (s); ^{29}Si {^{1}H}NMR (79.49 MHz, d_5-pyridine, 25°C) δ −65.59, −66.81, −66.86 (s, 1 : 4 : 3). ^{29}Si {^{1}H}NMR (79.49 MHz, $CDCl_3$, 25°C) δ −67.81, −68.58 (s, 1 : 7). MS (relative intensity) *m/e* 1103 (M^+, 100%), 1020 (M^+–C_6H_{11}, 32%), 938 (M^+–C_6H_{11}–C_6H_{11}, 7%).

4.9. Alternative Preparation of $Cy_7Si_8O_{12}(CH_2)_2C_5H_4N$ (2). Trisilanol $Cy_7Si_7O_9(OH)_3$ (**1**, 3.0 g, 3.1 mmol) was dissolved in 300 mL of freshly distilled toluene. When the stirred solution had become completely clear, triethylamine (1.28 mL, 9.2 mmol) was added. 4-(2-(trichlorosilyl)ethyl)-pyridine (0.74 g, 3.1 mmol) in toluene (60-70 mL) was added dropwise *via* a double-ended needle at room temperature. The reaction mixture was stirred for 5-6 h at room temperature and 1 h at 60°C (oil bath) until the transparent solution became cloudy white. Then the solution was concentrated to 150 mL and filtered off from the white sediment of $[Et_3NH]^+Cl^-$, and the sediment was washed twice with 100–150 mL of toluene. The solvent from the clear filtrate was removed completely and the white residue was dried under vacuum at +40°C. Yield 3.01 g (88%). The pure product could be obtained by slow diffusion of acetone into saturated chloroform solution.

4.10. Preparation of $[Cy_7Si_8O_{12}(CH_2)_2C_5H_4N^+CH_3]I^-$ (12). The 4-(2-ethyl)pyridine POSS derivative **2** (1.0 g, 0.837 mmol) was mixed with 5 mL of neat iodomethane. The mixture was refluxed at 80°C (oil bath) for 72 h. Then the iodomethane was removed under vacuum and the yellow residue was washed twice with diethyl ether giving the pure product. Yield 0.96 g (92%). Analysis calcd. for $C_{50}H_{88}INO_{12}Si_8$ (1246.83): C 48.17, H 7.11, N 1.12; found: C 49.39, H 6.83, N 1.41%. ^{1}H NMR (400.13 MHz, $CDCl_3$, 25°C) δ 9.19–9.17 (m, 2H-*pyr*), 7.82-7.81 (m, 2H-*pyr*), 4.70 (s, 3H, –CH_3), 3.52 (m, 2H-*pyr*), 1.96–1.52 (complex m, 35H-*cycl*), 1.46–1.09 (complex m, 35H-*cycl*), 1.02 (m, 2H-*pyr*), 0.84–0.21 (complex m, 7H-*cycl*); ^{13}C{^{1}H}NMR (100.61 MHz, $CDCl_3$, 25°C) δ 164.73 (s, C-*pyr*), 144.94, 127.13 (s, CH-*pyr*), 29.64 (s, CH_2-*pyr*), 27.38, 27.34, 26.79, 26.75, 26.63, 26.54, (s, CH_2-*cycl*), 22.99, 22.96 (s, 4 : 3 for CH-*cycl*), 12.02 (s, CH_2-*pyr*).

Acknowledgments

Financial support of the work by the Otto-von-Guericke-Universität Magdeburg is gratefully acknowledged. N. Kostenko thanks the Government of Saxony-Anhalt for a Ph.D. scholarship (Graduiertenförderung).

References

[1] D. S. Worley and G. Sun, "Biocidal polymers," *Trends in Polymer Science*, vol. 4, pp. 364–370, 1996.

[2] O. A. Legonkova, "Modern conception of biodegradable and biocide polymers and composite materials on their basis," in *New Topics in Monomer and Polymer Research*, pp. 61–73, Nova Science, Hauppauge, NY, U.S.A., 2007.

[3] J. Markarian, "Antimicrobials find new healthcare applications," *Plastics, Additives and Compounding*, vol. 11, no. 1, pp. 18–22, 2009.

[4] B. L. Rivas, E. Pereira, and A. Maureira, "Functional water-soluble polymers: polymer-metal ion removal and biocide properties," *Polymer International*, vol. 58, no. 10, pp. 1093–1114, 2009.

[5] J. C. Huang, C. B. He, Y. Xiao, K. Y. Mya, J. Dai, and Y. P. Siow, "Polyimide/POSS nanocomposites: interfacial interaction, thermal properties and mechanical properties," *Polymer*, vol. 44, no. 16, pp. 4491–4499, 2003.

[6] B. X. Fu, M. Y. Gelfer, B. S. Hsiao et al., "Physical gelation in ethylene-propylene copolymer melts induced by polyhedral oligomeric silsesquioxane (POSS) molecules," *Polymer*, vol. 44, no. 5, pp. 1499–1506, 2003.

[7] C. M. Leu, Y. T. Chang, and K. H. Wei, "Synthesis and dielectric properties of polyimide-tethered polyhedral oligomeric silsesquioxane (POSS) nanocomposites via poss-diamine," *Macromolecules*, vol. 36, no. 24, pp. 9122–9127, 2003.

[8] S. H. Phillips, T. S. Haddad, and S. J. Tomczak, "Developments in nanoscience: polyhedral oligomeric silsesquioxane (POSS)-polymers," *Current Opinion in Solid State and Materials Science*, vol. 8, no. 1, pp. 21–29, 2004.

[9] L. Zheng, S. Hong, G. Cardoen, E. Burgaz, S. P. Gido, and E. B. Coughlin, "Polymer nanocomposites through controlled self-assembly of cubic silsesquioxane scaffolds," *Macromolecules*, vol. 37, no. 23, pp. 8606–8611, 2004.

[10] Y. J. Lee, S. W. Kuo, W. J. Huang, H. Y. Lee, and F. C. Chang, "Miscibility, specific interactions, and self-assembly behavior of phenolic/polyhedral oligomeric silsesquioxane hybrids," *Journal of Polymer Science, Part B*, vol. 42, no. 6, pp. 1127–1136, 2004.

[11] A. Fina, D. Tabuani, A. Frache, and G. Camino, "Poly-propylene-polyhedral oligomeric silsesquioxanes (POSS) nanocomposites," *Polymer*, vol. 46, no. 19, pp. 7855–7866, 2005.

[12] J. Zeng, S. Kumar, S. Iyer, D. A. Schiraldi, and R. I. Gonzalez, "Reinforcement of poly(ethylene terephthalate) fibers with polyhedral oligomeric silsesquioxanes (POSS)," *High Performance Polymers*, vol. 17, no. 3, pp. 403–424, 2005.

[13] K. H. Yoon, M. B. Polk, J. H. Park, B. G. Min, and D. A. Schiraldi, "Properties of poly(ethylene terephthalate) containing epoxy-functionalized polyhedral oligomeric silsesquioxane," *Polymer International*, vol. 54, no. 1, pp. 47–53, 2005.

[14] R. Misra, B. X. Fu, and S. E. Morgan, "Surface energetics, dispersion, and nanotribomechanical behavior of POSS/PP hybrid nanocomposites," *Journal of Polymer Science, Part B*, vol. 45, no. 17, pp. 2441–2455, 2007.

[15] Y. Zhao and D. A. Schiraldi, "Thermal and mechanical properties of polyhedral oligomeric silsesquioxane (POSS)/polycarbonate composites," *Polymer*, vol. 46, no. 25, pp. 11640–11647, 2005.

[16] J. Wu, T. S. Haddad, G. M. Kim, and P. T. Mather, "Rheological behavior of entangled Polystyrene-Polyhedral Oligosilsesquioxane (POSS) copolymers," *Macromolecules*, vol. 40, no. 3, pp. 544–554, 2007.

[17] S. Roy, B. J. Lee, Z. M. Kakish, and S. C. Jana, "Exploiting POSS-Sorbitol interactions: issues of reinforcement of isotactic polypropylene spun fibers," *Macromolecules*, vol. 45, pp. 2420–2433, 2012.

[18] J. Wu and P. T. Mather, "POSS polymers: physical properties and biomaterials applications," *Polymer Reviews*, vol. 49, no. 1, pp. 25–63, 2009.

[19] F. J. Feher, D. A. Newman, and J. F. Walzer, "Silsesquioxanes as models for silica surfaces," *Journal of the American Chemical Society*, vol. 111, no. 5, pp. 1741–1748, 1989.

[20] F. J. Feher and T. A. Budzichowski, "Silasesquioxanes as ligands in inorganic and organometallic chemistry," *Polyhedron*, vol. 14, no. 22, pp. 3239–3253, 1995.

[21] V. Lorenz, A. Fischer, S. Gießmann et al., "Disiloxanediolates and polyhedral metallasilsesquioxanes of the early transition metals and *f*-elements," *Coordination Chemistry Reviews*, vol. 206-207, pp. 321–368, 2000.

[22] V. Lorenz and F. T. Edelmann, "Metallasilsesquioxanes," *Advances in Organometallic Chemistry*, vol. 53, pp. 101–153, 2005.

[23] D. B. Cordes, P. D. Lickiss, and F. Rataboul, "Recent developments in the chemistry of cubic polyhedral oligosilsesquioxanes," *Chemical Reviews*, vol. 110, no. 4, pp. 2081–2173, 2010.

[24] N. S. Nametkin, I. N. Lyashenko, T. I. Tchernysheva, S. N. Borisov, and V. A. Pestushevitch, *Doklady Akademija Nauk SSSR*, vol. 174, pp. 1105–1108, 1967.

[25] H.-R. Grüniger and G. Calzaferri, "Synthese von 4-Trichlorsilylmethylbenzonitril und 4-(2-Trichlorsilyläthyl)pyridin zur Oberflächenmodifikation von Zinndioxid," *Helvetica Chimica Acta*, vol. 62, pp. 2547–2550, 1979.

[26] M. G. Voronkov, N. N. Vlasova, S. A. Bolshakova, and S. V. Kirpichenko, "The catalytic reactions of triethyl- and triethoxysilane with unsaturated sulphides," *Journal of Organometallic Chemistry*, vol. 190, no. 4, pp. 335–341, 1980.

[27] W. Caseri and P. S. Pregosin, "Mechanistic aspects of the platinum catalysed hydrosilylation of $PhC{=}CH_2$ with Et_3SiH," *Journal of Organometallic Chemistry*, vol. 356, no. 2, pp. 259–269, 1988.

[28] C. Polizzi, A. M. Caporusso, G. Vitulli, P. Salvadori, and M. Pasero, "Supported platinum atoms derived catalysts in the hydrosilylation of unsaturated substrates," *Journal of Molecular Catalysis*, vol. 91, no. 1, pp. 83–90, 1994.

[29] M. F. Lappert and F. P. A. Scott, "The reaction pathway from Speier's to Karstedt's hydrosilylation catalyst," *Journal of Organometallic Chemistry*, vol. 492, no. 2, pp. C11–C13, 1995.

[30] S. Sakaki, N. Mizoe, M. Sugimoto, and Y. Musashi, "Pt-catalyzed hydrosilylation of ethylene. A theoretical study of the reaction mechanism," *Coordination Chemistry Reviews*, vol. 190–192, pp. 933–960, 1999.

[31] Q. J. Miao, Z. P. Fang, and G. P. Cai, "Silica-supported Karstedt-type catalyst for hydrosilylation reactions," *Catalysis Communications*, vol. 4, no. 12, pp. 637–639, 2003.

[32] J. Annand, H. C. Aspinall, and A. Steiner, "Novel heterometallic lanthanide silsesquioxane," *Inorganic Chemistry*, vol. 38, no. 17, pp. 3941–3943, 1999.

[33] V. Lorenz, S. Gießmann, Y. K. Gun'ko, A. K. Fischer, J. W. Gilje, and F. T. Edelmann, "Fully metalated silsesquioxanes: building blocks for the construction of catalyst models," *Angewandte Chemie*, vol. 43, no. 35, pp. 4603–4606, 2004.